Marcos Navascuez Lominchar

PhD. Thesis (Donostia, 2020)

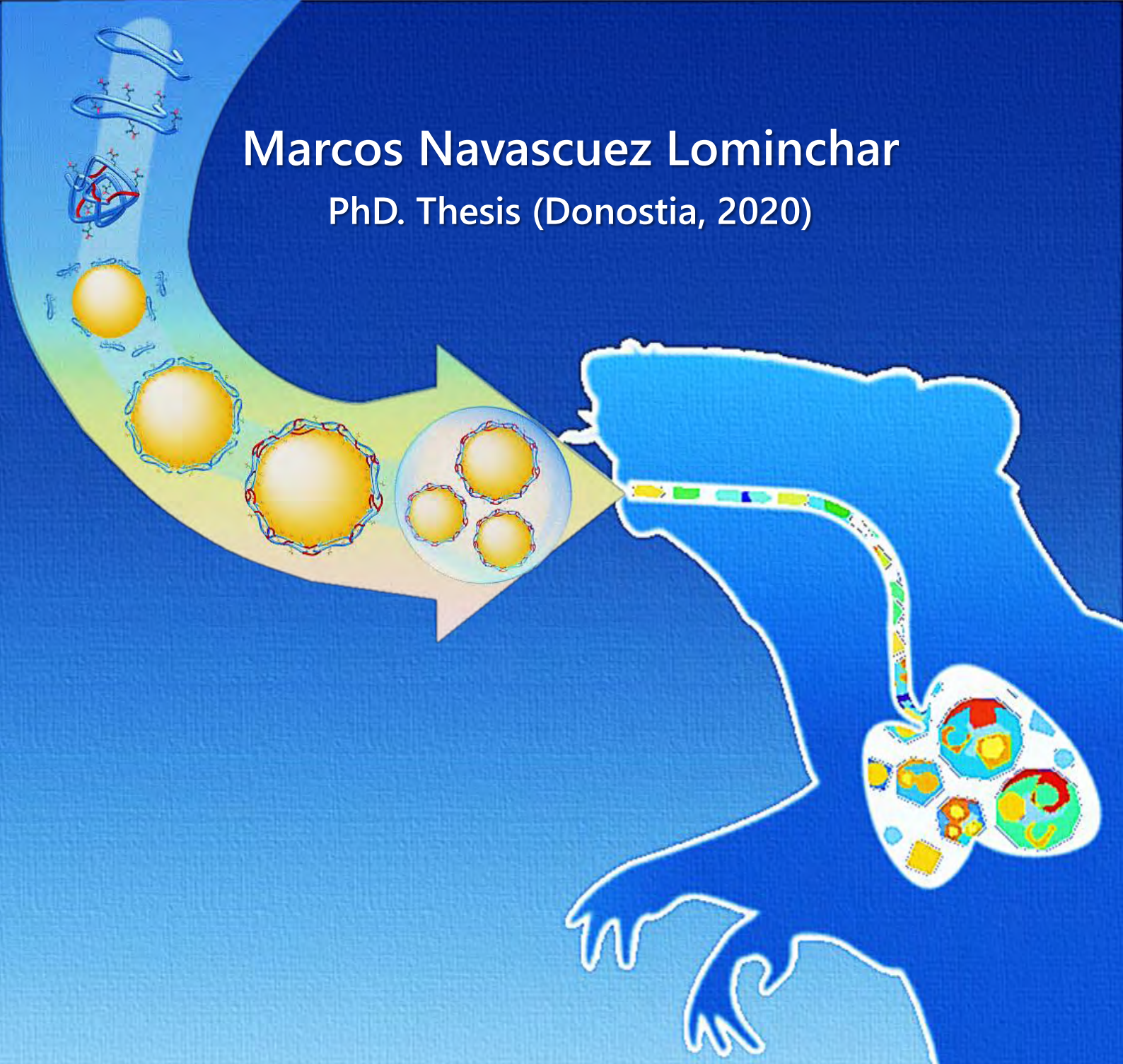

Nanoemulsions as drug carriers: preclinical evaluation of pulmonary delivered drug-loaded nanocapsules

eman ta zabal zazu

Universidad del País Vasco

Euskal Herriko Unibertsitatea

© 2020 Marcos Navascuez Lominchar

Nanoemulsions as drug carriers: Preclinical evaluation of pulmonary delivered drug-loaded nanocapsules

PhD Thesis

to obtain the Doctor of Philosophy degree in

Synthetic and Industrial Chemistry

at the University of the Basque Country (UPV/EHU)

by

Marcos Navascuez Lominchar

Donostia-San Sebastian, 2020

Thesis Supervisors: Dr. Jordi Llop Roig (Radiochemistry and Nuclear Imaging Group, CIC biomaGUNE) and Dra. Iraida Loinaz Bordonabe (Nanomedicine Institute, CIDETEC)

University Tutor: Dra. María Esther Lete Expósito (Department of Organic Chemistry II, Faculty of Science and Technology, University of the Basque Country (UPV/EHU))

Acknowledgments

Desde que vine a Donostia en Octubre del 2016 han tenido que pasar casi cuatro años y una pandemia para poder terminar esta tesis. Durante esta etapa he tenido la gran suerte de coincidir con muchas personas que me han ayudado muchísimo, tanto en lo personal como en lo profesional, y a las cuales quiero agradecer su apoyo aprovechando estas líneas.

En primer lugar, quiero agradecer a toda la gente del grupo de Radioquímica e Imagen Molecular del CIC **biomaGUNE**. A mi director Jordi; por tu confianza, optimismo, integridad e inteligencia con las que te has ganado todo mi respeto y admiración, llegando a convertirte, y lo digo absolutamente convencido, en el mejor modelo a seguir que podría haber tenido. Al crossfitero Unai, por tu predisposición a ayudar y compartir lo que sabes contribuyendo enormemente a que me sintiera parte del grupo desde el inicio (no siempre es fácil estando entre dos centros…) muchas gracias crack. A los figuras de la plataforma (Aitor, Víctor y Xabi) por vuestra paciencia conmigo y por toda vuestra ayuda, haciendo demasiadas veces de nuestros proyectos los vuestros. A Zuriñe, la mamá de todos, por ser tan tan tan buena y comprensiva con nosotros… no sabes lo que se agradece cuando estás lejos de casa. Tendría para escribir otra tesis agradeciendo a cada uno del grupo lo que me habéis ayudado, pero tengo que acortar jaja y no quiero dejarme a nadie sin mencionar: Ángel, Luka, Vanessa, Luís, Larraitz, Sameer, Irene, Riccardo, Ana B., Ana J., Rossana, Pilar, Cristina (quina paSienSia!! :P), Kepa (lung inflammation team!!), Krishna (my Lord and my MASTER) y Ane (mejores de la promoción RQ-Supervisors!!). No me puedo olvidar de mis compis de despacho: Lydia, Irati, Zuriñe, Susana, María Jesús y Ander (que suerte tuve de coincidir contigo tío, eres una de las mejores personas que he conocido). Por último; a toda la gente de animalario, a Pedro por su ayuda en edición y programación y a Fernando, por esa capacidad para contagiar optimismo y todas sus buenas directrices cuando estaba empezando.

De igual forma, tengo mucho que agradecer a toda la gente de la Unidad de **Cidetec Nanomedicine** y, más concretamente, a las líneas de SCPNs y Smart Colloids.

Empezando por mi directora Iraida, por saber escuchar y por todo su apoyo y su confianza en mí desde que llegué. A Raquel y Marco por su paciencia conmigo cuando estaba empezando. A la doctora Alkorta, por enseñarme el funcionamiento de Cidetec y ayudarme como antigua doctoranda del grupo, gracias a ti todo ha sido más fácil… y me has demostrado, en demasiadas ocasiones, que eres una tía 10. A Janire Pikabea, por esa eterna predisposición a ayudar a tod@s, siempre con una sonrisa. A ti Adrián, por tu comprensión y actitud dialogante que tanto hace falta en un equipo. Mención especial para el señor Cristian por ser tan buen tío y tan alegre, porque a pesar de que nunca te invitarás a una copa… no puedo dejar de reírme contigo (eso sí, te falta calle pesetas :P). A Damien, el JEFE, porque siempre tienes unos segundos para atenderme y siempre has respetado mis ideas e iniciativas, permitiéndome fallar al intentar llevarlas a cabo, aun sabiendo que no iban a funcionar (Lo sé, soy muy maño/cabezón. PD: gracias por tu paciencia, confianza y por transmitirme toda esa pasión por la ciencia). A mi VETERANA amiga Nati, porque has sido capaz de hacer a la vez el papel de colega, psicóloga, madre, técnico, científica… Porque tienes esa asombrosa capacidad de hacer que TODO sea más fácil para TODOS. Porque tu forma de ser inspira, y ojalá, llegar a ser como tú (cuando sea mayor :P). Por último, a toda la gente que forma o ha formado parte de la unidad y a los que siempre tendré palabras de agradecimiento por el trato que han tenido conmigo: Julie, Laura, Eider, Idoia, Bea, Naiara, Cristina, Xabi, Juliana, Aitziber, Andrea, Susana, Ana B., Luisa, June, Ainara, Edurne, Aintzane y Pablo… GRACIAS.

Nada de esto hubiera sido lo mismo sin mi gente de la **Kuadrilla.** Posiblemente seamos la kuadrilla más variopinta de Donosti pero no cambiaría por nada los momentos vividos con Juan, Dani, Imanol, Jorge, Plou, Barrio, Edu, Badía y Pesetas. Siempre voy a recordar nuestras salidas al monte, Burgos (y el Condotiero), Semana Grande (sobre todo la de Bilbo jaja), Santo Tomás, sidrerías y demás salidas. Muchas gracias por hacerme sentir parte de este grupo chavales. Agradecimiento especial también para La **Peña Zaragocista** CIC biomaGUNE y a sus socios cofundadores (Plou, Dani y Javi) que gestaron el viaje a Miranda (PD: importantísimo que haya pepinillos jajaj).

Vivir a caballo entre dos ciudades no siempre es fácil, y menos cuando no miras el WhatsApp ni aunque te paguen, por eso quiero agradecer a los cracks de **Fuckinianos** (Plano, Kevin, Sáez, Isaac, Cesar, Barrio, Erik, Jona, Borja, Paco, Aitor, Montes y Liscano) por las pochas, la campana, los finitos, BBQs en Pinseque, el templo, los Royal y todo lo demás. Porque siempre están ahí para recordarme quien soy y de dónde vengo, y porque, "*el que guarda… siempre tiene"* gracias chavales. A Borja, Bibi, Adri, Vallas, Luís, Alberto y demás **figuras del atletismo** que nunca fallan a las grandes citas… ni aunque acaben en Zarautz. Gracias por los Koalas, litros pinchados, llaves perdidas, competiciones de flexiones y bailoteos, también en el norte. A toda la gente de **Quimipandi** (Pablo, Javi, Amaya, Anamar, Alba, Ainhoa, Aitor, Llorens, Lorena, Badía, Cored, Fer, Diego, Juan, Casas, Rebe y Regi) por las sidrerías, casas rurales, el doble check, nuestras discusiones políticas interminables y todas las exaltaciones de la amistad.

Qué ganas tenía de escribir unas líneas a los **Nanomagnets**!! A mi mentora Raluca por convencerme (y convencer) para que acabara en Donosti, por confiar en mí y ayudarme siempre que lo he necesitado. Al figura de Edu, por compensar con la organización del JICI el desastre de la caída del campo de refugiados (espero que en tu futuro político recuerdes mis lecciones…). Al turolense más ilustre que conozco, Don Vito, al que aprovecho a pedir públicamente perdón por haber organizado la fiesta sidrera que casi causa su muerte y que le dio su primer patín de oro (PD: a Ralu también jaja). Lo prometido es deuda así que… a ti Vanessa, una de las personas más transparentes que conozco, por todos los ratos que me has dado para discutir, divagar, psicoanalizar y darnos cera. Siempre con buen humor e ironía pero sin callarnos ni media… se te echa de menos. No me olvido del resto de miembros de Bionanosurf/NAP (cada día os llamáis de una manera XD) con los que he pasado tan buenos ratos. Especialmente de mi MAPS Eva, que no solo me soporta sino que encima le caigo bien jajaj. Ahora te toca acabar a ti, pero recuerda, el Oliver es sólo un estado mental que compartimos tú, yo y el Tana… mucho ánimo ☺

Llegan los más fundamentales: mis compañeros de **Untzaene Kalea N^{o}4**. A ti **Íñigo**, por tu sarcasmo, ironía y humor negro. Por nuestros debates puramente dialécticos, sin opinión fundada ni posición definida, debatir por debatir vaya jajaj se te echa de menos. Me quedas tú **Badía**, compañero de penas y alegrías durante estos 4 años… creo que te puedo considerar mi relación sentimental más duradera (lo siento por la Rachel XD). Sin ti no hubiera llegado donde estoy, nuestra competitividad (SANA) en casa me ha llevado a progresar increíblemente y, a pesar de que no puedo estar más contento por acabar, no puedo estar más triste porque nuestros caminos se separan. Nos va a ir bien a los dos, nos lo merecemos y te lo mereces, porque las oportunidades son sólo una cuestión probabilística para el que se lo curra de verdad. Voy a echar de menos Fogones Bunsen y el choperismo… te aprecio mucho.

Por último, quiero agradecerle a mi **Familia** (aragonesa, alemana y valenciana) todo lo que ha hecho por mí. Estas pocas líneas son inversamente proporcionales a toda vuestra contribución. Mención especial para mi primo **David**; transmites pasión, alegría y optimismo en todo lo que haces y… me da que es contagioso, por eso cada vez que alguien me compara contigo no puedo sentir más que orgullo, gracias. También a mi tío **Juan**, me hubiera encantado que vieras terminado este trabajo. Me has inspirado mucho más de lo que te imaginas y voy a echar de menos tus lecciones camarada. Ya sabéis que confío mucho en mí mismo y en mis posibilidades pero eso no sirve de mucho si no vives en el mundo real. Por eso, quiero darte las gracias **MAMÁ**, por ponerme los pies en la tierra cuando me vengo arriba y me creo que puedo volar. Y por eso también, muchas gracias **PAPÁ**, por creer siempre que puedo volar… tenga alas o no. Y por supuesto muchas gracias **ELÍAS**, tu fe ciega en mí siempre me hizo creer que era alguien diferente, alguien importante, alguien al que merecía la pena seguir… y es por eso que he tratado de parecerme todos los días a esa versión de mí mismo que tú imaginaste. Creo firmemente que la suerte sólo existe en el momento del reparto de cartas, al empezar la partida, y que después el que mejor juega es el que más posibilidades tiene de ganar. Tengo claro que he llegado hasta aquí gracias a mi esfuerzo y dedicación pero, he de reconocer, que he tenido mucha suerte con las cartas que me tocaron al empezar la partida. OS QUIERO MUCHO.

List of Abbreviations and Acronyms

ALI	Acute lung injury
AMF	Ammonium formate
ARDS	Acute respiratory distress syndrome
Asp	Aspartate
BCS	Biopharmaceutical Classification System
BFCs	Bifunctional chelators
CMC	Critical Micelle Concentration
CALB	Candida Antarctica Lipase B
CL	Cross-linked
CT	Computational Tomography
COPD	Chronic obstructive pulmonary disease
COSAN	Cobalt *bis*(dicarbollide) anion ($[3,3'\text{-}Co(C_2B_9H_{11})_2]^-$)
Dh	Hydrodynamic diameter
Dh[4;3]	Volume diameter
DHA	Docosahexaenoic acid
DLS	Dynamic light Scattering
DMAP	4-(*N*,*N*-dimethylamino)pyridine
Dv50	Median diameter by volume
DODT	3,6-dioxa-1,8-octane-dithiol
DOTA	1,4,7,10-tetraazacyclododecane-tetraacetic acid
DS	Degree of substitution
DXT-MA	Dextran random coil polymer (MA functionalized)
DXT-F	Dextran random coil polymer (COOH functionalized)
DXT-SCPN-MA	Dextran single chain polymer nanoparticle (MA functionalized)
DXT-SCPN-F	Dextran single chain polymer nanoparticle (COOH functionalized)
DXT-R	Dextran derivatives
D (number)	Dextran derivatives labelling
E (number)	Emulsions labelling
FDG	2-deoxy-2-[^{18}F]fluoro-D-glucose
FES	16α-[^{18}F]Fluoroestradiol
FFA	Free fatty acid
FFA_{max}	Maximum percentage of free fatty acids
Glc	Glucose
GMA	Glycidyl methacrylate
Glu	Glutamate
His	Histidine

LD	Laser diffraction
MA	Methacrylate
MAG	Monoglyceride
MeCN	Acetonitrile
MPA	3-mercaptopropionic acid
MMSE	3-methoxymethyl-16β,17β-epiestriol-O-cyclic sulfone
NPs	Nanoparticles
NCs	Nanocarriers
NEs	Nanoemulsions
O/W or W/O	oil-in-water or water-in-oil
PBS	Phosphate buffer saline
PDI	Polydispersity index
PET	Positron Emission Tomography
PLA	Polylactide acid
PL	Pancreatic Lipase
PTA	Phosphotungstenic acid
RML	Rhizomucor miehei Lipase
ROL	Rhizopus oryzae Lipase
SCPNs	Single chain polymer nanoparticles
SEC	Size exclusion chromatography
SEM	Scanning Electron Microscopy
Ser	Serine
SEAr	Aromatic electrophilic substitution
SMEs	Small and medium enterprises
SPECT	Single Photon Emission Computerised Tomography
ST	Surface tension
TAG	Triacylglyceride
TEM	Transmission Electron Microscopy
TLC	Thin layer chromatography
TLL	Thermomyces lanuginosus Lipase
VOI	Volume of interest

Table of Contents

Summary

The use of nanomaterials for biomedical applications has been widely studied during the last decades. In medicine, nanomaterials constitute a very promising research field from an academic point of view in areas such as the development of medical devices, molecular imaging or drug delivery, among others. Advanced drug delivery systems can improve the pharmacological properties of conventional "free" drugs by modifying their biodistribution and pharmacokinetics. Ideally, nanocarriers should increase the bioavailability of the drug in the target organ while decreasing toxic and side effects. To this purpose; a proper size, shape and surface functionality of the carrier are required to prolong the biological half-life of the drug and to achieve the optimal dose in the diseased tissue while minimizing off-target side effects.

The administration route also plays a pivotal role in nanomedicine, and pulmonary delivery is attractive both for local and systemic therapies. The low thickness of the epithelium (0.1–0.5 µm in the alveolar region) and its huge surface area (75–150 m^2) lead to a faster onset of therapeutic action while avoiding the first-pass metabolic barriers. One of the main challenges in inhalation when the lungs are the target organ is to avoid or reduce the extremely fast clearance in the alveoli region. This effect is especially relevant for poorly water-soluble drugs which are highly permeable to biological membranes. However, the therapeutic efficacy of poorly-water soluble drugs can be significantly improved by optimizing the formulation design. In this context, oil-in-water (o/w)-nanoemulsions (NEs) have gained attention as hydrophobic drug carriers because of their high loading capacity. Emulsion stabilization usually requires the use of surfactants (surface-active substances) which are amphiphilic molecules able to reduce interfacial tension between the immiscible phases. Regarding to this, natural polymer grafting has appeared as novel strategy to produce biodegradable surfactants relevant to biomedical applications.

In this PhD thesis, pulmonary administration and *in vivo* molecular imaging have been pushed forward, with the ultimate aim of exploring the suitability of polymers and polymeric NPs to stabilize (o/w)-nanoemulsions as potential drug carriers for enhanced transport and delivery of poor water soluble drugs.

First, the capacity of dextran polymers and dextran-based single-chain polymer nanoparticles (SCPNs) to stabilize NEs was investigated (chapter 3). The main goal of this chapter was to produce stable and monodisperse dextran-based (o/w)-nanoemulsions below 500 nm suitable for pulmonary delivery. As pristine dextran (DXT, hydrophilic polysaccharide) is not able to sufficiently decrease the oil/water interfacial tension to produce (o/w)-nanoemulsions, chemical modification of dextran with hydrophobic or hydrophilic moieties (DXT-R) were carried out. Four dextran derivatives with the same degree of functionalization were synthesized while changing the functional group (methacrylic or carboxylic acid) and the three-dimensional structure (polymer coil or single chain polymer nanoparticle). Besides surfactant optimization (surfactant selection, determination of surfactant weight percentage and functionalization degree), other experimental conditions such as the parameters of the oil phase (selection of the oil and the oil/water proportions) were evaluated in order to fulfill droplet size and stability requirements for intratracheal instillation. Big efforts were conducted to achieve long-term stable emulsions. However, emulsion stability was compromised in highly ionic strength media, and NEs were rapidly destabilized under physiological conditions.

Aiming at improving the media stability of the NEs, cross-linking strategies were explored (chapter 4). More concretely, cross-linking was performed on the polymers after adsorption at the oil/water interface under mild reaction conditions using a surface active dithiol as the linker. Two different strategies for crosslinking (via the aqueous phase or the organic phase) were evaluated in order to avoid inter-droplet crosslinking. Successful intra-droplet crosslinking via the organic phase could be achieved, with consequent extensive improvement in emulsion long-term stability. The resulting cross-linked emulsions proved to be stable for months (up to 1 year) in any physiologically relevant medium. Moreover, the effect of the reaction on emulsion stability was assessed, both *in vitro* and *in vivo*, the latter using Positron Emission Tomography (PET). Fluoroestradiol was selected as model drug due to its hydrophobicity (log Kow=4.01) and easy labelling with the positron emitter ^{18}F (half-life of 109.8 minutes). Copper-64, a positron emitter with physical half-life of 12.7 hours,

was anchored to the polymeric surfactant to investigate the biodistribution of the nanocarrier.

Moving forward towards potential controlled drug delivery, the enzyme-responsive properties of the NEs were studied (chapter 5). Due to the presence of ester bonds generated during dextran functionalization and also present in the oil phase, our emulsions can be destabilized in the presence of esterase enzymes. Hence, we designed an experimental set up to unravel the mechanism of enzymatic destabilization by evaluating the response of the individual components (oil and surfactant) towards Candida Antarctica Lipase B (CALB) and the effect of the enzyme on droplet size. Finally, the studies were extended to Pancreatic Lipase.

Finally, with the aim of exploring less conventional amphiphiles as emulsion stabilizers, and taking advantage of the expertise of the research team in boron chemistry, the suitability of the boron-rich anionic complex cobalt bis(dicarbollide) (COSAN) to stabilize NEs was also assayed (chapter 6). Nanoemulsion stability was evaluated towards a wide range of stimuli: overtime, in relevant physiological media, in presence or absence of light, at different temperatures and in presence of lipases. Moreover, the capability of the resulting NEs to modulate the biodistribution of entrapped hydrophobic drugs after pulmonary administration was investigated in rodents using *in vivo* nuclear imaging. Previous results obtained with FES as model drug encouraged us to use the same model compound using COSAN-based NEs as pulmonary carriers. To get further information of the nanocarrier, we also explored the biodistribution of the stabiliser, i.e. the COSAN. In this case, COSAN was firstly functionalized with iodine and later on radiolabelled with the positron emitter ^{124}I (half-life of 4.2 days) via isotopic exchange. Our promising results suggest that the newly developed NEs can be applied for drug delivery of poor water soluble drugs when the lung is the target organ.

Resumen

La utilización de nanomateriales en aplicaciones biomédicas ha suscitado un gran interés durante las últimas décadas. En medicina, los nanomateriales constituyen un campo de investigación muy prometedor desde un punto de vista académico en áreas

como el desarrollo de dispositivos médicos, la imagen molecular o la liberación controlada de fármacos. Los nanomateriales avanzados para la administración controlada de medicamentos (*nanocarriers*) pueden mejorar las propiedades farmacológicas de los mismos en comparación con la administración del compuesto activo libre, debido a que consiguen modificar su biodistribución y farmacocinética. Idealmente, los *nanocarriers* deberían aumentar la biodisponibilidad del fármaco en el órgano a tratar, al mismo tiempo que disminuyen los efectos secundarios en el resto de los órganos. Para este fin se requieren una forma y tamaño adecuados, además de una funcionalización apropiada de la superficie del *nanocarrier* con el objetivo de prolongar la vida media biológica del fármaco. Esto ayudaría a alcanzar la dosis adecuada en el tejido/órgano afectado, minimizando a su vez los efectos secundarios fuera de la diana terapéutica.

La ruta de administración juega un papel fundamental en el uso de nanomateriales como *nanocarriers,* y en este contexto la inhalación de aerosoles a través del sistema respiratorio es considerada una ruta de administración muy atractiva tanto para terapias locales como sistémicas. El bajo grosor del epitelio (0.1–0.5 µm en la región alveolar) y su enorme área superficial (75–150 m^2) proporcionan un inicio más rápido de la acción terapéutica evitando las principales barreras metabólicas del cuerpo. Uno de los principales desafíos a superar cuando los pulmones son el órgano a tratar consiste en evitar o reducir la rápida eliminación del fármaco en la región de los alvéolos. Este efecto, que es especialmente relevante en fármacos poco solubles en agua que son altamente permeables a membranas biológicas, puede mitigarse optimizando el diseño de su formulación. Una opción para conseguir una formulación adecuada consiste en utilizar nanoemulsiones de aceite-en-agua (NEs) como portadores de fármacos hidrofóbicos, cuyo uso ha suscitado un gran interés científico debido, principalmente, a su gran capacidad de carga. La estabilización de la emulsión generalmente requiere del uso de tensoactivos, que son moléculas anfifílicas capaces de reducir la tensión interfacial entre fases inmiscibles. En este aspecto, el grafting o funcionalización de polímeros naturales ha emergido como una novedosa estrategia

para la producción de tensoactivos o estabilizadores biodegradables que puedan ser útiles en aplicaciones biomédicas.

En esta tesis doctoral, se ha utilizado la administración pulmonar y las técnicas de imagen molecular *in vivo* con el objetivo final de explorar la idoneidad de polímeros y NPs poliméricas basadas en dextrano para estabilizar nanoemulsiones de aceite en agua cuya principal función es la encapsulación, transporte y liberación controlada de fármacos poco solubles en agua.

Los polisacáridos son las biomacromoléculas más comunes en todo el mundo. La gran variedad de grupos reactivos y composición química, junto con su biodegradabilidad, han propiciado su uso en diferentes aplicaciones biomédicas. El dextrano (DXT) es un polisacárido hidrofílico incapaz de disminuir suficientemente la tensión interfacial entre agua y aceite como para producir emulsiones estables; en consecuencia, requiere de modificaciones químicas que le confieran propiedades como tensoactivo. El primer objetivo de la tesis, abordado en el capítulo 3, ha sido el de producir nanoemulsiones estabilizadas con derivados de dextrano (DXT-R), estables, monodispersas y con un diámetro inferior a 500 nm, con lo que serían adecuadas para la administración pulmonar. Con este propósito, se sintetizaron cuatro derivados de dextrano con el mismo grado de funcionalización pero cambiando de grupo funcional (metacrilato o ácido carboxílico) y la estructura tridimensional (polímero *random coil* o nanopartícula polimérica de cadena única). Además de la optimización del tensoactivo (selección del tensoactivo, determinación del porcentaje en peso del tensoactivo y su grado de funcionalización), se evaluaron otras condiciones experimentales como los parámetros relacionados con la fase oleosa (selección del aceite y las proporciones de aceite/agua) con el objetivo de cumplir con los criterios de tamaño, polidispersidad y estabilidad necesarios para la nebulización del aerosol. Todos los DXT-R han demostrado su capacidad para actuar como emulsificantes, incluidos los modificados hidrofílicamente. Sin embargo, DXT-MA (modificado con grupos metacrilatos, MA) ha sido seleccionado como el mejor estabilizante debido a la simplicidad en su síntesis química (sólo una etapa de funcionalización) y a su capacidad para generar las emulsiones con menor polidispersidad y menor diámetro de gota (**Figura 1**).

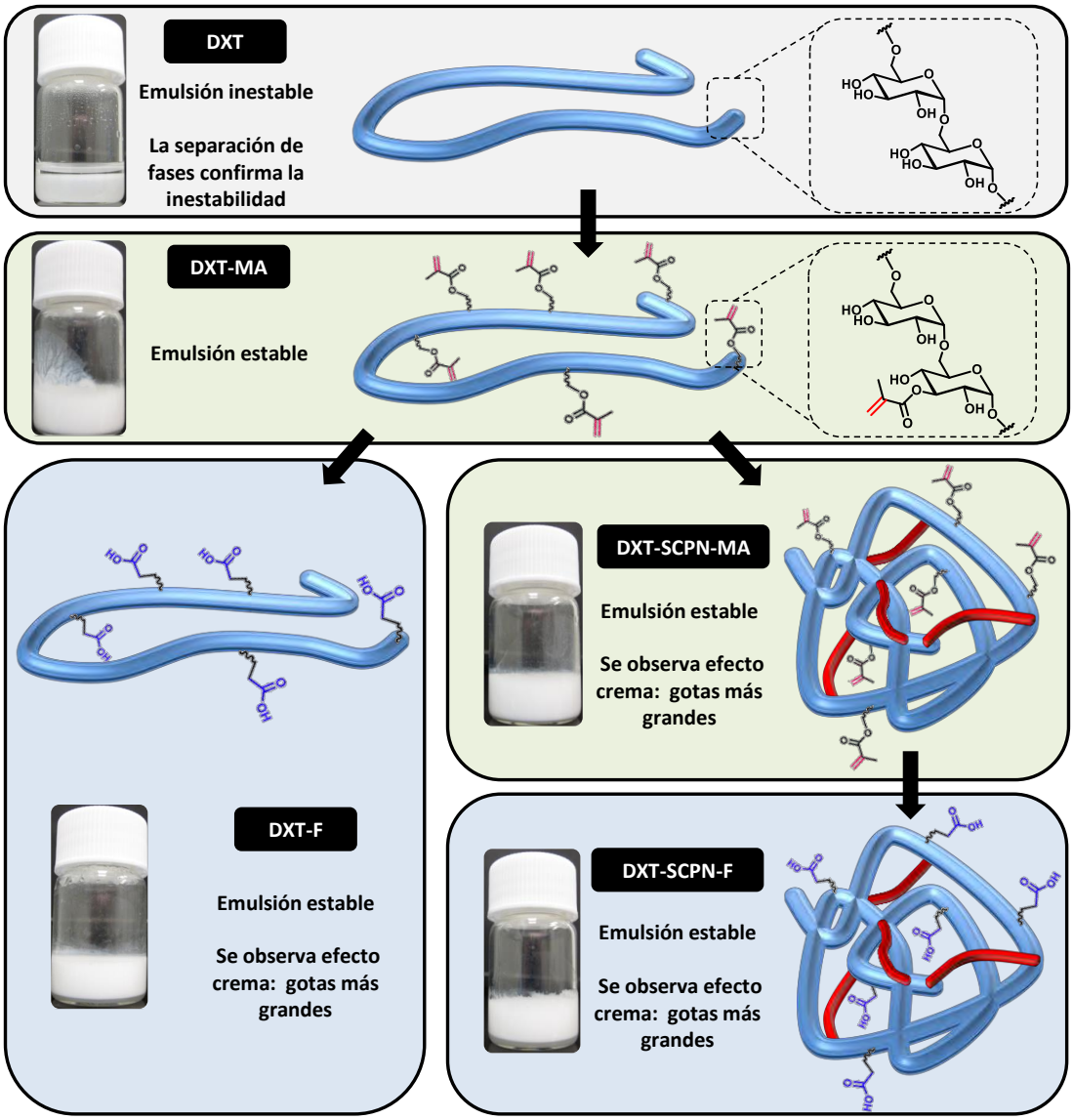

Figura 1. *Rutas sintéticas seguidas para la funcionalización del dextrano (DXT) y el uso de los diferentes derivados como estabilizadores de emulsiones de aceite en agua. Representación esquemática de la estructura fisicoquímica y los pasos sintéticos necesarios para obtener los diferentes derivados de dextrano (DXT, DXT-MA, DXT-F, DXT-SCPN-MA y DXT-SCPN-F) combinados con fotografías digitales de las emulsiones resultantes después de 24 horas en reposo. Las emulsiones se prepararon al 10% en peso de dodecano (fase aceite) y estabilizadas con 0,5% en peso de dextrano funcionalizado (emulsificante).*

Además, se han probado diferentes cantidades de estabilizante para encontrar el porcentaje en peso óptimo del mismo, que finalmente ha sido fijado en 0.5 wt. %. Por otro lado, el aceite de pescado (cuyo componente principal es el ácido docosahexenoico, DHA) dio como resultado las gotas más pequeñas y más estables con el porcentaje de fase oleosa del 10 wt. %, previamente seleccionado. Además, se

ha sintetizado DXT-MA con diferentes grados de sustitución (DS) para evaluar el efecto de los grupos MA en las propiedades de la emulsión. Los resultados sugieren que se necesita un DS mínimo para formar emulsiones estables. El DS mínimo se ha establecido como la sustitución mínima necesaria para obtener valores de tensión superficial (ST) inferiores a 60 mN/m a una concentración de 5 g/L. Nuestros resultados confirman que hay un número mínimo de grupos MA, en el rango de 10-15%, necesarios para producir emulsiones estables. Además, el diámetro de la gota aumenta al aumentar el DS lo que significa que existe un rango de sustitución óptimo (DS = 15-25%) que permite la producción de emulsiones estables, más pequeñas y menos polidispersas. Por último, se realizaron grandes esfuerzos para lograr emulsiones estables a largo plazo. Sin embargo, la estabilidad de la emulsión se vio comprometida en medios con elevada fuerza iónica, comprobando así que las nanoemulsiones se desestabilizaban rápidamente en condiciones fisiológicas.

Con el objetivo de mejorar la estabilidad en medios fisiológicos de las nanoemulsiones, en el capítulo 4 se exploraron dos estrategias diferentes para la reticulación (a través de la fase acuosa o la fase oleosa), procurando evitar la reticulación entre polímeros pertenecientes a distintas gotas. Más concretamente, dicha reticulación se llevó a cabo directamente sobre los polímeros adsorbidos en la interfase aceite/agua bajo condiciones suaves de reacción y utilizando el ditiol 2,2'-(etilendioxi)dietanetiol (DODT), con cierta actividad interfacial, como agente reticulante. Los resultados mostraron que se puede conseguir estabilizar la emulsión siguiendo la estrategia de adición del reticulante en la fase oleosa, permitiendo la reticulación polimérica intra-gota (**Figura 2**). Para demostrar la reticulación de las nanogotas se ha utilizado el método de DMSO/dioxano (70:30) que permite eliminar agua y aceite dejando aislado el polímero reticulado. Gracias a esto, se ha podido llevar a cabo la cuantificación por ^{1}H-RMN de la agente reticulador unido al polímero. Además, este método nos permitió visualizar la reticulación del material a través de las microgafías SEM del coloidosoma colapsado (**Figura 2c**). La estabilidad de las emulsiones reticuladas aumentó en medios de elevada fuerza iónica como en el tampón fosfato salino (PBS, 10 mM en fosfato), mientras que las emulsiones no reticuladas mostraron una rápida desestabilización

(efectos de coalescencia). Tal y como se planteó en las hipótesis de partida, las emulsiones reticuladas también demostraron ser estables en el tiempo al permanecer inalterado su tamaño durante meses (hasta 1 año) en cualquier medio fisiológicamente relevante (Figura 2).

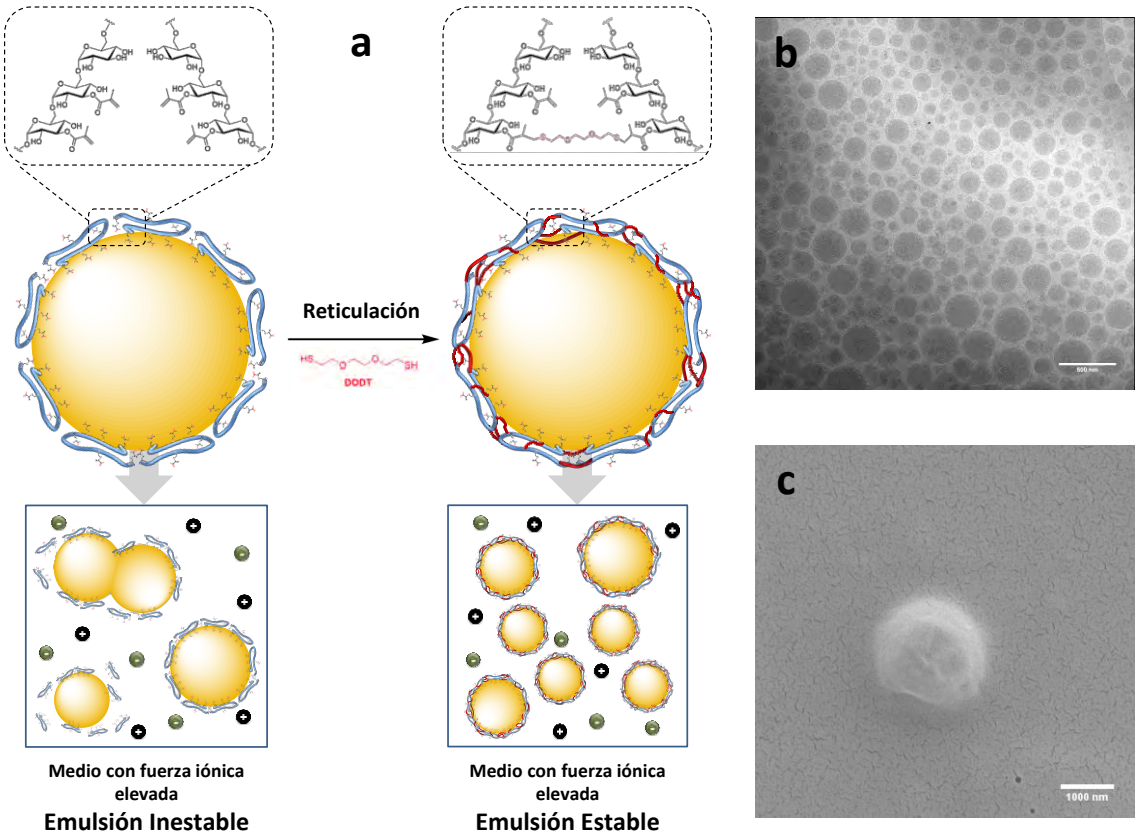

Figura 2. *a) Representación esquemática de la mejora de la estabilidad tras la reticulación en la interfase a través de la fase de oleosa. b) Micrografía Crio-TEM de una nanoemulsión reticulada. c) Imagen SEM del coloidosoma colapsado obtenido después de la extracción del aceite mediante el método del DMSO/dioxano.*

Además, este efecto estabilizador se evaluó *in vivo* utilizando tomografía por emisión de positrones (PET). El fluoroestradiol (FES) fue seleccionado como fármaco modelo debido a su hidrofobicidad (log Kow = 4.01) y a la facilidad para ser funcionalizado con el isótopo emisor de positrones ^{18}F (vida media de 109.8 minutos). La nanoemulsión prolongó 10 veces el tiempo de residencia del FES en los pulmones. Por otro lado, el cobre-64 que es un emisor de positrones con una vida media de 12.7 horas, se unió al tensioactivo polimérico mediante un agente quelante con el objetivo de investigar la biodistribución del *nanocarrier*. Para ello, se utilizó un derivado tiolado de DOTA

(DOTA-SH) que permitía por un lado la formación del complejo con el radiometal, y por otro su unión al polímero a través de los grupos metacrilato presentes en el DXT-MA. La biodistribución del DXT-MA confirmó que el estabilizador también es eliminado de los pulmones a una velocidad similar a la del FES encapsulado, lo que parece indicar que los componentes individuales de la emulsión permanecen juntos tras la administración *in vivo*.

Idealmente, los materiales utilizados para liberación controlada de fármacos deberían acumularse selectivamente en el órgano o tejido a tratar liberando su carga bajo estímulos concretos. La sobreexpresión de ciertas enzimas generalmente está relacionada con trastornos fisiológicos. Cuando dicha sobreexpresión se produce en el órgano diana, se puede utilizar como estímulo para iniciar la liberación del fármaco. Con esta idea, se utilizaron diferentes enzimas para evaluar si eran capaces de desestabilizar las nanoemulsiones. Debido a la presencia de enlaces éster generados durante la funcionalización del dextrano y los presentes en los triglicéridos de la fase oleosa, nuestras emulsiones podrían desestabilizarse en presencia de enzimas de tipo esterasa. Dentro de la familia de las esterasas se encuentran las de tipo lipasa, que son especialmente eficientes en la hidrólisis de enlaces éster procedentes de triglicéridos generando ácidos grasos y glicerol. En general, las lipasas necesitan ser activadas interfacialmente. Sin embargo, la presencia de nuestro tensoactivo basado en dextrano en la interfase nos llevó a estudiar el principal mecanismo de desestabilización enzimática (capítulo 5). Para ello, se evaluó la respuesta de los componentes individuales de la emulsión, aceite y surfactante, frente a la enzima *Candida Antártica Lipasa B (CALB)* y el efecto que ésta generaba en el tamaño de gota. La investigación del tamaño mediante difracción láser confirmó una disminución de la población principal con el tiempo, lo que sugiere que la estabilidad de la emulsión se ve comprometida como consecuencia de la actividad enzimática. Las principales diferencias en la velocidad de la demulsificación están relacionadas con las propiedades fisicoquímicas en la interfase, la naturaleza del enlace éster y el tamaño de gota inicial. El tamaño de la gota determina la superficie total disponible para el reconocimiento enzimático. En consecuencia, las gotas más pequeñas se degradan

más rápido debido al aumento del ratio superficie/volumen. El impedimento estérico del enlace éster presente en el emulsificante también juega un papel fundamental en la velocidad de degradación. Estos estudios se extendieron hacia el uso de una lipasa presente en humanos como es la lipasa pancreática y los resultados obtenidos demostraron que la velocidad de demulsificación puede ajustarse mediante un diseño apropiado de la nanoemulsión.

Por último y con el objetivo de explorar la utilización de compuestos anfifílicos poco convencionales, se evaluó la idoneidad del anión anfifílico conocido como COSAN, cobalto *bis*(dicarballuro), para la estabilización de nanoemulsiones (capítulo 6). La estabilidad de la nanoemulsión fue testeada frente a una amplia gama de estímulos: tiempo, medios fisiológicos relevantes, en presencia o ausencia de luz, a diferentes temperaturas y en presencia de lipasas. Además, se estudió la capacidad de las nanoemulsiones resultantes para modular la biodistribución de fármacos hidrófobos. Las técnicas de imagen nuclear sirvieron de nuevo para comprobar las diferencias obtenidas en las biodistribuciones del fármaco libre o encapsulado tras la administración pulmonar. Los resultados obtenidos anteriormente con FES, fármaco hidrofóbico modelo, nos animaron a repetir los estudios utilizando nanoemulsiones basadas en COSAN. Los estudios de imagen PET *in vivo* realizados con *[^{18}F]FES* y *NE-[^{18}F]FES* demostraron que las nanoemulsiones son capaces de prolongar el tiempo de residencia en los pulmones del FES después de la aerosolización intratraqueal (**Figura 3**). Para obtener más información sobre el *nanocarrier*, también se estudió la biodistribución del estabilizante, es decir, el COSAN. En un primer paso, el COSAN fue funcionalizado con yodo y posteriormente se realizó el marcaje radiactivo con el emisor de positrones ^{124}I (vida media de 4.2 días) mediante intercambio isotópico. Posteriormente se generó la nanoemulsión ([^{124}I]NE-FES). Los resultados de imagen demostraron que el emulsificante se elimina rápidamente de los pulmones después de la liberación del fármaco (**Figura 3c**). El conjunto de los resultados posiciona a las nanoemulsiones estabilizadas con COSAN como potenciales agentes de liberación controlada de fármacos poco solubles en agua cuando el pulmón es el órgano a tratar.

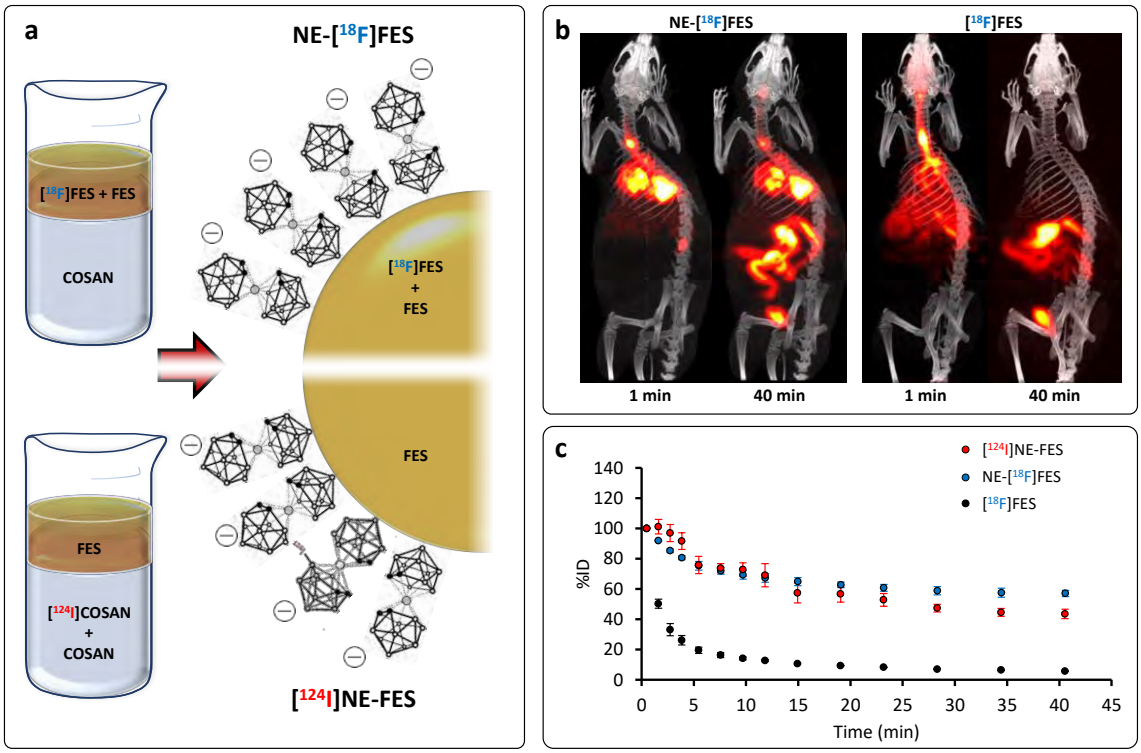

Figura 3. *a) Representación esquemática de la preparación de NE-[^{18}F]FES y [^{124}I]NE-FES; (b) imágenes de PET-CT representativas de la biodistribución de la radiactividad en diferentes puntos temporales tras la administración intratraqueal de NE-[^{18}F]FES (izquierda) y [^{18}F]FES (derecha). Las proyecciones de máxima intensidad de las imágenes PET se han corrregistrado con las imágenes CT; c) Curvas de la radioactividad en pulmón frente al tiempo después de la administración intratraqueal de [^{124}I]NE-FES, NE-[^{18}F]FES y [^{18}F]FES. Los resultados se expresan en porcentaje de la dosis inyectada (% DI). Los valores mostrados corresponden a la media ± desviación estándar, n = 2 por compuesto.*

Chapter 1. General introduction

1.1. Nanoparticles and nanomedicine

1.1.1. Nanoparticle: definition and applications

Nanoparticles (NPs) are generally defined as particles between 1 and 100 nanometres (nm) in size, in at least one dimension.[1] Due to their high surface-to-volume ratio, nanoparticles (NPs) have physico-chemical properties that differ from their respective bulk materials, turning them into very interesting materials in different market sectors such as energy, electronics, food, agriculture or health.[1,2] In addition, the properties of NPs can be tuned by functionalization of their surface, making them stable in different media and enabling the attachment of bioactive molecules which can develop a specific role for the final application. For these reasons, NPs have emerged as excellent candidates for their use in medicine.

1.1.2. Nanoparticles in medicine

The use of NPs for biomedical applications has been widely studied during the last decades. In medicine, NPs constitute a very promising research field from an academic point of view in areas such as the development of medical devices, molecular imaging or drug delivery, among others.[2] The unique properties of NPs, together with their size, turn NPs into genuine materials having a three-dimensional structure that confers certain advantages over small-molecule therapeutic or diagnostic agents.[3] These facts have resulted in the emergence of a new research field, nanomedicine, in which nanomaterials are designed to solve medical problems. Nanomedicine, as defined by the European Commission, includes different application areas: Drug delivery, drugs and therapies, *in vivo* imaging, *in vitro* diagnostics, biomaterials, and active implants.[4] The field has evolved creating nanomaterials to help medical doctors with early detection and prevention, improved diagnosis, personalized medicine and the follow-up of diseases.[5,6]

Nanomedicine research is not only focused on the academic area and has been also translated into industry. A recent study carried out by the European Commission

identified around 200 companies with nanomedicine activities, including 92 start-ups (44%), 67 small and medium enterprises (SMEs; 32%) and 41 large pharmaceutical or medical device companies (21%) (**Figure 1**). A detailed data analysis revealed that the relative proportion of corporations, SMEs and start-ups are similar in the US and the EU.[4] Drug delivery is the field of nanomedicine with higher development; 76% of the publications and 59% of the patents are related to drug development. In second position, and contributing only with 11% of the publications and 14% of the patents, the field of *in vitro* diagnosis has significantly lower economic impact than drug delivery.[4,7]

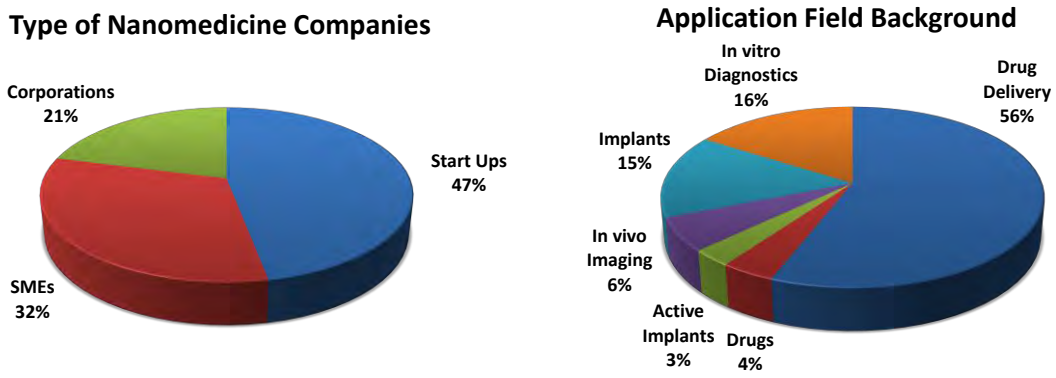

Figure 1. *Nanomedicine Sector: Types of companies and application field breakdown. Figure adapted from a European Commission report.*[4]

Advanced drug delivery systems can improve the pharmacological properties of conventional "free" drugs. This is because they are designed to modify the biodistribution and pharmacokinetics of their associated drugs. An ideal carrier should increase the bioavailability of the drug in the target organ while decreasing toxic and undesired side effects in the rest of the organs. Proper size, shape and surface functionality of the carrier contribute to prolong the biological half-live of the drug and may help in achieving the optimal dose in the targeted diseased tissue while minimizing off-target side effects.[8]

A wide variety of drug delivery systems with sizes below 1 micrometer have been reported as nanocarriers.[9–11] These systems can be classified depending on the final application, type of material or the type of drug that they carry. The active ingredients

can be either attached or adsorbed onto inorganic particle surfaces or dissolved, encapsulated and/or entrapped inside soft matter systems.[12] Drug-encapsulated liposomes and polymer–drug conjugates such as polyethyleneglycol-functionalized (PEGylated) drugs are predominant in clinical trials. Besides liposomes and polymeric conjugates, other nanocarriers such as polymeric nanoparticles, micelles, nanoemulsions, nanoshells, dendrimers, engineered viral nanoparticles, albumin-based nanoparticles, polysaccharide-based nanoparticles, metallic nanoparticles, and ceramic nanoparticles have been investigated.[13–15] A few examples of these drug delivery systems are represented in **Figure 2**.

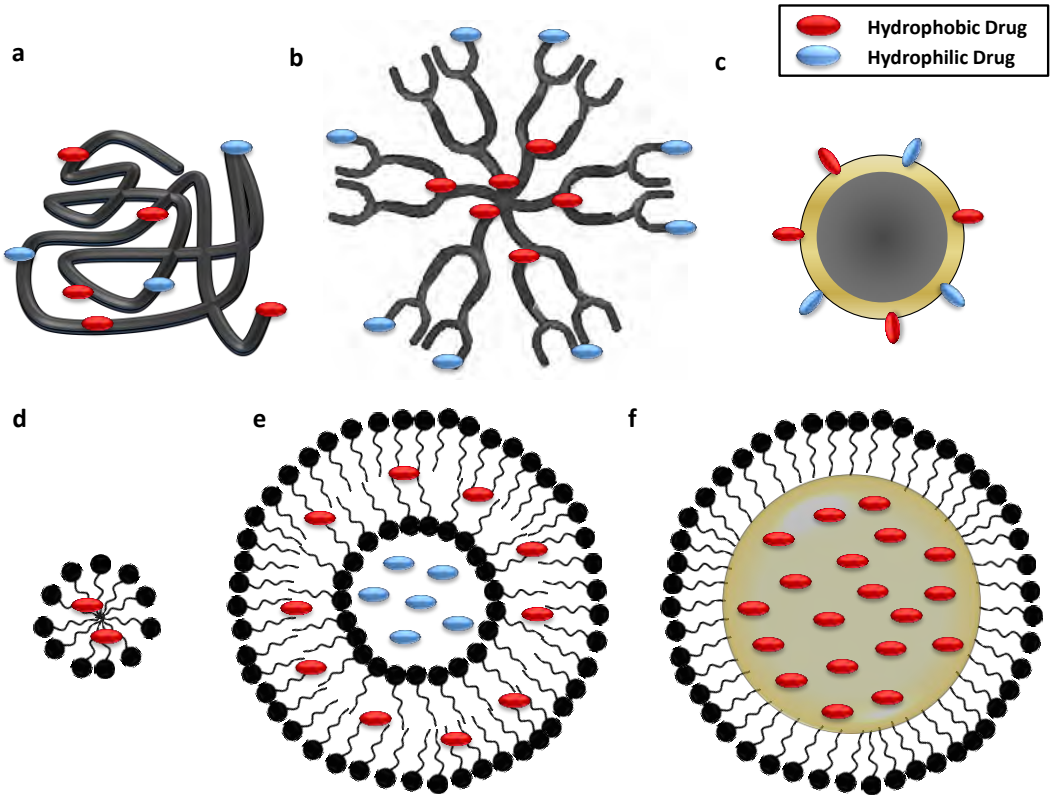

Figure 2. *Schematic illustration of therapeutic nanoparticle platforms in preclinical development: (a) polymer-drug conjugate, (b) dendrimer, (c) inorganic nanoparticles, (d) Micelle, (e) liposome and (f) nanoemulsion. Red dots represent hydrophobic drugs and blue dots represent hydrophoilic drugs.*

1.1.3. Nanocarriers for poorly water-soluble drugs

As mentioned above, NP formulations are being deeply investigated as drug delivery systems. This is especially relevant for poorly water-soluble drugs, for which direct administration has difficulties. The use of nanoformulations is advantageous due to three main reasons: (1) their size, which facilitates the accumulation in the target organ or tissue, e.g. preferential accumulation in the tumor tissue due to the well-known enhanced permeability and retention (EPR) effect;[16] (2) their high surface-to-volume ratio, which can confer genuine physical properties and enables multi-functionalization;[3] and (3) the possibility of loading a high amount of cargo while increasing its bioavailability, which turns NPs into ideal carriers for hydrophobic drugs.[17] Indeed, the presence of poorly water-soluble drugs has increased the pipeline of the drug discovery process.[18] According to US pharmacopeia, more than 40% of the drugs in the market are poorly water-soluble, and it is estimated that 60% of the drugs currently under development in pharmaceutical chemical laboratories are insoluble or poorly soluble in water.[18–20] Many of these, classified by the Biopharmaceutical Classification System (BCS) as BCS Class II-IV drugs (**Figure 3** [21]) have been successfully tested *in vitro*; however, they finally fail *in vivo* due to their poor solubility in blood (92% wt. content of water). To overcome this problem, different solubilization strategies have been used in pharmaceutical industry including prodrug formation, complexation and use of co-solvents and/or surfactants which usually generate undesirable side effects. For this reason, the use of nanodelivery systems (nanocarriers) is currently drawing attention.

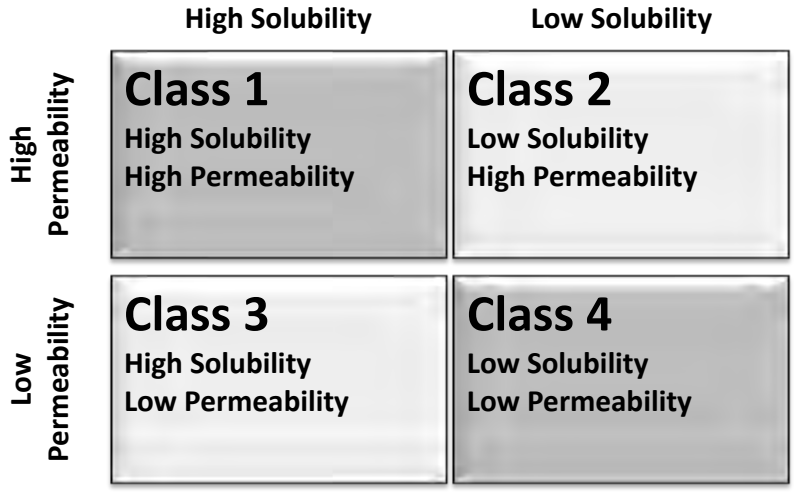

Figure 3. *Biopharmaceutics classification system of drugs.*[21]

In this PhD thesis, we have focused in the use of nanocarriers to improve the bioavailability of drugs classified as BCS Class II, which are highly permeable, and hence its bioavailability can be significantly enhanced by optimizing the formulation design to mitigate low water solubility. It is important to mention that BCS classification is mainly related to orally administered drugs but, in the absence of alternatives, it would be a good approach for inhalation. One strategy to achieve this is by using NPs. Historically; lipid-based nanocarriers have been mostly used for this purpose. Most commonly used lipid components are phospholipids, cholesterol and triglycerides.[22] These materials often derive from natural sources and hence are biodegradable and biocompatible *in vivo*. Thus, the use of physiological lipids as part of the nanocarriers prevents certain negative side effects. Lipid-based delivery systems include liposomes, micelles, solid lipid nanoparticles, nanosuspensions and nanoemulsions.[23,24]

Liposomes are vesicles that contain an aqueous core surrounded by phospholipid bilayers.[23] Vesicles can be mono- or multi-lamellar in a range of sizes between 50–2000 nm. Lipid and phospholipid micelles are nanomaterials (5–50 nm) generally composed by single units containing hydrophobic and hydrophilic regions that self-assemble spontaneously in aqueous media above their critical micelle concentrations (CMCs). In this case lipid monomers are able to form the micelle core while polar groups face outwards to the aqueous media constituting the outer layer of the particle (micelle).

On the other hand, when polar groups are self-oriented inside and outside of the lipidic membrane the final structure relies in the formation of a liposome.[25,26] Solid lipid nanoparticles are colloids that consist of a matrix based on lipids at solid state (50–1000 nm) dispersed in aqueous media. Some of these complexes demand the use of emulsifiers for increasing physical stability of the system.[23] Lipid-based nanosuspensions are submicron colloids (100–500 nm) of hydrophobic drug particles coated by lipid-derived surfactants which prevent self-aggregation.[25] Finally, a nanoemulsion consists in 2 immiscible liquids (typically oil and water) where the lipidic phase is dispersed in the aqueous phase (in the case of oil-in water nanoemulsion) in the form of nanosized droplets around 100-500 nm. Surfactants and/or co-surfactants are adsorbed at the oil/water interface in order to stabilize the system. Nanoemulsions are thermodynamically unstable but kinetically stable, and hence these nanosystems are suitable for drug delivery purposes.[25] This PhD thesis is based on the use of nanoemulsions as nanocarriers for poorly-water soluble drugs.

1.1.4. Nanoemulsions in nanomedicine

As mentioned above, lipid-based formulations have been widely used to improve the bioavailability of poorly water-soluble drugs,[24] and a wide range of lipid-based materials to generate such lipid-based formulations have been developed. Also, one other nanosystem widely investigated is emulsion based, which according to the IUPAC, are ***"fluid systems in which liquid droplets are dispersed in a liquid"***.[27] Liquids tend to minimize their surface area generating the geometrical form with the smallest surface/volume ratio. Therefore, a typical emulsion consists in two immiscible liquids (usually oil and water) where one phase is dispersed as small spherical droplets within the other.[12,24,28–30] In addition to the oil and water phases, stabilizers are needed in order to maintain the properties of the emulsion. Most common stabilizers are surfactants, which are surface-active substances that reduce the interfacial tension between the two immiscible liquids. Other stabilizers alter the properties of the continuous phase thus retarding emulsion breakdown processes. One example is emulsifiers, which are absorbed at the interface of the emulsion droplet forming a protective coating that prevents droplet aggregation and facilitates the disruption of

the initial emulsion droplets during homogenization, generating smaller droplets.[29] However, an energy input is required for the adsorption of the emulsifier at the oil-water interface. This is because the interfacial area between the two phases is enlarged during the homogenization of the bulk materials, resulting in an increment of the interfacial free energy of the system.[31]

Generally speaking, **surfactants comprise the simultaneous presence of hydrophilic and hydrophobic** parts in the same molecule. These molecules are defined as amphiphiles but these characteristics are not the only requirement to be surface active. Surfactants also need an adequate three-dimensional structure. In aqueous phase, surfactants tend to self-assembly as micelles, after overtaking the critical micelle concentration (CMC), where the hydrophobic parts form the core of the aggregate and the hydrophilic regions are in contact with the surrounding liquid. Other types of aggregates can also be formed, such as spherical or cylindrical micelles or lipid bilayers.[32] Thus, the final shape of the self-assembled structure also depends on the physicochemical properties of the surfactants. In droplet generation, the formation of spheres is resisted by the interfacial tension as determined by the Young-Laplace[33] equation:

Equation 1

$$p_\alpha - p_\beta = \frac{2\gamma}{r}$$

where γ is the surface (air-liquid) or interfacial (liquid-liquid) tension, p_α and p_β are the internal and external pressures of the spherical surface and r is its radius. This equation describes the pressure difference sustained across the interface between two static fluids. The surface tension acts to reduce the surface area and hence the volume of the drop, while the pressure difference (p_α-p_β) acts to increase the volume of the drop. The equilibrium condition is achieved when these two tendencies counterbalance each other. The Young–Laplace equation shows that the pressure difference increases if the radius becomes smaller and tends to infinity when r tends to zero. Following this, an extra energy is required to form smaller (highly curved) droplets for overtaking the large pressure that results from their small radius. For this reason, droplet formation is highly affected by the presence of surfactants because they lower the interfacial

tension and therefore the internal pressure of the droplets. Thus, surfactants act diminishing the stress required to break up a droplet and preventing new droplets from coalescing.[33,34]

Macromolecules containing both hydrophilic and hydrophobic parts are generally referred as polymeric surfactants. Compared to their low-molecular weight analogous, polymeric surfactants are structurally more complex (e.g. number and distribution of hydrophilic and hydrophobic moieties along the chain), which can result in different properties.[5] Usually, homopolymers, either hydrophilic or hydrophobic, have not enough interfacial activity to be adsorbed at the oil/water (o/w)-interface. However, copolymers or grafted polymers which contain both hydrophilic and hydrophobic segments are usually more surface active molecules. The adsorption of the polymer at the air-liquid or liquid-liquid interfaces strongly depends on the chemical segments but also on the structural conformation in the liquid media (see **Figure 4**).[5,31]

Other molecules or even particles without the abovementioned amphiphilic character have enough interfacial activity to stabilize emulsions. Particle stabilized emulsions, also known as Pickering emulsions, have been described for more than a century.[35,36] These solid particles tend to self-assembly at the oil/water interface depending on their wettability, contact angle and the total energy delivered to the system.[37–39] In this work we have tested polymers, polymeric particles and organometallic clusters as emulsion stabilizers for drug delivery purposes.

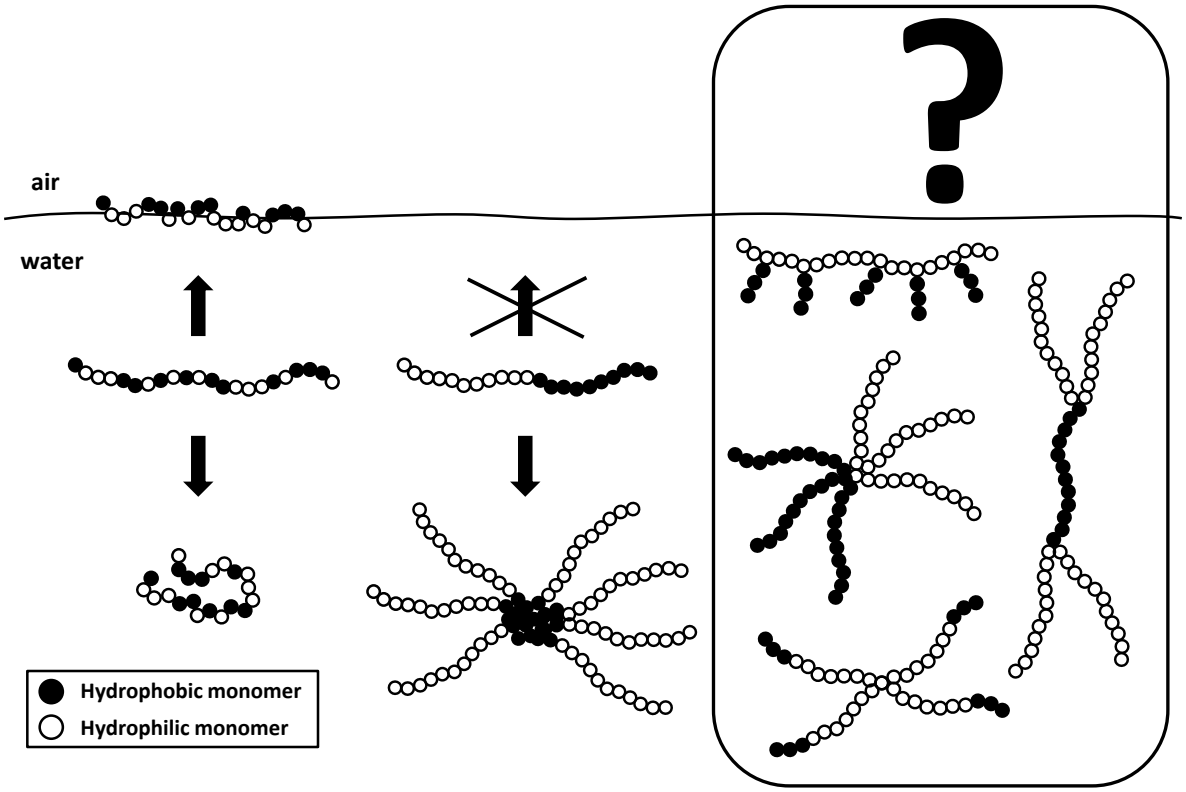

Figure 4. *Schematic representation of the different behavior displayed in solution and at the air/water interface by randomly amphiphilic polymers (left) and macrosurfactants (center). Very few data about the behavior of complex architectures is available (right). Figure adapted from Raffa et al.* [5]

Emulsions are mainly categorized depending on the characteristics of the dispersed phase or their droplet size. Regarding the dispersed phase, there are two principal emulsion types; oil-in-water (O/W) emulsions, where oil droplets are dispersed in an aqueous phase, and water-in-oil (W/O) emulsions if the water droplets are dispersed in an oil phase. On the other hand, emulsions can be classified by their hydrodynamic diameter as macro-emulsions (1-100 µm), mini-emulsions (50-1000 nm) and/or micro-emulsions (1-100 nm). In addition, the term nano-emulsions has been used for emulsions in the range of 100-500 nm despite of its discrepancy with recent definitions of a nanomaterial (one dimension below 100 nm). This terminology has been accepted in literature because previous categorization for micro-emulsions (1-100 nm) was appointed before scientists discover their nanoscale size.[30–32] Macroemulsions are integrated by large droplets and thus they are “unstable”; as a consequence, the dispersed and continuous phases tend to coalescence within time periods from a few

seconds to a few hours leading finally in phase separation. Miniemulsions are meta-stable systems which are thermodynamically unstable but kinetically dependent (stabilized against diffusion degradation) and they are usually stable for at least several days. Microemulsions are isotropic and thermodynamically stable systems where the domains of the dispersed phase are either globular or interconnected.[27] Recent trends suggest that NEs in the range 100-500 nm should be described as miniemulsions.[25,32,40,41]

The term "emulsion stability" is usually referred to the capability of an emulsion to resist changes in its physicochemical properties over time.[31] For this reason, a complete emulsion characterization requires the investigation of its long-term stability under storage conditions. Emulsions for drug delivery use to be thermodynamically unstable but kinetically stable systems and size is the parameter that mainly drives emulsion breakdown processes. Other parameters also related with destabilization are the volume concentration of the dispersed phase, properties and composition of both phases, and interactions among dispersed phase particles or between particles and continuous phase constituents.[29,42] As dispersion quality criteria, the state and properties of the dispersion must be the same throughout the whole material.[42]

Knowledge about the destabilization mechanisms is paramount to achieve a proper characterization of the emulsion and to improve such stability. By identifying the dominant physical and/or chemical destabilization mechanism, effective strategies to improve stability can be implemented. Most typical mechanisms involved are flocculation, coalescence, partial coalescence, gravitational separation (creaming or sedimentation), phase inversion and Ostwald ripening [29] which have been summarized in **Figure 5**.

Flocculation is the process whereby two or more droplets come closer to each other because of attractive interactions and finally form an aggregate, in which the integrity of the individuals is maintained but they move as single entity. In contrast, during coalescence two or more droplets merge to form a single larger droplet. Partial coalescence is usually produced by partly crystalline droplets which form a single

irregularly shaped aggregate due to the penetration of solid crystals from one droplet into a fluid region of another.

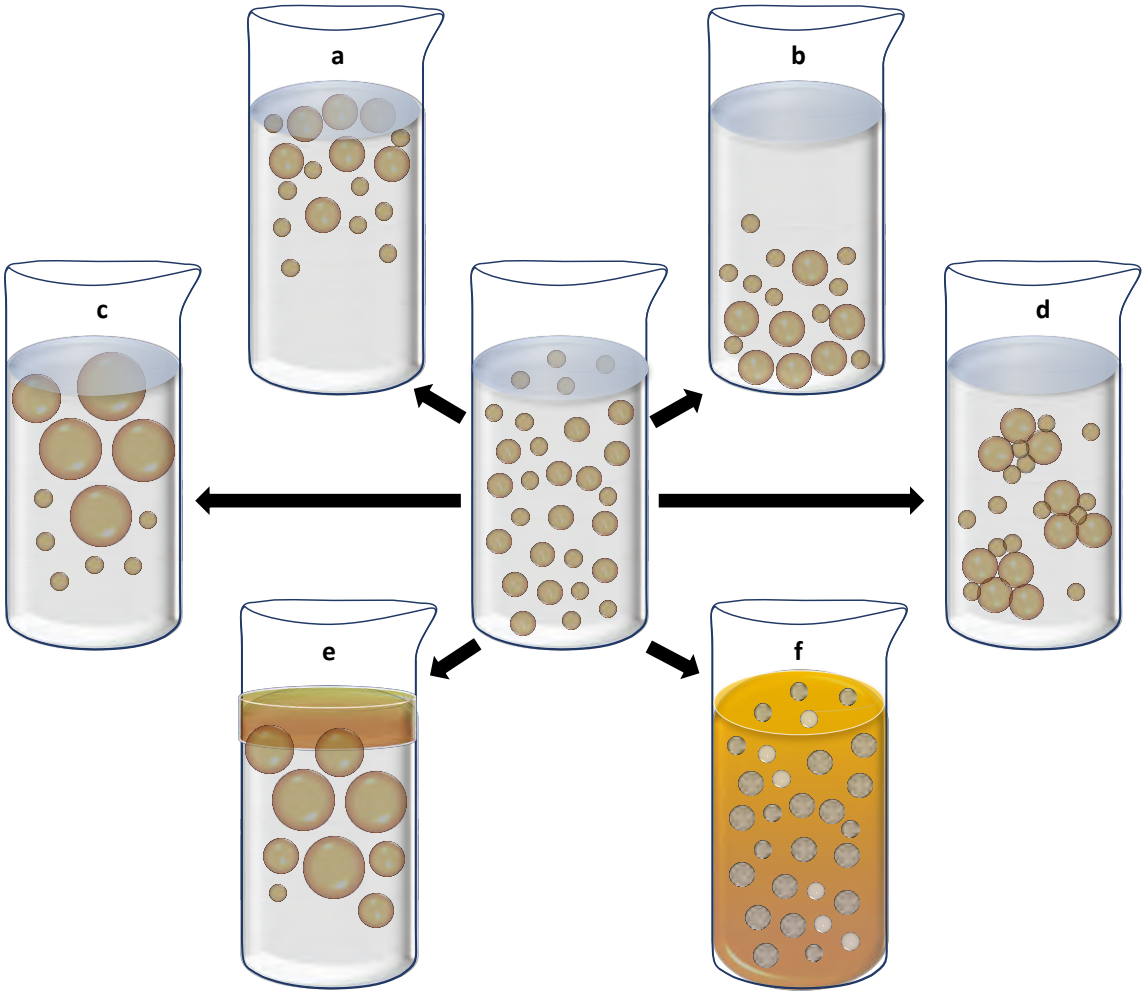

Figure 5. *Different unstabilization pathways due to physical and/or physicochemical phenomena: (a) Creaming, (b) Sedimentation, (c) Ostwald ripening, (d) Flocculation/agglomeration, (e) Coalescence + phase separation and (f) phase inversion.*

Often, the presence of an emulsifier layer at the interface induces repulsive forces due to steric interactions between the droplets which prevent flocculation and coalescence. This phenomenon is stronger in (nano/micro)-emulsions as the thickness of the emulsifier layer (≈ 10 nm) is similar to droplet size.[29,32] Gravitational separation processes in dispersions mainly depend on density differences between dispersed and dispersant phases. If droplets have lower density than the dispersant phase, they move upwards by buoyancy and the process is called “creaming”. On the contrary, if droplets

have higher density than the dispersant phase, they move downwards and the process is called “sedimentation”. Creaming predominates when buoyant force dominates over the Brownian motion, and it is insignificant in miniemulsions with droplet size below a few microns.[32] Phase inversion is produced when an oil-in-water emulsion changes to a water-in-oil emulsion, or vice versa. Ostwald ripening is the process whereby larger droplets grow at the expense of smaller droplets due to mass transfer of dispersed phase material through the continuous phase. There are many factors which can contribute to Ostwald ripening as for example: dispersed phase solubility, polydispersity and ionic strength. Solubility of the dispersed phase in the continuous phase is critical for Ostwald ripening rate, because dispersed phase molecules with high solubility in the continuous phase will lead to faster destabilization. Ostwald ripening is also faster at higher temperatures because both solubility and diffusivity are temperature dependent. Polydispersity affects the Ostwald ripening rate significantly because higher polydispersity represents higher chemical potential differences between droplets. Finally, ionic strength of the continuous phase also promotes Ostwald ripening by reducing the repulsive barrier between droplets. It is important to mention that these instability mechanisms are often interrelated. For example, an increment of the main droplet population size due to flocculation, coalescence or Ostwald ripening usually leads to an increment of the instability of the droplets by gravitational separation. However, if droplets due to gravitational separation or flocculation come closer and stick together for long enough, they become more susceptible to coalescence. Consequently, the instability mechanism responsible for the visible manifestation of emulsion breakdown is not unique and depends of each system.[29,32,42]

At the industrial level, the traditional method employed for emulsion production consists of the homogenization of the bulk materials (oil and water) by applying energy to the system. Usually, this energy is implemented by mechanical agitation or ultrasonication of the liquid mixture.[29,40] Food, pharmaceutical and cosmetic industries have been developing and using emulsions for drug delivery since the last century. This is because the production is simple and robust; furthermore, emulsions have higher

loading capacity than other drug delivery systems such as liposomes and vesicles (only surfactant shell conforms the hydrophobic domain while the inner core is hydrophilic) or micelles (small volume of the hydrophobic inner core).[32,40] Regarding to this, *Rosenblatt et al.* described that the concentration of encapsulated ibuprofen was almost double for emulsions (14 mg/mL) than for other colloidal suspensions (2-8 mg/mL).[43] Generally, mini-emulsions (50-1000 nm) are extensively used because their size makes them kinetically stable over a time period (e.g., a few days, weeks, months or years) so they can suit the shelf-life requirements for pharma industry. Specifically, (o/w)-miniemulsions, which can carry poorly water-soluble drugs, have been employed to increase solubility and bioavailability.[25,32] Furthermore, emulsions are highly tunable systems, and their charge and rheology can be adapted to the requirements dictated by their final application. For medical purposes, (o/w)-emulsions below 1 µm are the most suitable drug delivery systems due to their long-term stability and adequate size. Nanoemulsions have been tested in a wide number of drug delivery applications using different administration routes including topical, dermal, intravenous, intranasal and oral.[44,45] In this work, we describe the use of (o/w)-nanoemulsions (150-400 nm) as hydrophobic drug carriers for *in vivo* applications.

1.1.5. Polysaccharides

Polysaccharides are the most abundant biomacromolecules on the planet.[46,47] They are **biopolymers made of monosaccharides (sugars)** linked together through glycosidic bonds. Polysaccharides have a general formula of $C_x(H_2O)_y$ where x is usually a large number between 200 and 2.500. Considering that the monomer units in the polymer backbone are often six-carbon monosaccharides, the general formula commonly used to represent polysaccharides is $(C_6H_{10}O_5)_n$ where $40 \leq n \leq 3.000$ [48]. Depending on the bond type between sugar monomers, the polymeric structure can give random coil shapes (e.g. dextran), semiflexible chains (e.g. cellulose derivatives), or interrupted helical structures (e.g. amylose) (

Figure 6).[47,49] Polysaccharides usually have a large number of reactive groups per molecule and they can cover a wide range of molecular weights. Both conditions determine their physicochemical structure and properties making them highly versatile

materials.[50] Due to this diversity, polysaccharides play diverse and important roles in a huge number of biological processes. Most common functions are storing energy (e.g. starch and glycogen) or their use as structural components (e.g. cellulose in plants and chitin in arthropods). However, they are also involved in signal recognition, communication between cells and different functionalities related with the immune system. As they come from biological sources they are highly biocompatible systems. Biocompatibility, together with availability and tuneability turn them into interesting materials for different *in vivo* applications.[46] Polysaccharides can also generate polymeric networks for improving drug bioavailability and targeting, stimuli-responsiveness, enhanced permeability and modulated drug release, among others.[51] Chemical or biochemical modifications have been widely studied in order to produce highly stable, safe, non-toxic, amphiphilic, ionic or non-ionic molecules and also to transform these polymers into more complex structures (e.g. hydrogels). This tuneability has to be aligned with their inherent material properties, biodegradability and/or bioactivity, especially for their use in drug delivery.[46,48,50]

Proteins and polysaccharides are usually applied as emulsifiers/stabilizers in food and pharmaceutical industries. Many proteins can act as emulsifiers as far as they have amphiphilic properties that allow their adsorbance at the (o/w)-interface. However, polysaccharides act as stabilizers by increasing the emulsion viscosity and forming an extended network in the continuous phase, and not acting as surfactants.[52] Pioneering work of Landoll demonstrates that cellulose can also act as surfactant by the appropriate functionalization with alkyl chains.[53] Since this pioneering work, different studies have confirmed that hydrophobic modification of polysaccharides contributes not only to reduce surface and interfacial tension, but also to (o/w)-emulsion stabilization by thickening aqueous phase.

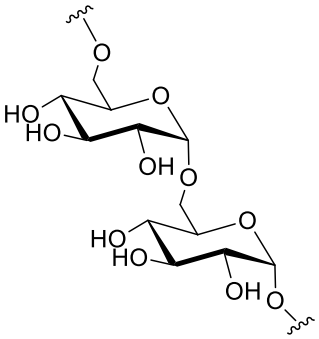

Dextran

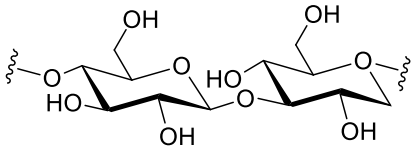

Amylopectin

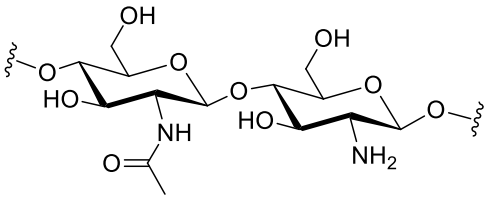

Chitin / Chitosan

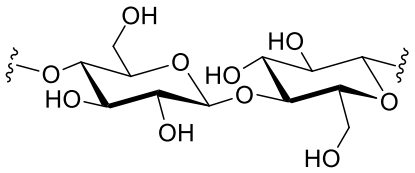

Cellulose

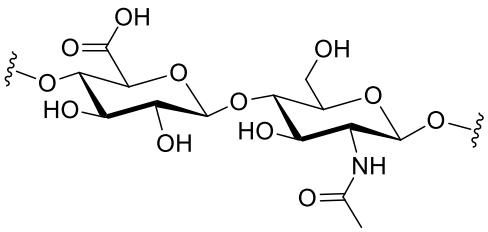

Hyaluronic acid

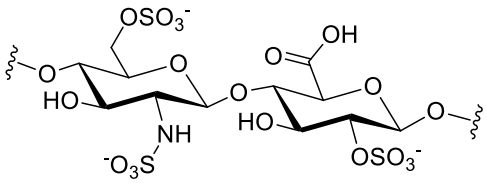

Heparin

Figure 6. *Structures of polysaccharides used in the development of drug-delivery systems and the possible modified site.*

Recently, the **hydrophobic modification of polysaccharides** has gained increasing attention because functionalized polysaccharides show amphiphilic behavior, and hence can be applied as rheology modifiers, emulsion stabilizers, surface modifiers for liposomes and self-assembling units.[31] Intrinsic self-assembly at the aqueous phase (micelle formation) or adsorption at the interface of (o/w)-emulsions induces the

generation of hydrophobic cores surrounded by hydrophilic outer shells. Both conformations allow the incorporation of hydrophobic drugs in the inner core, because of the hydrophobic interactions between both, making them suitable for drug delivery. In this work, we have functionalized polysaccharides, especially dextran, generating sufficient interfacial activity for their adsorption at the oil/water interface stabilizing (o/w)-emulsions and preventing their coalescence.

Dextran (DEX) is a natural polysaccharide formed by the condensation of glucose monomers in a complex branched structure of varying lengths (from 3 to 2.000 kDa). According to the IUPAC dextran is defined as "Branched poly-α-D-glucosides of microbial origin having glycosidic bonds predominantly (1→6)".[54] This composition makes dextran hydrophilic and electrically neutral. These properties, together with its biodegradability and the possibility of functionalization promote its uses in drug delivery. Hydrophobically modified dextran has been previously used in the synthesis of hydrogels or as polymeric surfactant.[55,56] Dextran grafting with phenoxy groups,[57] n-butyl cyanoacrylate,[58] polylactic acid[59,60] and alkyl, dialkyl or bile acids[61] have generated amphiphilic derivatives with adequate properties to stabilize (o/w)-emulsions. For the use of modified dextran as a surfactant, the degree of functionalization, the hydrophobic character of the molecule attached and the chain length affect both, size and polidispersity of (o/w)-emulsions. Generally, long hydrophobic chains and high grafting grades result in more stable and less polydisperse. In this context, few authors have demonstrated that polylactide(PLA)-grafted dextran can stabilize (o/w)-nanoemulsions even with short-length PLA chains[59,60] while Rouzes and coworkers have proved the efficiency of low substituted phenoxy-grafted dextran to stabilize emulsions.[57,62] In our approach, a facile modification of natural dextran with relatively short hydrophobic but reactive functional groups (methacrylate moieties, MA) appeared sufficient to confer interfacial activity to the biocompatible polymer producing stable methacrylate-functionalized dextran (DXT-MA) stabilized emulsions.

1.1.6. Enzyme-responsive materials to trigger drug release

Stimuli-responsive or smart materials are versatile systems with dynamic properties which can be switched on or off depending on the external signals.[63] Main strategies to achieve smart materials are the combination of different material properties as forming composites or generating chemical modifications that change the physico-chemical properties of the original material. Nowadays, they have gained attention in different research areas being their use as drug delivery systems one of the most interested fields of application. This is because drug delivery systems are expected to selectively accumulate in the target organ or tissue and release their cargo in a controlled manner. To that aim, drug delivery systems have been developed to change its properties as response to their local environment (pH, temperature, shear forces, enzymes …) or remotely applied stimuli (magnetic or electric fields, light …).[63–65] Most common stimuli-responsive materials used in drug delivery are based on biodegradable polymers as i.e. polysaccharides. As described above, polysaccharides are natural polymers which have been extensively used in medicine for their biocompatibility and biodegradability. This is because, in most of the cases, natural origin confers a specific biodegradation route which can be used as stimulus to selectively trigger drug release.[66–68] Following this, enzymes have emerged as potential stimulus to trigger drug release. **Enzymes** are biological catalyzers which have been evolved for years to fulfil the selectivity and specificity requirements of living organisms. Thus, enzymes are highly specialized in biochemical reactions performed under mild conditions and in aqueous media.[69] Furthermore, enzymes can be classified depending on their specific substrate (e.g. lipase hydrolyzes lipids generating fatty acids and glycerol) or englobing a family of reactions (e.g. esterases hydrolyze ester bonds).[70] Overexpression of certain enzymes is generally related to physiological disorders.[71] When such overexpression occurs in the target organ, this stimulus can be used to trigger drug release by using enzyme-responsive materials. In this process, the interaction between the enzyme and the substrate often results in degradation of the carrier (triggering drug release), and this interaction can be some extent controlled by the modification of either involved in the catalytic cycle.

Lipases are carboxyl-esterases naturally designed for lipid digestion. Generally speaking, lipid digestion consists in the cleavage of long-chain acylglycerides (mono-, di-, and triglycerides) into polar lipids (fatty acids). Triglycerides can be cleaved at all three ester bonds or specifically at only one or two positions. Moreover, lipases show very different specificities depending on the lengths of the fatty acids. Opposite polarity between the enzyme (hydrophilic) and substrates (hydrophobic) demands reaction occurs at the oil-water interface.[72–75] Lipases, on the contrary to other esterases which primarily hydrolyze water-soluble esters, demand the presence of (o/w)-emulsions to be activated in a phenomenon called "interfacial activation". A close contact between the enzyme and the hydrophobic interface lead in the movement of the lid domain that is covering the active site. This enzymatic recognition is paramount to leave the active site available for substrate binding and processing.[74] In the first step the water-soluble enzyme is adsorbed at the interface leading to a more favorable state of energy (E*) (**Figure 7**). Secondly, active site of the adsorbed enzyme binds the substrate molecule (S) achieving the complex enzyme-substrate (E*S).

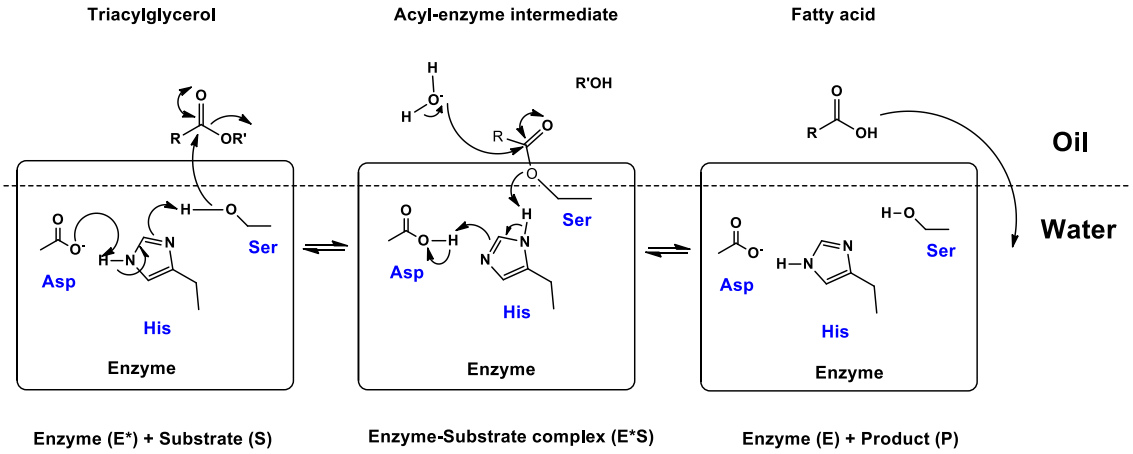

Figure 7. *Mechanism of lipase catalysis adapted from De Simone.[76] The active site of lipase is formed by catalytic triad of aspartic acid, histidine and serine. First, His deprotonates the OH group of Ser. Then, Ser attacks the carboxyl group of the triacylglycerol and an acyl-enzyme intermediate is formed (center). Diacylglycerol (R'OH) is released during this step. Subsequently, a deprotonated water molecule acts as nucleophile, adding to the acyl group. Finally, a free fatty is released and the catalytic residues are regenerated.*

Then, lipase catalytic triad (composed of serine, histidine and aspartate or glutamate) facilitates ester hydrolysis following the mechanism described in **Figure 7**. Finally, ester hydrolysis generates the product (P*) that is solubilized and released into the aqueous phase (P).[76]

In this PhD thesis two different lipases have been employed, Candida Antarctica Lipase B (CALB) and Pancreatic Lipase (PL), as both enabled ester hydrolysis of (o/w)-emulsions. Thus, a brief description of the characteristics of each lipase is included below. **Candida Antarctica Lipase B** is a monomeric protein composed by 317 amino acids with a molecular weight of 33 kDa. CALB structure appears to be in an "open" conformation with a rather restricted entrance to the active site. This is because, unlike most lipases, CALB has no lid to cover the entrance to the active site and thus do not show interfacial activation. The relatively low activity of the enzyme on large triglyceride substrates together with the absence of lid suggests that CALB may be an intermediate between an esterase and a true, interfacially activated lipase.[77,78] **Pancreatic Lipase** is a single-chain glycoprotein composed by 449 amino acids with a molecular weight of 51 kDa. As most of lipases, PL has the hydrolytic site covered by a lid which loop (opening/closing motion) in water is closed being inaccessible to the solvent. This loop is opened upon interfacial adsorption leading in enzyme activation. Furthermore, this enzyme is located in the duodenum of mammals where various amphiphiles (bile salts, soaps, phospholipids, etc.) are hindering interfacial activation and thus demanding the use of cofactors (colipases) to promote *in vivo* digestion.[75,79,80]

1.1.7. Nanoparticles in pulmonary delivery

Pulmonary delivery is an attractive administration route for either local or systemic therapies.[81,82] Lung administration for systemic delivery has many advantages in comparison with other noninvasive routes as oral. The low thickness of the epithelium (0.1–0.5 µm in alveolar region) and its huge surface area (75–150 m^2) lead to a faster onset of therapeutic action while avoiding the first-pass metabolic barriers.[82,83] Furthermore, **pulmonary delivery is the main administration route when the lung is**

the target organ, as local administration of therapeutics reduce the overall dose and negative side effects by decreasing systemic drug exposure.[84]

After direct administration, lung clearance can take place following different mechanisms such as mucociliar clearance, phagocytosis by macrophages, intracellular catabolism or permeation through the alveolar epithelium, among others.[82] One of the main challenges of topic treatments in lungs by inhalation is to avoid or reduce the extremely fast clearance in the alveoli region. In this context, NPs have emerged as attractive tools because they can be retained within the lungs, thus prolonging the residence time of the therapeutic agent and providing controlled drug release. In parallel, they can aid in administering poorly water-soluble drugs. Thus, there are many studies involving NPs and focused on pulmonary delivery for the treatment of respiratory diseases such as asthma, interstitial lung diseases (e.g. cystic fibrosis), acute lung injury (ALI), acute respiratory distress syndrome (ARDS) or chronic obstructive pulmonary disease (COPD).[83–85] Therefore, the nebulization of submicron (o/w)-emulsions is becoming an upcoming research area. However, successful formulations of inhalable NEs have to be studied deeply in order to understand how particles are deposit along the respiratory tract and overcoming possible adverse effects of surfactants and oils on lung alveoli function (adverse interactions with lung surfactant).[83,84,86,87]

1.2. Tracing NPs *in vivo*: Nuclear Imaging Techniques

1.2.1. Why we need to track NPs?

Nanoformulations for *in vivo* applications have to fulfill strict requirements to reach the market, as any other drug. NPs for drug delivery need to be biocompatible and accumulate a sufficient amount of drug in the target organ or tissue while minimizing accumulation in off-target organs to minimize adverse effects. Furthermore, they should be cleared from the body to enable subsequent treatments to the patient. Because of this, a complete understanding of the pharmacokinetics and biological fate of the nanocarrier and the drug is extremely important in order to ensure the safety

and efficacy of the treatment and to select the therapeutic doses. However, nanoformulations are difficult to track once distributed *in vivo*. One strategy to overcome this limitation consists of labeling the different components of the nanoformultaion with radionuclides, which enable the detection and quantification of the different components with high sensitivity and in a non-invasive way by using molecular imaging techniques such as single-photon emission computed tomography (SPECT) and positron emission tomography (PET). The use of these techniques is gaining relevance in the pharmacokinetic evaluation of novel nanosystems.[10,88,89]

1.2.2. Nuclear imaging

Nuclear imaging techniques rely on the administration of a trace amount of the molecule/material to be investigated previously labeled with a radionuclide, i.e. a positron or gamma emitter. Radionuclides spontaneously decay, resulting in the emission of positrons or gamma rays. The annihilation of a positron with an electron occurs rapidly and results in the formation of gamma rays. Hence, both positron and gamma emitters ultimately lead to emission of gamma rays, which have high penetration power and can "escape" from the body and reach the detectors. By detecting such gamma rays, three dimensional, time-resolved images accounting for the concentration of the radioactivity in different regions can be generated. Positron Emission Tomography (PET) and Single Photon Emission Computerised Tomography (SPECT) are the most commonly used nuclear imaging techniques. In the context of this PhD thesis, only PET has been used, and hence a brief introduction on the principles is included in this chapter. For a detailed description of SPECT the reader is referred to *Israel et al.* [90]

1.2.3. Positron Emission Tomography

Positron emitters are radioactive nuclides that spontaneously decay by emitting a positron, the electron antimatter with equivalent mass but positive electrical charge. Positrons interact with the media and progressively lose their kinetic energy; when it is almost at rest, a positron annihilates with an electron, a phenomenon that results in

the emission of two gamma rays traveling in opposite directions with an energy of 511 keV each.[91]

When a positron emitter-labeled molecule is injected into a living subject, millions of annihilations occur within the organism, thus generating millions of gamma-ray pairs. Images are acquired with PET cameras, which consist of an array of detectors arranged in a ring surrounding the organism. Because gamma ray pairs are emitted in opposite directions, the simultaneous detection (within i.e. 1 nanosecond) of two gamma rays by two detectors defines a "line of response", in which the annihilation took place[92] (**Figure 8**). This is known as "electronic" collimation. The detection of hundreds of thousands of gamma ray pairs can be translated into a three-dimensional, time-resolved image that accounts for the regional concentration of radioactivity.

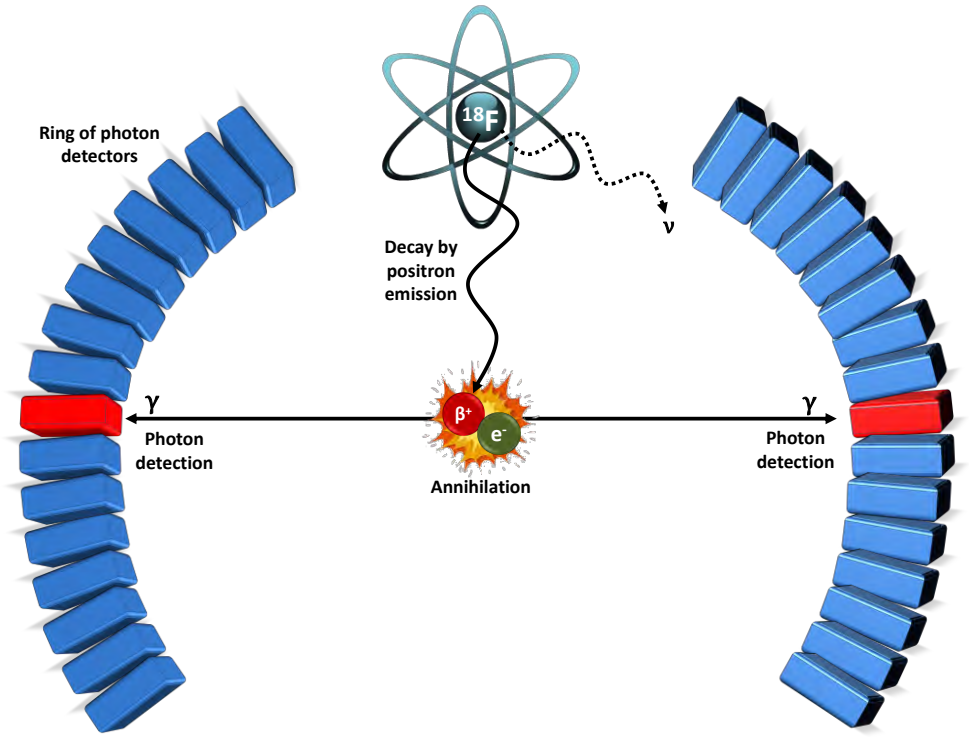

Figure 8. *Schematic representation of positron/electron annihilation and detection in Positron Emission Tomography (PET).*

PET images offer molecular information. In order to unambiguously localize the radioactive signal, PET images are usually corregistered with anatomical images, typically obtained by computerized tomography (CT). Hence, typical practice both in the pre-clinical and clinical fields consists of acquiring consecutive PET and CT images

and analyze them together. The anatomical image can be used to define volumes of interest (VOIs) in different regions. Such VOIs are then translated to the PET images, in order to obtain quantitative information regarding the concentration of radioactivity as a function of time.

One key parameter in PET radionuclides is their **physical half-life**, defined as the time period required for the amount of radioactivity to decrease to one half of the initial value. Half-life values for PET radionuclides typically used in biomedical applications range from few minutes to few days (

Table 1).

Table 1. Typical positron emitters used in nuclear imaging (with half-life and positron energy).

Isotope	Half-Life	β^+ Energy$_{max}$ (β^+ Fraction)*
^{18}F	109.8 min	0.63 MeV (0.97)
^{64}Cu	12.7 h	0.66 MeV (0.18)
^{11}C	20.4 min	0.96 MeV (1.00)
^{13}N	9.97 min	1.20 MeV (1.00)
^{15}O	122 s	1.73 MeV (1.00)
^{68}Ga	67.6 min	1.89 MeV (0.89)
^{124}I	4.18 days	2.14 MeV (0.23)

* The positrons are not emitted with a single energy. The energies of the positrons emitted by a radionuclide follow a Poisson distribution. The maximum value of the distribution is presented in the table.

The selection of the right isotope with adequate half-life is paramount to guarantee successful pharmacokinetic evaluation of new entities. Ideally, the radionuclide should have a physical half-life similar to the biological half-life of the molecule or nanosystem under investigation. If the physical half-life is too short, the radionuclide will completely decay before the compound is eliminated from the organism, and part of the information will be lost. If the half-life is too long, the subject under investigation will be exposed to an unnecessary dose of radiation.

In this PhD thesis ^{18}F, ^{64}Cu and ^{124}I have been employed, as they enabled the radiolabelling and *in vivo* investigations of the nanocarriers and drugs assayed. A brief description of the production and radiochemical applications of these radionuclides is included below.

1.2.4. Properties, production and radiochemistry of the positron emitters ^{18}F, ^{64}Cu and ^{124}I.

Fluorine-18 (^{18}F) is considered as an ideal PET radioisotope. It decays almost quantitatively by positron emission (97%) and it has a low β^+ energy ($E_{\beta max}$ = 0.635 MeV), enabling the acquisition of images with higher resolution than other positron emitters (see

Table 1). Moreover, its half-live of 109.8 min is very convenient for different uses such as drug development or *in vivo* diagnosis. Indeed, ^{18}F is the most commonly used positron emitter world-wide due to its application in the preparation of the glucose analogue 2-deoxy-2-[^{18}F]fluoro-D-glucose ([^{18}F]FDG, an indirect proliferation marker which is used in the early diagnose and the evaluation of the response to treatment of different types of cancer, inflammatory processes and other diseases.[93]

^{18}F can be generated in biomedical cyclotrons in two chemical forms, i.e. [^{18}F]F^- and [^{18}F]F_2, by using different nuclear reactions. Usually, production of [^{18}F]F^- is achieved by irradiation of ^{18}O-enriched water (95-98%) with protons in an energy range of 8-18 MeV following the nuclear reaction of $^{18}O(p,n)^{18}F$.[94] Once the nuclear reaction is produced, the enriched water containing $^{18}F^-$ is transferred to a shielded hot cell and processed. $^{18}F^-$ is then used to prepare ^{18}F-radiotracers using nucleophilic substitution reactions on a precursor bearing a good leaving group.[95,96] Production of [^{18}F]F_2 is based on a double irradiation approach. In a first step, [^{18}O]O_2 is irradiated with protons to generate ^{18}F, which remains absorbed on the walls of the target chamber. The oxygen gas is then removed from the target by cryogenic trapping, and the target is filled with a Ne/F_2 mixture. A second irradiation induces isotopic exchange reaction with the consequent formation of [^{18}F]F_2,[97] which is then transferred to the hot cell and used for labeling.

Radiolabeling with ^{18}F is generally approached by using two different strategies: "direct" or "indirect" fluorination. Direct fluorination consists of the introduction of ^{18}F, either as $[^{18}F]F^-$ or $[^{18}F]F_2$, in the target molecule in a single step;[95] indirect fluorination consists of radiolabelling a reactive prosthetic group, which is subsequently attached to the target molecule (multistep synthesis).[98,99] The latest is commonly applied to the radiolabelling of biomolecules that can be unstable under the harsh reaction conditions required for direct fluorination. ^{18}F-fluoroalkylation, ^{18}F-fluoroacylation, or ^{18}F-fluoroamidation of primary amino groups or thiol residues or cycloaddition reactions are usually exploited for indirect labeling.

For direct fluorination, the most commonly used reactions are based on the nucleophilic substitution of $[^{18}F]F^-$ on a molecule bearing a good leaving group;[95,96] the most representative example is the production of $[^{18}F]$FDG, in which $^{18}F^-$ is reacted with 1,3,4,6-tetra-*O*-acetyl-2-*O*-trifluoromethanesulfonyl-beta-D-mannopyranose (mannose triflate) in acetonitrile.[93] In some occasions, when nucleophilic substitution reactions are not feasible, ^{18}F is introduced to the target molecule via electrophilic aromatic substitution reactions using $[^{18}F]F_2$,[94] although this strategy is technically more challenging due to difficulties associated with the generation and manipulation of $[^{18}F]F_2$.

In the current PhD thesis, **direct fluorination of 17β-estradiol was achieved via nucleophilic substitution**. The ^{18}F atom was incorporated after the reaction of $[^{18}F]F^-$ with the precursor 3-methoxymethyl-16β,17β-epiestriol-O-cyclic sulfone (MMSE) followed by acid hydrolysis.[100]

Copper-64 (^{64}Cu) is a radionuclide which exhibits three different decay routes and a relatively long half-life (12.7 hours). It can undergo by electron capture (ε, 43.8%), β^+ emission to ^{64}Ni (17.8%), and β^- emission to ^{64}Zn (38.4%). The half-life and positron-branch turn ^{64}Cu into a suitable candidate for diagnostic imaging, while the β^- and electron capture decay modes are useful for therapy. Copper-64 production can be done by reactor-based or accelerator-based methods. Reactor-based methods consist in the irradiation of the target material with thermal (relatively low energy) or fast

(highly energetic) neutrons. In the first case, the irradiation of stable ^{63}Cu (69.1% natural abundance) with thermal neutrons produces ^{64}Cu with low specific activity *via* the ^{63}Cu(n,γ)^{64}Cu nuclear reaction. Irradiation of ^{64}Zn with high energy neutrons generates ^{64}Cu with high-specific activity *via* the ^{64}Zn(n,p)^{64}Cu nuclear reaction. As an alternative to reactor-based production methods, biomedical cyclotrons can be used to produce ^{64}Cu *via* the ^{64}Ni(p,n)^{64}Cu nuclear reaction. This methodology firstly proposed by Szelecsenyi *et al.*[101] is based on the irradiation of enriched ^{64}Ni, previously electroplated onto a gold disk. Because of the low natural abundance of ^{64}Ni, it has a high cost (a few tens € per mg). Thus, after irradiation, the target material is dissolved in concentrated HCl, and the resulting solution is eluted through an anion exchange column with different acid concentrations, allowing the separation of ^{64}Cu from the nickel fraction which can be reused.[102]

^{64}Cu has a suitable half-life for tracking both small and large molecules. This advantage, together with its well-known coordination chemistry and redox behaviour, dominated by oxidation states I and II, make ^{64}Cu very attractive in comparison with other metal radioisotopes, especially for the radiolabelling of NPs, which can be achieved via one of the following routes: (i) incorporation of a chelator in the nanoparticle and subsequent radiolabeling by formation of a radiometal-chelator complex;[103–105] (ii) formation of a pre-labeled chelator bearing a reactive residue and subsequent attachment to the NP;[106] and (iii) direct incorporation of the radionuclide within the NP,[107] typically within the crystal lattice of inorganic NPs.

The use of chelators finds its main application in the radiolabelling of soft-matter NPs, and to date a wide variety of chelating agents bearing a reactive moiety (so called bifunctional chelators, BFCs) have been developed and are currently commercially available.[108] The choice of the chelator is critical for *in vivo* applications, as dissociation of the chelator-radiometal complex could lead to misinterpretation of the imaging results. Thus, stability studies to guarantee that the labelled NP remains intact over the duration of the study need to be performed. Due to its relatively large cavity and chelating properties, 1,4,7,10-tetraazacyclododecane-tetraacetic acid (DOTA) and its

derivatives (**Figure 9**) are widely used for medical diagnostics and in the preclinical setting.[109]

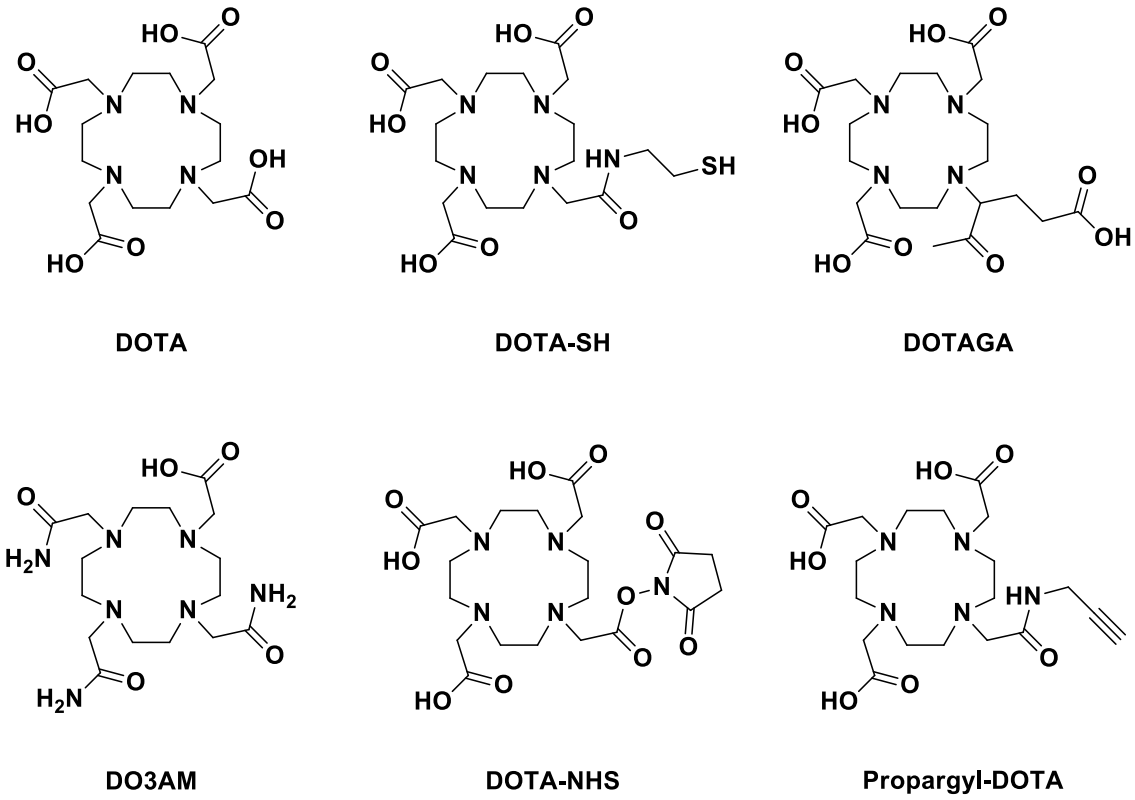

Figure 9. *DOTA and commercially available derivatives of DOTA functionalized for use as bifunctional chelating agents.*

In this PhD thesis, ^{64}Cu has been used to radiolabel the polymers employed to stabilize the emulsions, and this has been achieved by using bifunctional chelators. Due to the presence of double bonds in DXT-MA, which are susceptible to react with thiol groups via thio-Michael addition, we used a pre-labeled thiolated DOTA (DOTA-SH) as bifunctional chelator (**Figure 9**).

Iodine has mainly four radioisotopes with interest in the field of *in vivo* imaging, namely: ^{123}I, ^{124}I, ^{125}I and ^{131}I. For PET imaging **^{124}I**, which is a positron emitter, has become a very useful labelling tool due to its long half-life (4.17 days). Its decay route entails the emission of high energy γ-rays (0.603 MeV, 63.0% abundance) and high energy positrons ($E_{\beta max}$ = 2.14 MeV, 23% abundance). Due to its relatively long half-life, Iodine-124 can be obtained from commercial suppliers. The production is carried out

in solid targets *via* the ^{124}Te(d,2n)^{124}I or the ^{124}Te(p,n)^{124}I nuclear reactions.[110] The target material consist of tellurium or tellurium oxide which is irradiated and thereupon recovered by heating at 750^{o}C (dry distillation) or by dissolution in an oxidizing alkaline medium with the subsequent chemical reduction to I^- state and the final purification by solid phase extraction.[111] Despite the methodology for the production of this isotope looks simple, different parameters must be optimized and, as a consequence, the cost remains relatively high.

Labeling with radioiodine has been widely described in the literature.[111–113] The main radiolabelling routes (see **Figure 10** for scheme) are: (i) in situ oxidation of the anionic species (I^-) and subsequent aromatic electrophilic substitution (SEAr) in an activated aromatic ring;[113] (ii) indirect methods based on pre-labeling using a prosthetic group and further functionalization via covalent bond with the target molecule;[112] and (iii) catalyst-assisted isotopic exchange, only applicable when an iodine atom is already present in the target molecule.[114] Methods (i) and (ii) usually result in high yields, and have been widely applied to the radiolabelling of proteins and peptides, among others. Isotopic exchange often leads to low specific activity values of the final radiotracer and is less often employed.

In this PhD thesis, ^{124}I has been used for the radiolabeling of the cobalt *bis*(dicarbollide) anion ([3,3'-Co($C_2B_9H_{11}$)$_2$]$^-$ (COSAN), a metallocarborane compound consisting of a central cobalt (Co^{3+}) atom sandwiched between two η^5-bonding $[C_2B_9H_{11}]^{2-}$ moieties which has been used as stabilizer of (o/w)-emulsions. The labeling was carried out by isotopic exchange.

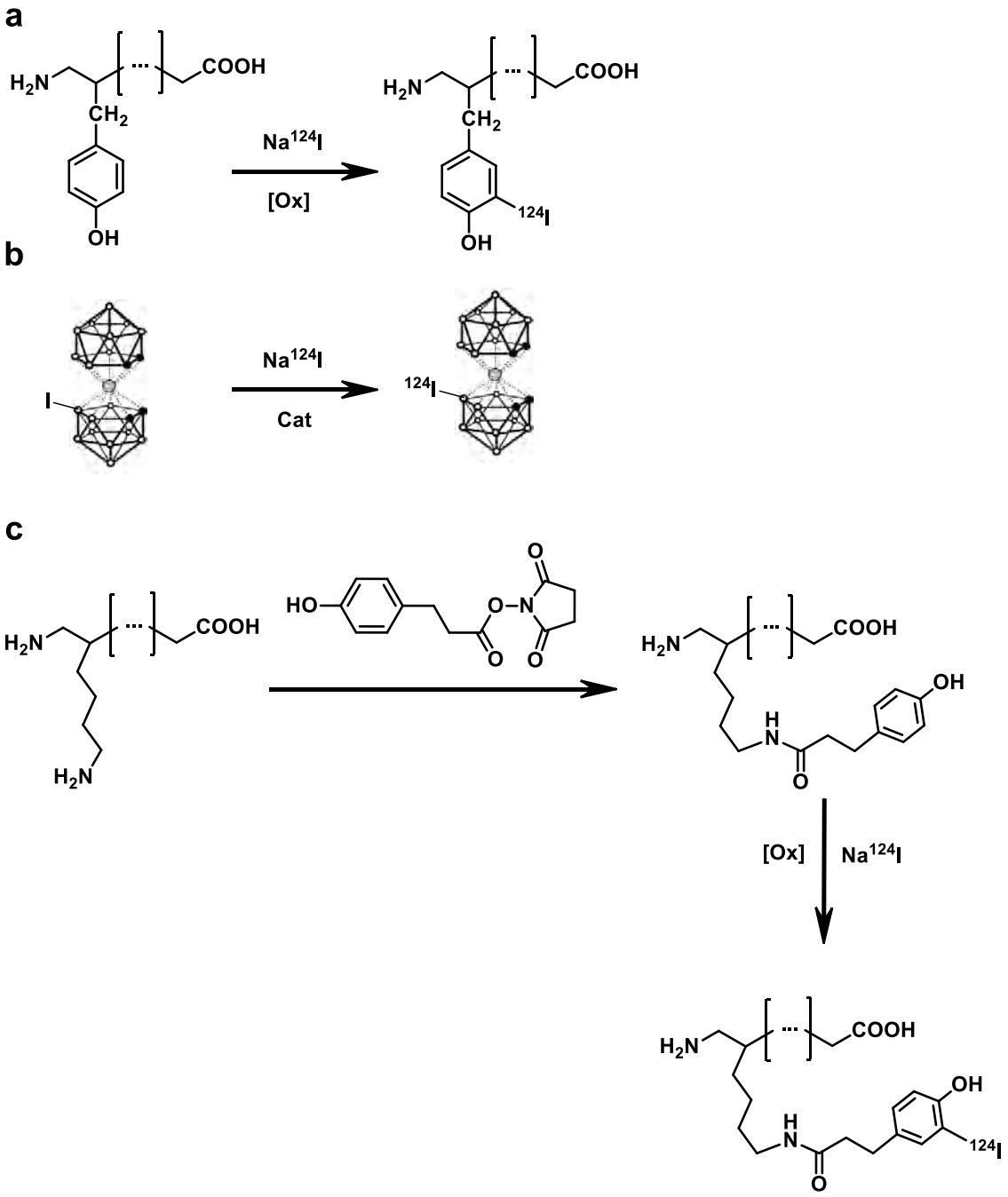

Figure 10. *Schematic representation of the main strategies used for the radioiodination of different molecules; (a) electrophilic substitution, (b) isotopic exchange and (c) pre-labeling using a prosthetic group. Examples are shown with ^{124}I; these strategies can be extended to other iodine radioisotopes.*

1.3. References

1. Ramsden, J. J. The nanotechnology industry. *Nanotechnol. Perceptions* **9**, 102–118 (2013).

2. Etheridge, M. L. *et al.* The big picture on nanomedicine: The state of investigational and approved nanomedicine products. *Nanomedicine Nanotechnology, Biol. Med.* **9**, 1–14 (2013).

3. Doane, T. L. & Burda, C. The unique role of nanoparticles in nanomedicine: Imaging, drug delivery and therapy. *Chem. Soc. Rev.* **41**, 2885–2911 (2012).

4. Wagner, V., Husing, B., Gaisser, S. & Bock, A.-K. Nanomedicine : Drivers for development and possible impacts. *Eur. Comm. Jt. Res. Cent. Rep. No. 46744* 1–116 (2006).

5. Nikalje, A. Nanotechnology and its Applications in Medicine. *Med. Chem. (Los. Angeles).* **5**, 081–089 (2015).

6. Roco, M. C. Nanotechnology: Convergence with modern biology and medicine. *Curr. Opin. Biotechnol.* **14**, 337–346 (2003).

7. Morigi, V. *et al.* Nanotechnology in Medicine: From Inception to Market Domination. *J. Drug Deliv.* **2012**, 1–7 (2012).

8. Allen, T. M. & Cullis, P. R. Drug Delivery Systems: Entering the Mainstream. *Science (80-.).* **303**, 1818–1822 (2004).

9. Patra, J. K. *et al.* Nano based drug delivery systems: Recent developments and future prospects 10 Technology 1007 Nanotechnology 03 Chemical Sciences 0306 Physical Chemistry (incl. Structural) 03 Chemical Sciences 0303 Macromolecular and Materials Chemistry 11 Medical and He. *J. Nanobiotechnology* **16**, 1–33 (2018).

10. Smith, B. R. & Gambhir, S. S. Nanomaterials for *in Vivo* Imaging. *Chem. Rev.* **117**, 901–986 (2017).

11. Singh, R. & Lillard, J. W. Nanoparticle-based targeted drug delivery. *Exp. Mol. Pathol.* **86**, 215–223 (2009).

12. Mishra, B., Patel, B. B. & Tiwari, S. Colloidal nanocarriers: a review on formulation technology, types and applications toward targeted drug delivery. *Nanomedicine Nanotechnology, Biol. Med.* **6**, 9–24 (2010).

13. Zhang, L. Nanoparticles in Medicine: Therapeutic Applications and Developments. *Clin. Pharmacol. Ther.* **83**, 761–769 (2007).

14. Peer, D. *et al.* Nanocarriers as an emerging platform forcancer therapy. *Nat. Nanotechnol.* **2**, 751–760 (2007).

15. Yohan, D. & Chithrani, B. D. Applications of nanoparticles in nanomedicine. *J. Biomed. Nanotechnol.* **10**, 2371–2392 (2014).

16. Maeda, H. Macromolecular therapeutics in cancer treatment: The EPR effect and beyond. *J. Control. Release* **164**, 138–144 (2012).

17. Narvekar, M., Xue, H. Y., Eoh, J. Y. & Wong, H. L. Nanocarrier for poorly water-soluble anticancer drugs - Barriers of translation and solutions. *AAPS PharmSciTech* **15**, 822–833 (2014).

18. Van Hoogevest, P., Liu, X. & Fahr, A. Drug delivery strategies for poorly water-soluble drugs: The industrial perspective. *Expert Opin. Drug Deliv.* **8**, 1481–1500 (2011).

19. Giliyar C. , Fikstad D. T., T. S. *Challenges and opportunities in oral delivery of poorly water-soluble drugs. Drug Delivery Technology* vol. 6 (2006).

20. Lipinski C. A., Lombardo F., Dominy B.W., Experimental and computational approaches to estimate solubility and permeability in drug discovery and development settings. *Adv. Drug Deliv. Rev.* **46**, 3–26 (2001).

21. Internationalcouncil for harmonisation of technical requirements for pharmaceuticals for humans. *Biopharmaceutics classification system-based*. (2018).

22. Rawat, M., Singh, D., Saraf, S. & Saraf, S. Lipid carriers: A versatile delivery vehicle for proteins and peptides. *Yakugaku Zasshi* **128**, 269–280 (2008).

23. Lim, S. B., Banerjee, A. & Önyüksel, H. Improvement of drug safety by the use of lipid-based nanocarriers. *J. Control. Release* **163**, 34–45 (2012).

24. Gursoy, R. N. & Benita, S. Self-emulsifying drug delivery systems (SEDDS) for improved oral delivery of lipophilic drugs. *Biomed. Pharmacother.* **58**, 173–182 (2004).

25. Constantinides, P. P., Chaubal, M. V & Shorr, R. Advances in lipid nanodispersions for parenteral drug delivery and targeting. *Adv. Drug Deliv. Rev.* **60**, 757–767 (2008).

26. Torchilin, V. P. Micellar nanocarriers: Pharmaceutical perspectives. *Pharm. Res.* **24**, 1–16 (2007).

27. Slomkowski, S. *et al.* Terminology of polymers and polymerization processes in dispersed systems (IUPAC recommendations 2011). *Pure Appl. Chem.* **83**, 2229–2259 (2011).

28. McClements, D. J., Decker, E. A. & Weiss, J. Emulsion-based delivery systems for lipophilic bioactive components. *J. Food Sci.* **72**, 109–124 (2007).

29. McClements, D. J. Critical review of techniques and methodologies for characterization of emulsion stability. *Crit. Rev. Food Sci. Nutr.* **47**, 611–649 (2007).

30. Hayn, M. H., Averch, T. D. & Jackman, S. V. Transperitoneal laparoscopic radical and partial nephrectomy in patients with cirrhosis: report of three cases. *Can. J. Urol.* **16**, 4770–4773 (2009).

31. Frazier, R. A. *Physical Chemistry of Foods*. *Food Chemistry* vol. 85 (2004).

32. Gupta, A., Eral, H. B., Hatton, T. A. & Doyle, P. S. Nanoemulsions: formation, properties and applications. *R. Soc. Chem.* **12**, 2826–2841 (2016).

33. Pellicer, J., García-Morales, V. & Hernández, M. J. On the demonstration of the young-laplace equation in introductory physics courses. *Phys. Educ.* **35**, 126–129 (2000).

34. Xu, J. *et al.* Effect of surfactant headgroups on the oil/water interface: An interfacial tension measurement and simulation study. *J. Mol. Struct.* **1052**, 50–56 (2013).

35. Finkle, P., Draper, H. D. & Hildebrand, J. H. The theory of emulsification. *J. Am. Chem. Soc.* **45**, 2780–2788 (1923).

36. Dutta, S. K., Knowlton, E. & Blair, D. L. Emulsions. *Fluids, Colloids Soft Mater. An Introd. to Soft Matter Phys.* **91**, 2001–2021 (1907).

37. Morse, A. J. *et al.* Novel Pickering Emulsi fi ers Based on pH-Responsive Poly(2-(diethylamino)ethyl methacrylate) Latexes. *Langmuir* **29**, 5446–5475 (2013).

38. Chevalier, Y. & Bolzinger, M. A. Emulsions stabilized with solid nanoparticles: Pickering emulsions. *Colloids Surfaces A Physicochem. Eng. Asp.* **439**, 23–34 (2013).

39. Wang, H., Singh, V. & Behrens, S. H. Image charge effects on the formation of pickering emulsions. *J. Phys. Chem. Lett.* **3**, 2986–2990 (2012).

40. Kentish, S. *et al.* The use of ultrasonics for nanoemulsion preparation. *Innov. Food Sci. Emerg. Technol.* **9**, 170–175 (2008).

41. Azeem, A. *et al.* Nanoemulsion components screening and selection: A technical note. *AAPS PharmSciTech* **10**, 69–76 (2009).

42. Lerche, D. & Sobisch, T. Direct and accelerated characterization of formulation stability. *J. Dispers. Sci. Technol.* **32**, 1799–1811 (2011).

43. Rosenblatt, K. M. & Bunjes, H. Evaluation of the drug loading capacity of different lipid nanoparticle dispersions by passive drug loading. *Eur. J. Pharm. Biopharm.* **117**, 49–59 (2017).

44. Ganta, S., Talekar, M., Singh, A., Coleman, T. P. & Amiji, M. M. Nanoemulsions in translational research - Opportunities and challenges in targeted cancer therapy. *AAPS PharmSciTech* **15**, 694–708 (2014).

45. Tayeb, H. H. & Sainsbury, F. Nanoemulsions in drug delivery: Formulation to medical application. *Nanomedicine* **13**, 2507–2525 (2018).

46. Liu, J., Willför, S. & Xu, C. A review of bioactive plant polysaccharides: Biological activities, functionalization, and biomedical applications. *Bioact. Carbohydrates Diet. Fibre* **5**, 31–61 (2015).

47. Zhang, N., Wardwell, P. R. & Bader, R. A. Polysaccharide-based micelles for drug delivery. *Pharmaceutics* **5**, 329–352 (2013).

48. Zong, A., Cao, H. & Wang, F. Anticancer polysaccharides from natural resources: A review of recent research. *Carbohydr. Polym.* **90**, 1395–1410 (2012).

49. Bais, D., Trevisan, A., Lapasin, R., Partal, P. & Gallegos, C. Rheological characterization of polysaccharide-surfactant matrices for cosmetic O/W emulsions. *J. Colloid Interface Sci.* **290**, 546–556 (2005).

50. Sinha, V. R. & Kumria, R. Polysaccharides in colon-specific drug delivery. *Int. J. Pharm.* **224**, 19–38 (2001).

51. Ngwuluka, N. C. *Responsive polysaccharides and polysaccharides-based nanoparticles for drug delivery*. *Stimuli Responsive Polymeric Nanocarriers for Drug Delivery Applications, Volume 1* (Elsevier Ltd., 2018). doi:10.1016/b978-0-08-101997-9.00023-0.

52. Bouyer, E., Mekhloufi, G., Rosilio, V., Grossiord, J. L. & Agnely, F. Proteins, polysaccharides, and their complexes used as stabilizers for emulsions: Alternatives to synthetic surfactants in the pharmaceutical field? *Int. J. Pharm.* **436**, 359–378 (2012).

53. Landoll, L. M. Nonionic Polymer Surfactants. *J. Polym. Sci. A1.* **20**, 443–455 (1982).

54. Moss, G. P., Smith, P. A. S. & Tavernier, D. Glossary of class names of organic compounds and reactive intermediates based on structure (IUPAC recommendations 1995). *Pure Appl. Chem.* **67**, 1307–1375 (1995).

55. van Dijk-Wotthuis, W. N. E. *et al.* Synthesis, Characterization, and Polymerization of Glycidyl Methacrylate Derivatized Dextran. *Macromolecules* **28**, 6317–6322 (1995).

56. van Dijk-Wolthuis, W. N. E., Kettenes-van den Bosch, J. J., van der Kerk-van Hoof, A. & Hennink, W. E. Reaction of Dextran with Glycidyl Methacrylate: An Unexpected Transesterification. *Macromolecules* **30**, 3411–3413 (1997).

57. Rouzes, C., Durand, A., Leonard, M. & Dellacherie, E. Surface activity and emulsification properties of hydrophobically modified dextrins. *Colloids Surfaces A Physicochem. Eng. Asp.* **364**, 55–60 (2010).

58. Wu, M., Dellacherie, E., Durand, A. & Marie, E. Poly(n-butyl cyanoacrylate) nanoparticles via miniemulsion polymerization (1): Dextran-based surfactants. *Colloids Surfaces B Biointerfaces* **69**, 141–146 (2009).

59. Raynaud, J. *et al.* Emulsifying properties of biodegradable polylactide-grafted dextran copolymers. *Biomacromolecules* **9**, 1014–1021 (2008).

60. Nouvel, C. *et al.* Biodegradable nanoparticles made from polylactide-grafted dextran copolymers. *J. Colloid Interface Sci.* **330**, 337–343 (2009).

61. Nichifor, M., Mocanu, G. & Stanciu, M. C. Micelle-like association of polysaccharides with hydrophobic end groups. *Carbohydr. Polym.* **110**, 209–218 (2014).

62. Rouzes, C., Durand, A., Leonard, M. & Dellacherie, E. Surface activity and emulsification properties of hydrophobically modified dextrans. *J. Colloid Interface Sci.* **253**, 217–223 (2002).

63. Chan, A., Orme, R. P., Fricker, R. A. & Roach, P. Remote and local control of stimuli responsive materials for therapeutic applications. *Adv. Drug Deliv. Rev.* **65**, 497–514 (2013).

64. Theato, P., Sumerlin, B. S., O'reilly, R. K. & Epp, T. H. Stimuli responsive materials. *Chem. Soc. Rev.* **42**, 7055–7056 (2013).

65. de la Rica, R., Aili, D. & Stevens, M. M. Enzyme-responsive nanoparticles for drug release and diagnostics. *Adv. Drug Deliv. Rev.* **64**, 967–978 (2012).

66. Zelzer, M. & Ulijn, R. V. *Enzyme-responsive polymers: Properties, synthesis and applications*. *Smart Polymers and their Applications* (Woodhead Publishing Limited, 2014). doi:10.1533/9780857097026.1.166.

67. Ulijn, R. V. Enzyme-responsive materials: A new class of smart biomaterials. *J. Mater. Chem.* **16**, 2217–2225 (2006).

68. Namazi, H., Fathi, F. & Heydari, A. Nanoparticles Based on Modified Polysaccharides. *Deliv. Nanoparticles* (2012) doi:10.5772/34795.

69. Abedi, D., Zhang, L., Pyne, M. & Perry Chou, C. *Enzyme Biocatalysis*. *Comprehensive Biotechnology, Second Edition* vol. 1 (2011).

70. De Simone, A. *Engineering the genetic code of Escherichia coli with methionine analogues and bioorthogonal amino acids for protein immobilization*. (2016).

71. Nomura, D. K. & Casida, J. E. Lipases and their inhibitors in health and disease. *Chem. Biol. Interact.* **259**, 211–222 (2016).

72. McClements, D. J. & Li, Y. Structured emulsion-based delivery systems: Controlling the digestion and release of lipophilic food components. *Adv. Colloid Interface Sci.* **159**, 213–228 (2010).

73. Lee, S. J., Choi, S. J., Li, Y., Decker, E. A. & McClements, D. J. Protein-stabilized nanoemulsions and emulsions: Comparison of physicochemical stability, lipid oxidation, and lipase digestibility. *J. Agric. Food Chem.* **59**, 415–427 (2011).

74. Reis, P., Holmberg, K., Watzke, H., Leser, M. E. & Miller, R. Lipases at interfaces: A review. *Adv. Colloid Interface Sci.* **147–148**, 237–250 (2009).

75. Mukherjee, A. K. Hydrophobic-hydrophilic interaction in lipase catalytic triad and possibility of a cofactor mediated catalysis. *Int. J. Agric. Food Sci.* **4**, 84–89 (2014).

76. De Simone, A. *Engineering the genetic code of Escherichia coli with methionine analogues and bioorthogonal amino acids for protein immobilization*. (2016).

77. Brito e Cunha, D. A. *et al.* Structural differences of commercial and recombinant lipase B from Candida antarctica: An important implication on enzymes thermostability. *Int. J. Biol. Macromol.* **140**, 761–770 (2019).

78. Rabbani, G. *et al.* Impact of structural stability of cold adapted Candida antarctica lipase B (CaLB): In relation to pH, chemical and thermal denaturation. *RSC Adv.* **5**, 20115–20131 (2015).

79. De Caro, J. *et al.* Porcine pancreatic lipase. Completion of the primary structure. *BBA - Protein Struct.* **671**, 129–138 (1981).

80. Mun, S., Decker, E. A. & McClements, D. J. Influence of emulsifier type on *in vitro* digestibility of lipid droplets by pancreatic lipase. *Food Res. Int.* **40**, 770–781 (2007).

81. Azarmi, S., Roa, W. H. & Löbenberg, R. Targeted delivery of nanoparticles for the treatment of lung diseases. *Adv. Drug Deliv. Rev.* **60**, 863–875 (2008).

82. Andrade, F., Videira, M., Ferreira, D. & Sarmento, B. Nanocarriers for pulmonary administration of peptides and therapeutic proteins. *Nanomedicine* **6**, 123–141 (2011).

83. Mansour, H. M., Rhee, Y. S. & Wu, X. Nanomedicine in pulmonary delivery. *Int. J. Nanomedicine* **4**, 299–319 (2009).

84. Sung, J. C., Pulliam, B. L. & Edwards, D. A. Nanoparticles for drug delivery to the lungs. *Trends Biotechnol.* **25**, 563–570 (2007).

85. Scherer, P. M. & Chen, D. L. Imaging pulmonary inflammation. *J. Nucl. Med.* **57**, 1764–1770 (2016).

86. Gurzell, E. A. *et al.* DHA-enriched fish oil targets B cell lipid microdomains and enhances ex vivo and *in vivo* B cell function. *J. Leukoc. Biol.* **93**, 463–470 (2013).

87. Shaikh, S. R., Fessler, M. B. & Gowdy, K. M. Role for phospholipid acyl chains and cholesterol in pulmonary infections and inflammation. *J. Leukoc. Biol.* **100**, 1–13 (2016).

88. Padmanabhan, P., Kumar, A., Kumar, S., Chaudhary, R. K. & Gulyás, B. Nanoparticles in practice for molecular-imaging applications: An overview. *Acta Biomater.* **41**, 1–16 (2016).

89. Kim, J., Lee, N. & Hyeon, T. Recent development of nanoparticles for molecular imaging. *Philos. Trans. R. Soc. A Math. Phys. Eng. Sci.* **375**, (2017).

90. Israel, O. *et al.* Two decades of SPECT/CT – the coming of age of a technology: An updated review of literature evidence. *Eur. J. Nucl. Med. Mol. Imaging* **46**, 1990–2012 (2019).

91. Conti, M. & Eriksson, L. Physics of pure and non-pure positron emitters for PET: A review and a discussion. *EJNMMI Phys.* **3**, (2016).

92. Rahmim, A. & Zaidi, H. Pet versus spect: Strengths, limitations and challenges. *Nucl. Med. Commun.* **29**, 193–207 (2008).

93. Vallabhajosula, S. 18F-Labeled Positron Emission Tomographic Radiopharmaceuticals in Oncology: An Overview of Radiochemistry and Mechanisms of Tumor Localization. *Semin. Nucl. Med.* **37**, 400–419 (2007).

94. Teare, H. *et al.* Radiosynthesis and evaluation of [18F]Selectfluor bis(triflate). *Angew. Chemie - Int. Ed.* **49**, 6821–6824 (2010).

95. Urakami, T. *et al.* Novel amphiphilic probes for [18F]-radiolabeling preformed liposomes and determination of liposomal trafficking by positron emission tomography. *J. Med. Chem.* **50**, 6454–6457 (2007).

96. Marik, J. *et al.* Long-circulating liposomes radiolabeled with [18F]fluorodipalmitin ([18F]FDP). *Nucl. Med. Biol.* **34**, 165–171 (2007).

97. Roberts, A. D., Oakes, T. R. & Nickles, R. J. Development of an improved target for [18F]F2 production. *Appl. Radiat. Isot.* **46**, 87–91 (1995).

98. Guerrero, S. *et al.* Synthesis and *in vivo* evaluation of the biodistribution of a 18F-labeled conjugate gold-nanoparticle-peptide with potential biomedical application. *Bioconjug. Chem.* **23**, 399–408 (2012).

99. Rojas, S. *et al.* Biodistribution of amino-functionalized diamond nanoparticles. *in vivo* studies based on 18F radionuclide emission. *ACS Nano* **5**, 5552–5559 (2011).

100. Römer, J., Füchtner, F., Steinbach, J. & Johannsen, B. Automated production of 16α- [18F]fluoroestradiol for breast cancer imaging. *Nucl. Med. Biol.* **26**, 473–479 (1999).

101. Szelecsfinyi, F. Excitation Functions of Proton Induced Nuclear Reactions on Enriched 61Ni and 64Ni : Possibility of Production of 61 Cu and 64cu at a Small Cyclotron. *Production* **44**, 575–580 (1993).

102. McCarthy, D. W. *et al.* High purity production and potential applications of copper-60 and copper-61. *Nucl. Med. Biol.* **26**, 351–358 (1999).

103. Schjoeth-Eskesen, C. *et al.* -labelled trastuzumab: Optimisation of labelling by DOTA and NODAGA conjugation and initial evaluation in mice. *J. Label. Compd. Radiopharm.* **58**, 227–233 (2015).

104. Ghosh, S. C. *et al.* Comparison of DOTA and NODAGA as chelators for 64Cu-labeled immunoconjugates. *Nucl. Med. Biol.* **42**, 177–183 (2015).

105. Zhu, H. *et al.* Radiolabeling and evaluation of 64Cu-DOTA-F56 peptide targeting vascular endothelial growth factor receptor 1 in the molecular imaging of gastric cancer. *Am. J. Cancer Res.* **5**, 3301–3310 (2015).

106. Hanaoka, H. *et al.* Evaluation of 64Cu-labeled DOTA-d-Phe1-Tyr 3-octreotide (64Cu-DOTA-TOC) for imaging somatostatin receptor-expressing tumors. *Ann. Nucl. Med.* **23**, 559–567 (2009).

107. Boros, E., Bowen, A. M., Josephson, L., Vasdev, N. & Holland, J. P. Chelate-free metal ion binding and heat-induced radiolabeling of iron oxide nanoparticles. *Chem. Sci.* **6**, 225–236 (2015).

108. Lattuada, L., Barge, A., Cravotto, G., Giovenzana, G. B. & Tei, L. The synthesis and application of polyamino polycarboxylic bifunctional chelating agents. *Chem. Soc. Rev.* **40**, 3019–3049 (2011).

109. Stasiuk, G. J. & Long, N. J. The ubiquitous DOTA and its derivatives: The impact of 1,4,7,10- tetraazacyclododecane-1,4,7,10-tetraacetic acid on biomedical imaging. *Chem. Commun.* **49**, 2732–2746 (2013).

110. Clem, R. G. & Lambrecht, R. M. Te targets for production of. *Nucl. Instruments Methods Phys. Res. Sect. A* **303**, 115–118 (1991).

111. Seevers, R. H. & Counsell, R. E. Radioiodination Techniques for Small Organic Molecules. *Chem. Rev.* **82**, 575–590 (1982).

112. Bolton, A. E. & Hunter, W. M. The labelling of proteins to high specific radioactivities by conjugation to a 125I containing acylating agent. Application to the radioimmunoassay. *Biochem. J.* **133**, 529–538 (1973).

113. Wellman, H. W. & Wilson, A. T. 1962 Nature Publishing Group. *Group* **194**, 1097–1098 (1962).

114. Weichert, J. P., Van Dort, M. E., Groziak, M. P. & Counsell, R. E. Radioiodination via isotope exchange in pivalic acid. *Int. J. Radiat. Appl. Instrumentation. Part* **37**, 907–913 (1986).

Chapter 2. Motivation, Hypothesis and Objectives of the Thesis

2.1. Motivation and Hypothesis

The work carried out in this PhD thesis has been co-supervised by Dr. Iraida Loinaz (Director of the Nanomedicine Institute, CIDETEC) and Dr. Jordi Llop (Principal Investigator of the Radiochemistry and Nuclear Imaging group, CIC biomaGUNE). In a previous collaborative effort in the context of an EU funded project, both groups worked on the development of polymeric nanoparticle-based formulations for direct pulmonary administration of new antibiotics to treat antibiotic-resistant bacterial infections. This previous work, which was conducted in a cross-sectorial and international effort and in tight collaboration with European experts in areas such as lung infection, pulmonary delivery and nanotechnology, brought to the groups a strong expertise and tracked record in the use of nanovehicles for direct pulmonary administration of drugs and the use of imaging modalities for their investigation *in vivo*.[1,2] Both groups explored the use of single-chain polymer nanoparticles based on dextran for lung delivery. This strategy was proven ideal for lung-delivery of hydrophilic peptides.[3,4] However, it was not adequate for the delivery of poorly water-soluble drugs where the loading was reduced and hardly reproducible. In order to force the loading and control drug release, other groups employed hydrophobic backbone to force drug loading through non covalent hydrophobic interactions with a maximum loading of 16%.[5]

The use of dextran modified with hydrophobic motives was previously described to reduce interfacial tension and to generate nanoemulsions.[6–8] Furthermore, hydrophilic particles were reported as Pickering stabilizers for (o/w)-emulsions being those hydrophobic useful for (w/o)-emulsions.[9]

With the aim of solving this limitation of dextran based single chain polymer nanoparticles, in this PhD thesis, we proposed to explore the suitability of polymers and polymeric NPs to stabilize oil-in-water (o/w)-nanoemulsions as potential drug carriers for enhanced transport and delivery of poor water soluble drugs.

We hypothesized that nanoemulsions could be stabilized by dextran polymers and dextran-based NPs in order to obtain monodisperse droplets below 500 nm, suitable for nebulization. We envisaged that introduction of hydrophobic modifications on dextran (hydrophilic polymer) could decrease the interfacial tension between oil and water[8] when compared to the hydrophilically-modified homologous polymers. Altogether, encourage us to study the use of functionalized dextran-based polymers and NPs for (o/w)-emulsion stabilization.[10] Furthermore, we also hypothesized that long-term stability in different media could be improved by using cross-linking strategies at the oil/water interface,[11] as this could avoid adsorption/desorption equilibrium and slow down phase separation.[12] Moving forward towards potential controlled drug delivery, we hypothesized that esterase enzymes may trigger nanoemulsion destabilization due to the presence of ester bonds in both surfactant and oil phase.[13] Finally, and with the aim of exploring less conventional amphyphiles as emulsion stabilizers, we envisioned the formation of nanoemulsions using the anionic complex cobalt bis(dicarbollide) as the stabiliser.[14,15] Our final hypothesis was that the newly generated (o/w)-nanoemulsions should be able to modulate the biodistribution of entrapped hydrophobic drugs after pulmonary administration in rodents, and that this hypothesis could be confirmed with the aid of *in vivo* nuclear imaging.

2.2. Objectives

The main aim of the PhD thesis was the development, characterization and evaluation of nanoemulsions as drug carriers for pulmonary administration of poor water-soluble drugs. To achieve this ambitious goal and prove our hypotheses, the following objectives were defined:

1. To evaluate the capacity of different dextran derivatives to stabilize (o/w)-emulsions, and optimize experimental conditions to achieve small-sized, monodisperse nanodroplets.
2. To optimize the methodology for polymer cross-linking at the O/W interface to improve nanoemulsion stability in strong ionic media and over time.

3. To evaluate the *in vivo* stability of cross-linked nanoemulsions and their capacity to modulate the biodistribution of entrapped drugs by using *in vivo* imaging techniques
4. To investigate the demulsification mechanism of polymeric nanoparticle-stabilized oil-in-water emulsions in the presence of selected Lipases and to evaluate the effect of composition and crosslinking on the stability.
5. To prepare and characterize COSAN-stabilized (o/w)-emulsions and evaluate the *in vivo* stability and the capacity of the resulting nanoemulsions to modulate the biodistribution of entrapped drugs.

2.3. References

1. Gracia, R. *et al.* Synthesis and functionalization of dextran-based single-chain nanoparticles in aqueous media. *J. Mater. Chem. B* **5**, 1143–1147 (2017).

2. Cossío, U. *et al.* Preclinical evaluation of aerosol administration systems using Positron Emission Tomography. *Eur. J. Pharm. Biopharm.* **130**, 59–65 (2018).

3. Falciani, C. *et al.* Antimicrobial peptide-loaded nanoparticles as inhalation therapy for Pseudomonas aeruginosa infections. *Int. J. Nanomedicine* **15**, 1117–1128 (2020).

4. van der Weide, H. *et al.* Therapeutic efficacy of novel antimicrobial peptide AA139-nanomedicines in a multidrug-resistant Klebsiella pneumoniae pneumonia-septicemia model in rats . *Antimicrob. Agents Chemother.* (2020) doi:10.1128/aac.00517-20.

5. Pia P. Kröger, A. P. P., Hamelmann, N. M., Juan, A., Lindhoud, S. & Paulusse, J. M. J. Biocompatible single-chain polymer nanoparticles for drug deliverya dual approach. *ACS Appl. Mater. Interfaces* **10**, 30946–30951 (2018).

6. Raynaud, J. *et al.* Emulsifying properties of biodegradable polylactide-grafted dextran copolymers. *Biomacromolecules* **9**, 1014–1021 (2008).

7. Nouvel, C. *et al.* Biodegradable nanoparticles made from polylactide-grafted dextran copolymers. *J. Colloid Interface Sci.* **330**, 337–343 (2009).

8. Rouzes, C., Durand, A., Leonard, M. & Dellacherie, E. Surfac activity and emulsification properties of hydrophobically modified dextrans. *J. Colloid Interface Sci.* **253**, 217–223 (2002).

9. Aveyard, R., Binks, B. P. & Clint, J. H. Emulsions stabilised solely by colloidal particles. *Adv. Colloid Interface Sci.* **100**–**102**, 503–506 (2003).

10. Wu, J. & Ma, G. H. Recent Studies of Pickering Emulsions: Particles Make the Difference. *Small* **12**, 4633–4648 (2016).

11. Thompson, K. L., Williams, M. & Armes, S. P. Colloidosomes: Synthesis, properties and applications. *J. Colloid Interface Sci.* **447**, 217–228 (2014).

12. Thompson, K. L. *et al.* Covalently cross-linked colloidosomes. *Macromolecules* **43**, 10466–10474 (2010).

13. McClements, D. J. & Li, Y. Review of in vitro digestion models for rapid screening of emulsion-based systems. *Food Funct.* **1**, 32–59 (2010).

14. Verdiá-Báguena, C. *et al.* Amphiphilic COSAN and I2-COSAN crossing synthetic lipid membranes: Planar bilayers and liposomes. *Chem. Commun.* **50**, 6700–6703 (2014).

15. Bauduin, P. *et al.* A theta-shaped amphiphilic cobaltabisdicarbollide anion: Transition from monolayer vesicles to micelles. *Angew. Chemie - Int. Ed.* **50**, 5298–5300 (2011).

Chapter 3. Dextran derivatives as stabilizers of oil-in-water (o/w)-emulsions

3.1. Introduction

Polysaccharides are the most common biomacromolecules worldwide. They have a wide variety of reactive groups, variable chemical composition and cover a large range of molecular weights, all these contributing to their diversity in structure and properties. Also, after appropriate chemical modification with hydrophobic moieties, they can present amphiphilic behavior which is extremely interesting for a wide range of applications, for instance as rheology modifiers, emulsion stabilizers, surface modifiers, and targeting moieties for drug delivery systems, among others.[1,2]

In recent years, the self-assembling capacity of hydrophobically modified polysaccharides has received increasing attention in biomedicine.[3] In the presence of water, the hydrophobic cores of these polymers are surrounded by hydrophilic outer shells, resulting in the formation of nanoparticles in which the inner core can be used for the encapsulation of hydrophobic drugs.[4–6] As mentioned in the introductory chapter (see **Chapter 1. General introduction**), these nano-sized objects (nanoparticles, NPs), have physicochemical properties that differ from the bulk materials. These properties can be tuned by modifying the size, shape and surface functionalization, turning nanomaterials into promising drug carriers.[1,3]

Modified polysaccharides have been also used as o/w-emulsion stabilizers to produce stable hydrophilic nanoparticles by different methods,[7–9] one example is the work published by Landoll, who demonstrates that cellulose can also act as surfactant by the appropriate functionalization with alkyl chains.[10] Specifically, dextran (DXT), a natural biocompatible polysaccharide consisting of a (1→6) linear chain linked to D-glucopyranosyl units with (1→2), (1→3), and (1→4) ramifications, can be easily modified with methacrylate (MA) groups (DXT-MA). One of the synthetic routes proposed by van Dijk-Wolthuis and coworkers was the nucleophilic attack of one hydroxyl group of dextran at the methylene carbon of the epoxy group of glycidyl

methacrylate (GMA) obtaining DXT-GMA.[11] A couple of years later, the same authors reported an unexpected transesterification of the methacryloyl group from GMA to dextran, yielding DXT-MA.[12] This transesterification reaction became very useful because DXT-MA can undergo chemical cross-linking reactions,[12,13] which can be also used to produce dextran-based single chain polymer nanoparticles (SCPNs).[14] The collapse of a single polymer chain has been used to produce NPs ranging between 1.5 and 20 nm diameters, also known as SCPNs.[15] The necessity of controlled sizes and tailored arrangement of functional groups, highly desirable in nanomedicine, are becoming interesting in fields like drug delivery and imaging.[16]

On the other hand, Pickering described the use of particles, instead of surfactants, to stabilize emulsions one century ago.[17] Despite being ignored for a long period, Pickering emulsions demonstrated better stability against coalescence than classical emulsions due to the limited adsorption and desorption at the interface in comparison with classical surfactants equilibrium.[18] In this context, dextran-based SCPNs are promising Pickering emulsion stabilizers for biomedical applications.

In this chapter, we describe a straightforward route for the chemical modification of natural polysaccharides with hydrophobic or hydrophilic reactive functional groups, which confers sufficient interfacial activity to enable the production of stable DXT-R based emulsions. To that purpose, four dextran derivatives were synthesized with the same degree of glucose functionalization but changing the functional group (methacrylic or carboxylic acid groups) and the three-dimensional structure (polymer coil or single chain polymer nanoparticle) following the methodology previously developed by *Gracia et al.*[14] It is important to mention that the hydrodynamic diameter (Dh) is characterized only for SCPNs and not for polymer coils because the latter are not internally crosslinked forming a particle in water media. Similarly, zeta-potential values have been only described for particles with carboxylic acid groups.

The presence of reactive groups at the surface of the emulsion should enable the subsequent functionalization of the nanodroplets to add targeting molecules or other relevant agents.[14,19] The hydrophobic nature of the oily core of the nanoemulsions

offers potential applications as delivery agents for hydrophobic drugs. Experimental conditions were optimized to achieve small-sized (<500 nm), stable and monodispersed nanodroplets. To reach this goal, the rational design of the work included in this chapter consisted of the synthesis and characterization of different dextran derivatives and the selection/optimization of all the emulsion components: emulsifier (DXT-R), oil phase and aqueous phase. For clarity reasons, each dextran functionalization has been labelled with "D" followed by the corresponding identification number. Similarly, each emulsion produced has been labelled with "E" followed by the corresponding identification number.

3.2. Objectives

1- To evaluate the capacity of different dextran derivatives to stabilize (o/w)-emulsions.
2- To optimize experimental conditions (emulsifier weight percentage and degree of substitution; oil and oil weight percentage) to achieve small-sized (ca. 500 nm), monodisperse nanodroplets.

3.3. Results and discussion

3.3.1. Dextran derivatives (DXT-R)

Methacrylated dextran polymer (DXT-MA) (D1-D14)

Our first goal was to synthesize MA-functionalised dextran polymers in order to evaluate their capacity to stabilise mono-disperse, small sized NEs. For the synthesis of DXT-MA, a protocol previously established in our lab was used.[14] The method was based on the reaction of dextran (DXT-40, 1g) with glycidyl methacrylate (GMA, 1.2 mmol) in the presence of 4-(*N*,*N*-dimethylamino)pyridine (DMAP, 1.6 mmol) as the base and dimethyl sulfoxide (DMSO) as the solvent at room temperature. This reaction unexpectedly undergoes via trans-esterification of the glycidyl methacrylate, instead of

epoxy ring-opening, as described by Van Dijk-Wolthuis and coworkers.[6] At different time-points, the reaction was quenched by addition of 0.1M HCl and the modified dextran was purified by dialysis. Ester bonds are very sensitive to acid or basic hydrolysis thus it is important to control the pH during all process. The kinetic of the functionalization reaction was monitored by determining the degree of substitution (DS) using ^{1}H NMR. DS was calculated as the ratio between the unsubstituted glucose and the sum of both substituted and unsubstituted glucoses, expressed in percentage. Thus, assuming that for example only one hydroxyl group per glucose reacts with one MA, modified dextran having a degree of substitution of 80% implies that 80% of the repeating units of the dextran (i.e. 80% of the glucoses of the dextran) have, as an average, one hydroxyl group modified by a methacrylate group.

Pure dextran ^{1}H NMR showed proton signals corresponding to 6 glucose positions (H2-H7) in the region of 3.3-4.2 ppm and another signal at 5.0 ppm related to the anomeric proton (H1), as displayed in **Figure 11**. MA functionalization is predominant in position 3 (H3) shifting this proton signal to 5.5-4.8 region, leaving only 5 of the substituted protons in the region of 3.3-4.2 ppm. DS calculation by ^{1}H NMR is carried out by comparing the integration of the MA proton signal at 6.3-6.1 ppm (one proton) with respect to the signals at 3.3-4.2 ppm, the latter corresponding to the protons of the glucose (Glc) moiety (6 protons for unsubstituted Glc, 5 protons for substituted Glc) (see **Figure 12**).

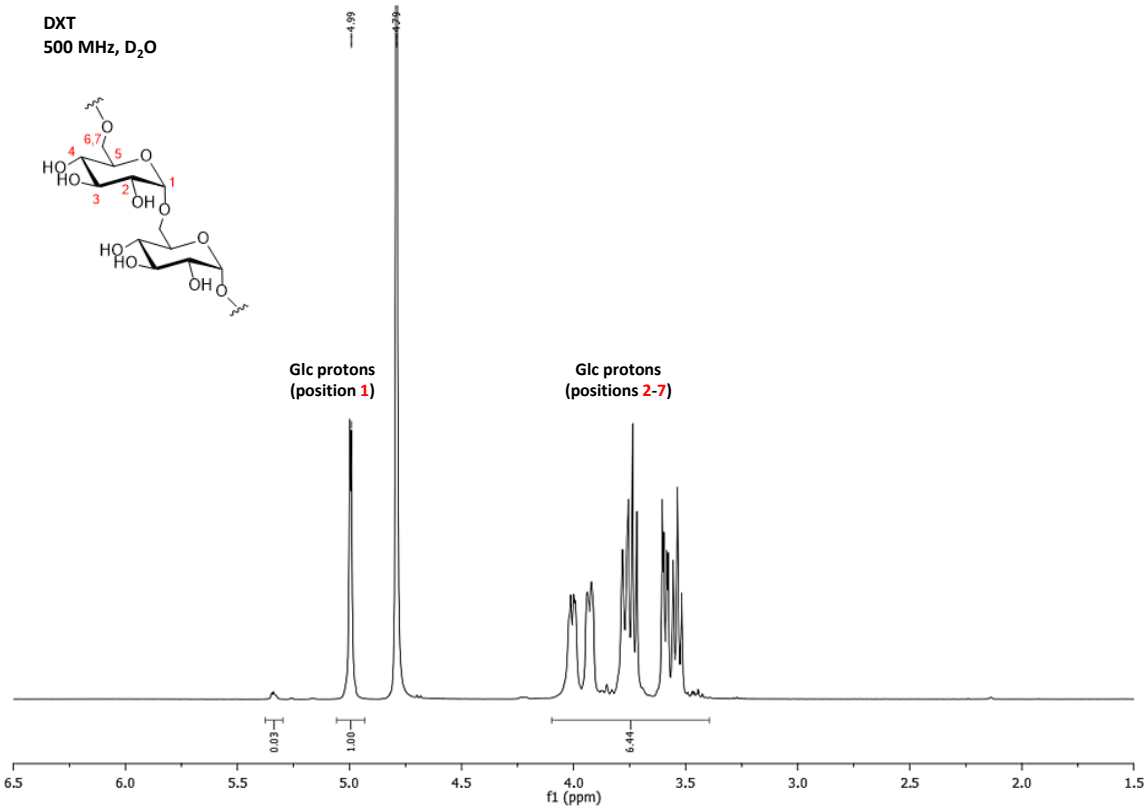

Figure 11. *^{1}H NMR spectrum (D_2O, 500 MHz) of pure DXT. DXT has been drawn as linear polysaccharide (α-1,6 glucosidic linkages) although it is known to be branched, as ramifications (α-1,3 glucosidic linkages) are also present. Protons corresponding to each glucose position (H1-H7) have been labelled in red.*

An example of this calculation with DS 52% (**D12** in table 1) is described in **Figure 12**. For this degree of substitution, the most representative signals for DS calculation in the ^{1}H NMR (500 MHz, D_2O) spectrum are those at 6.35-6.10 ppm (m, 1H, TRANS-methacrylic-CH), 5.92-5.72 ppm (m, 1H, CIS-methacrylic-CH) and 4.20-3.33 ppm (10.3H, m, rest of hydrogen atoms of Glc). Reference signals for both molecules involved in the reaction are required. Integrals of protons 1'-1 are too broad to be a clear reference and the integral of 3', despite being the main functionalized position, did not integrate the same as the methacrylic protons (1H) due to the polymer branching and the lack of selectivity of the reaction. For these reasons, DS calculation requires the subtraction of 5H corresponding to the substituted Glc in the region of 3.3-4.2 ppm (10.33 – 5 = 5.33). This difference corresponds to 6 Hydrogen atoms of unmodified Glc. Integration of one single proton present in unmodified Glc moiety was

obtained by the subsequent division against the total number of protons involved in the integral (5.33 / 6 = 0.89). DS was calculated as the ratio between the substituted Glc and the sum of both integrations (Glc + $Glc_{substituted}$) following the formula:

Equation 2. DS calculation example (D12)

$$DS(\%) = \frac{Glc_{substituted}}{Glc + Glc_{substituted}} \; x \; 100 = \frac{1}{0.89 + 1} \; x \; 100 = 52 \; \%$$

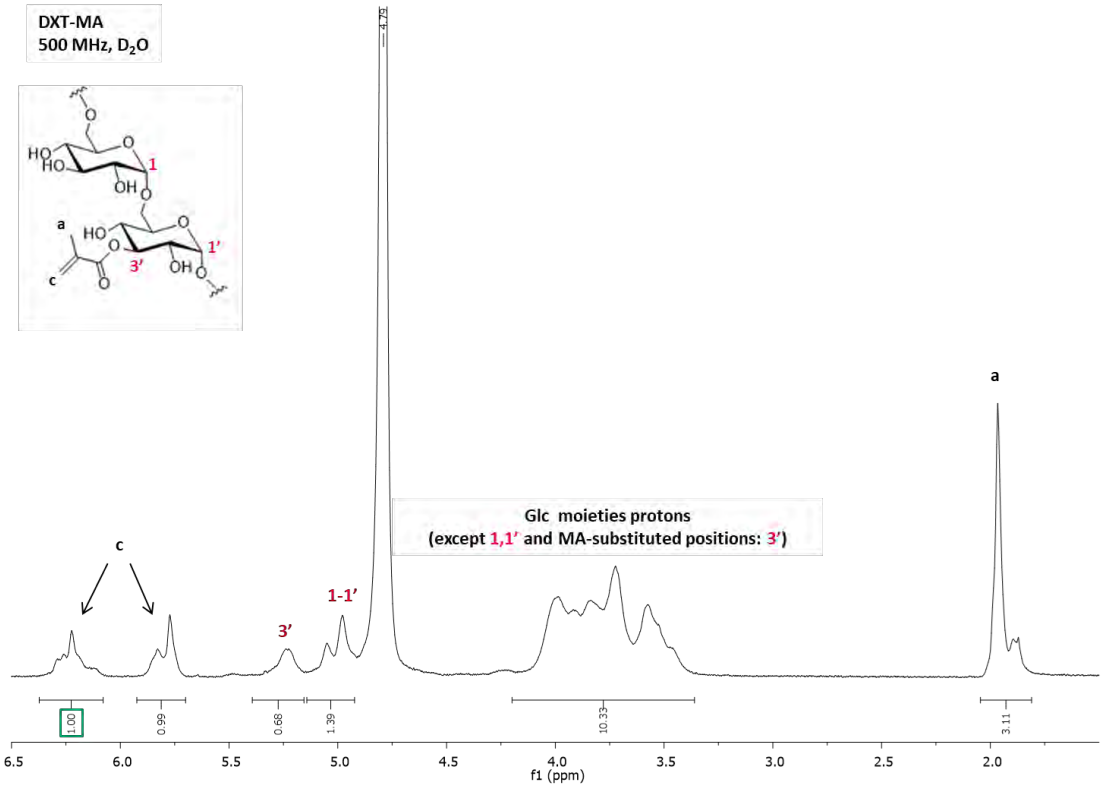

Figure 12. *^{1}H NMR spectrum (D_2O, 500 MHz) of DXT-MA with DS=52% (D12 in Table 1). For clarity reasons, only MA substitution at position 3 of glucose (Glc) has been depicted in the chemical structure insert. Protons shifted from Glc region of 3.3-4.2 ppm (H1, H1' and H3') are labelled in red and protons from MA moiety are described with letters "c" (2H, methacrylic-CH) and "a" (3H, methacrylic-CH_3).*

The DS values obtained at different reaction times are summarized in Table 1. Due to the poor solubility and branching of the polymer, DS variability at early times is significantly high. Furthermore, it is important to mention that ^{1}H NMR quantification accuracy has limitations but DS calculations are a useful tool for determining the ratios

between the species of interest. Similarly to results obtained by van Dijk-Wolthuis and coworkers,[20] the DS increases when increasing reaction time.

Table 2. Degree of substitution (DS) at different reaction times for the DXT modified with methacrylate group after reaction in DMSO with GMA at 25°C, in the presence of DMAP as the catalyzer.

Name	DS (%)	Time (hours)
D1	1	3
D2	8	7
D3	10	15
D4-D7	18 ± 5*	16
D8	28	24
D9	36	31
D10	45	48
D11	50	55
D12	52	66
D13	55	72
D14	70	104

*DS (Mean ± SD %) calculation based on polymers obtained after 16 hours reaction: D4 (DS=13%), D5 (DS=15%), D6 (DS=19%) and D7 (DS=24%).

Dextran-MA based single-chain polymer nanoparticles (DXT-SCPN-MA) (D15)

Single-chain polymer nanoparticles (SCPNs) based on synthetic polymers allow the rational design of precursors that can result in SCPNs with a desired size and functionality. Synthetic routes to obtain SCPNs are mainly based on intra-chain coupling or cross-linking-induced collapse of the pre-functionalized polymers. In this case, DXT-MA was reacted with 3,6-dioxa-1,8-octane-dithiol (DODT) through thiol-ene Michael addition at pH= 9.5 and room temperature following a previously established method[14]. **D15** was purified by dialysis and the hydrodynamic diameter (Dh = 13 ± 8 nm) and polydispersity index (PDI = 0.2) were determined by DLS (Figure 13). Crosslinking degree was measured by ^{1}H NMR (**Figure 14**). In this case, crosslinking results in the decrease of the methacrylic-CH signals due to the addition of the thiol functional groups of the DODT linker into the methacrylate group. Furthermore, new proton signals appeared in the 3.06-2.53 ppm region (5H: b', c' and d) and at 1.3 ppm (3H: a') corresponding to the protons of DODT linker. Both signals allow the

quantification of the crosslinking degree. To simplify, the region of 3.06-2.53 ppm has been selected to estimate the degree of crosslinking of the SCPNs. With that aim, single proton integration value from DODT moiety has been calculated by determining the ratio between the previously mentioned integral, corresponding to 5 protons at 3.06-2.53 ppm, and the total number of protons involved in the signal (integral value / number of protons = 5 / 5 = 1). Thus, proton integrals due to glucose-MA and glucose-linker moieties equal 1, which means that both show the same degree of substitution/crosslinking. Reaction yield was complete because SCPNs formation required 0.5 thiol equivalents based on the total MA groups present in DXT-MA, which correspond to 0.25 equivalents of DODT crosslinker (which possess 2 thiol groups). In this approach, DXT-SCPN-MA (**D15**) has 26% of MA substitution and 26% of MA-crosslinker substitution leading to the original DS of 52%.

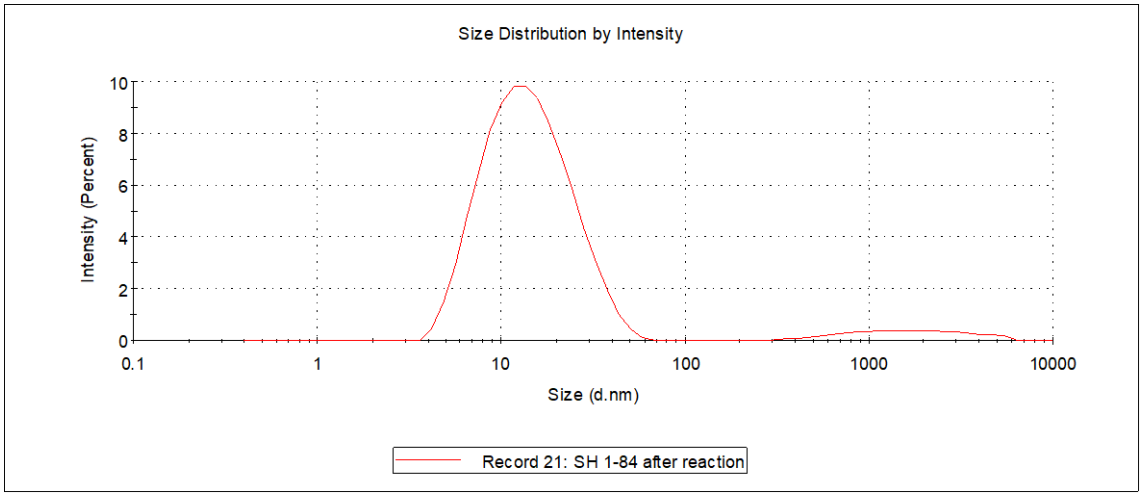

Figure 13. Size distribution of intensity-average diameter *for DXT-SCPN-MA **(D15)** obtained by DLS in PBS at 10 mM, pH 7.4, and 25°C. Reprinted from Gracia et al* [14] *with permission.*

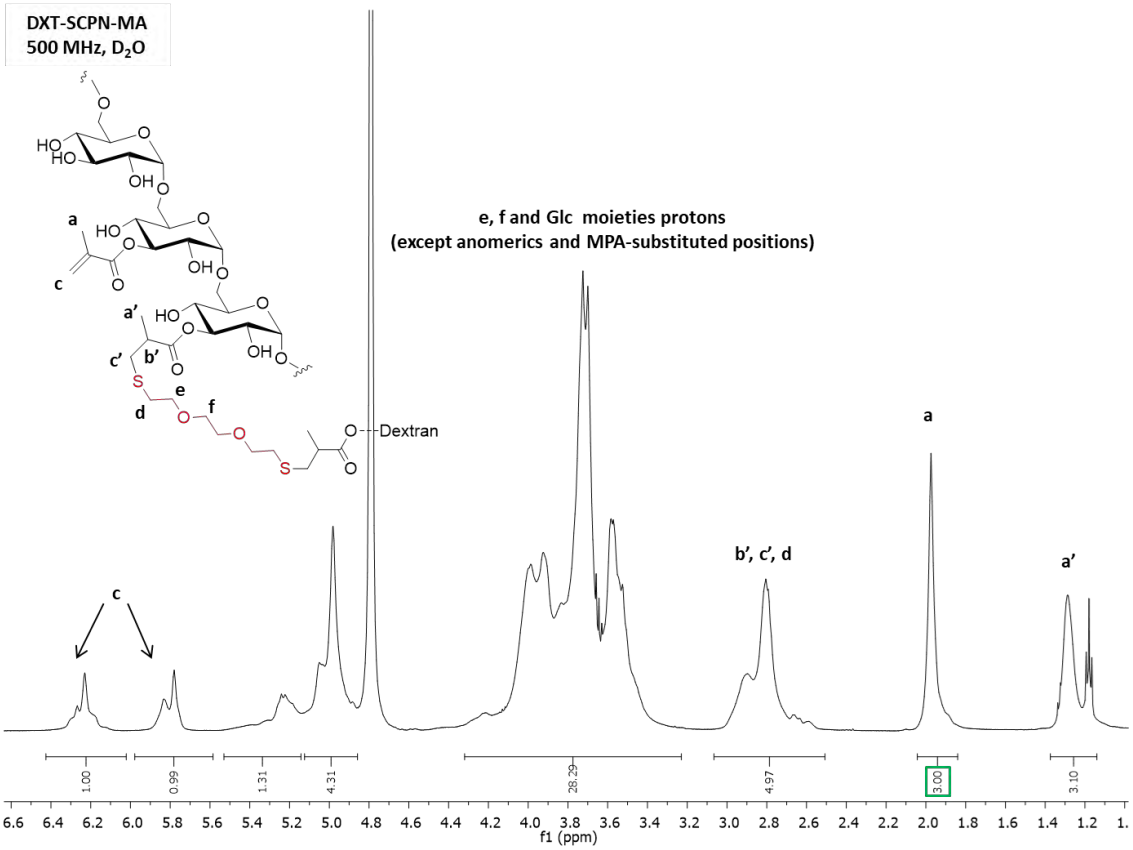

Figure 14. *^{1}H NMR spectrum (D_2O, 500 MHz) of DXT-SCPN-MA* ***(D15).*** *For clarity reasons, only protons from the functionalized moieties (MA and MA-Crosslinker) have been labeled.*

Dextran-quenched single-chain polymer nanoparticles (DXT-SCPN-F) (D16)

To study the effect of the functional group on the interfacial activity, DXT-SCPN-MA was quenched, changing MA groups by carboxylic acids, based on a previously reported method.[14] The functionalized DXT-SCPN-F was achieved by slow addition of 3-mercapto propionic acid (MPA, 7.5 µmol) to the reaction flask containing **D15** at pH= 9.5. Thio-Michael addition was performed on the unreacted MA groups leading the final SCPN structure with terminal carboxylic acid groups (-COOH). After purification by dialysis, the resulting solution was freeze-dried to obtain nanoparticles as a white solid powder that were characterised using ^{1}H NMR (**Figure 15**, **D16**). In this case, a new signal appeared in the range of 2.75-2.33 ppm corresponding to 2H (CH_2S, g) of MPA. Quantitative reaction of the methacrylic functional groups was confirmed by ^{1}H-NMR,

where the signals corresponding to both methacrylic-CH bonds above 5.5 ppms, disappeared completely.

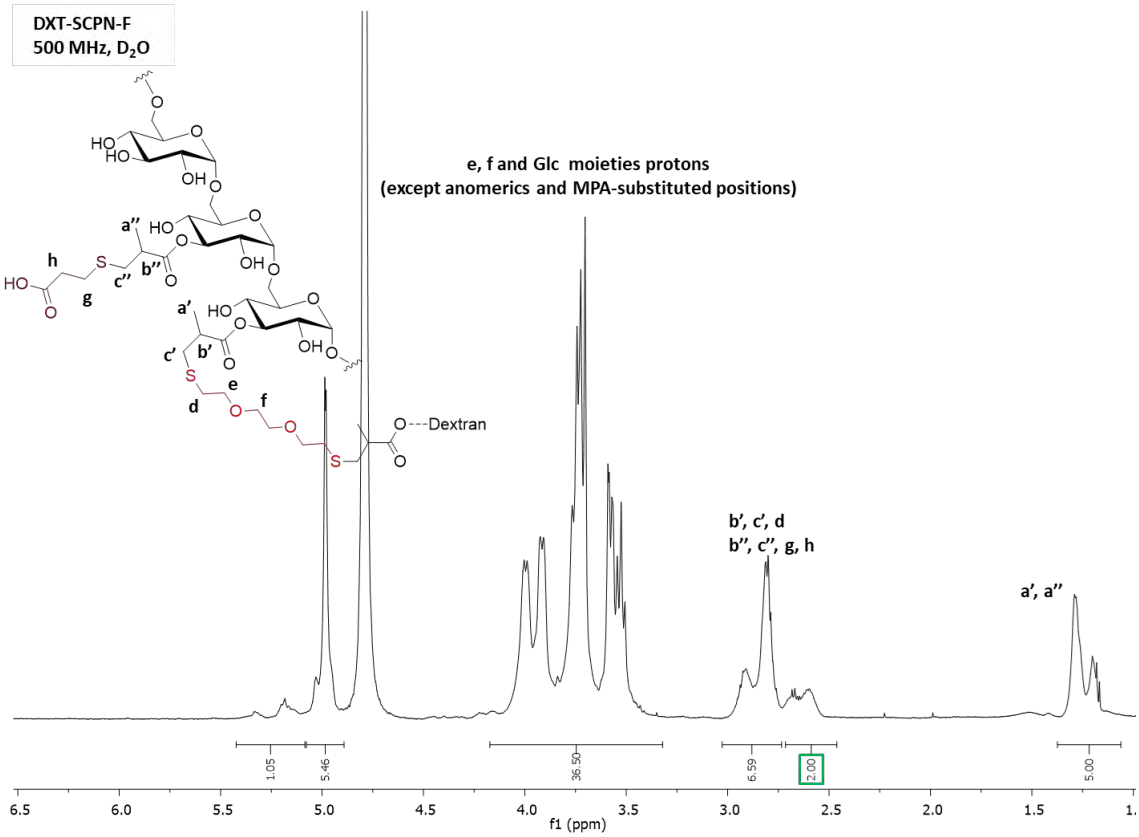

Figure 15. *^{1}H NMR spectrum (D_2O, 500 MHz) of DXT-SCPN-F (**D16**). For clarity reasons, only protons from the functionalized moieties (MPA and MA-Crosslinker) have been labeled.*

TEM images (**Figure 16**) showed an average diameter of 13 ± 3 nm, while Dh and Zeta-potential were 15 ± 4 nm (PDI 0.2) and -20mV ± 5 (pH = 7.2, 25°C), respectively.

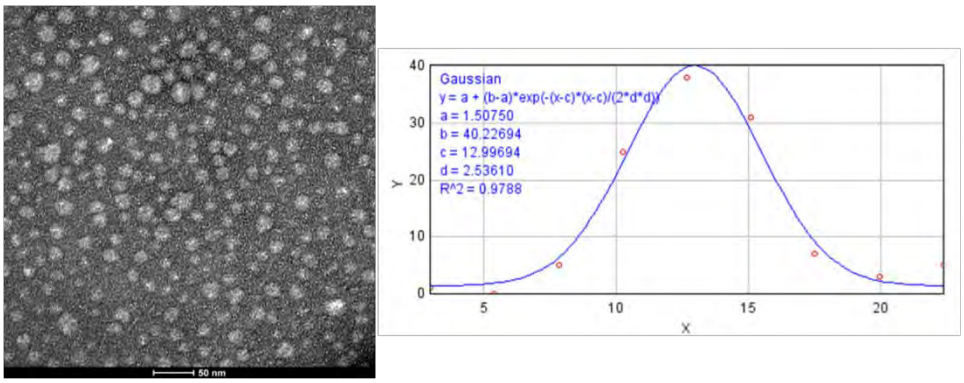

Figure 16. *TEM picture (uranyl staining) and distribution analysis (number-average diameter calculated by ImageJ platform using a Gaussian curve fitting after counting about 300 nanoparticles) of DXT-SCPN-F **(D16)**. Reprinted from Gracia et al [14] with permission.*

Carboxylate functionalized dextran polymer (DXT-F) (D17)

The methacrylate group of DXT-MA was also substituted by a carboxylic acid to evaluate the effect of the functional group on the interfacial properties of modified DXT. Carboxylate functionalized polymer (**D17**) was synthesized following a similar process to that described for **D16**. A solution of 3-mercaptopropionic acid (4.9 µmol) was slowly added to a previously prepared solution containing 350 mg of DXT-MA (**D12**, **Table 2**) at pH=9.5. The reaction was maintained under constant stirring for 12 h to functionalize all MA groups and then purified by dialysis to yield the quenched polymer as a white solid. As shown in the ^{1}H NMR spectrum (**Figure 17**), proton signals from methacrylic-CH above 5.5 ppm disappear, confirming total quenching of the unmodified MA groups presented in original polymer DXT-MA (**D12**). Zeta potential values were -12 mV ± 7 (pH = 7.2).

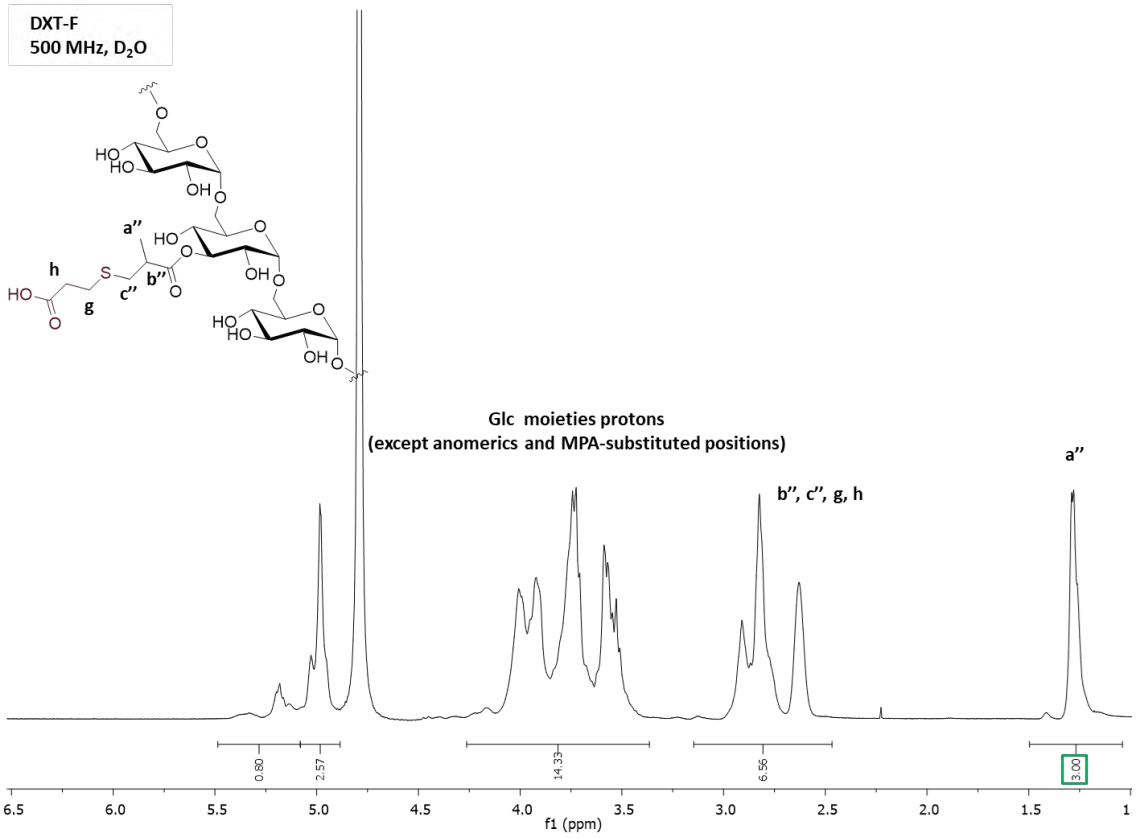

Figure 17. *^{1}H NMR spectrum (D_2O, 500 MHz) of DXT-MA functionalized with mercaptopropionic acid (DXT-F)* ***(D17)****. For clarity reasons, only protons from the MPA-functionalized moieties have been labeled.*

3.3.2 Modified dextran as oil-in-water (o/w)-emulsion stabilizer

Optimization of the emulsion

DXT-based SCPNs previously patented in our research group (**WO 2016/071258 A1**)[21] are very hydrophilic, and this limits their capacity to carry hydrophobic drugs. Hence, we considered their potential use as oil-in-water emulsion stabilisers; as such emulsions could become excellent nanocarriers capable to entrap hydrophobic drugs. Emulsion droplet size distribution has been characterized using: Dynamic Light Scattering (DLS; *Z-average*), Laser Diffraction (LD; *volume-average*) and Transmission Electron Microscopy (TEM; *number-average*). For a better comparison of the four DXT derivatives, the resulting emulsions were evaluated based on droplet size (diameters < 500 nm are preferable) and predefined stability criteria. More concretely, emulsions have to fulfil two criterion to be stable and hence allowing droplet size characterization; (i) preservation of emulsion physical integrity (no phase separation) as judged by visual inspection for a minimum of 5 days and (ii) size distribution of at least 5 consecutive LD measurements must be overlapped.

It is important to mention LD is performed under recirculation (1000-3000 rpm) while DLS measurements are performed statically, which may result in sedimentation, agglomeration, creaming or related effects in many cases. Recirculation of the samples inherent to LD measurement gives a fairly good indication of the stability of the emulsion under low shear, with the overlapping of at least 5 consecutive measurements. DLS technique has been optimised for monodispersed populations in a range of 1-1000 nm. On the contrary, LD is more suitable for non-uniform dispersions in a range of 1-1000 µm.[22] Considering that ultrasounds production of emulsions is unable to generate highly monodisperse emulsions and taking into account that the main size population is above 100 nm, LD has been considered more appropriate than DLS for size distribution characterization.

In our first approach, an aqueous solution of dextran based SCPN (DXT-SCPN-F, **D16**) (1 mL, 1 wt%) was emulsified via sonication during 2 min in the presence of dodecane oil (1 g) generating a characteristic milky emulsion **(E4)**. However, creaming effect

(migration of the lighter oil droplet to the top of the aqueous phase) was observed. Unexpectedly, this emulsion was actually stable for 3 weeks, in spite of the fact that the presence of carboxylic acids confers a highly hydrophilic character to the SCPN. This result was in disagreement with those reported by Morse and coworkers,[23] where the increase in hydrophilicity of the pickering stabilizer finally leads to demuslficiation. In this case, demulsification did not occur until the third week, and hence, more work would be required to obtain meaningful conclusions about the stabilization mechanism. On the other hand, the presence of DODT linker that has been also used to stabilize (o/w)-emulsions in section **4.3.2. Crosslinking assessment by PBS challenge** could confer certain interfacial activity to DXT-SCPN-F to produce stable emulsions. As DXT-SCPN-F proved to be a relatively good emulsifier for dodecane oil, it was decided to verify the interfacial activity of all the starting and intermediate materials involved in the preparation of the NPs, i.e. pristine dextran, methacrylate-functionalized dextran polymer (DXT-MA, **D12**), carboxylate functionalized dextran polymer (DXT-F, **D17**) and methacrylate-functionalized dextran SCPN (DXT-SCPN-MA, **D15**). Results suggested that DODT linker is not responsible for the interfacial properties to DXT-SCPN-F or DXT-SCPN-MA because even without linker, DXT-MA or DXT-F, stable emulsions were produced. The unmodified dextran polymer did not show any interfacial activity as a clear phase separation was observed one hour after emulsification with dodecane oil (**Figure 18, E0**). On the other hand, all modified dextran with functional group, containing either methacrylate or carboxylic acid, could act as efficient stabilizers for dodecane oil droplets **(E1, E2** and **E3)** at 50 wt% using 1 wt% of modified DXT based on the oil phase, as seen in **Figure 18**.

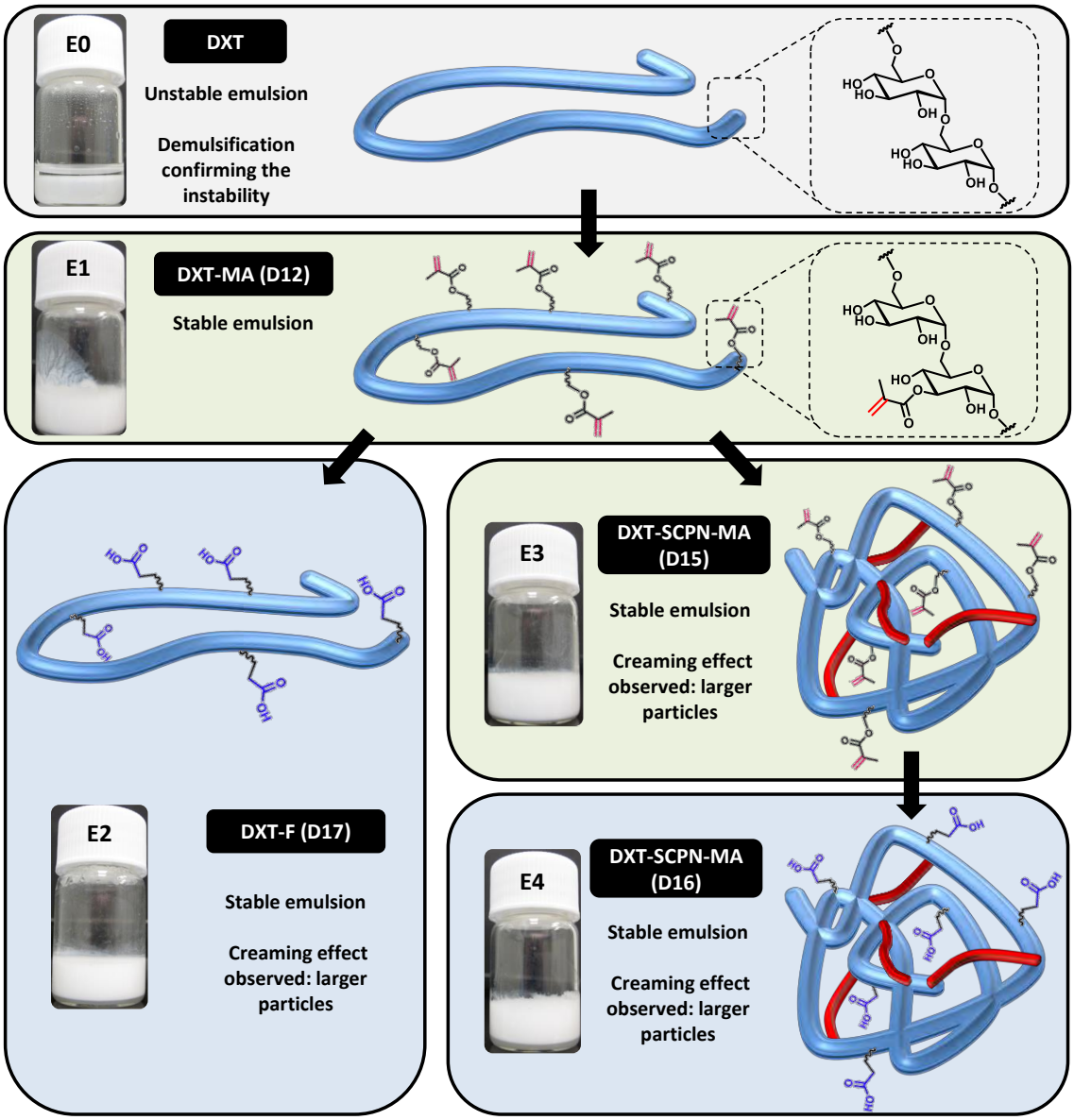

Figure 18. *Dextran functionalization and its use as oil-in-water emulsion stabilizer. Schematic representation of physicochemical structure and synthetic steps required for functionalized dextrans (DXT, D12, D17, D15 and D16) combined with digital photographs of the resulting O/W emulsions after 24 hours at rest (E0, E1, E2, E3 and E4, respectively) prepared at 10 wt.% dodecane oil and stabilized with 0.5% wt. of functionalized dextran.*

Characterization of the obtained emulsions demonstrated that oil-in-water type emulsions were achieved in all cases when DXT-F, DXT-MA, DXT-SCPN-MA, DXT-SCPN-F were used as stabilizers (**Appendix I. Production and Characterization of dextran-based emulsions**). Determination of the droplet size was carried out by means of DLS and LD. Noteworthy, sizes obtained for the emulsion produced at 50 wt% dodecane oil

are in the upper limit of the DLS detection; hence, laser diffraction was considered to be more appropriate to obtain a reliable estimation of the droplet size. The smaller droplet diameters were obtained when the emulsifier contained methacrylate groups, while larger droplets were obtained carboxylic acid-functionalised dextran. Such results were expected as the presence of methacrylate group confers hydrophobicity to the polymeric material, consequently increasing its affinity towards the hydrophobic oil. Thus, the creaming effect observed for DXT-F and DXT-SCPN-F was in good agreement with the larger droplet size obtained.

The results obtained suggested that slight hydrophilic and hydrophobic modifications on the dextran can confer interfacial activity to the natural polysaccharide. In our preliminary experiments described above, only dodecane was tested (E0-E4). However, this oil is not really relevant for bio applications. Hence, we tackled the evaluation of the interfacial properties of the different modified DXT with different oils, such as olive oil, sunflower oil, fish oil (rich in Omega 3 which has shown anti-inflammatory effect [24,25]), peppermint oil and eucalyptus oil (see **Appendix I. Production and Characterization of dextran-based emulsions**). Unfortunately, low quality and unstable emulsions were obtained with the latter two. Interestingly, the different modified dextran could stabilize emulsions prepared with olive, sunflower and fish oil. To evaluate their differences, growing amounts of dextran modified emulsifiers, DXT-F (**D17**), DXT-MA (**D12**), DXT-SCPN-F (**D16**) and DXT-SCPN-MA (**D15**), were used to generate (o/w)-emulsions using 10% wt. olive (**E9**, **E17**, **E36-E45**; **Appendix I**) or sunflower (**E14**, **E20**, **E46-E55**; **Appendix I**) oils. Size characterization was also performed by Laser diffraction (LD) and Dynamic Light Scattering (DLS) in order to determine the most suitable stabilizer for producing submicrometer and monodisperse (o/w)-emulsions (**Figure 19**).

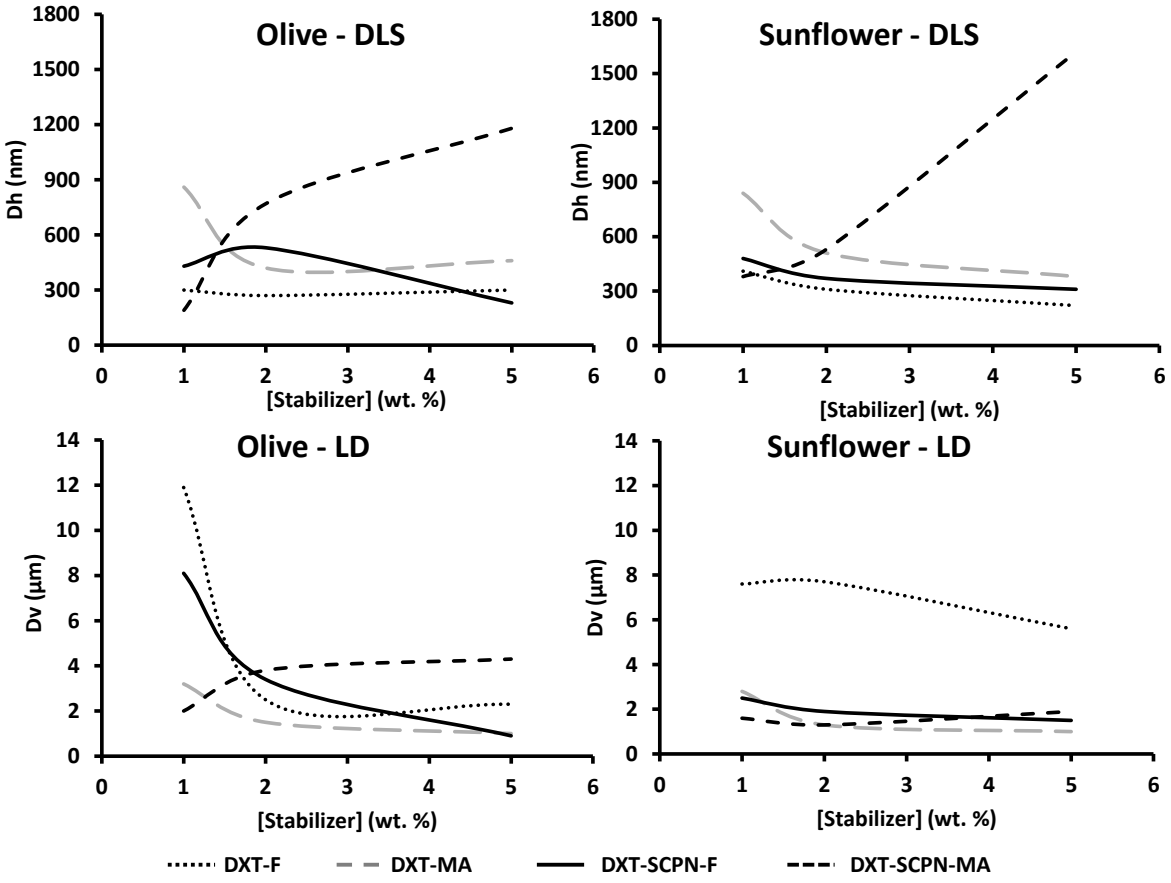

Figure 19. *Effect of the type of emulsifier (DXT-F, DXT-MA, DXT-SCPN-F and DXT-SCPN-MA) and its concentration (1% wt., 2% wt. and 5% wt. related to the oil phase) on the droplet size of oil-in-water emulsion prepared at 10% wt. oil phase (olive or sunflower) measured by Laser diffraction (LD) and by Dynamic Light Scattering (DLS), which Volume-average diameter (Dv) and Hydrodynamic diameter (Dh), respectively.*

Regarding to the emulsifier content, an aqueous solution containing 0.5 wt% of modified dextran (5 wt% based on the oil phase) seems the most suitable concentration to obtain smaller droplets with the lowest polydispersity. A rational understanding suggests that increasing amounts of emulsifier would lead in decreasing droplet diameter. This pattern was observed in all cases except for DXT-SCPN-MA in DLS which tendency is just the opposite for both oils. However, this emulsifier is not following the same tendency when using LD. One explanation could be related to the restricted morphology of DXT-SCPN-MA, due to the presence of DODT cross-linker, because some MA groups can be facing the water phase once located at droplet interface. This could generate droplet aggregation when measurement is performed in

a static fluid (i.e. DLS), due to the presence of non-polar interactions between the water-faced MA groups of the surrounding droplets. On contrary, same functionalization without internal restrictions, as the case of DXT-MA, is not generating aggregation when increasing concentration (see **Figure 19**). Thus, DXT-MA would be able to self-orientate MA moieties to majority face the oil phase avoiding droplet aggregation. Another explanation for this phenomenon, considering that DXT-SCPN-MA is worse emulsifier than DXT-MA at the same concentration, is related to the "real" droplet size of DXT-SCPN-MA stabilized emulsions. At low emulsifier concentrations, most of the droplets would be too big to be visualized by DLS because of the fast creaming effect (**Figure 19**). However, when increasing emulsifier concentration smaller droplets would be generated contributing to slow down the creaming effect. These effect would allow the observation of big droplets which were not enough big to rapidly escape from the field of view of DLS during the measurement. Generally speaking, DXT-F emulsions showed the smallest droplet size for each experimental condition when using DLS. However, broad and multimodal size distributions obtained by LD suggested a non-optimal assembly of this polymer at the interface as observed in **Figure 20**.

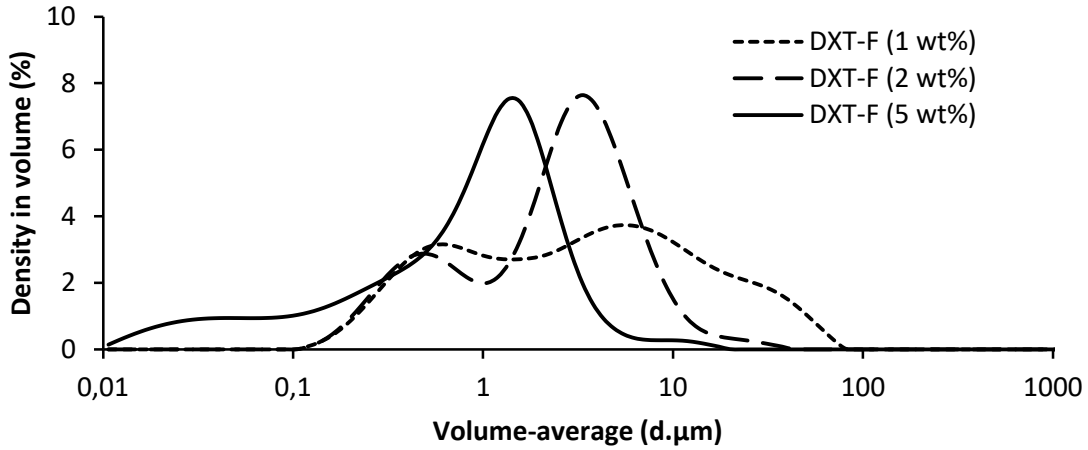

Figure 20. *Effect of DXT-F weight percentage (1% wt., 2% wt. and 5% wt. related to the oil phase) on the droplet size distribution of (o/w)-emulsions prepared at 10% wt. olive oil measured by Laser diffraction (LD).*

On the other hand, DXT-SCPN-F showed consistency for the droplet diameter obtained with both techniques, as the diameter decrease with increasing amount of emulsifier,

except for olive oil at 2% wt of emulsifier as judged by DLS (**Figure 19**). This diameter was very similar to that obtained for 1% wt of DXT-SCPN-F suggesting an experimental failure occurred. A similar trend was observed with DXT-MA. It is worth pointing that using DXT-MA emulsifier resulted in an emulsion with the smallest droplets as measured by LD. Furthermore, the preparation of DXT-MA is much easier (and less costly) as this is the first modification of DXT sufficient to confer interfacial activity to the polysaccharide. Thus, DXT-MA was selected as the best dextran functionalization to produce (o/w)-nanoemulsions being 0.5 wt% of emulsifier considered for the rest of the study.

Concerning the oil, results were not enough robust to consider olive or sunflower as the oil phase for the following experiments. High variability between emulsifiers did not allow a proper oil phase selection. To that aim, previously selected emulsifier, DXT-MA (**D12**), was evaluated again including fish oil because of the benefit of providing anti-inflammatory response.[24] As it can be seen in **Figure 21**, results clearly indicate that fish oil generates smaller droplets. This experimental fact, together with the anti-inflammatory properties, was taken into consideration to select fish oil as the best choice for further investigations.

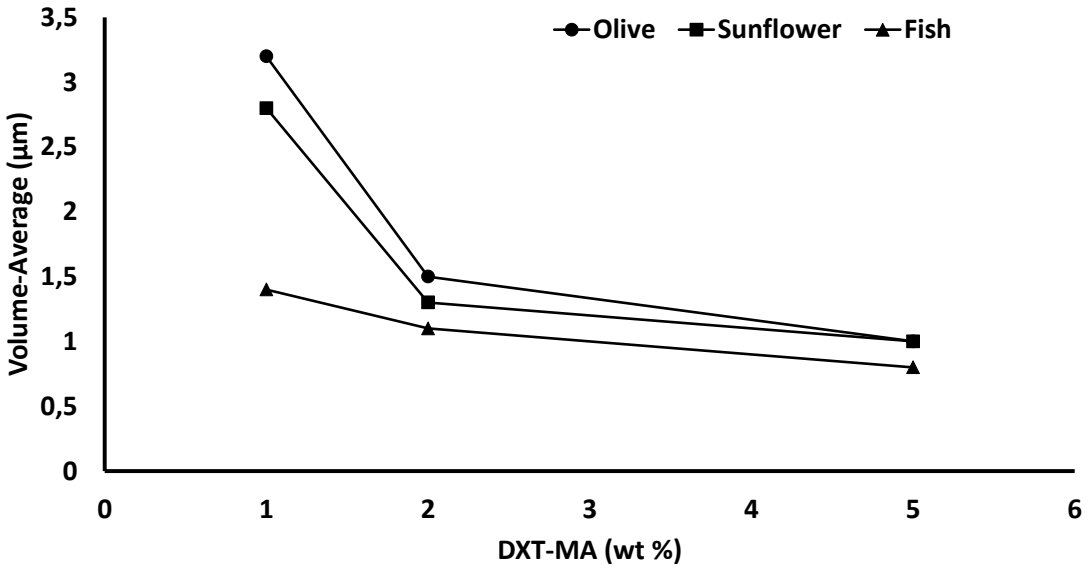

Figure 21. *Effect of the amount of DXT-MA (**D12**) emulsifier (based on the oil phase) on the droplet size of oil-in-water emulsions produced at 10% wt. for different commercial oils, i.e. olive, sunflower and fish oils, measured by Laser diffraction (LD).*

Effect of the degree of substitution (DS) on emulsion droplet size

With a selected formulation based on DXT-MA at 0.5 wt% and fish oil at 10 wt%, the effect of the DS of the polysaccharide was studied. First, functionalization with methacrylate groups was investigated and DXT-MA with 1 **(D1)**, 8 **(D2)**, 15 **(D5)**, 19 **(D6)**, 28 **(D8)**, 36 **(D9)** and 50 **(D11)** % of methacrylate groups were produced. The droplet diameters were found to be between 250 and 700 nm as judged by DLS while LD confirmed that droplets with a diameter between 0.6 and 1.9 microns (**E59-E65, Appendix I**) were obtained with monomodal distribution. However, visual inspection of the emulsions demonstrated that DXT-MA containing less than 8 % methacrylate lead to phase separation in less than 2 days while emulsions stabilized with DXT-MA in the range of 8-15 % MA remained stable up to 5 days. On contrary, emulsions stabilized with MA substitutions above 15 % remained stable for weeks (stored in water media at 4^{o}C).

Thus, the smaller droplet size for the production of stable emulsions was obtained for DXT-MA with DS between 15 and 28 % of methacrylate groups (**Figure 22**), as judged by laser diffraction. Surprisingly, higher degree of functionalization resulted in larger droplet diameter. DXT-MA functionalized with more MA groups would expect to wet better the oil, contributing to decrease the interfacial tension, which should lead to smaller droplets. Despite this tendency, new size population below 100 nm appeared when 50 % MA substitution suggesting that higher DS could eventually lead to smaller droplets or broader size distributions (**Figure 22**).

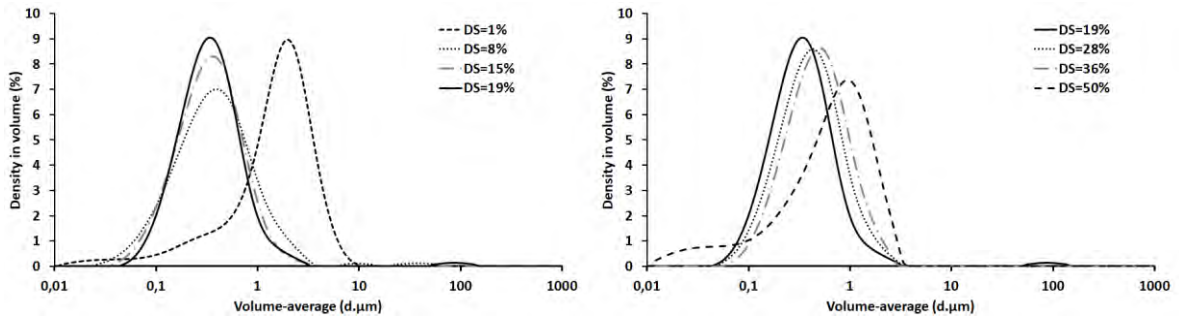

Figure 22. *Size determination by laser diffraction of emulsions with 10% wt. of fish oil (DHA) and 5% wt. of DXT-MA with MA substitution percentages of* 1 (**D1**, **E59**), 8 (**D2**, **E60**), 15 (**D5**, **E61**), 19 (**D6**, **E62**), 28 (**D8**, **E63**), 36 (**D9**, **E64**) and 50 (**D11**, **E65**).

To confirm these preliminary results in other oils and to identify the minimum DS required to obtain stable emulsions, DXT-MA polymers were produced with DS of 13, 36, 50 and 70 %. Those DXT-MA were prepared and tested as emulsifiers using 10% wt. of sunflower oil as dispersed phase. In that case, all emulsions prepared showed good stability over time except for DS=13% which remained stable during one week. A closer look at the diameter measured by laser diffraction confirmed that increasing the degree of substitution of the DXT-MA resulted in an increase of the final droplet diameter (**Figure 23**). Thus, the selection of the optimum DS is based on (i) emulsion stability and (ii) droplet size. Emulsion stability criteria was defined as the absence of phase separation, along with the overlapping of 5 consecutive runs in LD, after one-week stored at 4°C. Once stable, droplet size distributions should be monomodal having the minimum possible diameter. Following this criteria, the optimum DS for DXT-MA to obtain the smaller, monomodal and at least one-week stable droplets, based on this study, was found between 13 and 36 %.

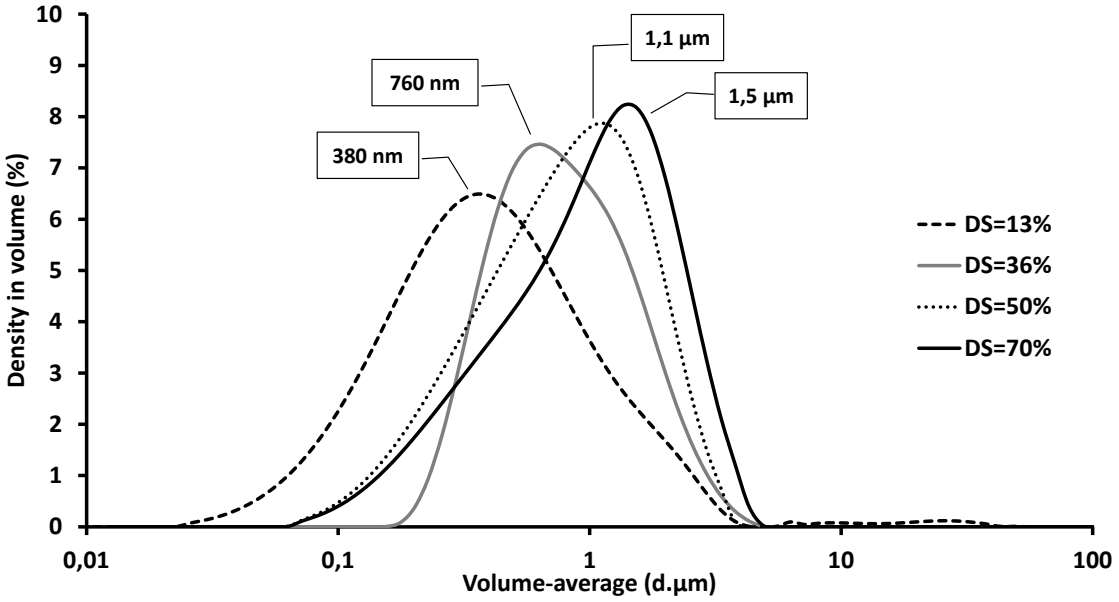

Figure 23. *Size comparison by laser diffraction of emulsions with 10% wt. of sunflower oil and 5% wt. DXT-MA. DS from left to right: 13% (**D4**, **E66**), 36% (**D9**, **E67**), 50% (**D11**, **E68**) and 70% (**D14**, **E69**).*

Regarding the broad size distribution for 13 % substitution and the lack of stability after one-week storage, we decided to fix the minimum DS necessary in 15 %. Therefore, DS values in the range 15-36% were considered optimal for our study purposes as they provided small and highly stable emulsion droplets with low polydispersivity. Moreover, emulsions were analysed by TEM to obtain meaningful conclusions about droplet morphology. It is worth to point out that staining is necessary for soft matter visualization in TEM. Nevertheless, this technique is only useful for shape characterization but not for size distribution analysis. This is because drying process related to staining could lead to droplet smash overestimating droplet diameter, hence, Cryo-TEM analysis would be needed to properly evaluate droplet size. On the other hand, phosphotungstenic acid (PTA) negative staining of a representative example of a nanoemulsion with DS=24% demonstrated droplets spherical shape (**Figure 24**).

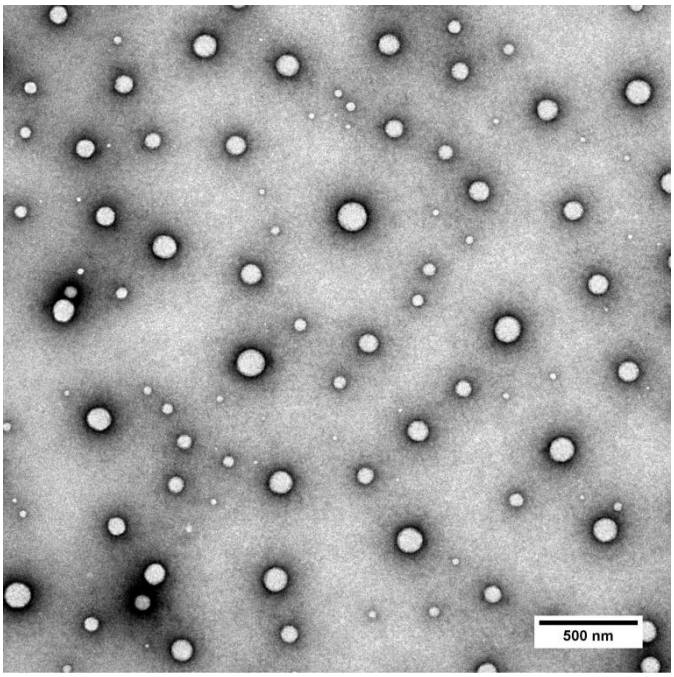

Figure 24. *TEM of DXT-MA-(D7, DS=24%) based (o/w)-emulsion (**E70**) seen by negative-stain electron microscopy. Negative staining with phosphotungstenic acid solution (PTA, 1% w/v).*

Effect of DS in surface tension (ST)

As described in section **1.1.4. Nanoemulsions in nanomedicine** of the introduction chapter, the formation of spheres is resisted by the interfacial tension as determined by the Young-Laplace equation.[26] The surface tension acts to reduce the surface area and hence the volume of the drop, while the pressure difference (p_α-p_β) acts to increase the volume of the drop. Surfactants act diminishing the surface tension, which contributes to droplet formation and stabilization by allowing the counterbalance of these two tendencies to achieve the equilibrium condition.

The surface-active properties of DXT-MA have been determined by measuring the steady state surface tension of water as a function of the polymer concentration. The results were plotted against the logarithm of the polymer concentration in water, as shown in **Figure 25**.

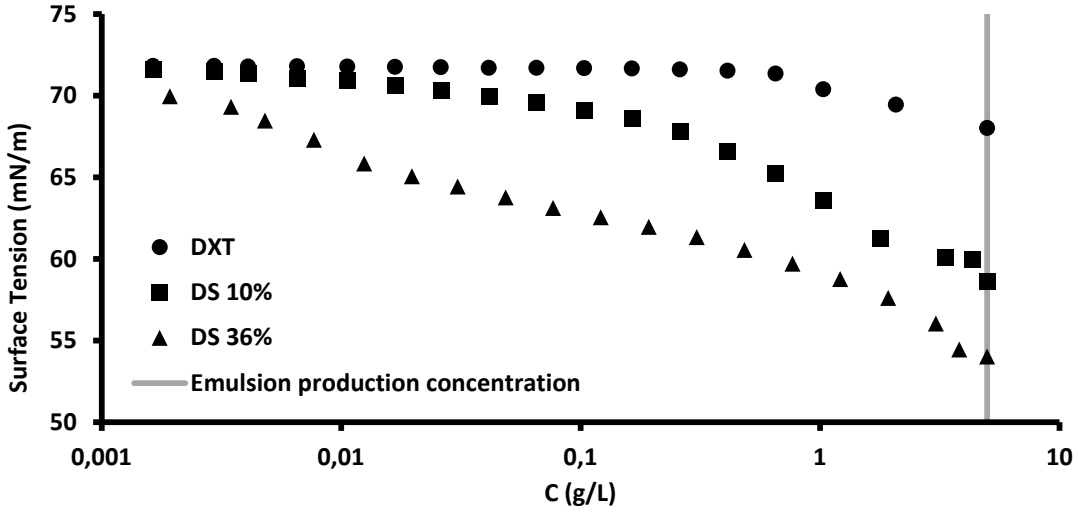

Figure 25. *Graphic representation of surface tension of aqueous polymer solutions, for pure dextran (DXT), D3 (DS=10%) and D9 (DS=36%) versus polymer concentration and a representative line at the optimal concentration fixed for emulsions production (5 g/L).*

As can be seen, higher DS values lead to lower surface tension values at the same surfactant concentration, irrespective of the concentration in the range 0.002-5 g/L. These results are in accordance with those observed in the production of DXT-MA stabilized emulsions with different DS. This means, polymers with higher DS values

seems better surfactants as far as they can reach lower ST at lower surfactant concentration. To confirm this, and taking into account that the surfactant concentration for the production of emulsions was initially fixed at 0.5% wt. = 5 g/L (see above), the surface tension of DXT-MA with different DS, in the range 0-57%, was measured at this particular concentration (**Figure 26**). The results confirm that higher DS values lead to progressive decrease in ST values, as expected. Thus, functionalization is clearly affecting the interfacial properties of the polymer. Noteworthy, ST values for D3 and D5, with DS at 10 and 15 % respectively, are around 58 mN/m. These results combined with those obtained for emulsion formation and stability suggest that 58 mN/m is the minimum ST required to stabilize emulsions, nevertheless, DS above 15% are required to fulfil the predefined stability criteria.

Name	DS (%)	ST (mN/m)
DXT	0	68,02
D2	8	65,62
D3	10	58,53
D5	15	58,61
D9	36	54,02
D11	50	46,82
D13	57	44,30

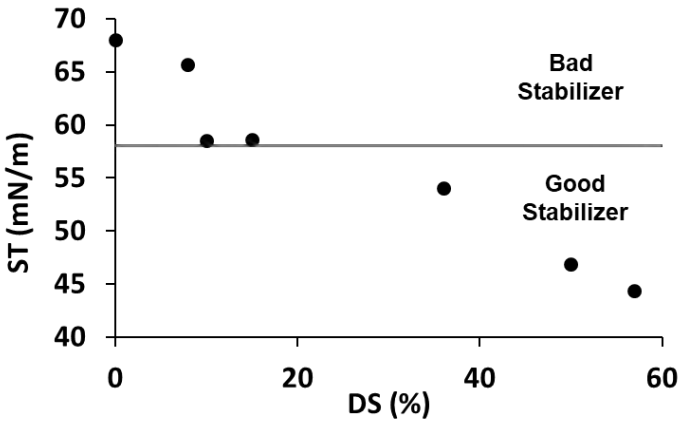

Figure 26. From left to right; Surface tension (ST) of DXT and DXT-MA with different DS, *Graphical criterion to define the minimum DS needed for this application.*

For a better understanding of this phenomena, a simple experiment was carried out with the same aqueous DXT-MA solutions described above by shacking vigorously for 20 s the vials in order to verify the adsorption of the modified polysaccharides at the air/water interface, via the formation of foam (**Figure 27**). Clearly, DXT-MA with higher DS generates more foam, as judged by visual inspection, which is also related with the reduction of the ST. Moreover, pristine dextran and DXT-MA with DS at only 8 % did not show any foam formation and similar values of ST (68.02 and 65.62, respectively) indicating that these polymers are not enough surface actives to produce stable

emulsions at these conditions. On the other hand, despite DS at 10 and 15 % achieved similar ST values (58.53 and 58.61, respectively), only 15 % have demonstrated their capability to produce foams. This result was in good agreement with those obtained previously, suggesting 15 % of MA groups as the minimum substitution required for producing stable emulsions at the concentration of 5 g/L. Thus, we have selected this criterion, ST<58 mN/m at 5 g/L, together with the predefined stability criteria to fix the minimum DS needed for each DXT to act as emulsion stabilizer in 15 %.

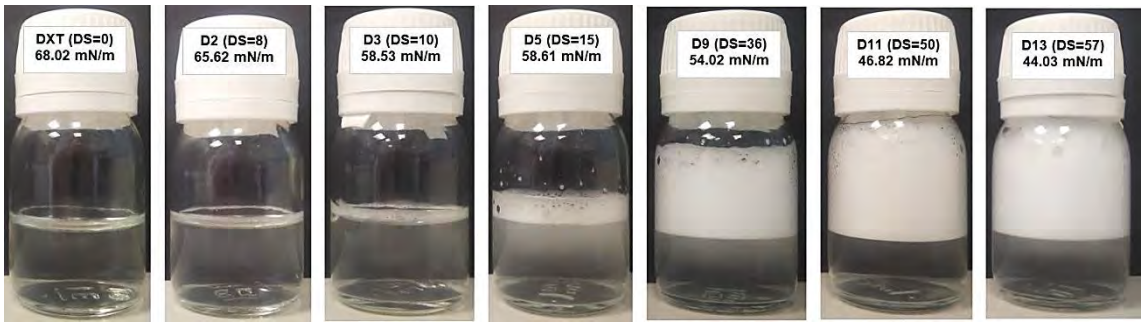

Figure 27. *Digital pictures of aqueous solutions of DXT-MA (DS: 0-57 %) at the concentration of 5 g/L after being shacked for 20 seconds.*

3.4. Summary and Conclusion

Pure dextran is not able to act as oil-in-water (o/w) emulsion stabilizer. However, simple dextran modifications (DXT-R) can confer interfacial activity to the polysaccharide. All DXT-R prove their capability to act as emulsifiers, including those modified hydrophilically. Nevertheless, DXT-MA (modified with methacrylated groups, MA) has been selected as the best stabilizer for the final application due to its facile synthesis in addition to the lower polidispersity and smaller droplet diameter obtained when used as emulsifier for oil-in-water emulsion. Different stabilizer amounts have been tested in order to find the optimum emulsifier weight percentage which has been finally established at 0.5 wt. %. fish oil because resulted in smaller and more stable droplets with the selected oil phase percentage of 10 wt. %.

Furthermore, DXT-MA with different substitution degrees (DS) has been synthetized in order to evaluate the effect of MA groups in the emulsion properties. Results suggest

that there is a minimum DS needed to form stable emulsions. Minimum DS has been established as the minimum substitution needed to obtain ST values below 58 mN/m at the concentration of 5 g/L that can produce stable emulsions (the avoidance of phase separation for at least 5 days and the overlapping of 5 consecutive runs in LD). Following this, our results confirm that 15 % is the minimum number of MA groups needed to produce stable emulsions. Moreover, droplet diameter increases with increasing the DS. This means there are an optimal substitution range (DS=15-36%) which allows the production of smaller, monomodal and stable emulsions.

3.5. Materials and methods

3.5.1. Materials

Dextran from Leuconostoc spp. (DXT-40, Mr ~40 kDa), glycidyl methacrylate (GMA) (97%), dimethyl sulfoxide (DMSO) (98%), 3-mercaptopropionic acid (≥99%), acryloyl chloride (99%) and 2,2'-(ethylenedioxy)diethanethiol [3,6-dioxa-1,8-octane-dithiol (DODT)] (95%) were purchased from Aldrich and used as received. Phosphate-buffered saline (PBS) and dichloromethane were purchased from Scharlau and used as received. 4-(Dimethylamino)pyridine (DMAP) was purchased from Acros-Organics. Water (H_2O) used in the syntheses, unless otherwise stated, was ultrapure water from a MilliQ A10 Gradient equipment (Millipore). Docosahexaenoic acid (DHA) rich oil (> 95 wt%) extracted from fish oil was kindly provided by SENDABIO S.L.

3.5.2. Characterization Methods

- *Dynamic Light Scattering* (DLS): DLS analyses were conducted using a Zetasizer Nano ZS, ZEN3600 Model (Malvern Instruments Ltd). All measurements were performed in disposable sizing cuvettes at a laser wavelength of 633 nm and a scattering angle of 173°. Zeta-potential measurements were performed in disposable zeta potential cells (pH 7.4, 25°C). Before the measurement, DXT functionalized samples were dispersed in saline solution (0.9 wt% NaCl for size measurements and 1 mM NaCl for zeta-potential measurements) at a concentration

of 1 mg/mL. Emulsion samples were dispersed in ultrapure water at a concentration of 2 mg oil/mL. Each measurement was repeated three times per sample at 25°C.

- *Nuclear magnetic resonance* (^{1}H NMR): NMR spectra were recorded on a Bruker AVANCE III spectrometer at 500 MHz and 25°C. Chemical shifts (δ) are expressed in ppm relative to the residual signal of the solvent. Splitting patterns: b, broad; s, singlet; d, doublet; t, triplet; q, quartet; m, multiplet.
- *Laser diffraction (LD)*: LD analyses were conducted using a Mastersizer 3000 laser diffraction system (Malvern Instruments Ltd). All measurements were performed at a laser wavelength of 430 nm using 600 mL of deionized water in a glass beaker. Five measurements (5 seconds each) were performed per sample at 25°C following Mie dispersion model.
- *Transmission Electron Microscopy (TEM)*: TEM analyses of Single Chain Polymeric Nanoparticles (SCPNs) were performed in a TECNAI G2 20 TWIN microscope (FEI, Eindhoven, The Netherlands), operating at an accelerating voltage of 200 KeV in a bright-field image mode. One drop of the sample dispersion in water (~3 µL, 0.035 mg/mL) was deposited on a carbon film supported on a copper grid (300 mesh). The sample was hydrophilized by a glow discharge process just prior to use. After staining for 20 seconds with uranyl acetate (aqueous solution, 1% w/v), the sample was spin-dried at room temperature. Number-averaged diameter was calculated on ca. 300 nanoparticles using ImageJ analysis software and Gaussian curve fitting. TEM analyses of emulsions were performed in a LaB6-TEM JEOL JEM-1400PLUS (40kV - 120kV) system equipped with a GATAN US1000 CCD camera (2k x 2k). One drop of the sample dispersion in water (~20 µL, 1 mg oil/mL emulsion) was deposited on a carbon film supported on a copper grid (300 mesh) and hydrophilized by a glow discharge process just prior to use. After washing three times with ultrapure water, the staining was carried out for 40 seconds with phosphotungstenic acid solution (PTA, 1% w/v) and the sample was dried at room temperature overnight.
- *Surface tension (ST):* ST measurements were performed in a KSV Sigma 700 Force tensiometer following the Ring Method and using a Standard Ring (R-ring = 9.58

mm, R-wire = 0.185 mm). Automatic measurements of the "critical micelle concentration (CMC)" were performed by dissolving dextran polymer in water (200 mL) until a final concentration of 2.5 g/L was reached. After each addition, the sample was stirred for 60 seconds and kept at rest during 120 seconds. Description of the experimental setup: Standard Vessel (diameter = 66 mm, max. volume = 110 mL), heavy phase (water) and light phase (air). Individual surface tension measurements were performed using "Surface Tension" program at the concentration of 5 g/L. Each sample was measured without stirring until surface tension stabilization (stabilization criteria: 4 runs with a variation below 1.5%). Description of the experimental setup: Small Vessel (diameter = 50 mm, max. volume = 70 mL), heavy phase (water) and light phase (air). Digital photography: each dextran polymer was solved in water at the concentration of 5 g/L and mixtures were shaken vigorously during 20 seconds and kept at rest for 10 seconds before digital picture acquisition.

3.5.3. Synthesis of methacrylated dextran polymer (DXT-MA) (D1-D14)

Our first goal was to tackle the preparation of dextran methacrylated polymer (DXT-MA), which was synthesized following a slightly modified published procedure.[20] First, dextran (DXT-40, 1g) was dissolved in 30 mL of dimethyl sulfoxide (DMSO) under a nitrogen atmosphere. To this solution, 200 mg of 4-(N,N-dimethylamino)pyridine (DMAP, 1.6 mmol) was added. Then, 1 mL of glycidyl methacrylate (GMA, 1.2 mmol) was incorporated and the mixture was stirred at room temperature until reach the appropriate substitution degree (DS, percent of modified hydroxyl groups per repeating unit). The reaction was stopped by adding an equimolar amount of concentrated HCl solution (37% v/v, 1.6 mmol, 0.132 mL) to neutralize DMAP. The modified dextran solution was purified by dialysis against ultrapure water (MWCO 3,500 Da) at room temperature until reaching deionized water conductivity values < 1µS (9 days, refreshing with 4 L of deionized water twice per day). ^{1}H NMR (500 MHz, D_2O) (δ ppm) **(D12)**: 6.35-6.10 (m, 1H, methacrylic-CH), 5.92-5.72 (m, 1H, methacrylic-CH), 5.54-4.86 (2.1H, including H-1 and H-2/3 MA-substituted), 4.20-3.33 (10.3H, m, rest of hydrogen atoms of Glc), 1.98 (s, 3H, methacrylic-CH_3).

3.5.4. Preparation of dextran-based single-chain polymer nanoparticles (DXT-SCPN-MA) (D15)

In a standard procedure based on *Gracia et al* (2017),[14] 0.37 mL of a previously prepared 0.15 M solution (2 mL, MeOH/PBS, 1:1, v/v, adjusted to pH= 9.5) of cross-linker DODT (0.06 mmol, 49 µL) was added dropwise using a syringe pump (0.04 mL/h) over a 0.02 M solution of DXT-MA (D12, **Table 2**) (100 mg, 0.024 mmol, 13 mL PBS, adjusted to pH= 9.5) during 8 h at room temperature and under constant stirring. After addition, the reaction was maintained stirred at room temperature for 12 h. Then, the disappearance of the -SH groups from the cross-linker DODT was checked by Ellamn´s test. Further characterization studies were carried out after purification of 5 mL sample from the reaction mixture by dialysis against ultrapure water (MWCO 3500 Da) until reaching deionized water conductivity values < 1µS (5 days, refreshing with 4 L of deionized water twice per day). Finally, the resulting aqueous solution was freeze-dried to obtain nanoparticles as a white solid. Yield >90%. ^{1}H NMR spectrum (500 MHz, D_2O; δ ppm) **(D15)**: 6.34-6.12 (m, 1H, methacrylic-CH), 5.94-5.70 (m, 1H, methacrylic-CH), 5.55-4.85 (5.6H, including H-1 and H-2/3 MA-substituted), 4.34-3.28 (28.3H, m, rest of Glc and 2xCH_2O of cross-linker), 3.06-2.53 (5H, m, $CH(CH_3)CH_2S$, CH_2S of cross-linker), 1.98 (s, 3H, methacrylic-CH_3), 1.29 (s, 3H, cross-linker-CH_3). Dh (DLS) = 13 ± 8 nm; PDI 0.2.

3.5.5. Functionalization of DXT-SCPN-MA with 3-mercaptopropionic acid (DXT-SCPN-F) (D16)

One batch synthesis of the functionalized DXT-SCPN-F was achieved by adding slowly 2 mL of an aqueous solution of 3-mercapto propionic acid (61.4 µL, 7.5 mmol, pH= 9.5) to the reaction flask in the previously reported synthesis of the DXT-SCPN-MA **(D15)**. The reaction was stirred for 24 h and the excess acid was removed by dialysis against ultrapure water (MWCO 3,500Da) until reaching deionized water conductivity values < 1µS (5 days, refreshing with 4L of deionized water twice per day). The resulting aqueous solution was freeze-dried to obtain nanoparticles as a white solid. Yield >90%. ^{1}H NMR spectrum (500 MHz, D_2O; δ ppm) **(D16)**: 5.55-4.85 (6.5H, including H-1 and H-2/3 MA-substituted), 4.34-3.28 (36.5H, m, rest of Glc and 2xCH_2O of cross-linker), 3.11-

2.81 (6.6H, m, $CH(CH_3)CH_2S$, CH_2S of cross-linker), 2.75-2.33 (2H, m, CH_2S of MPA), 1.98-1.29 (5H, including MA-CH_3 and cross-linker-CH_3). Dh (DLS) = 15 ± 4 nm; PDI 0.2. Zeta-potential (pH = 7.2) = -20mV ± 5.

3.5.6. Functionalization of the DXT-MA (52%) with 3-mercaptopropionic acid (DXT-F) (D17)

An aqueous solution of 3-mercaptopropionic acid (430 µL, 5 mL H_2O, pH= 9.5) was slowly added to a previously prepared solution of DXT-MA (**D12**, **Table 2**) (350 mg, 20 mL H_2O, pH= 9.5). The reaction was maintained under constant stirring for 12 h and then purified by dialysis against ultrapure water (MWCO 3,500Da). The resulting aqueous solution was freeze-dried to obtain the resulting quenched polymer as a white solid. ^{1}H NMR (500 MHz, D2O) δ ppm **(D17)**: 5.41-4.86 (3.4H, including H-1 and H-2/3 MPA-substituted), 4.20-3.33 (14.3H, m, rest of Glc), 3.02-2.49 (6.6H, m, MPA except CH_3), 1.29 (s, 3H, MA-CH_3). Zetapotential (pH = 7.2) = -12 mV ± 7.

3.5.7. Production of oil-in-water (O/W) emulsions based on functionalized dextran (DXT-R) (M1)

DXT-R was dissolved in deionized water in an 8 mL glass vial. To this solution, the oil was added. The relative amounts of DXT-R, water and oil were modified to reach always a final amount of 2g. The emulsion was then formed by sonication (0°C, no stirring) using an UP400S (Hielscher) system at 100% of amplitude and pulse during 4 minutes (400 W) with a H3 sonotrode tip (3 mm diameter, 100 mm length).

3.5.8. Optimised production of O/W emulsions based on DXT-MA (M2)

Dextran methacrylate polymer (20 mg, 5% wt. based on the oil phase) was dissolved in deionized water (aqueous phase, 3.6 mL, 90% wt.) in an 8 mL glass vial. To this solution, 0.4 g of triglyceride based oil (oil phase, 10% wt.) was added. The emulsion was then formed by sonication (0°C, no stirring) using an UP400S (Hielscher) system at 100% of amplitude and pulse during 4 minutes (400 W) with a H3 sonotrode tip (3 mm diameter, 100 mm length).

3.6. References

1. Namazi, H., Fathi, F. & Heydari, A. Nanoparticles Based on Modified Polysaccharides. *Deliv. Nanoparticles* (2012) doi:10.5772/34795.

2. Krstonošić, V., Dokić, L., Nikolić, I. & Milanović, M. Influence of xanthan gum on oil-in-water emulsion characteristics stabilized by OSA starch. *Food Hydrocoll.* **45**, 9–17 (2015).

3. Debele, T. A., Mekuria, S. L. & Tsai, H. C. Polysaccharide based nanogels in the drug delivery system: Application as the carrier of pharmaceutical agents. *Mater. Sci. Eng. C* **68**, 964–981 (2016).

4. Janes, K. A., Calvo, P. & Alonso, M. J. Polysaccharide colloidal particles as delivery systems for macromolecules. *Adv. Drug Deliv. Rev.* **47**, 83–97 (2001).

5. Bouyer, E., Mekhloufi, G., Rosilio, V., Grossiord, J. L. & Agnely, F. Proteins, polysaccharides, and their complexes used as stabilizers for emulsions: Alternatives to synthetic surfactants in the pharmaceutical field? *Int. J. Pharm.* **436**, 359–378 (2012).

6. Bais, D., Trevisan, A., Lapasin, R., Partal, P. & Gallegos, C. Rheological characterization of polysaccharide-surfactant matrices for cosmetic O/W emulsions. *J. Colloid Interface Sci.* **290**, 546–556 (2005).

7. Liu, J., Willför, S. & Xu, C. A review of bioactive plant polysaccharides: Biological activities, functionalization, and biomedical applications. *Bioact. Carbohydrates Diet. Fibre* **5**, 31–61 (2015).

8. Sinha, V. R. & Kumria, R. Polysaccharides in colon-specific drug delivery. *Int. J. Pharm.* **224**, 19–38 (2001).

9. Zong, A., Cao, H. & Wang, F. Anticancer polysaccharides from natural resources: A review of recent research. *Carbohydr. Polym.* **90**, 1395–1410 (2012).

10. Landoll, L. M. Nonionic Polymer Surfactants. *J. Polym. Sci. A1.* **20**, 443–455 (1982).

11. Steenbergenj, V. *et al.* Synthesis, Characterization, and Polymerization of Glycidyl Methacrylate Derivatized Dextran. *Macromolecules* **28**, 6317–6322 (1995).

12. van Dijk-Wolthuis, W. N. E., Kettenes-van den Bosch, J. J., van der Kerk-van Hoof, A. & Hennink, W. E. Reaction of Dextran with Glycidyl Methacrylate: An Unexpected Transesterification. *Macromolecules* **30**, 3411–3413 (1997).

13. Kim, S. H. & Chu, C. C. Synthesis and characterization of dextran-methacrylate hydrogels and structural study by SEM. *J. Biomed. Mater. Res.* **49**, 517–527 (2000).

14. Gracia, R. *et al.* Synthesis and functionalization of dextran-based single-chain nanoparticles in aqueous media. *J. Mater. Chem. B* **5**, 1143–1147 (2017).

15. Aiertza, M. K., Odriozola, I., Cabañero, G., Grande, H. J. & Loinaz, I. Single-chain polymer nanoparticles. *Cell. Mol. Life Sci.* **69**, 337–346 (2012).

16. Benito, A. B. *et al.* Functional Single-Chain Polymer Nanoparticles: Targeting and Imaging Pancreatic Tumors *in Vivo*. *Biomacromolecules* **17**, 3213–3221 (2016).

17. Dutta, S. K., Knowlton, E. & Blair, D. L. Emulsions. *Fluids, Colloids Soft Mater. An Introd. to Soft Matter Phys.* **91**, 2001–2021 (1907).

18. Finkle, P., Draper, H. D. & Hildebrand, J. H. The theory of emulsification. *J. Am. Chem. Soc.* **45**, 2780–2788 (1923).

19. Gracia, R. *et al.* Biocompatible single-chain polymer nanoparticles loaded with an antigen mimetic as potential anticancer vaccine. *ACS Macro Lett.* **7**, 196–200 (2018).

20. van Dijk-Wotthuis, W. N. E. *et al.* Synthesis, Characterization, and Polymerization of Glycidyl Methacrylate Derivatized Dextran. *Macromolecules* **28**, 6317–6322 (1995).

21. Aiertza otxotorena, M., Karmele. Sanchez Abella, Laura; Benito Collado, A. B. L., Bordonabe, Iraida; Cabanero, G., Grande, H.-J. M. & Marco; Gracia Espana, R. WO 2016/071258 Al. 35 (2016).

22. Malvern. A basic guide to particle characterization. *Malvern whitepaper* (2015).

23. Morse, A. J. *et al.* Novel Pickering Emulsi fi ers Based on pH-Responsive Poly(2-(diethylamino)ethyl methacrylate) Latexes. *Langmuir* **29**, 5446–5475 (2013).

24. Maroon, J. C. & Bost, J. W. x -3 Fatty acids (fish oil) as an anti-inflammatory : an alternative to nonsteroidal anti-inflammatory drugs for discogenic pain y. *Surg. Neurol.* **65**, 326–331 (2006).

25. Van Biervliet, S., Van Biervliet, J. P., Robberecht, E. & Christophe, A. Docosahexaenoic acid trials in cystic fibrosis: A review of the rationale behind the clinical trials. *J. Cyst. Fibros.* **4**, 27–34 (2005).

26. Pellicer, J., García-Morales, V. & Hernández, M. J. On the demonstration of the young-laplace equation in introductory physics courses. *Phys. Educ.* **35**, 126–129 (2000).

Chapter 4. Stability enhancement: crosslinking at the oil/water interface.

4.1 Introduction

The relative low stability of emulsion droplets is one major drawback for their application. Such instability arises from the fact that emulsions are thermodynamically unstable systems, and consequently, they are very sensitive to changes in pH, temperature and ionic strength.[1–5] However, emulsions are kinetically more stable when smaller meaning that larger droplets easily rely in emulsion breakdown, as described in the introduction chapter. Furthermore, we have predefined the stability criteria as the absence of phase separation, along with the overlapping of 5 consecutive runs in LD, after one-week stored at 4^{o}C. This criteria was very useful to optimize emulsion formulation, but useless from an application point of view because drug delivery systems often demand higher stability in the long-term. To enhance stability, several approaches have been investigated; including the use of proper surfactants,[6] the addition of co-surfactants [7] or the use of particles as stabilizers, which result in the formation of the so-called Pickering emulsions.[8–10] Additionally, application of different treatments at the oil/water interface including thermal annealing,[9] gel trapping,[11] polyelectrolyte complexation,[12] polymerization of droplet phase [13] and crosslinking [14–17] have also been used. However, these stabilizing strategies have been reported for particle-stabilized emulsions, but not for emulsions stabilized with other molecular modalities.

Here, we decided to investigate the covalent fixation of the adsorbed emulsifier at the interface, inspired on previously developed Pickering strategies, to improve emulsion stability.[14–16] More concretely, cross-linking reactions of the polymer adsorbed at the oil/water interface were carried out via thio-Michael addition reaction using 2,2'-(ethylenedioxy)diethanethiol (DODT) as the linker. We have demonstrated that the stability of the emulsions can be enhanced by appropriate cross-linking at the (o/w)-interface. The resulting cross-linked emulsions proved stable for months (up to 1 year)

in any physiologically relevant medium. This stability improvement is very interesting for *in vivo* applications regarding the possibility of incorporate higher amounts of drug than other nanocarriers like micelles [18] or liposomes [19].

4.2 Objectives

The specific objectives of this work are:

1. To optimize the methodology for polymer cross-linking at the O/W interface to improve nanoemulsion stability.
2. To characterize the resulting nanoemulsions.
3. To fine tune the method developed in objective 1 in order to improve stability in strong ionic media (PBS 1X) and over time.
4. To evaluate the *in vivo* biodistribution of the resulting nanoemulsions and their capacity to modulate the release of entrapped drugs, by applying a dual labeling strategy followed by *in vivo* imaging using positron emission tomography.

4.3. Emulsions Cross-linked at the oil/water interface

4.3.1. Emulsion production and characterization

DXT-MA stabilised NEs were generated as described in section **3.5.8. Optimised production of O/W emulsions based on DXT-MA (M2)**. First, DXT-MA with a degree of functionalization of 24 % **(D7)** as determined by ^{1}H NMR was selected for a preliminary study. Nanoemulsions (**E71**, **E72** and **E78**, see **Appendix II. Production and Characterization of Cross-linked emulsions**) were subsequently prepared by sonication of 10 wt.% fish oil with 0.5 wt.% of **D7**. Droplet diameter values of 300 and 380 nm were obtained as judged by DLS (Z-Average) and LD (Dv50), respectively (**Figure 28**). These values are similar to those obtained in previous experiments under equivalent experimental conditions, thus confirming the reproducibility of our method.

Moreover, the overlapping of 5 runs in LD measurements confirmed emulsion stability towards recirculation.

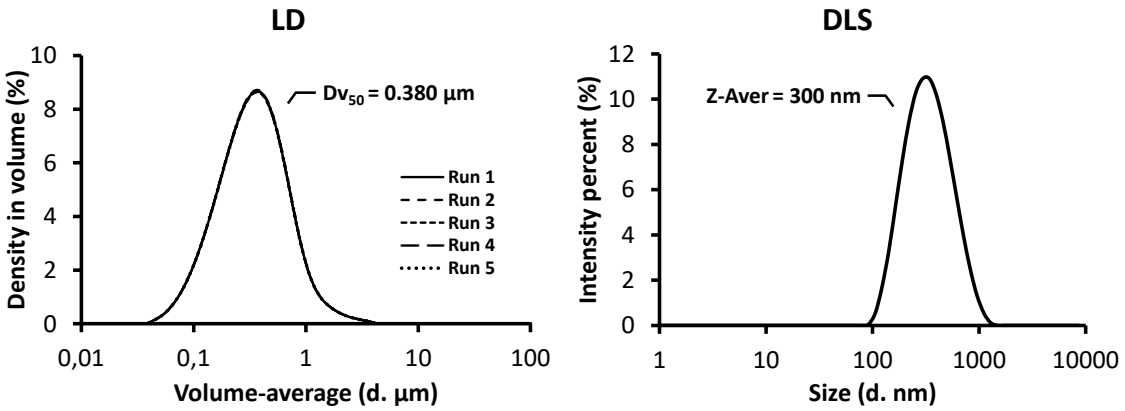

Figure 28. *Size distribution of **E71** emulsion as determined by laser diffraction (LD; deionized water, 2000 rpm, 25 °C) and dynamic light scattering (DLS; deionized water, 25 °C).*

The emulsions proved to be highly stable in water. However, a slight increase in droplet diameter was observed in PBS 1X (137 mM NaCl, 2.7 mM KCl, 10 mM Na_2HPO_4, 2 mM KH_2PO_4, pH 7.4). Despite DXT-MA is non-ionic, it is a poor surfactant as demonstrated by the low decrease of surface tension reported in section **3.3.2 Modified dextran as oil-in-water (o/w)-emulsion stabilizer**, and hence, it was expected that a slight increase in the ionic strength resulted in the formation of bigger droplets.

In order to enhance stability in this medium, the possibility of polymer cross-linking to force DXT-MA stabilizer to remain at the oil/water interface avoiding its desorption was foreseen (**Figure 29a**) by taking advantage of the presence of methacrylate groups on the dextran groups and using the same thio-Michael addition as for the formation of DXT-SCPNS (see section **3.3.1. Dextran derivatives (DXT-R)**).

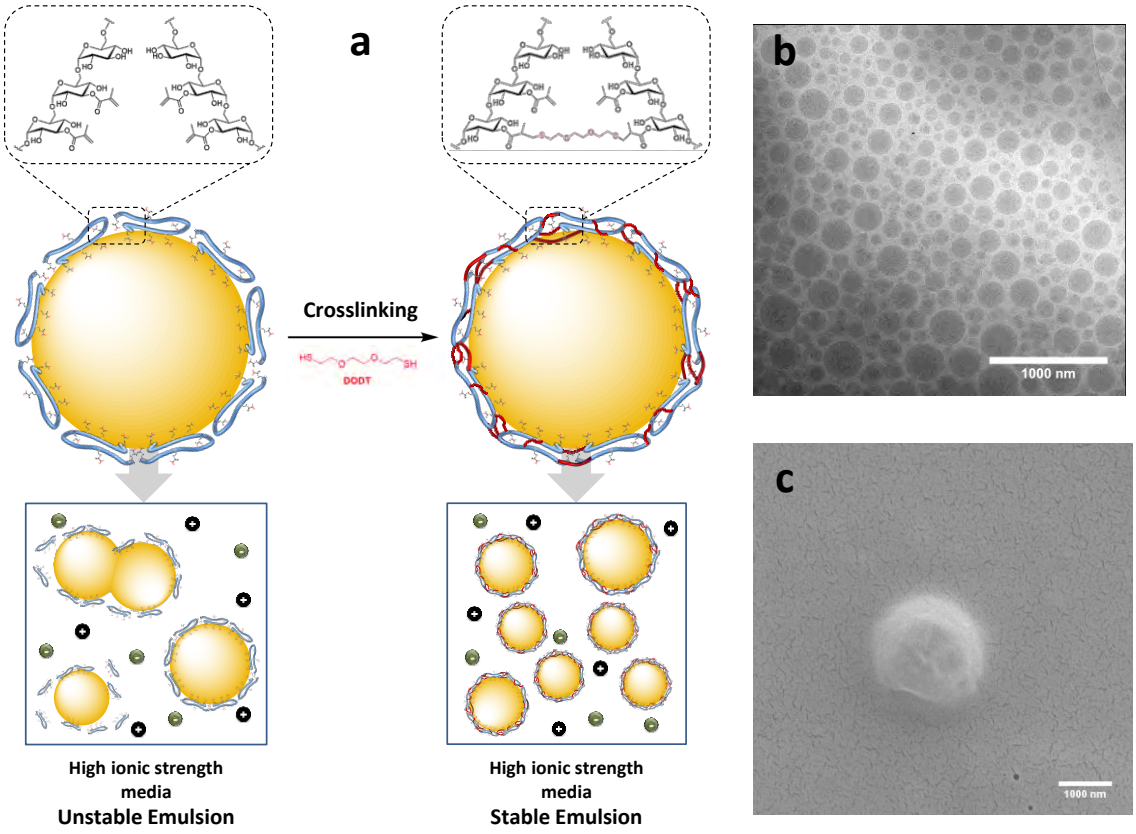

Figure 29. *a) Schematic representation of the stability enhancement after cross-linking at the O/W interface via oil dispersed phase. b) Cryo-TEM micrograph of an interfacial cross-linked nanoemulsion (**E74**). c) SEM image of the collapsed colloidosome obtained after DMSO/dioxane challenge of **E74**.*

Two different strategies for cross-linking were carried out. In our first strategy, different amounts of DODT, based on the number of MA presented in DXT-MA, were added to the aqueous phase of an emulsion previously produced. It is worth mentioning that the droplet dispersion concentration was decreased to 1 wt.% to avoid inter-droplet cross-linking. Although the emulsion appeared to remain visually stable during this cross-linking reaction, LD measurements suggested a lack of stability as the droplet diameter was increasing with higher amounts of DODT. For a better understanding of the process, an (o/w)-emulsion based on 0.5% wt. DXT-MA (**D9**, DS=36%) with a big amount of oil, 60% wt. olive oil (Nile Red 0.2 mg/mL oil), was produced in order to generate droplets above 1 µm which can be analyzed by Optical Microscopy (OM). Optical microscope images finally demonstrated droplet diameter

remained stable but few droplets aggregates appeared (see **Figure 30**). Moreover, the number of aggregates increased when the amount of cross-linker was increased. These results suggest that in spite of our efforts to work at relatively low concentration (1 wt. %), inter-droplets cross-linking occurred when the cross-linker was added to the water phase. This behaviour differed from that obtained by Walsh and co-workers where colloidosomes formed from an (o/w)-Pickering emulsion were successfully cross-linked via the aqueous continuous phase.[20] Obviously, this undesired inter-droplet cross-linking could be avoided by diluting even more the emulsion or reducing the DODT equivalents, although further dilution would result in low-concentration dispersions and DODT reduction would imply harsh reaction conditions, which could be a limitation for the translation of the methodology for industrial applications.

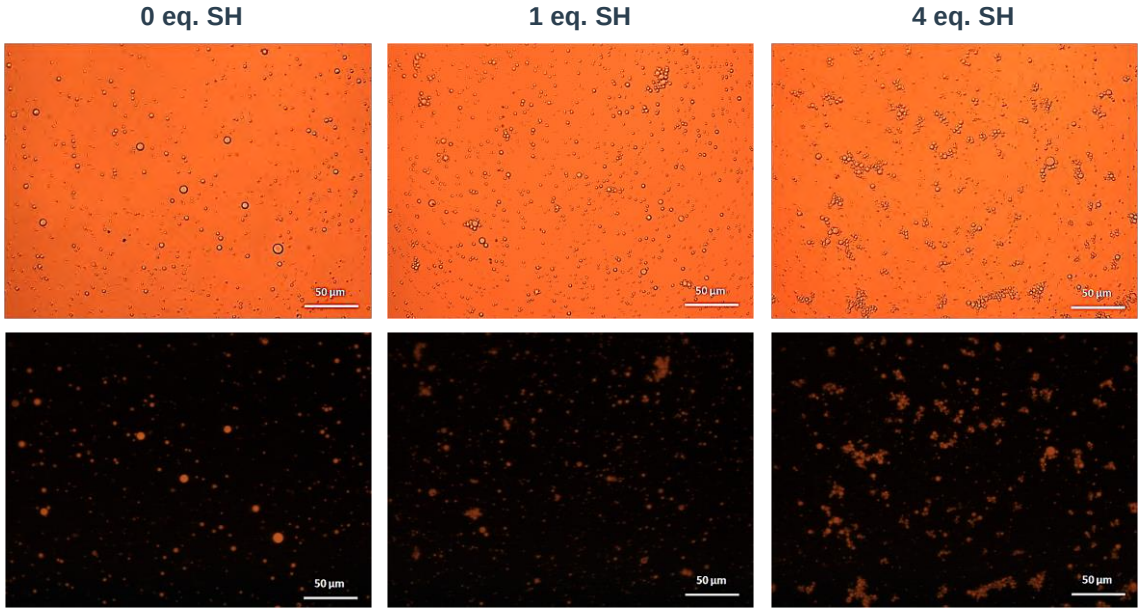

Figure 30. *Images of (o/w)-emulsions based on 0.5% wt. DXT-MA (D9, DS=36%), 60% wt. olive oil (Nile Red 0.2 mg/mL oil) as judged by Optical Microscopy (top) or Fluorescence Microscopy (bottom). From left to right: non-crosslinked, crosslinked via the aqueous phase using 1 or 4 thiol equivalents of DODT per MA group.*

To avoid inter-cross-linking of the droplets, we decided to investigate a second strategy, based on the addition of the DODT cross-linker into the dispersed phase, i.e. previously dissolved in the oil phase prior to the emulsification process **(4.6.3. Production of O/W emulsions cross-linked at the O/W interface (method 3, M3))**. In

this scenario, the cross-linking reaction should occur from the inside of the droplet, only when the droplets are formed and once DXT-MA emulsifier is adsorbed at the interface. Hence, the possibilities of inter-crosslinking are dramatically minimised, assuming that DODT is not transferred to the aqueous phase. In brief, **D7** (20 mg, 5% wt. related to oil phase) was dissolved in 3.6 mL of deionized water (aqueous phase, 90% wt.) and 0.4 g of fish oil (oil phase, 10% wt.) was added. Then, DODT was carefully added over the oil phase and the pH in the aqueous phase was adjusted to 9.5 (as required for the thio-Michael addition reaction) using 1M NaOH. The mixture was immediately sonicated, to prevent basic hydrolysis of the ester groups present in **D7**, for 4 min in an ice bath and under magnetic stirring. By using this approach, DXT-MA could be successfully cross-linked at the (o/w)-interface, using different DODT equivalents with respect to the amount of methacrylate (see **Appendix II. Production and Characterization of Cross-linked emulsions** for experimental conditions and emulsion properties; **E73**-**E77** and **E79**-**E81**).

Determination of nanodroplet size distribution by LD (expressed as Dv(50), median particle size by volume) confirms that the size of the nanodroplets decreased when the amount of cross-linker was increased (see **Table 3**). However, when looking at Dh[4;3] (volume diameter) it was observed that smaller droplets were actually obtained for a certain range of DODT (0.5-1 equivalents of -SH groups based on the total amount of methacrylate present in the solution). Noteworthy, LD measurements are useful to determine size distribution and stability under recirculation but it is not working to a proper size characterization. Furthermore, Dv(50) as the median is usually characteristic of emulsion main population, when distribution is mainly monomodal, meanwhile Dh[4;3] is the volume moment mean and reflects the size of those particles which constitute the bulk of the sample volume. Thus, Dh[4;3] is most sensitive to the presence of large droplets in the size.[21] For these reasons, droplet size and shape of crosslinking emulsions were characterized by Cryo-TEM (see **Figure 29b** for example of **E71**). In general terms, the cross-linking process did not have an effect neither on the shape nor the size of the emulsions.

Table 3. Dh[4,3], Dv(50) and uniformity values of different cross-linked nanoemulsions obtained under different experimental conditions; the amount of DODT was varied, leading to different molar equivalents of -SH related to the number of MA groups present in D7 (20 mg, DS~24%).

Emulsion	DODT (µL)	SH eq.	Dh [4;3]	Dv (50)	Uniformity
E72	0	0	431	339	0.66
E73	0.5	0.25	435	340	0.67
E74	1.0	0.50	381	297	0.67
E75	1.5	0.75	381	291	0.69
E76	2.0	1	385	284	0.75
E77	3.0	1.5	469	271	1.15

At 1.5 eq of -SH, an increase of Dh[4;3] values was observed as the distribution showed the presence of larger droplets (see **Table 3**). Furthermore, uniformity (parameter related with sample polydispersity) is increasing when increasing DODT amounts. This increment is significantly more pronounced when using more than one thiol equivalents. This could be explained by the uncontrolled inter-droplet crosslinking at relatively high amounts of DODT linker (i.e. 1.5 SH eq.; Uniformity = 1.15). A control experiment using only DODT as stabiliser to check its interfacial activity showed a resulting emulsion with Dh[4;3] values close to 1.1 micron. It is worth to mention that the interfacial activity of DODT will facilitate the cross-linking of the DXT-MA as both compounds will be highly concentrated at the (o/w)-interface. Then, too much DODT would result in a high competition against DXT-MA for the stabilization of the oil droplets and hence some DODT, which have reacted with only one MA group, might be exposed to the water phase offering the option for interdroplet cross-linking. Altogether, these results suggest that there is an optimal range in the relative amount of cross-linker that is actually required to cross-link the polymer adsorbed at the interface, without compromising the characteristics of the nanodroplets. The result is not contra-intuitive, as it can be expected that, due to the conformation of the DXT-MA adsorbed at the interface, a fraction of the methacrylate moieties are “wetting the oil” being available for the intra-droplet cross-linking, while the remaining are less accessible for the cross-linker which eventually leads in a single-thiol reaction. Thus, DODT length is paramount for cross-linking MA groups located at certain distance. If

distance between MA groups is higher than DODT length thio-Michael addition would be produced only for one SH leaving the unreacted as free terminal group attached to the droplet interface.

Successful cross-linking was assessed by a DMSO/dioxane (70:30, v/v) challenge. Similar strategy to visualize the effect of cross-linking was investigated by Thomson et al. They reported the "ethanol challenge" as a way to dissolve all emulsion components to see differences if cross-linked or not. They dissolve both emulsions, cross-linked and non-cross-linked, in a large excess of ethanol and the resulting dispersions were analysed by optical microscope. Results demonstrated that cross-linked emulsions remained spherical despite collapsed while no microcapsules were observed for the non-cross-linked.[14] With that aim, the cross-linked emulsion (1.5 mL) was dissolved in 30 mL of DMSO/dioxane solution (which acts as a solvent for both the water and oil phases). After 12 hours, the oil phase was removed by liquid-liquid extraction with hexane and the aqueous phase, containing DMSO, water and the cross-linked (CL) polymer (**D7-CL**) was collected and purified by dialysis. The resulting aqueous solution was freeze-dried to obtain **D7-CL** as a white solid. Oil traces were removed via solid-liquid extraction with hexane, whereby solid dextran was centrifuged and the supernatant was removed. SEM images obtained after DMSO/dioxane challenge show the collapsed structure of the droplet shell once the oil phase is removed (**Figure 29c**). It is important to point out that spherical morphology is hard to identify because the thin layer of cross-linked polymer, which is acting as a shell, is too fragile to remain as spherical as the original oil droplet and hence most of them are destroyed during the process.

^{1}H NMR (500 MHz, D_2O) studies were carried out on the cross-linked polymers isolated from the emulsions **E72**-**E77,** as described in **Table 4**, to determine the amount of methacrylate groups still present on the polymer after cross-linking (Glc-MA), the degree of DODT successfully reacted (Glc-DODT) and the amount of unmodified pristine glucose units (Glc unmodified), following the procedure described in section **3.3.1. Dextran derivatives (DXT-R).**

Table 4. Summary of the quantification of extracted DXT-MA reacted with DODT by ^{1}H NMR (D_2O, 500 MHz) of emulsions based on D7 (DS=24% before crosslinking at the O/W interface) after crosslinking with different thiol equivalents of DODT linker (0-1.5 eq. SH) based on the number of MA groups assuming that all the diblock copolymer is located at the oil/water interface.

Emulsions based on D7	E72 (0 eq.)	E73 (0.25 eq.)	E74 (0.5 eq.)	E75 (0.75 eq.)	E76 (1 eq.)	E77 (1.5 eq.)
DS. (Glc unmodified)	79	75	75	80	76	73
DS. (Glc-MA)	21	19	16	8	7	6
DS. (Glc-DODT)	0	6	9	12	17	21
DS. Final (Glc-MA + Glc-DODT)	21	25	25	20	24	27
% initial MA reacted	0	25	39	60	72	88

For the particular case of **E74**, which is presented as an example (**Figure 31**), ^{1}H NMR (500 MHz, D_2O; δ ppm) signals for the extracted cross-linked polymer were found at 6.38-6.08 (m, 1H, methacrylic-CH), 5.95-5.67 (m, 1H, methacrylic-CH), 5.55-4.85 (8.2H, including H-1 and H-2/3 MA-substituted), 4.38-3.25 (40H, m, rest of Glc and 2xCH_2O of cross-linker), 3.06-2.58 (3.3H, m, $CH(CH_3)CH_2S$, CH_2S of cross-linker), 1.98 (s, 3.7H, methacrylic-CH_3), and 1.36-1.12 (b, 1.7H, cross-linker-CH_3). The decrease of signal intensity of the methacrylic group between 5.6-6.4 ppm and the appearance of the signal of the reacted methyl group of the methacrylate t 1.2-1.4 ppm confirmed that the thio-Michael addition did occur.

^{1}H NMR showed that the polymers did not suffer hydrolysis during the cross-linking reaction, as the values of DS. Final (Glc-MA + Glc-DODT) remain close to 24%, which is the initial DS of **D7** (see **Table 4**). On the other hand, the amount of reacted MA groups increased with increasing amount of DODT cross-linker. It is important to point out that even in those scenarios with the highest amount of cross-linker, some MA groups remained unreacted. This is clearly observed by comparing the percentage of initial MA reacted for 0.25 eq. (all SH equivalents have reacted: 25% of initial MA) and 0.5 eq. (only 39% of SH equivalents have reacted instead of theoretical 50%). Furthermore, the transfer to the water phase of DODT might have occurred in some extent but it seems irrelevant as more than 10 % of MA remained free after using 1.5 eq. of SH.

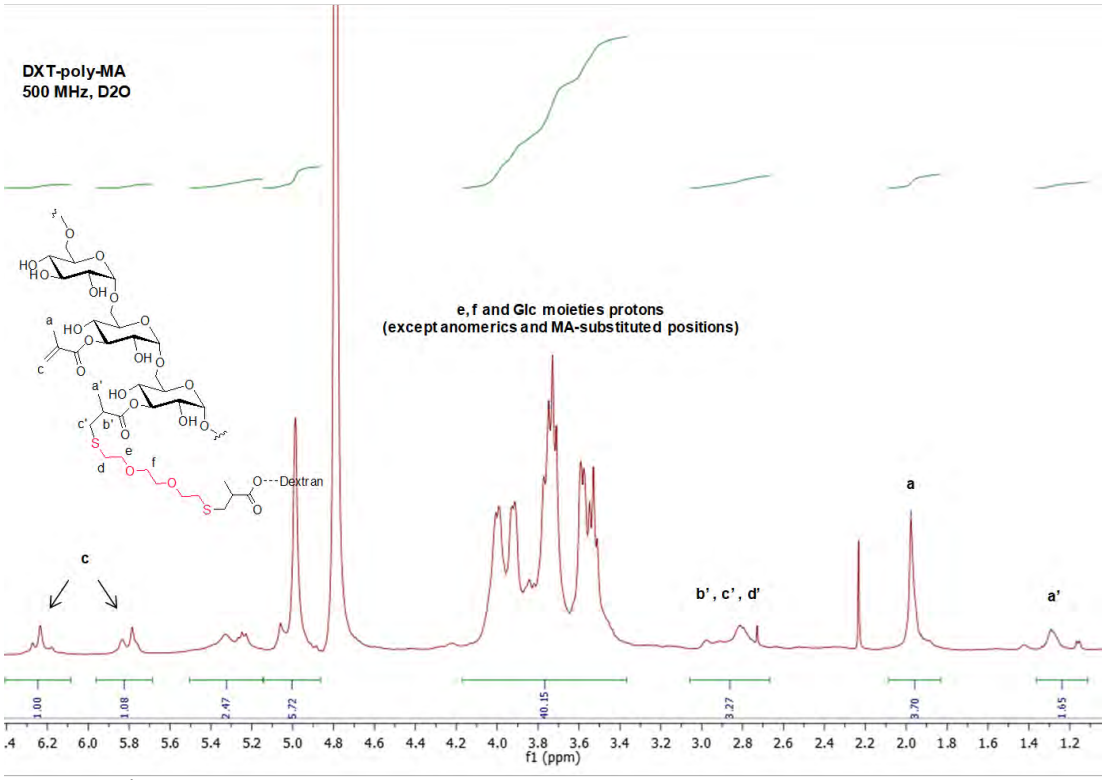

Figure 31. *^{1}H NMR (D_2O, 500 MHz) of **D7-CL** from **E74**.*

These results confirmed the hypothesis that some of the MA groups are unavailable for reaction because oriented towards the water phase and/or the short length of DODT linker is avoiding the equimolar reaction between MA and SH. This fact has a positive outcome: those unreacted MA groups present on the outside of the droplet offers the possibility to further functionalize the droplet with targeting agents and/or compounds to adjust its surface chemistry (e.g. zeta potential by reacting with thiolated compounds with different charges).

4.3.2. Crosslinking assessment by PBS challenge

As mentioned above, some destabilization of non-cross-linked emulsions was observed when redispersed in PBS (10 mM phosphate). Presence of salts in solution usually leads to an increment of the interfacial tension between oil and aqueous phases because increasing the polarity of the aqueous solution. This destabilization phenomenon has been widely described in literature even with the presence of non-ionic surfactants.[2,3,5] This effect can be prevented by cross-linking the surfactant at the interface to avoid its desorption due to changes in the interfacial tension. However, authors usually performed cross-linking strategies with Pickering emulsifiers[10,14] being

quite challenging to perform chemical reactions in molecules located at the interface without compromising emulsion stability.

To study the effect of cross-linking in highly ionic strength media, emulsions were diluted twice in ultrapure water and PBS. Actually, in PBS media pristine non-cross-linked NEs showed a clear increase in droplet diameter together with the appearance of large droplets just below 10 microns (**Figure 32;** 0 eq. SH).

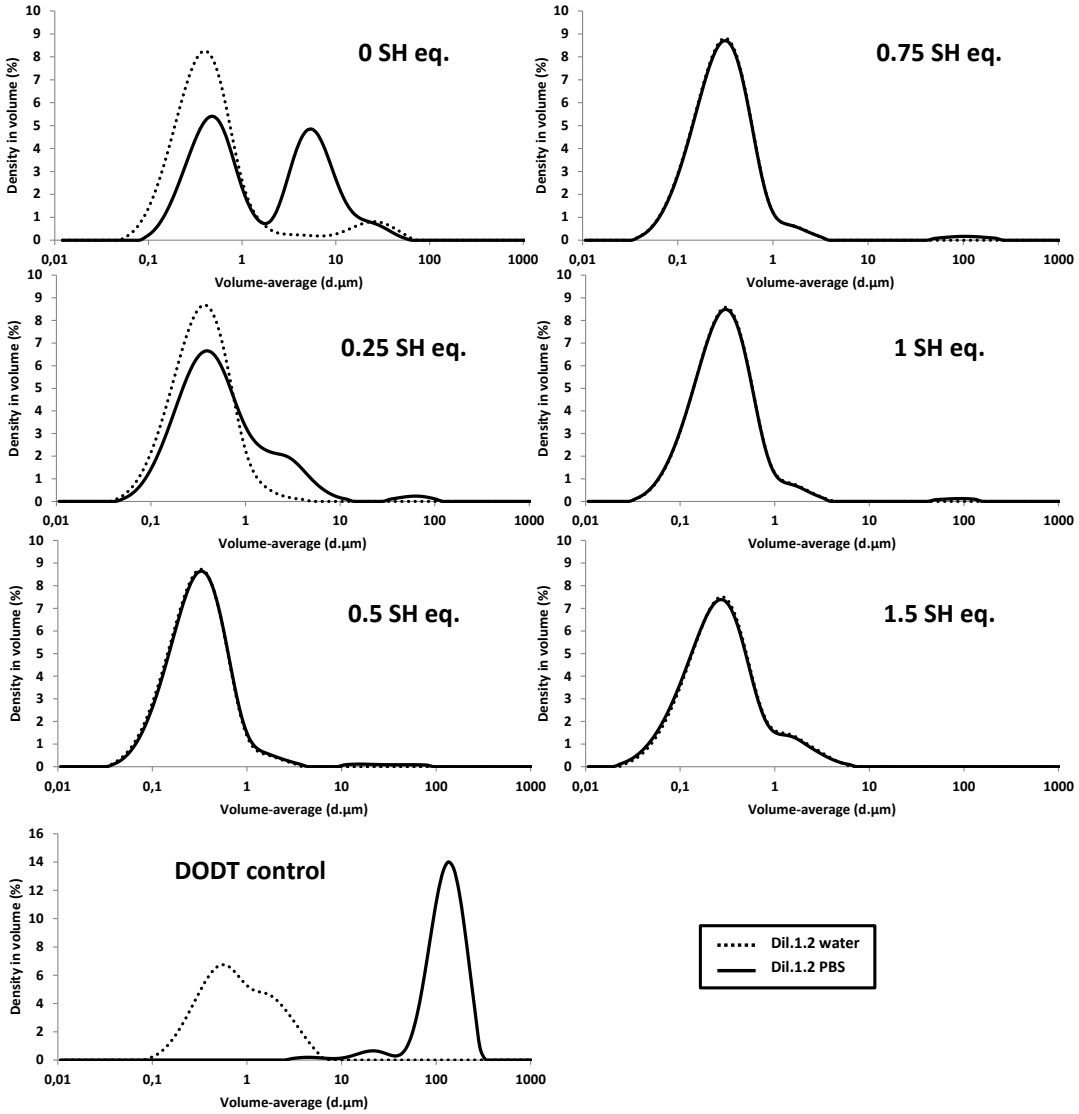

Figure 32. *Size distribution as determined by laser diffraction (LD; deionized water, 2000 rpm, 25 ^{o}C) of D7 based emulsions obtained after addition of different thiol (-SH) equivalents; 0 (**E72**), 0.25 (**E73**), 0.5 (**E74**), 0.75 (**E75**), 1 (**E76**) and 1.5 (**E77**) as DODT. Samples were diluted in deionized water:PBS (1:2) and stored at 4°C in the darkness for 48 h. Control emulsion without **D7** (only 1 SH eq. of DODT) was prepared using the same procedure.*

We took advantage of this low stability to demonstrate the positive effect of cross-linking. Addition of 0.25 eq of -SH as DODT significantly reduced the population of large droplets after dilution in PBS and the emulsion main population remained mostly unchanged. This result also indicates that the cross-linking reaction occurs partially. However, the use of higher amounts of DODT cross-linker resulted in size distributions of the emulsion diluted in PBS perfectly matching the one obtained in deionised water, as determined by LD (**Figure 32**). This result demonstrates that the cross-linking reaction confers high stability to the droplets, and such stability can be achieved with as low as 0.5 equivalents of SH, related to the total amount of MA groups present in the dispersion. A control experiment was carried out with DODT (1 eq) as surfactant but without adding D7 resulted in poor stability, confirming that DODT itself cannot produce stable emulsions in PBS (1X).

4.3.3. Emulsion stability in physiological media (PBS, 1X)

In order to actually prove cross-linking enhances media stability under recirculation in physiological conditions, an example of non-crosslinked **(E78)** and cross-linked **(E79)** emulsions were evaluated in extreme dilution conditions (>Dil. 1:500) in PBS (10 mM phosphate) at 1500 rpm. It is worth to point out that the same experiment carried out in deionized water did not show any instability issues. Both emulsions were prepared using 10 wt. % of fish oil and 0.5 wt. % of DXT-MA (DS=16%, **D5**). **E79** crosslinking was performed with 0.5 thiol equivalents. As shown in **Figure 33**, the non-cross-linked emulsion **E78** was less stable than the CL emulsion (**E79**). After 10 minutes, **E78** main population shifted from the original $D_v(50)$ = 0.46 µm to 0.77 µm. Longer times further increase this shift, while a new population of droplets at ca. 10 µm progressively appears. On the other hand, **E79** main population remained constant during the whole experiment, proving the enhanced stability due to crosslinking and suggesting that cross-linked NEs can be applied under physiological conditions. Noteworthy, **E79** measurements did not perfectly overlap, as observed in deionized water, suggesting that cross-linking can be also improved.

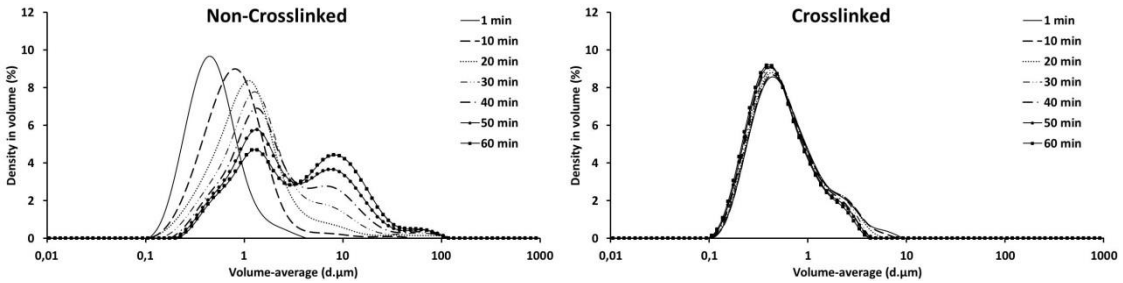

Figure 33. *LD (PBS 1X, 1500 rpm, 25 °C) measurements of **D7** based emulsions crosslinked (right, **E79**) or not (left, **E78**) at different time points.*

4.3.4. Long-term stability at different storing conditions (accelerated test conditions)

Long-term stability of emulsions is a key factor for potential industrial or biomedical applications. To demonstrate the long-term stability in water media of non-cross-linked and cross-linked NEs, **E79** (cross-linked, 0.5 thiol equivalents) and **E78** (non-crosslinked) were stored 4 different conditions for three months: A, light at room temperature (r.t.); B, dark at r.t.; C, dark at 5 °C; and D, dark at 40 °C. Emulsion stability was subsequently evaluated by visual inspection. Additionally, the hydrodynamic diameter was monitored over time (1, 2 and 3 months) by DLS (**Table 5**) and volume average diameter was assessed using LD (**Figure 34**).

Table 5. Size distribution characterized by DLS (Z-Average, PDI) of non-crosslinked (E78) o/w-emulsion after being stored at 4 different conditions (A: light at r.t., B: dark at r.t., C: dark at 5 °C and D: dark at 40 °C) at 3 different time points (1 month, 2 months and 3 months) where the final concentration of the emulsion is 1 mg fish oil per milliliter of water. Freshly prepared emulsion characteristics: Z-average=300 nm, PDI=0.24. Samples unable to fulfill DLS quality criteria (Malvern Instruments) are depicted as not available measurements (N/A) and creaming effect is depicted by (*).

		Light + r.t.		Dark + r.t.		Dark + 5°C		Dark + 40°C	
Emulsion	**Time point**	**Z-average (d.nm)**	**PDI**	**Z-average (d.nm)**	**PDI**	**Z-average (d.nm)**	**PDI**	**Z-average (d.nm)**	**PDI**
non-CL (E78)	**Month 1**	N/A	N/A	1100*	0.36*	630*	0.29*	N/A	N/A
	Month 2	N/A	N/A	N/A	N/A	N/A	N/A	N/A	N/A
	Month 3	N/A	N/A	N/A	N/A	N/A	N/A	N/A	N/A
CL (E79)	**Month 1**	290	0.22	300	0.23	290	0.23	320	0.30
	Month 2	300	0.26	300	0.24	300	0.23	320	0.27
	Month 3	280	0.23	800*	0.17*	310	0.26	290	0.23

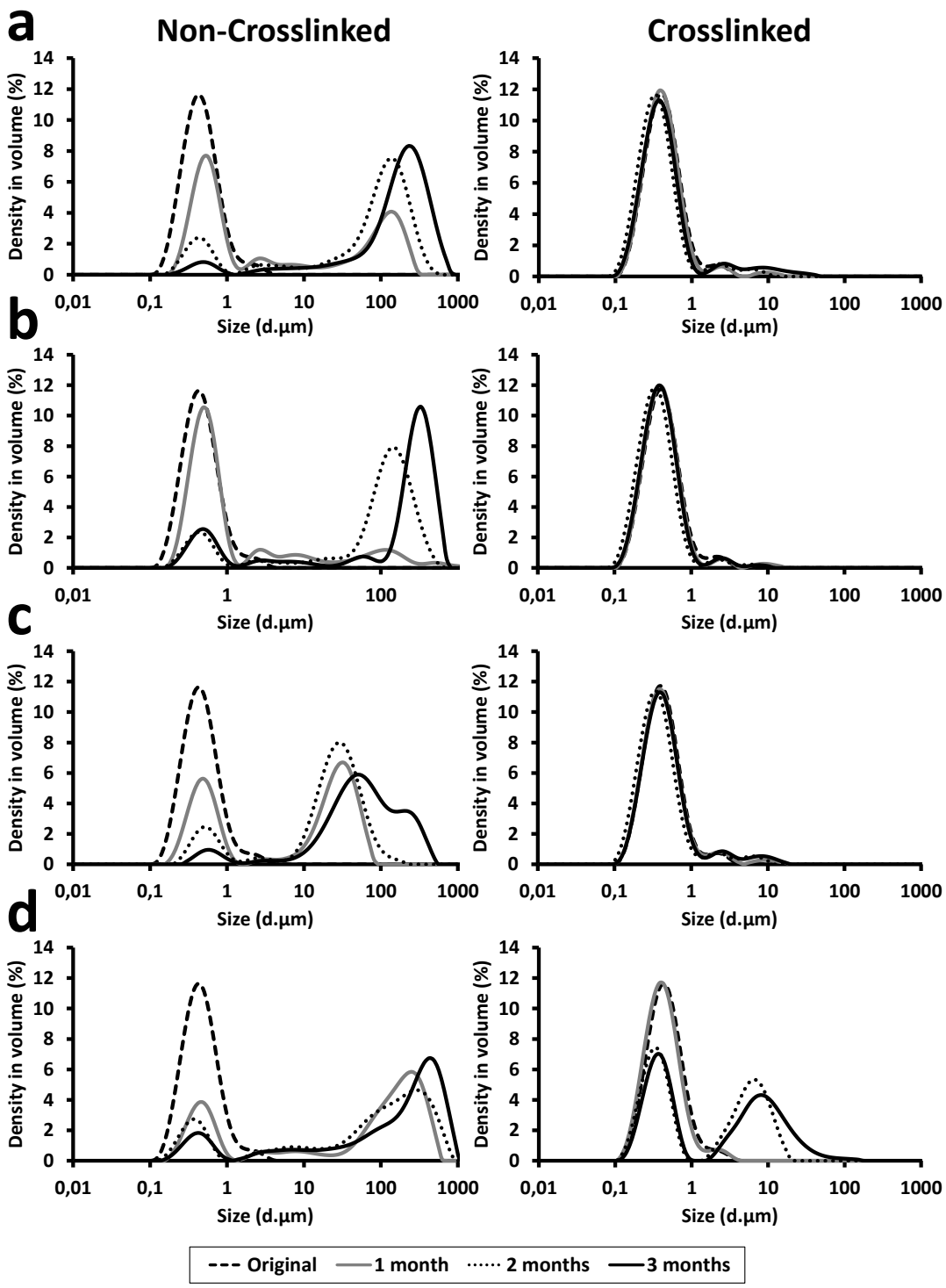

Figure 34. *Size distribution as determined by laser diffraction (LD; deionized water, 2000 rpm, 25 °C) of non-crosslinked (E78, left) and crosslinked (E79, right) o/w-emulsions freshly prepared (original) and at 3 different time points (1 month, 2 months and 3 months) after being stored at 4 different conditions (**a**: light at r.t., **b**: dark at r.t., **c**: dark at 5 °C and **d**: dark at 40 °C).*

Visual inspection demonstrates that **E78** did not suffer phase separation for 1 month; nevertheless, size population was affected by coalescence and subsequent creaming effect; irrespective of the storage conditions (see **Figure 34**).

The presence of larger droplets impeded to perform DLS measurements with the quality criteria required for this technique in most of the cases (see **Table 5**). After 1 month, the stability was completely lost in all samples, except for the emulsions stored in darkness at room temperature and at 5 °C. Our results suggest that non-cross-linked NEs prepared with DXT-MA polymers with a DS=15% are not enough stable to maintain the original droplet size distribution independently of the storing conditions. However, the use of higher DS values for the DXT-MA starting polymer may affect the stability of the resulting nanodroplets, although this was not tested in the current PhD thesis. On the other hand, **E79** proved to be more stable, irrespective of the storage conditions. Coalescence and creaming effects were not observed, and droplet sizes remained stable during the first month in all conditions with the exception of "D" (dark at 40 °C) as showed in **Figure 34** and **Table 5**. It is quite surprising that **E79** was stable in daylight but not in the dark indicating that fish oil, which is known to be very sensitive to light and temperature, is efficiently protected against light but not temperature. This fact explains the presence of large droplet populations at long times under certain conditions, i.e. when stored at 40°C. Interestingly, droplet size increase was not observed during the first month when stored at room temperature and the light, but size increase was observed at months 2 and 3. Moreover, **E79** seems to suffer coalescence at the third month storage in dark and at room temperature as judged by DLS (Z-Average = 800 nm, see **Table 5**) but this effect was not observed by LD (**Figure 34**) confirming that the main emulsion population remained stable. Altogether, our results confirm that crosslinking is a very attractive method to stabilise NEs in the long term.

4.4. Radiochemistry: Biodistribution studies

4.4.1. In vivo biodistribution of free and encapsulated 16α-[18F]Fluoroestradiol (FES)

One of the potential applications of our NEs is in the biomedical field as drug carriers. In this context, it is paramount to investigate the biological fate of the NEs and their capacity to modulate the pharmacokinetic parameters of the encapsulated drugs. In addition, only cross-linked emulsion has been evaluated *in vivo* due to the poor stability achieved by non-cross-linked at 40^{o}C and PBS media.

In order to prove the capacity of the cross-linked NEs to act as drug carriers and modulate drug pharmacokinetics, we selected a hydrophobic model drug (fluoroestradiol, FES) and carried out *in vivo* biodistribution studies. Due to its hydrophobic character, FES is a good candidate to test how drug encapsulation can affect the biodistribution after administration into living organisms. As a control, we also investigated the biodistribution of the free drug. With that aim, we radiolabelled FES with the positron emitter ^{18}F, which enabled *in vivo* studies using positron emission tomography. The free [^{18}F]FES was dissolved in physiological saline solution just before administration. To achieve encapsulation in the nanoemulsion, [^{18}F]FES was dissolved in a small aliquot of dichloromethane and poured into the oil phase just before the sonication step (see Materials and Methods section for detailed description of the process, **E80**). Biodistribution studies with free and encapsulated [^{18}F]FES were carried out in healthy female rats (n=2) after intratracheal administration.

In both cases, the radioactivity was initially in the lungs, and progressively accumulated in the liver even at short times after administration. At longer times, the radioactivity progressively translocated to the gastrointestinal track (**Figure 37**). Despite this qualitative equivalence, quantitative data obtained from the PET images revealed that drug encapsulation significantly prolongs the residence time in the lungs. As it can be seen in **Figure 37**, two minutes after administration of the free [^{18}F]FES, the percentage of radioactivity in the lungs is just 50% of the administered dose, and this value decreases to 10% at t=10 min after administration. Contrarily, for encapsulated

FES (NE-[^{18}F]FES), more than 70% of the radioactivity was still in the lungs at t=10 min. This difference is also observed at t=40 min after administration. At this time point, the % of injected dose remaining in the lungs is 5% and 60% for the free and encapsulated drugs, respectively. These results confirm the suitability of the NEs to prolong the residence time of hydrophobic drugs in the lungs and suggest that these NEs can be used as drug delivery agents.

4.4.2. Preliminary study of ^{64}Cu-DOTA complexation and DXT-MA labeling

As demonstrated in the *in vivo* studies described above, the pharmacokinetics properties of FES can be modified by the proper encapsulation with our DXT-MA emulsifier. However, the pharmacokinetics of the carrier needs to be investigated as well. With that aim, we tackled the radiolabelling of the nanodroplets by covalent attachment of the chelating agent DOTA-SH via thio-Michael reaction on the double bond present in the DXT-MA polymer, preceded by formation of a ^{64}Cu-DOTA complex. This radionuclide is extremely convenient, because its long half-life (ca. 13 hours) enables longitudinal follow-up of the nanodroplets over days.

Chelator choice is crucial for *in vivo* tracking in order to avoid the potential dissociation of the complex chelator-metal, which could result in misinterpretation of the images. As mentioned in the introduction, due to its relatively large cavity and chelating properties, 1,4,7,10-tetraazacyclododecane-tetraacetic acid (DOTA) is one of the most commonly used for *in vivo* imaging. In this specific case, the most convenient method to attach ^{64}Cu to the emulsifier was by using the bifunctional DOTA-SH, due to the presence of double bonds in DXT-MA, which are susceptible to react with thiol groups (-SH) via thio-Michael addition. Furthermore, to preserve the interfacial activity of DXT-MA is mandatory to perform the labeling after the emulsion production following two steps: (i) ^{64}Cu complexation with DOTA-SH and (ii) thio-Michael addition of the complex (^{64}Cu-DOTA-SH) to the DXT-MA present in the interface of the nanoemulsion droplets (see **Figure 36a**).

The incorporation of the radiolabelled bi-functional chelator on the surface of the nanodroplets may significantly modify the surface properties. Because of this, it is

general practice to use the minimum amount of chelator needed to achieve sufficient radiochemical yields to enable *in vivo* imaging. Hence, a preliminary study with pristine DOTA was performed, in order to determine the minimum amount of chelator needed to quantitatively complex ^{64}Cu. To that aim, increasing amounts of DOTA (0, 0.1, 0.3, 1, 3, 10, 30 and 100 nmols) were poured into a buffered sodium acetate solution (pH=5.7) containing ^{64}Cu. After 1 hour at room temperature the complexation was evaluated by radio thin layer chromatography (radio-TLC) on cellulose gel using aqueous NaOH solution (0.001M) as the mobile phase. As shown in **Figure 35b**, free copper (green area) is retained at the seeding spot, while ^{64}Cu-DOTA-SH complex (red area) is eluted. The efficiency of the complexation was evaluated as the ratio between the areas under the two peaks (**Figure 35a**). As it can be seen, below 3 nmols of DOTA no complexation takes place, while a *plateau* is reached at 10 nmols with 100% conversion. In view of the results, we decided to fix the amount of chelator at 100 nmols to ensure quantitative complexation in subsequent experiments.

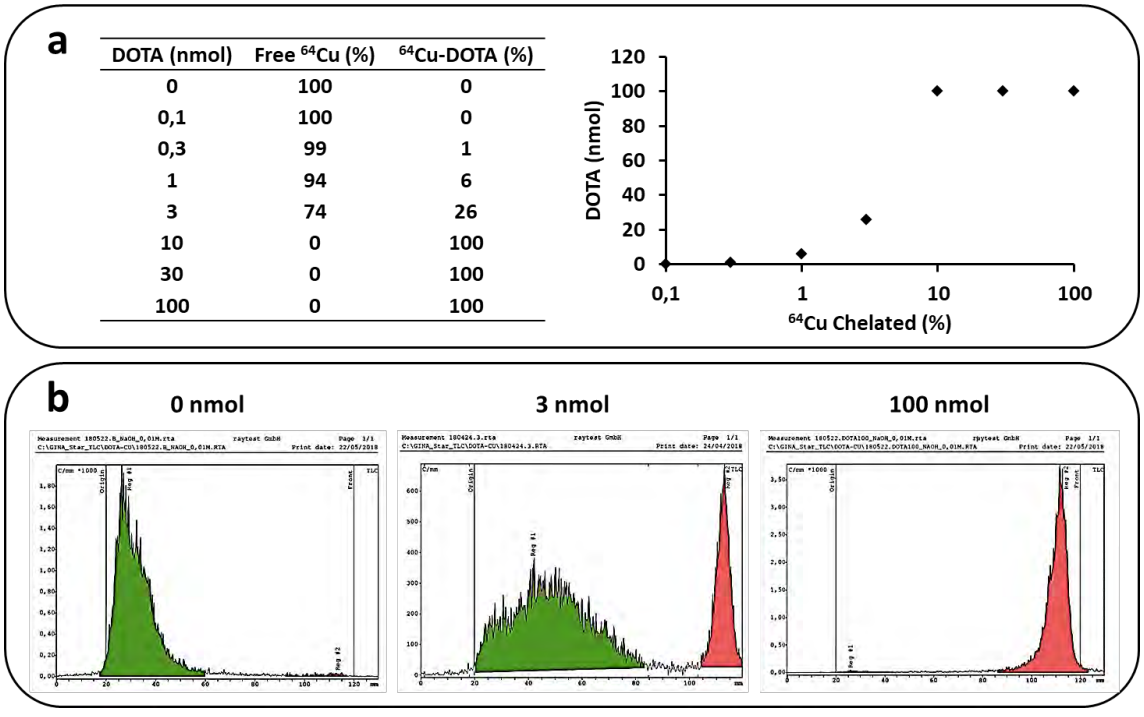

Figure 35. *a) ^{64}Cu complexation percentages obtained by radio-TLC for increasing amounts of DOTA (0, 0.1, 0.3, 1, 3, 10, 30 and 100 nmols). b) Representative radio-TLC images of complexation with 0, 3 and 100 nmols of DOTA; Free ^{64}Cu: green area; ^{64}Cu-DOTA-SH: red area.*

After fixing the amount of chelator at 100 nmol, the reaction with the thiolated chelator was carried out, followed by attachment of the labeled chelator to the surface of the NEs. One-hour reaction resulted in non-quantitative yields, and hence a purification step was required to remove the unreacted free complex. To that aim, size exclusion chromatography (SEC) was performed using a PD-10 column and ultrapure water as the eluent. The eluted solution was collected in 1 mL fractions and the amount of radioactivity in each fraction was determined using a gamma counter (**Figure 36b-c**). As it can be seen in **Figure 36b**, maximum amount of radioactivity was detected in fractions 5 and 13. Fractions 4-6, containing the labelled NEs and showing the aspect of a milky emulsion, were joined and used for *in vivo* experiments. The other fractions containing radioactivity (9-16) were discarded.

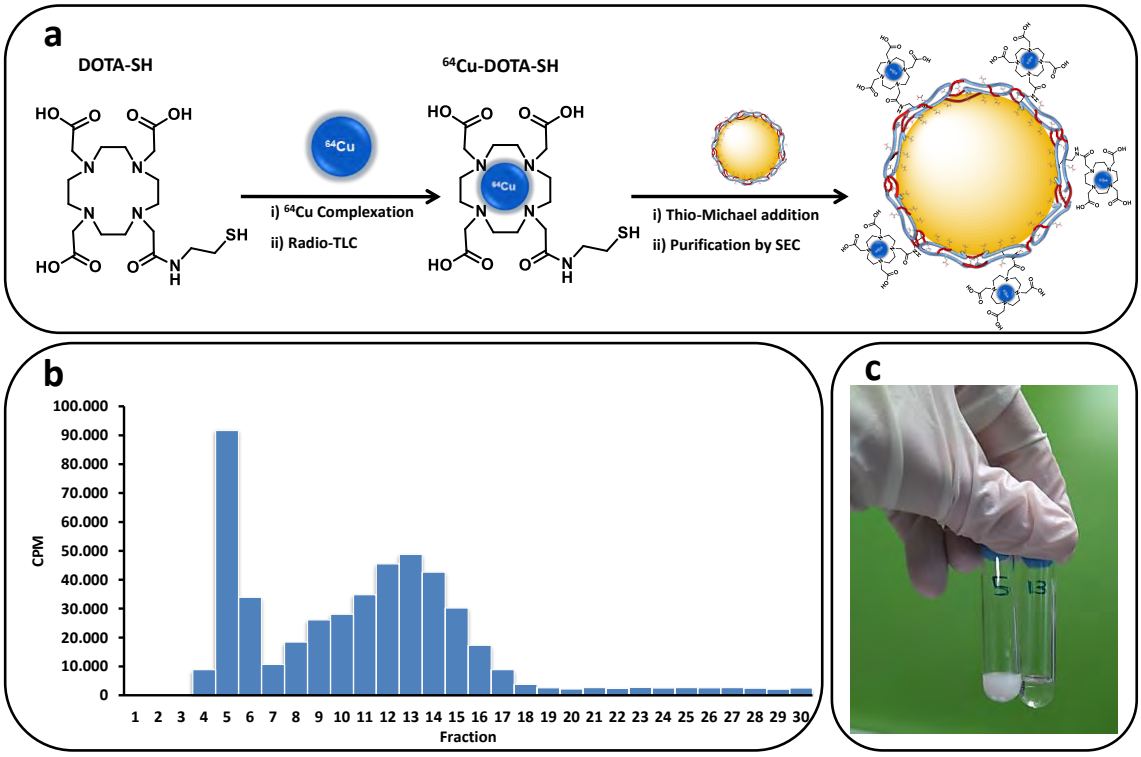

Figure 36. *a) Schematic representation of ^{64}Cu radiolabeling in two steps: (1) ^{64}Cu complexation with DOTA-SH and (2) thio-Michael addition of the complex (^{64}Cu-DOTA-SH) to the DXT-MA present in the interface of the nanoemulsion droplets. b) Graphical representation of the radioactivity (counts per minute, cpm) in the different fractions collected after purification using size exclusion chromatography. c) Digital photograph of maximum activity fractions: Fraction 5 (nanoemulsion) and Fraction 13 (free ^{64}Cu-DOTA-SH).*

4.4.3. *In vivo* biodistribution of DXT-MA

In order to conduct *in vivo* experiments, the radiolabelled cross-linked nanoemulsion (**E81**) prepared as above was administered by intratracheal aerosolization in healthy female rats (n=2) and dynamic PET images were acquired for 40 min. Most of the activity remained in the lungs at early time points, and was progressively translocated to the gastrointestinal track. Focusing on the lungs, more than 70% of the radioactivity was still in this organ at t=10 min, and at t=40 min around 60% of the administered dose still remained. These results perfectly match those obtained for encapsulated [^{18}F]FES, (**Figure 37**) indicating that the nanoemulsion stabilizer (DXT-MA; [^{64}Cu]NE-FES) and the entrapped drug (NE-[^{18}F]FES) remain together.

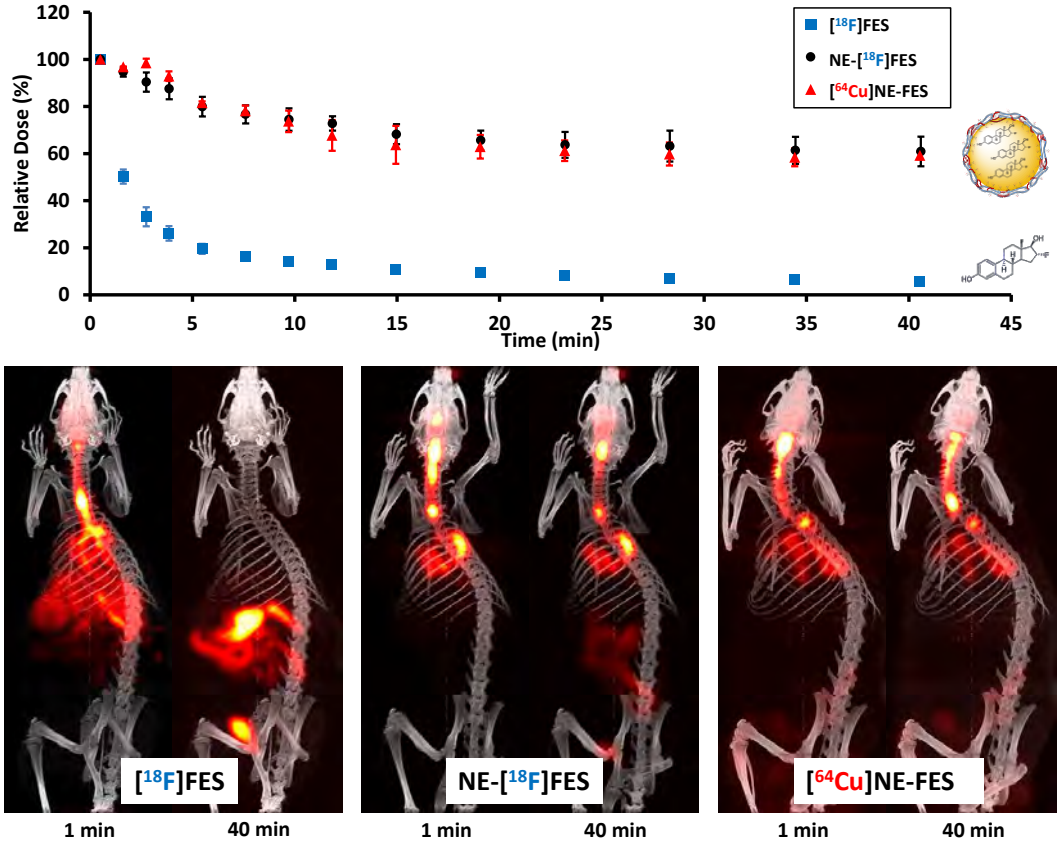

Figure 37. *Top: Percentage of administered dose in lungs at different time points (0-42 min) after intratracheal administration of free FES ([^{18}F]FES; blue), encapsulated FES (NE-[^{18}F]FES; **E80**, black) and DXT-MA ([^{64}Cu]NE-FES; **E81**, red) in healthy female rats (n=2). Bottom: representative PET-CT images (3D coronal projections) at 1 min and at 42 min after intratracheal administration of free FES (left), encapsulated FES (centre) and DXT-emulsion (right).*

The results suggest that as long as the drug remains entrapped, the nanoemulsion also remains in the lungs. Once the drug is released, probably due to destabilization of the emulsion, it is rapidly translocated together with the polymer.

4.5. Summary and Conclusion

Emulsion stability can be enhanced via cross-linking reaction at the oil-water interface. The cross-linking is satisfactory when the cross-linker is dissolved in the oily phase. Stability of cross-linked emulsions was proven in high ionic strength media (PBS, 10 mM phosphate), whereas non-crosslinked emulsions showed fast destabilization (coalescence effects). The minimum amount of DODT required for maintaining the droplet size constant in PBS media was fixed at 0.5 thiol equivalents, related to the number of MA groups. Furthermore, cross-linked emulsions demonstrated to stable up to 3 months in all storage conditions with the exception of darkness and T = 40^{o}C. *In vivo* imaging showed the capacity of the nanoemulsions to modulate the biodistribution of hydrophobic drugs, using FES as model compound. The nanoemulsion prolonged the residence time in the lungs of the encapsulated drug. Radiolabelling of the nanoemulsion confirms that the stabilizer is translocated after drug release, the latter probably triggered by destabilization of the nanodroplets.

4.6. Materials and methods

4.6.1. Materials

Dextran from Leuconostoc spp. (DXT-40, Mr ~40 kDa), glycidyl methacrylate (GMA) (97%), dimethyl sulfoxide (DMSO) (98%), 1,4-Dioxane anhydrous (Dioxane) (99.8%), 2,2'-(ethylenedioxy)diethanethiol [3,6-dioxa-1,8-octane-dithiol (DODT)] (95%) and Kryptofix $K_{2.2.2}$ were purchased from Aldrich and used as received. Docosahexaeonic acid oil (DHA) (80%) was kindly provided by SendaBio. Phosphate-buffered saline (PBS), acetonitrile (MeCN) and dichloromethane were purchased from Scharlau and used as received. 4-(Dimethylamino)pyridine (DMAP) was purchased from Acros-Organics. 1,4,7,10-Tetraazacyclododecane-1,4,7-tris(acetic acid)-10-(2-thioethyl)acetamide

(DOTA-SH) (94%) was purchased from Macrocyclics. 3-methoxymethyl-16β,17β-epiestriol-O-cyclic sulfone (MMSE) was purchased from ABX Advance. Illustra NAP TM-5 columns were purchased from GE Healthcare Life Sciences. Ultrapure water was obtained from a Milli-Q A10 Gradient equipment (Millipore).

4.6.2. Characterization Methods

- *Dynamic Light Scattering* (DLS): DLS analyses were conducted using a Zetasizer Nano ZS, ZEN3600 Model (Malvern Instruments Ltd). All measurements were performed in disposable sizing cuvettes at a laser wavelength of 633 nm and a scattering angle of 173°, while the zeta-potential measurements were performed in disposable zeta potential cells (pH 7.4, 25°C). Emulsion samples were dispersed in deionized water at a concentration of 2 mg oil/mL. Each measurement was repeated for three runs per sample at 25°C.
- *Nuclear magnetic resonance* (^{1}H NMR): NMR spectra were recorded on a Bruker AVANCE III spectrometer at 500 MHz and 25°C. Chemical shifts (δ) are given in ppm relative to the residual signal of the solvent. Splitting patterns: b, broad; s, singlet; d, doublet; t, triplet; q, quartet; m, multiplet.
- *Laser diffraction (LD)*: LD analyses were conducted using Mastersizer 3000 laser diffraction system (Malvern Instruments Ltd). All measurements were performed at a laser wavelength of 430 nm using 600 mL of deionized water in a glass beaker. Each measurement was repeated for five runs per sample and 5 seconds per run at 25°C following Mie dispersion model.
- *Cryo Transmission Electron Microscopy (Cryo-TEM)*: Cryo-TEM analysis of (o/w)-emulsions were performed on a JEM-2200FS/CR (JEOL Europe, Croissy-sur-Seine, France) transmission electron microscope. This microscope is equipped with a field emission gun (FEG) operated at 200 kV and an in-column Ω energy filter. During imaging, no-tilted zero-loss two-dimensional (2D) images were recorded under low-dose conditions, utilizing the 'Minimum Dose System (MDS)' of Jeol software, with a total dose on the order of 10-20 electrons/Å² per exposure, at defocus values ranging from 1.5 to 4.0 µm. The in-column Omega energy filter of the microscope help us to record images with improved signal-to-noise ratio (SNR) by zero-loss

filtering, using an energy selecting slit width of 30 eV centered at the zero-loss peak of the energy spectra. Digital images were recorded on a 4K × 4K (15 µm pixels) Ultrascan4000™ charge-coupled device (CCD) camera (Gatan Inc.) using DigitalMicrograph™ (Gatan Inc.) software, at different nominal magnifications from 4000× to 60,000×.

- *Field-Emission Scanning Electron Microscopy (FE-SEM).* Micrographs were obtained using a ULTRA plus ZEISS Field-Emission Scanning Electron Microscope (FE-SEM) instrument operating at 5 kV. 1 drop of the particles dispersion at 0.1 wt% was added on an aluminium SEM stub and left dried during a couple of hours. Prior to inspection, all samples were sputter-coated (SDC 005, Bal-Tec) with a thin overlayer of gold to prevent sample-charging effects. ImageJ software was used to analyse the FE-SEM micrographs to determine the number-average diameter and size distributions.

4.6.3. Production of O/W emulsions cross-linked at the O/W interface (method 3, M3)

DXT-MA **(D7;** 20 mg, 5% wt. related to oil phase) was dissolved in 3.6 mL of deionized water (aqueous phase, 90% wt.) in a 8 mL glass vial. To this solution 0.4 g of DHA (oil phase, 10% wt.) were added. Then, DODT (0.5-3 µL; 0.25-1.5 SH eq.) was carefully added over the oil phase and pH was adjusted to 9.5. Emulsion was formed using an UP400S (Hielscher) system at 100% of amplitude and pulse during 4 minutes (400 W) with a H3 sonotrode tip (3 mm diameter, 100 mm length). Sonication step was realized at 0°C, using an ice bath, and under magnetic stirring.

4.6.4. DMSO/Dioxane (70:30, v/v) challenge

Cross-linked emulsion (i.e. E74; 1.5 mL) was dissolved in 30 mL (Dil. 1:20) of DMSO/Dioxane (70:30, v/v) overnight, at room temperature and under magnetic stirring. The oil phase was removed by liquid-liquid extraction with hexane (3x80 mL). The aqueous phase was collected and purified by dialysis against ultrapure water (MWCO 3,500Da) during 4 days, refreshing with 4 L of deionized water twice per day. The resulting aqueous solution was freeze-dried to obtain the cross-linked polymer **(D7-CL)** as a white solid. Oil traces were removed via solid-liquid extraction with

hexane (3x1 mL) using a vortex. Purification was performed by 3 centrifugation cycles (14000 rpm, 5 min, r.t.), whereby supernatant was removed. The polymer (solid) was finally dried at 70°C for 2 hours. ^{1}H NMR (500 MHz, D_2O) δ ppm: 6.38-6.08 (m, 1H, methacrylic-CH), 5.95-5.67 (m, 1H, methacrylic-CH), 5.55-4.85 (8.2H, including H-1 and H-2/3 MA-substituted), 4.38-3.25 (40H, m, rest of Glc and 2xCH_2O of cross-linker), 3.06-2.58 (3.3H, m, $CH(CH_3)CH_2S$, CH_2S of cross-linker), 1.98 (s, 3.7H, methacrylic-CH_3), 1.36-1.12 (b, 1.7H, cross-linker-CH_3).

4.6.5. Crosslinking assessment by PBS (1X) challenge

Medium stability studies were carried out by diluting (Dil. 1:2) the emulsions (E72, E73, E74, E75, E76 and E77) with deionized water or phosphate buffered saline (PBS, 10 mM phosphate). All samples were stored at 4°C in darkness for 48 h. Then, size distribution was measured by LD.

4.6.6. Medium stability over time in PBS (1X)

Medium stability studies were also performed over time and under recirculation in phosphate buffered saline (PBS, 10 mM phosphate) followed by volume-weighted size distribution at regular intervals of 10 minutes, determined using a Mastersizer 3000 laser diffraction system (Malvern Instruments Ltd). With that aim, nanoemulsions were added dropwise over 100 mL of PBS (10 mM phosphate) in the Hydro SM (Small volume entry level wet dispersion unit) at 1500 rpm.

4.6.7. Long-term stability at different storing conditions

Time stability studies were done by storing the cross-linked and non-cross-inked NEs at 4 different conditions (A: light at r.t., B: dark at r.t., C: dark at 5 °C and D: dark at 40 °C) during 3 months. Emulsion stability was subsequently evaluated by visual inspection; hydrodynamic diameter and volume average diameter were determined by DLS and LD at 3 different time points (1 month, 2 months and 3 months).

4.6.8. Radiochemistry (I): Synthesis of 16α-[^{18}F]Fluoroestradiol (FES) (Core)

[^{18}F]fluorine was produced by irradiation of [^{18}O]H_2O with 18MeV protons using an IBA Cyclone 18/9 cyclotron based on Römer *et al.* (1999) [22]. [^{18}F]F^- was trapped in an

Accell™ Plus QMA anion exchange resin (Waters) and eluted into a V-shaped vial using sequentially a solution of Kryptofix $K_{2.2.2}$ in MeCN (15 mg/mL; 1 mL) and an aqueous K_2CO_3 solution (6 mg/mL; 0.5 mL). The solvent was evaporated to dryness via azeotropic distillation in two steps (80°C, 10 min; 100°C, 5 min) under helium flow. Subsequently, a solution containing 1 mg of 3-methoxymethyl-16β,17β-epiestriol-O-cyclic sulfone (MMSE) in anhydrous MeCN (1 mL) was added and the mixture was heated at 100°C for 10 min. After fluorination, a 0.1M HCl solution in CH_3CN (prepared by mixing 9 parts of MeCN and 1 part of 1 M HCl) was added and the solvent was evaporated to dryness at 100°C under helium flow. After repeating this operation and cooling to 40°C, the reaction crude was diluted with Water/MeCN (40/60, 2.5 mL) and the resulting mixture was eluted through a Sep-Pak C18 plus cartridge (Waters) and purified by high performance liquid chromatography (HPLC) using radioactive detection. A Nucleosil™ 100-7 C18 column (10 x 250 mm, 5 µm) was used as stationary phase and Water/MeCN (40/60) as the mobile phase at a flow rate of 5 mL/min. The desired fraction (retention time ~ 12 min) was collected, diluted with water (40 mL) and reformulated by trapping in a Sep-Pak C18 Plus Short Cartridge (waters) and further eluting with dichloromethane (2 mL). Quality control analysis was performed using a Mediterranea Teknokroma C18 column (150 mm) as stationary phase. The column was eluted with A (water) and B (Acetonitrile) using a gradient: t=0 min, 80% A, 20% B; t=2min, 80% A, 20% B; t=10 min, 10% A, 90% B; t=12 min, 10% A, 90% B; t=14 min, 80% A, 20% B at 1 mL/min flow rate. The retention time was 9 min.

4.6.9. Radiochemistry (II): Radiolabeling of DXT-MA with ^{64}Cu (shell)

^{64}Cu was produced at by irradiation of ^{64}Ni (Isoflex USA, 99.53% atom) at 14 MeV following a previously described method by Kume *et al* (2012)[23]. The solution containing $^{64}CuCl_2$ in 0.1M HCl (1 mL) containing ca. 970 MBq of ^{64}Cu was evaporated to dryness and the residue was reconstituted with 0.2M sodium acetate buffer solution (800 µL, pH=5.7). To this solution, DOTA-SH (750 µL, 1 mg/mL, aqueous solution) was added and the reaction was allowed to occur for 1h at room temperature. The reaction progress was monitored by thin layer chromatography (TLC) on cellulose gel using aqueous NaOH solution (0.001M) as the mobile phase. After

completion of the reaction, the mixture was eluted through a sep-pak C18 plus cartridge to selectively retain ^{64}Cu-DOTA-SH, which was further eluted with Ethanol (1 mL). Ethanol was evaporated and the residue was reconstituted with 0.01M NaOH solution (500 µL). To this solution, 500 µL of cross-linked emulsion (5% wt. of DHA oil and 0.25%wt. of DXT-MA) were added. The solution was brought to pH=10 and the reaction was allowed to occur at room temperature for 1 hour. Excess chelator was removed by size exclusion chromatography using a PD-10 column eluted with ultrapure water, and 1 mL fractions were collected. Only those fractions containing the highest concentration of radioactivity (140-360 MBq) were used subsequently.

4.6.10. Animal experiments

The animals were maintained and handled in accordance with the Guidelines for Accommodation and Care of Animals (European Convention for Protection of Vertebrate Animals Used for Experimental and Other Scientific Purposes) and internal guidelines. Experimental procedures were approved by the ethical committee and local authorities. All animals were housed in ventilate cages and fed on standard diet ad libitum.

4.6.11. Aerosol administration

Endotracheal insufflations were carried out using the Penn-Century MicroSprayer® Aerosolizer (FMJ-250 High Pressure Syringe Model, Penn-Century. Inc. Wyndmoor, USA; henceforth “Penn-Century Aerosolizer”) following a previously reported method by Cossío *et al.* (2018) [24]. In brief, deep sedation was induced to the animals by inhalation of 5% isoflurane in pure O_2. The tip of the delivery needle was carefully positioned just above the carina and 50 µL of injectable emulsion diluted with ultrapure water (1:10) containing ca. 1.85-9.32 MBq was administered. A small animal Laryngoscope (Penn-Century, Model LS-2) was used for correct visualization of the epiglottis. Immediately after administration, rats were submitted to *in vivo* imaging studies.

4.6.12. *In vivo* Imaging experiments

After aerosol administration and without recovering from sedation, animals were positioned in an eXploreVista-CT small animal PET-CT system (GE Healthcare, USA) to perform *in vivo* studies. During imaging, rats were kept normothermic using a heating blanket (Homeothermic Blanket Control Unit; Bruker). Anesthesia was maintained by inhalation of 1.5-2% isoflurane in pure O_2. Dynamic PET images (energy window: 400-700 KeV) were acquired with the following frames: 4 x 15 s, 4 x 30 s, 3 x 60 s and 3 x 90 seconds. In all cases, four beds were defined to acquire whole body images (total acquisition time = 42 min). After each PET acquisition, a CT scan (X-Ray energy: 40 kV, intensity: 140 µA) was performed for a later attenuation correction in the image reconstruction and for unequivocal localization of the radioactivity. PET Images were reconstructed using random and scatter corrections using filtered back projection. PET-CT images of the same animal were co-registered and analyzed using PMOD image analysis software (PMOD Technologies Ltd, Zürich, Switzerland). Volumes of interest (VOIs) were manually delineated on the organs of interest on CT images. VOIs were transferred to PET images and time–activity curves (decay corrected) were obtained as cps/cm^3 in each VOI and values were then normalised to the starting amount of radioactivity.

4.7. References

1. Demetriades, K., Coupland, J. N. & McClements, D. J. Physicochemical properties of whey protein-stabilized emulsions as affected by heating and ionic strength. *J. Food Sci.* **62**, 462–467 (1997).

2. Ishikawa, Y., Katoh, Y. & Ohshima, H. Colloidal stability of aqueous polymeric dispersions: Effect of pH and salt concentration. *Colloids Surfaces B Biointerfaces* **42**, 53–58 (2005).

3. Rangsansarid, J. & Fukada, K. Factors affecting the stability of O/W emulsion in BSA solution: Stabilization by electrically neutral protein at high ionic strength. *J. Colloid Interface Sci.* **316**, 779–786 (2007).

4. Dickinson, E. Hydrocolloids as emulsifiers and emulsion stabilizers. *Food Hydrocoll.* **23**, 1473–1482 (2009).

5. Bizmark, N. & Ioannidis, M. A. Effects of Ionic Strength on the Colloidal Stability and Interfacial Assembly of Hydrophobic Ethyl Cellulose Nanoparticles. *Langmuir* **31**, 9282–9289 (2015).

6. Leng, L., Li, H., Yuan, X., Zhou, W. & Huang, H. Bio-oil upgrading by emulsification/microemulsification: A review. *Energy* **161**, 214–232 (2018).

7. Chircov, C. & Grumezescu, A. M. *Nanoemulsion preparation, characterization, and application in the field of biomedicine*. *Nanoarchitectonics in Biomedicine* (Elsevier Inc., 2019). doi:10.1016/b978-0-12-816200-2.00019-0.

8. Chevalier, Y. & Bolzinger, M. A. Emulsions stabilized with solid nanoparticles: Pickering emulsions. *Colloids Surfaces A Physicochem. Eng. Asp.* **439**, 23–34 (2013).

9. Salari, J. W. O., Van Heck, J. & Klumperman, B. Steric stabilization of pickering emulsions for the efficient synthesis of polymeric microcapsules. *Langmuir* **26**, 14929–14936 (2010).

10. Morse, A. J. *et al.* Novel Pickering Emulsi fi ers Based on pH-Responsive Poly(2-(diethylamino)ethyl methacrylate) Latexes. *Langmuir* **29**, 5446–5475 (2013).

11. Cayre, O. J., Noble, P. F. & Paunov, V. N. Fabrication of novel colloidosome microcapsules with gelled aqueous cores. *J. Mater. Chem.* **14**, 3351–3355 (2004).

12. Gordon, V. D. *et al.* Self-assembled polymer membrane capsules inflated by osmotic pressure. *J. Am. Chem. Soc.* **126**, 14117–14122 (2004).

13. Bon, S. A. F., Cauvin, S. & Colver, P. J. Colloidosomes as micron-sized polymerisation vessels to create supracolloidal interpenetrating polymer network reinforced capsules. *Soft Matter* **3**, 194–199 (2007).

14. Thompson, K. L. *et al.* Covalently cross-linked colloidosomes. *Macromolecules* **43**, 10466–10474 (2010).

15. Thompson, K. L., Chambon, P., Verber, R. & Armes, S. P. Can polymersomes form colloidosomes? *J. Am. Chem. Soc.* **134**, 12450–12453 (2012).

16. Thompson, K. L., Williams, M. & Armes, S. P. Colloidosomes: Synthesis, properties and applications. *J. Colloid Interface Sci.* **447**, 217–228 (2014).

17. Færgemand, M., Murray, B. S. & Dickinson, E. Cross-Linking of Milk Proteins with Transglutaminase at the Oil-Water Interface. *J. Agric. Food Chem.* **45**, 2514–2519 (1997).

18. Torchilin, V. P. Micellar nanocarriers: Pharmaceutical perspectives. *Pharm. Res.* **24**, 1–16 (2007).

19. Xing, H., Hwang, K. & Lu, Y. Recent developments of liposomes as nanocarriers for theranostic applications. *Theranostics* **6**, 1336–1352 (2016).

20. Walsh, A., Thompson, K. L., Armes, S. P. & York, D. W. Polyamine-functional sterically stabilized latexes for covalently cross-linkable colloidosomes. *Langmuir* **26**, 18039–18048 (2010).

21. Malvern. A basic guide to particle characterization. *Malvern whitepaper* (2015).

22. Römer, J., Füchtner, F., Steinbach, J. & Johannsen, B. Automated production of 16α- [18F]fluoroestradiol for breast cancer imaging. *Nucl. Med. Biol.* **26**, 473–479 (1999).

23. Kume, M. *et al.* A semi-automated system for the routine production of copper-64. *Appl. Radiat. Isot.* **70**, 1803–1806 (2012).

24. Cossío, U. *et al.* Preclinical evaluation of aerosol administration systems using Positron Emission Tomography. *Eur. J. Pharm. Biopharm.* **130**, 59–65 (2018).

Chapter 5. Nanoemulsions as lipase-responsive materials

5.1. Introduction

Drug delivery systems are expected to selectively accumulate in the target organ or tissue and release the cargo in a controlled manner. Overexpression of certain enzymes is generally related to physiological disorders. When such overexpression occurs locally in the target organ, it can be used to trigger drug release by using enzyme-responsive materials.[1,2] In this process, the interaction between the enzyme and the substrate results in degradation of the carrier (triggering drug release), and this interaction can be controlled to some extent by introducing physical barriers between the encapsulated substrate and the surrounding aqueous phase where enzymes use to be located. The introduction of thick or unalterable barriers hampers enzyme-substrate interaction and results in delayed or limited drug release, with the consequent lack effectiveness of the treatment. Contrarily, the introduction of extremely soft and/or reactive materials can result in an uncontrolled and non-specific release of the cargo, with the consequent potential off-target side effects. The selection of the right substrate and precise composition of the above-mentioned physical barriers is essential to achieve selective or preferential delivery in the target organ. Because of this, the investigation of enzyme-responsive materials as drug delivery systems has gained attention in the last decades.[3–5]

Biodegradation of biopolymers usually relies on the action of enzymes (i.e. dextran is degraded by dextranase).[6] However, unmodified polymers are rarely used in nanomedicine, because the introduction of functional properties usually requires chemical modification of the enzymatically degradable chains. Such modifications may result in a reduction of the enzymatic degradability, although this is not always the case. For example, *Franssen et al.* demonstrated that methacrylated dextrans were enzymatically degraded by dextranase at a similar rate as the native dextran, even at high substitution degrees.[7] In our nanosystems, the presence of ester bonds generated during attachment of methacrylate (MA) to dextran (DXT) suggests that lipases or esterases may induce hydrolysis, compromising the stability of the emulsion,

eventually leading to release of the cargo. Moreover, the kinetics of drug release might be adjusted by crosslinking the functionalized polysaccharides adsorbed at the oil/water interface.

In this chapter, we demonstrate that DXT-MA-stabilized oil-in-water emulsions can be enzymatically degraded, and that drug release triggered by the enzymatic action can be significantly retarded by crosslinking the stabilizer at the oil/water interface. *Candida Antarctica Lipase B* (CALB) [8,9] was selected for preliminary studies tackling the elucidation of destabilization mechanism, while *Pancreatic Lipase* (PL) [10,11] was selected to evaluate the stability of the emulsions towards a human lipase in an *in vitro* model designed to simulate lipid digestion by pH-stat method.[5,12]

5.2 Objectives

The specific objectives of this work are:

1. To select the appropriate enzyme
2. To investigate the demulsification mechanism of DTX-MA-stabilized oil-in-water emulsions in the presence of *Candida Antarctica Lipase B*.
3. To evaluate the effect of: (i) crosslinking; (ii) emulsifier; (iii) droplet size; and (iv) triglyceride oil type, on the stability of DTX-MA-stabilized oil-in-water emulsions in the presence of *Lipases.*

5.3. Modified dextran as emulsifier with enzyme-responsiveness

5.3.1. Enzyme selection

The functionalization of the DXT with MA leads to ester bonds formation. Because of this, we anticipated that instability could be induced by using enzymes specifically adapted to hydrolyse ester bonds: esterases and lipases. Esterases are more selective to ester bonds of water-soluble molecules; meanwhile, lipases have evolved to be interfacially activated by the recognition of hydrophobic regions at the oil/water

interface.[13] Consequently and regarding emulsion characteristics, especially the presence of ester bonds in both surfactant and oil phase, lipases were selected to selectively trigger interfacial ester hydrolysis instead of esterases. A Preliminary proof of concept to elucidate how lipases trigger demulsification was performed following the products generated during the enzymatic action by ^{1}H-NMR. To that purpose, an emulsion based on sunflower oil at 40 wt% stabilized with 0.5 wt% of DXT-SCPN-MA (see **Appendix III. Production and Characterization of Lipase-Responsive Emulsions**; **E82**) was incubated towards *Rhizopus oryzae Lipase* (ROL), a microbial lipase widely used for the conversion of sunflower oil to biodiesel.[14,15]

In this experimental procedure, ^{1}H-NMR has been used to prove the presence of glycerol and linoleic acid, major components of the ester hydrolysis of sunflower oil, in the water media (**Figure 38**).

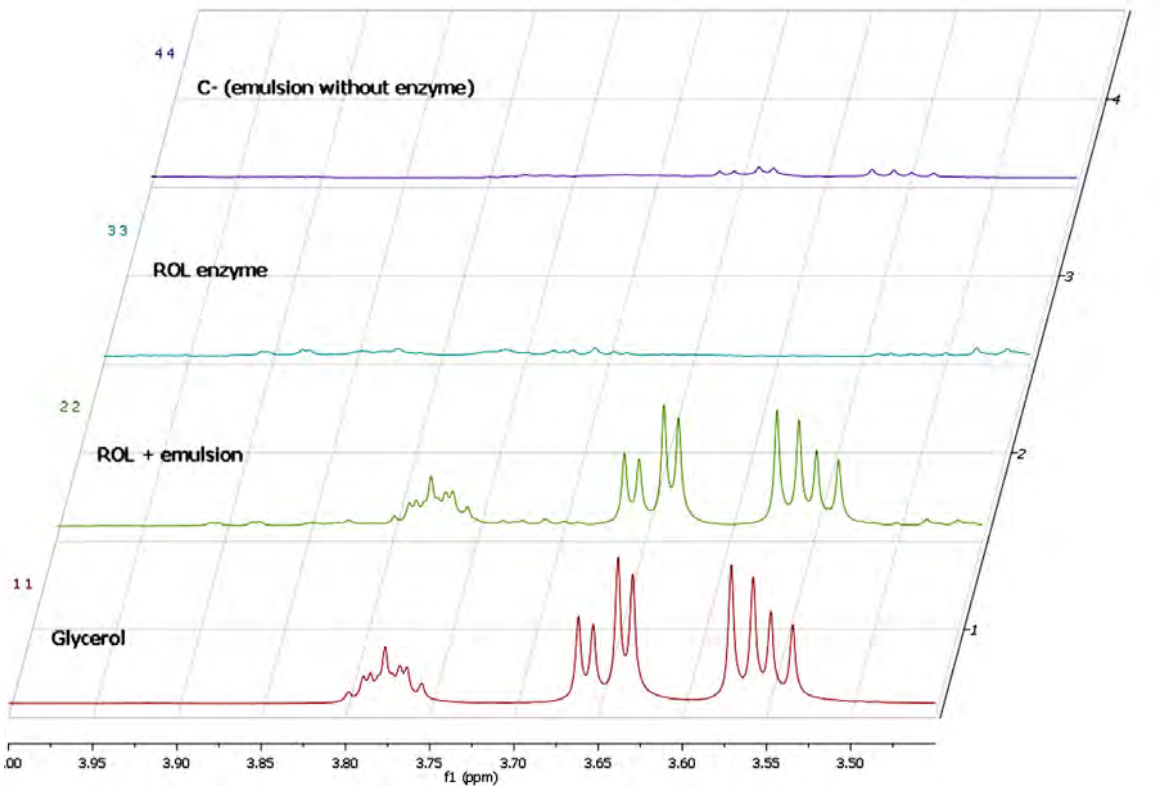

Figure 38. *^{1}H NMR (D_2O, 500 MHz) of: (1.1) isolated glycerol, (2.2) water phase of emulsion in the presence of ROL, (3.3) isolated ROL and (4.4) water phase of emulsion control (without ROL).*

The ^{1}H-NMR spectra demonstrated that the incubation of the emulsion with ROL generates glycerol as consequence of the lipase-catalyzed hydrolysis of the triacylglycerol from the sunflower oil presented forming the emulsion. Glycerol only appears where enzyme and emulsion are in contact; otherwise, the glycerol is not generated. Furthermore, the combination of the signals obtained for isolated ROL and isolated glycerol was in agreement with those obtained for the hydrolysis of sunflower (ROL + emulsion) as showed in **Figure 38**.

As second proof of concept assay, **E82** was incubated with ROL and other lipases from microbial origins that have proven their affinity towards sunflower oil (major emulsion component), i.e. *Candida Antarctica Lipase B* (CALB),[16,17] *Rhizomucor miehei Lipase* (RML),[18,19] and *Thermomyces lanuginosus Lipase* (TLL),[20,21] and the resulting emulsions were visually inspected over time. The addition of CALB, RML and ROL severely affected the stability of the emulsion after 40 h of incubation, with a clear creaming effect and formation of an oil layer at the top of the emulsion (**Figure 39**).

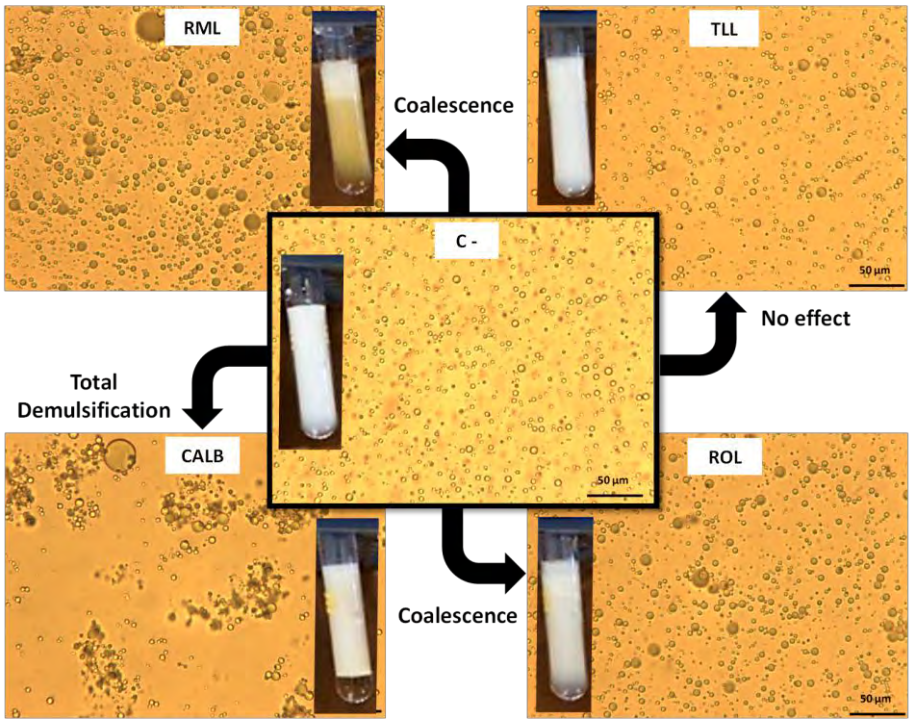

Figure 39. *Photographies (t=40 h of incubation) and optical microscopy images (t=20 h of incubation) obtained after incubation of* ***E82*** *emulsion with the lipases RML, TLL, CALB and ROL. A control emulsion (incubated without addition of enzyme) is also included (C-).*

At the same time point, the control emulsion ("C" in the Figure, no enzyme) remained unaltered. These results were confirmed by optical microscopy. Images obtained at 20 h of incubation clearly demonstrated that the presence of the enzyme altered the physical stability of the emulsion. The presence of either CALB, ROL or RML produced an increase in droplet size due to coalescence, flocculation and related effects (see Introduction chapter section **1.1.4. Nanoemulsions in nanomedicine**), as suggested by visual inspection in which phase separation and creaming effect could be observed, especially for CALB. This could be related to the high affinity of CALB towards methacrylated esters, similarly to those presented in DXT-SCPN-MA, as described in methacrylate functionalized polyester catalysis by polycondensation[22] or to obtain methacrylate-terminated polyisobutylenes by transesterification of vinyl methacrylate[23]. Furthermore, CALB do not need interfacial activation, because of the absence of lid covering the active site, being always in an "open" conformation.[8,9] Contrarily, the enzyme TLL did not affect the stability of the emulsion. It has been reported that the catalytic activity of TLL in transesterification is highly affected by the structure of the acyl donors involved. The initial reaction rate and the maximum substrate conversion increased with the elongation of the vinyl ester chain, being the stronger interactions obtained for medium-chain acyl groups (C8-C14).[24] However, branched-chains and short (C2-C8) or extremely long (C14-C18) chains were reported as the poorest substrates in these terms. This suggests that esters attached to MA groups present in highly hindered short-chain polymers, as DXT-SCPN-MA, are less reactive contributing to slow down the demulsification rate. To sum up, emulsion stability has been compromised by the presence of certain type of lipases suggesting their potential use as enzyme-responsive carriers to achieve controlled drug release. CALB was selected for the rest of the study because of achieving the fastest emulsion destabilization.

5.3.2. Effect of emulsion components on the enzyme-trigger demulsification efficiency

The preliminary results described above suggest that our NEs can be used as enzyme-responsive drug delivery systems. However, a good understanding of the

demulsification process is required to enable the preparation of tailored emulsions. First, we decided to investigate if the destabilization of the nanoemulsion was actually due to enzymatic cleavage of the ester bonds, or otherwise it was dominated by the physicochemical interactions at the oil-water interface. Lipase enzymes are adapted to hydrolyze ester bonds with certain characteristics. In our systems, ester bonds are present both in the emulsifier and the triglyceride oil, and different factors can affect the emulsion destabilization mechanism, including steric hindrance, droplet size, selectivity and specificity of the enzyme, emulsion dilution, temperature, stirring, etc.[10,13,25] Thus, a qualitative study to investigate the enzymatic degradation of major emulsion components separately (emulsifier and oil phase) was carried out to evaluate which one plays a more significant role in demulsification. Five emulsifiers were selected to evaluate the capacity of lipases to hydrolyze ester bonds presented in an aqueous solution of each emulsifier before emulsion generation. To that aim, emulsifiers with different physicochemical characteristics (electric charge, presence or absence of ester bonds and steric hindrance on the ester bond; **Table 6**) were incubated towards CALB for a week. After one-week incubation, sunflower oil (triacylglycerol mainly composed by oleic and linoleic acids) was incorporated to each emulsifier solution for evaluating the capacity of the emulsifiers to produce emulsions after being in the presence of the enzyme. On the other hand, to evaluate the enzyme capacity to hydrolyze esters in a non-aqueous media, CALB was dissolved in pure sunflower oil and the mixture was also incubated for a week (see section **5.5.8. Sunflower oil as enzyme substrate**).

Table 6. Main characteristics of the emulsifiers selected to investigate response to CALB enzyme.

Emulsifier	Emulsion	Electrochemical properties	Ester bonds	Steric hindrance
DXT-SCPN-MA **(D15)**	E83	Non ionic	Yes	+++
DXT-MA **(D12)**	E84	Non ionic	Yes	++
DXT-F **(D17)**	E85	Anionic	Yes	++
Tween20	E86	Non ionic	Yes	-
Triton-X100	E87	Non ionic	No	-

In a typical procedure, CALB was added to an aqueous solution containing 0.5% wt of each emulsifier. In the case of sunflower, 0.2 mg of CALB were poured into 0.4 g of the oil (**Figure 40**). All mixtures were homogenized using a roller mixer at room temperature for 7 days. Clear solutions of DXT-SCPN-MA (**D15**), DXT-MA (**D12**), Tween 20 and Triton X-100 became progressively turbid and white precipitates appeared in DXT-SCPN-MA and DXT-MA solutions. No alteration was observed for DXT-F (**D17**). In order to study the capability of the emulsifiers to stabilize oil droplets, the solutions incubated for one week were used together with the rest of the components needed to produce the emulsions.

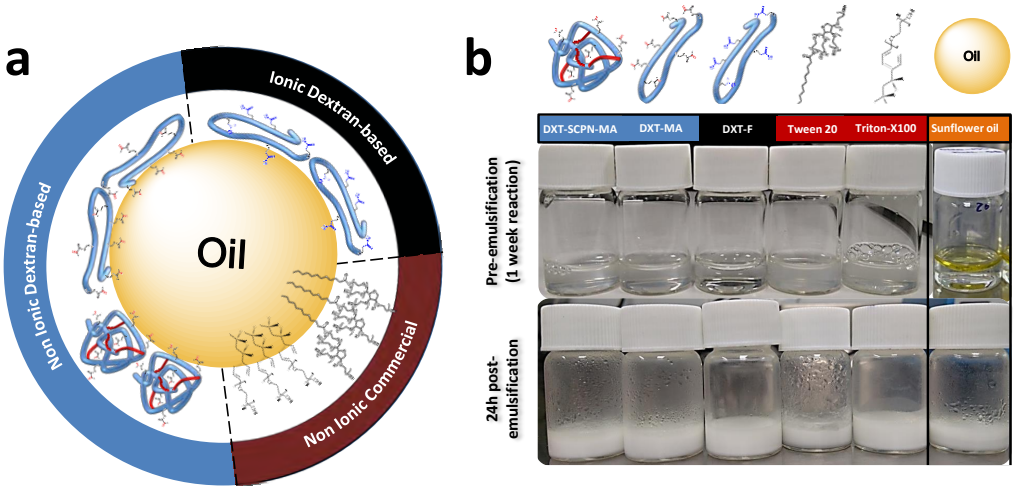

Figure 40. *a) Schematic representation of sunflower oil-in-water (O/W)-emulsions with 5 different emulsifiers. b) Digital photographies of (o/w)-emulsions (10% wt. sunflower oil, 90% wt. Milli-Q water and 0.1% wt. stabilizer) stabilized by DXT-SCPN-MA (**D15, E83**), DXT-MA (**D12, E84**), DXT-F (**D17, E85**), Tween20 (**E86**) and Triton-X100 (**E87**) after the addition of CALB (10 µL, 20 mg/mL) to the aqueous phase (Milli-Q water + emulsifier) and oil phase (sunflower oil, **E88**). Top: before emulsion production (after 1 week reaction); Bottom: 24 h after emulsion production.*

For the mixtures of emulsifier-CALB in water, only the dispersed phase (sunflower oil) was added, whereas an aqueous phase containing DXT-SCPN-MA (**D15**, 0.1% wt.) as surfactant was incorporated to the hydrolyzed sunflower oil. The mixtures were sonicated during 4 min. After 24 h, visual inspection of the emulsions confirmed the formation of oil droplets for DXT-SCPN-MA (**D15**), DXT-MA (**D12**) and Tween 20 (**Figure 40**), all of them containing ester bonds attached to a non-polar alkyl chain. However,

this did not happen in the case of DXT-F (**D17**), which has ester bonds attached to an anionic group (-COOH), and Triton-X100, which does not have ester bonds. Results obtained suggest that enzymatic activity of CALB is highly dependent on the ester bond type, with ester bonds directly attached to an alkyl chain showing higher reactivity towards the enzyme. Results are in agreement with literature data. Indeed, it is reported that lipase enzymes demand a non-polar chain attached to the ester bond to be recognized as a substrate.[11,26,27]

A similar effect was observed in the case of sunflower oil indicating enzyme is able to hydrolyze esters present in the oil phase (**Figure 40**). All these signs suggest emulsion destabilization is produced by the enzymatic activity (related to emulsifier, oil or both) and not by changes in the surface tension at the oil-water interface or related phenomena.

5.3.3. CALB effects in droplet size.

Destabilization of a DXT-SCPN-MA based emulsion (**E83**; sunflower oil) was monitored by LD over 16 hours (**Figure 41**). As control experiment, an enzyme-free emulsion was also monitored. In the absence of the enzyme, droplet size remained unaltered, although some alterations in the size distribution were identified in the 10-500 µm region. Contrarily, addition of CALB enzyme resulted in a significant decrease in main population droplet size and the formation of smaller droplets in the region of 0.01-0.1 µm. The decrease on density in volume (%) of the main population suggests lack of stability which results in the demulsification of the system. Furthermore, the new population with diameter close to 0.1 µm is compatible with the size of DXT-SCPN-MA (**D15**) aggregates, suggesting again instability of the emulsion.

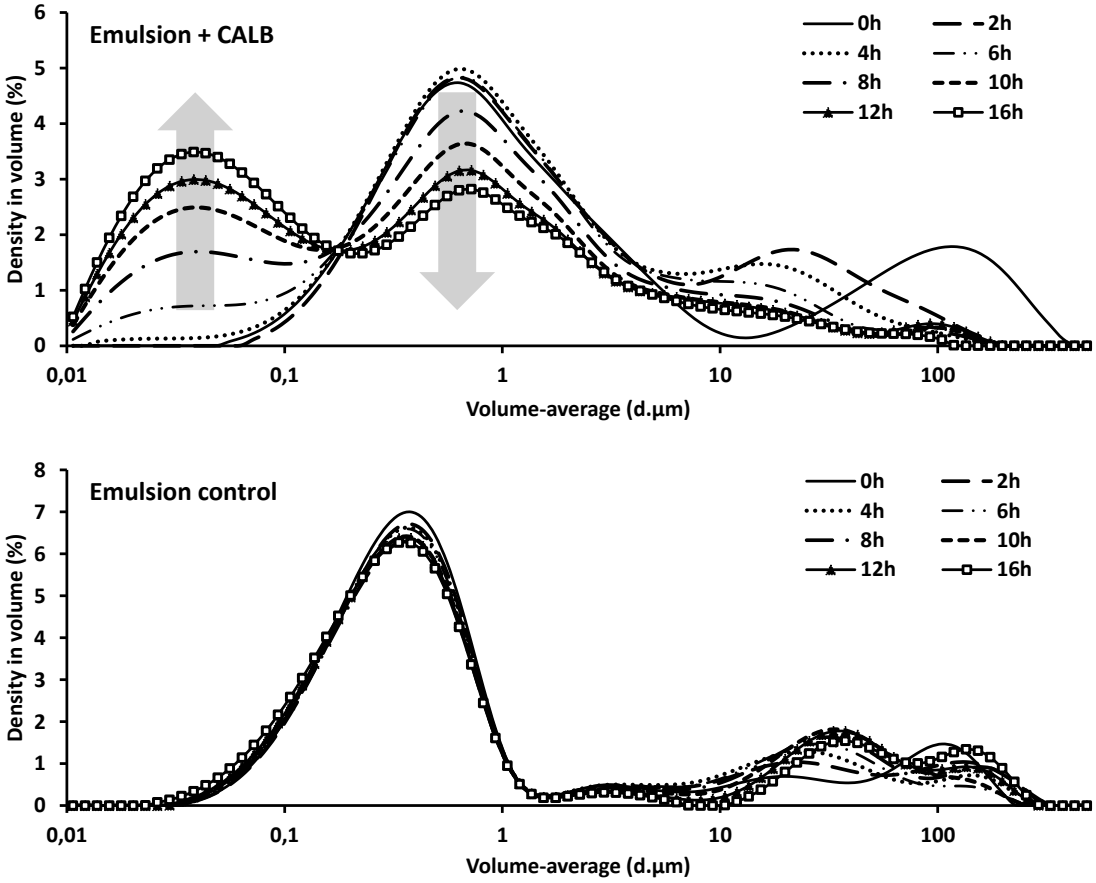

Figure 41. *Laser diffraction studies at different times after incubation of the emulsion based on sunflower oil stabilized with 0.5 wt% of DXT-SCPN-MA (**D15**, **E83**); top: in the presence of CALB enzyme*; bottom: in the absence of enzyme.

For a better understanding about the demulsification mechanism, we decided to switch the surfactant to DXT-MA and test the effect of the oil composition. To that aim, we produced emulsions based on olive, sunflower and fish oils at 10 wt% stabilized with 0.5 wt% of DXT-MA (**D7**) and droplet size was evaluated by LD over 20 hours (**Figure 42**). All emulsions were apparently stable in the absence of enzyme, although a slight decrease in the intensity of the main size population was observed specially for sunflower and fish oil (**Figure 42c** and **42e**). After the addition of CALB Lipase, a clear decrease of the main droplet size population was observed and this was progressively shifted to bigger diameters. On contrary to DXT-SCPN-MA stabilized emulsions, DXT-MA stabilized showed classical destabilization phenomena described for (o/w)-emulsion: coalescence (generation of bigger droplets) and phase separation (oil appeared on the top of emulsion at final stages).

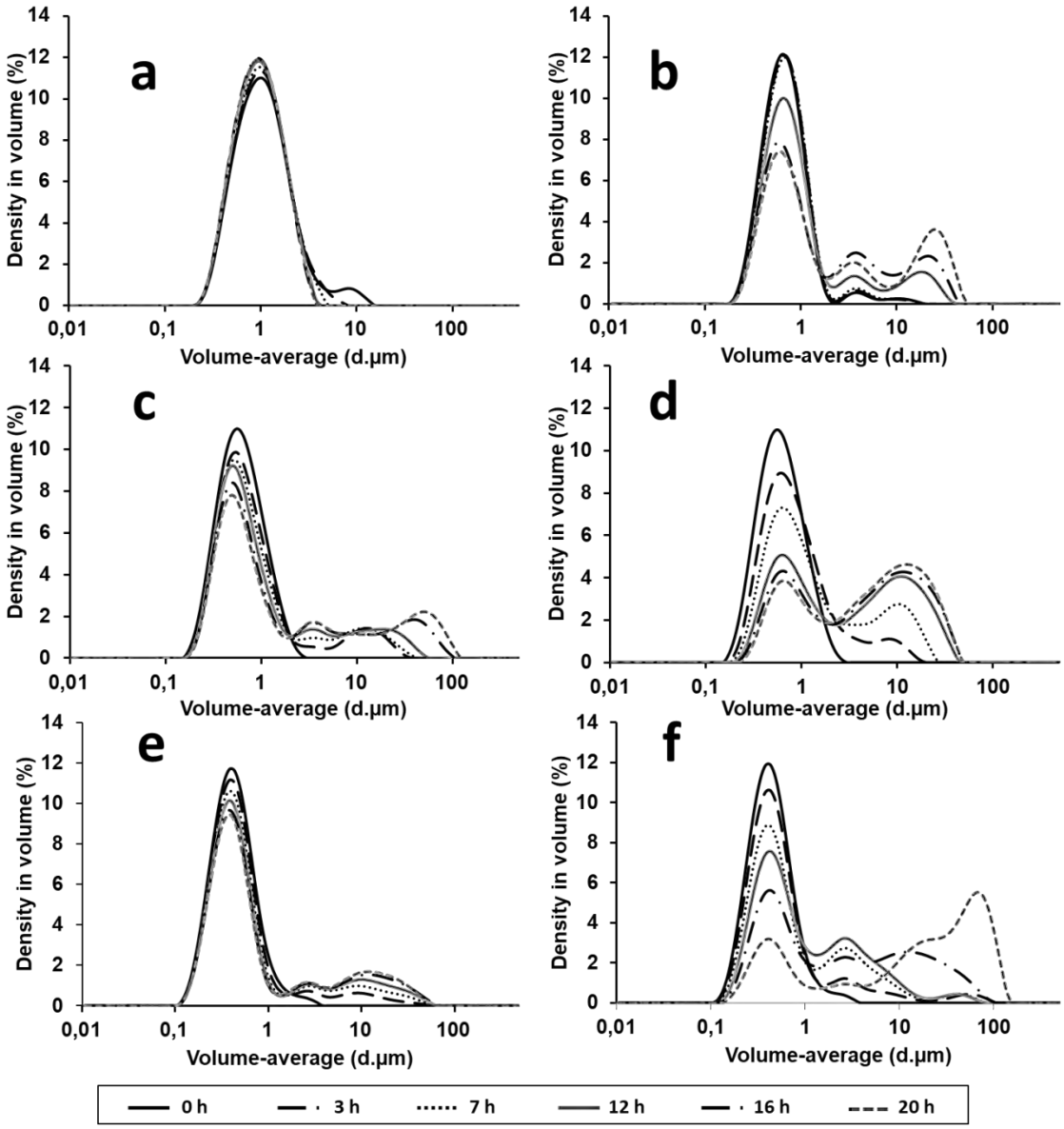

Figure 42. *Laser diffraction studies (deionized water, 2000 rpm, 25 ^{o}C) performed at different incubation times of (o/w)-emulsions stabilized with 0.5% wt. of DXT-MA (**D7**) based on 10% wt. of different oil phases; a) Olive oil (**E89**), b) Olive oil (**E89**) + CALB, c) Sunflower oil (**E90**), d) Sunflower oil (**E90**) + CALB, a) Fish oil (**E91**), b) Fish oil (**E91**) + CALB.*

Interestingly, all emulsions suffered similar destabilization phenomena being difficult to evaluate the enzyme-substrate relation between the oil and CALB. On the other hand, destabilization seems to be faster for sunflower and fish (**Figure 42d** and **42f**, respectively), probably due to the lack of stability of their respective controls against recirculation (**Figure 42c** and **42e**). Those results encouraged us to improve the

stability of emulsions against the enzyme by the appropriate cross-linking at the oil-water interface.

To that purpose, enzyme responsiveness of a fish oil emulsion, cross-linked or not, at 10 wt% stabilized with 0.5 wt% of DXT-MA (**D7**) was investigated. In this case, crosslinked (**E92**) and non-crosslinked (**E91**) emulsions were incubated in the presence and absence of the enzyme and the droplet size was monitored over time (**Figure 43**). Both emulsions were apparently stable in the absence of enzyme, although a slight decrease in the intensity of the main size population could be observed for the non-cross-linked emulsion. Such decrease was not observed in the cross-linked emulsion. After the addition of CALB Lipase, a clear decrease of the main droplet size population was observed for both emulsions (**Figure 43c** and **43d**).

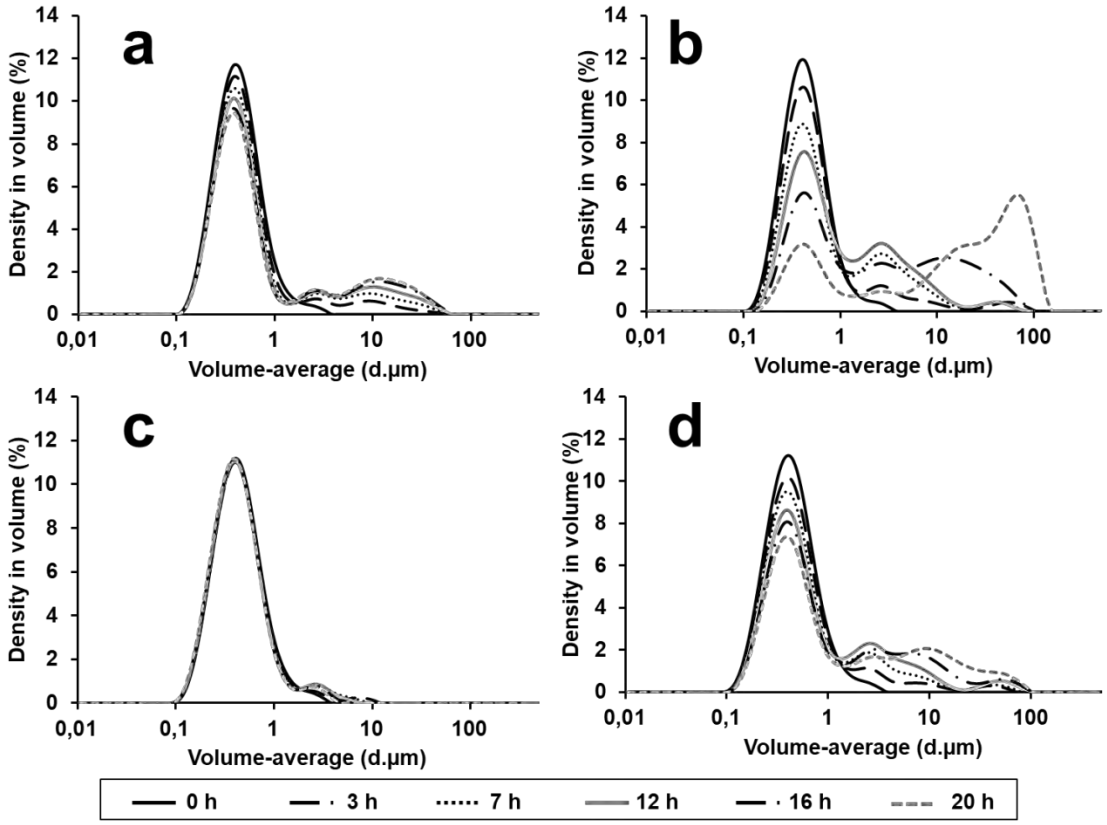

Figure 43. *Laser diffraction studies (deionized water, 2000 rpm, 25 ^{o}C) performed at different incubation times on fish oil based emulsion stabilized with DXT-MA (**D7**); a) Non-crosslinked (**E91**), b) Non-crosslinked (**E91**) + CALB lipase, c) Crosslinked (**E92**) and d) Crosslinked (**E92**) + CALB lipase.*

These results indicate that the presence of cross-linking bonds prevents the enzymatic degradation of the nanodroplets, and hence DXT-MA acts as an enzyme-responsive emulsifier irrespective of the presence of cross-linking. Interestingly, a clear difference in the kinetics of destabilization was observed. As it is showed in **Figure 43**, demulsification occurs faster for the non-cross-linked stabilizer, with full demulsification observed after 16 h (**Figure 43c**). However, a significant fraction of the nanodroplets stabilized with cross-linked DXT-MA remained stable after 16 h (**Figure 43d**). These results confirm that the degradation kinetics, and hence the release of the cargo, can be adjusted by tuning the degree of cross-linking.

5.3.4. Investigation of the enzyme-driven demulsification kinetics

The results presented so far qualitatively demonstrate that emulsion components containing non-polar moieties attached to ester bonds are susceptible to be degraded by lipase enzymes. However, degradation rates have not been evaluated quantitatively. In order to get quantitative data, we decided to prepare different formulas based on triglyceride oils and investigate the degradation by means of the pH-stat method. Such method, which allows a fast comparison of enzyme-responsive emulsions, consists of determining the acidity of free fatty acids (FFA) generated during the enzymatic digestion of the oil. The enzymatic degradation usually results in the formation of 2 free fatty acids (FFA) and 1 monoglyceride (MAG) per triacylglyceride (TAG) instead of 3 FFAs per TAG.[5] This said, completion of the reaction is often hampered by the poor solubility of long-chain FFAs which tend to accumulate at the oil-water interface inhibiting lipase activity.[4] Additionally, the progressive accumulation of lipid content and FFA (long hydrophobic chains) in water can change the polarity of the media leading in the displacement of pKa values from 4.7-4.9 (typical for carboxylic acids with short chains) to ca. pKa≈12, preventing complete deprotonation during the assay and thus losing titration sensitivity.[5,12] In our experiments, FFA percentage was calculated considering that 100% corresponds to all TAG molecules delivering 2 FFA and 1 MAG. The initial reaction velocity (V_o), calculated as the slope of the %FFA-time curve at early stages (t<5 min), enables a better comparison of emulsions in terms of droplet size and emulsifier characteristics.[28]

The experiment was carried out in PBS (0.7 mM phosphate) media ensuring a stable catalytic activity during the whole experiment by maintaining unalterable the pH and temperature. A solution of NaOH (0.1 M) was used as the titrant agent, and the parameters considered for data interpretation were differences in terms of degradation rate (slope of the curve at the early stages) and maximum percentage of free fatty acids FFA_{max} (*plateau*).

Demulsification kinetics towards *Candida Antarctica Lipase B* (CALB)

The demulsification ratio was evaluated towards CALB enzyme by modifying three different parameters; (i) emulsifier type, (ii) droplet size, and (iii) triglyceride oil type. In the first case, emulsions based on sunflower oil (**E93, E94** and **E95**) were produced using 3 different emulsifiers (DXT-MA (**D7**), Tween20 and Triton-X-100, respectively). Droplet size is directly related to the total surface area accessible to the enzyme, and hence special attention was paid to use emulsions with similar droplet size (ca. 300 nm). In addition, another DXT-MA emulsion (**D9, E96**) with a mean droplet diameter around 4000 nm was evaluated. With this set of emulsions, we were able to investigate how enzymatic degradation is affected by steric hindrance of the ester bond present in the emulsifier (by comparing **E93, E94** and **E95**), but also by droplet size (by comparing **E93** and **E96**). Comparison of the slopes at early reaction stages (t < 5 min) showed degradation rates for 300 nm emulsions following this sequence: Tween20 > DXT-MA > Triton-X100 (**Table 7**).

Table 7. Quantification of free fatty acids percentage (%FFA) or concentration of FFA per milligram of enzyme (FFA_{mol} ·mg lipase· L^{-1}) released over time obtained from different (o/w)-emulsions towards Candida Antarctica Lipase B using pH-stat method.

			V_o (t < 5 min)		FFA_{max} (%)	
Emulsifier	**Oil**	**Size (nm)**	**(%) FFA min^{-1}**	**FFA_{mol}·mg lipase·L^{-1}**	**t=2 h**	**t=15 h**
Triton-X-100	Sunflower	300	0,015	1,53E-07	2	5
Tween20	Sunflower	300	0,707	7,04E-06	16	26
DXT-MA (D7)	Sunflower	300	0,356	3,55E-06	16	30
DXT-MA (D9)	Sunflower	4000	0,118	1,17E-06	14	26
DXT-MA (D7)	Olive	300	0,604	5,97E-06	15	19
DXT-MA (D7)	Sunflower	300	0,363	3,62E-06	11	29
DXT-MA (D7)	Fish	300	0,271	2,34E-06	16	34

The molecular surfactant Tween20 owns an ester group directly related with its interfacial properties because of acting as joint group between hydrophobic and hydrophilic parts of the molecule (see **Figure 40**). For this reason, enzyme activity towards a few ester groups dramatically increases destabilization. This explains why Tween20 emulsion showed fast FFA release with a plateau (15% FFA) reached in less than 30 min (**Figure 44**). DXT-MA showed slower FFA release rate due to the higher steric hindrance of their ester bonds (15% of FFA *plateau* reached at t≈1.5 hrs). Finally, Triton-X100 emulsion, which has no ester bonds present in its molecular structure, reached only 2% of FFA after 2 hours. In good agreement with our previous results (see above), these results confirm that the emulsifier plays a key role in the demulsification process. Noteworthy, the presence of FFA when Triton-X100 emulsion was evaluated suggests that despite demulsification mechanism seems to be more related with the degradation of the emulsifier, the oil phase can also be degraded to lower extent (possibly due to a lack in the overtime stability independent of the enzymatic activity).

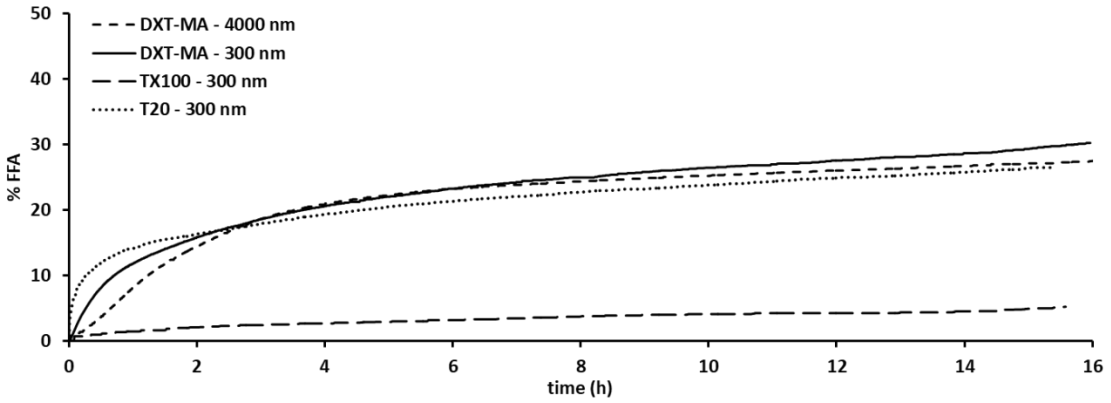

Figure 44. *Quantification of free fatty acids percentage (%FFA) released over time from sunflower based (o/w)-emulsions towards CALB lipase using pH-stat method. Comparison of sunflower oil based emulsions stabilized with DXT-MA (**D7, E93**: 300 nm; and **D7**, **E96:** 4000 nm), Tween20 (**E94:** 300 nm) and Triton-X100 (**E95:** 300 nm) as emulsifiers.*

The studies comparing degradation rate as a function of droplet size also provided expected results. Small droplets, which have higher surface area available for the enzyme, resulted in faster demulsification rates: 300 nm (**E93**) > 4000 nm (**E96**). DXT-MA-4000 reached only 15% of FFA at 2.5 h (compared to 1.5 h for DXT-MA-300). The final %FFA released in all cases was similar (FFA_{max} ≈ 26-30%) irrespectively of the

emulsifier, except in the case of Triton-X100 emulsion (FFA_{max} ≈ 5%) where the absence of ester bonds retards degradation.

We next explored the effect of the triglyceride composition on degradation rate, by investigating NEs formed with olive, sunflower and fish oils. FFA_{max} was in the range 19-34 %. At early stages of the reaction, CALB lipase seems to be more efficient degrading TAG with short chain length (C18 > C22) and lower number of unsaturations (n): Olive (80% oleic acid, C18, ω-9, n=1) > Sunflower (60% linoleic acid, C18, ω-6, n=2) > Fish (85% docosahexaeonic acid, C22, ω-3, n=6) (see **Table 7**). However, FFA_{max} follows an opposite trend: Fish (34%) > sunflower (29%) > olive (19%). Despite of the tiny differences observed between oils, it is worth to mention that olive and sunflower emulsions have reached a *plateau*, whereas in the case of fish oil emulsion, a sustained release is observed, suggesting incomplete reaction at the end of the experiment. These results are in good agreement with the low specificity of CALB described in literature.[29–33]

Proposed mechanism for enzymatic demulsification

Our results confirm that demulsification rate is strongly dependent of the emulsifier type, triglyceride composition and droplet size. Thus, degradation mechanism involves a wide number of parameters that are interplaying. Combining pH-stat information with the effect of the enzyme in droplet size, we can propose a two-step mechanism. First step involves the hydrolysis of the ester presented in the emulsifier and this usually relies in the formation of bigger droplets due to coalescence, creaming and related phenomena and the second step consisted in the degradation of the encapsulated oil (**Figure 45**). First step strongly influences the second because droplet coalescence acts reducing the emulsion surface area. Thus, emulsifiers that present highly reactive esters (related with their interfacial properties) lead to higher demulsification rates at early stages generating coalescence, creaming and phase separation which implies a reduction in FFA_{max} at the end of the experiment (see **Figure 45**). On the other hand, emulsifiers that present less reactive esters and/or generate thicker physical barriers, between oil and enzyme, slowly increase emulsion droplet size. This behavior resulted in a more sustained release of FFAs because droplet size

maintenance increases emulsion permeability over time, preventing fast phase separation and hence avoiding water saturation of FFAs that would result in enzyme inhibition.

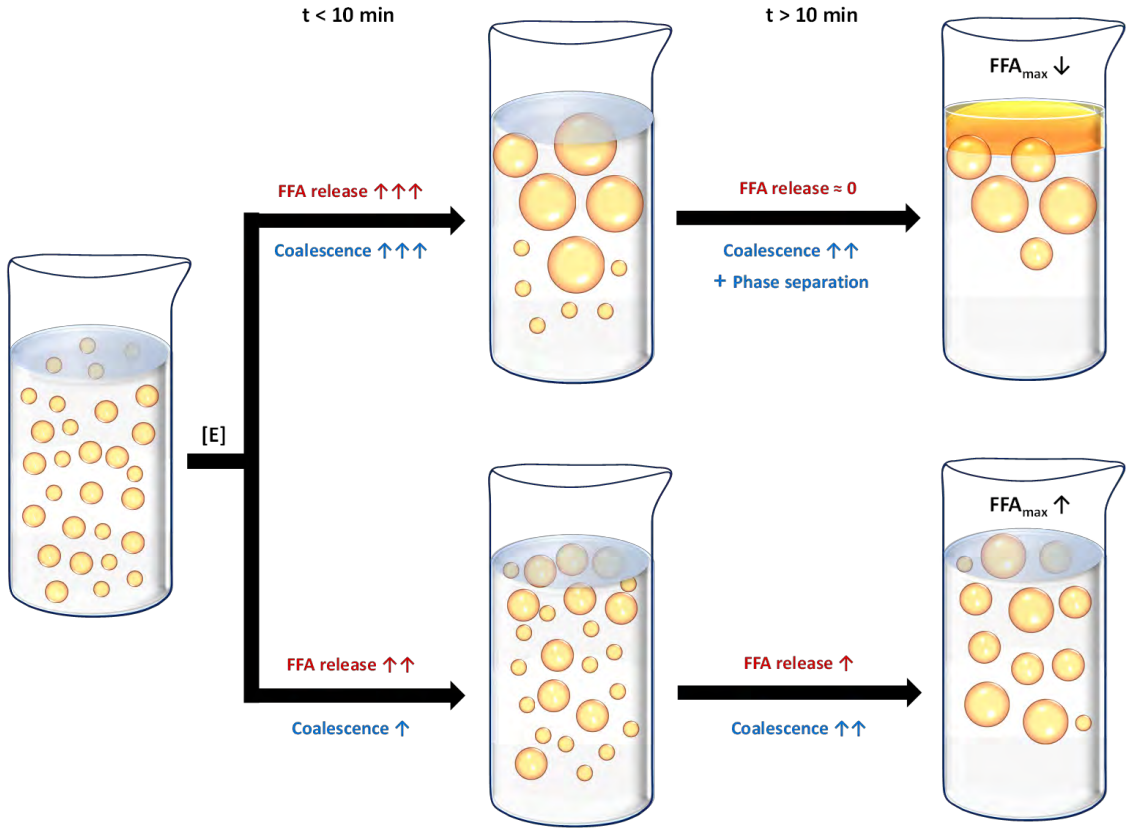

Figure 45. *Proposed mechanism for enzymatic demulsification. Top) High degradation rates at early reaction stages (t < 10 min) resulted in droplet coalescence and phase separation diminishing FFA_{max}, Bottom) Low degradation rates at early reaction stages (t < 10 min) slow down droplet coalescence increasing FFA_{max}.*

Thus, this kind of emulsifiers will reach higher FFA_{max} values at the end of the experiment when using the same oil phase. Finally, when oil is acting as enzyme substrate (second step), further investigation of each individual oil composition towards its corresponding lipase might be required in order to obtain meaningful conclusions.

Demulsification kinetics towards Pancreatic Lipase (PL)

Droplet size and substrate nature are strongly related to the demulsification process towards lipases. Results described above were very useful to investigate the

demulsification mechanism. Nevertheless, the potential application of these NEs as drug carriers demands evaluation towards a human lipase. Because certain diseases overexpress specific lipases,[34] a controlled released of the emulsion cargo in the target organ or tissue could be achieved by designing NEs susceptible of degradation in the presence of such lipases.[34–36] Nowadays, several drugs are currently approved or are in clinical trials for obesity, pain, inflammation, anxiety, and cardiovascular diseases.[37–39] The specificity of the lipase/substrate interaction could prevent undesired off-target delivery of the cargo, thus minimizing side and toxic effects.

In our study, we selected *Pancreatic Lipase* (PL), a specific lipase located preferentially in the pancreas,[10] and investigated the effect of (i) triglyceride oil type; (ii) steric hindrance; and (iii) cross-linking, on the degradation rate.

Emulsions formulated with sunflower (**E98**) and olive (**E97**) oils showed similar degradation patterns in the presence of *Pancreatic Lipase* (**Table 8**). In both cases, degradation rates observed at early reaction stages (0,279 and 0,355 %FFA min^{-1}, respectively) resulted in a *plateau* at t=2 h (FFA_{max} = 12 %). However, fish oil emulsion (**E99**) showed a lower degradation rate at early stages (0,151 %FFA min^{-1}), but a dramatic FFA increase was observed after 4 hours (**Figure 46**). *Plateau* was reached (FFA_{max} = 100 %) after 12 hours confirming complete degradation.

Table 8. Quantification of free fatty acids percentage (%FFA) or concentration of FFA per milligram of enzyme (FFA_{mol}·mg lipase·L^{-1}) released over time obtained from DXT-MA(D7)-stabilized (o/w)-emulsions towards Pancreatic lipase using pH-stat method.

		V_o (t < 5 min)		FFA_{max} (%)	
Oil	**Cross-linking**	**(%) FFA min^{-1}**	**FFA_{mol} · mg lipase· L^{-1} min^{-1}**	**t=2 h**	**t=15 h**
Olive	No	0,279	2,76E-06	12	12
Sunflower	No	0,355	3,54E-06	12	18
Fish	No	0,151	1,30E-06	11	100
Olive	Yes	0,262	2,60E-06	14	47
Sunflower	Yes	0,217	2,16E-06	14	25
Fish	Yes	0,231	1,99E-06	14	27

Our results suggest that PL is less reactive than CALB for olive and sunflower oils, at least in terms of maximum FFA percentages, but highly active towards fish oil. Few authors have described the resistance of oils coming from marine sources towards enzymatic hydrolysis postulating that double bond near the carboxyl group is

exercising an inhibitory effect.[40,41] Following this, *Brockerhoff et al.* demonstrated that the resistance of unsaturated or branched acids is due to steric hindrance during the formation of the activated complex (enzyme-substrate) but disappears for structures longer than C5.[41] Interestingly, larger structures with double bonds in positions 2-5 or methyl groups in position 2, 3 and 4 strongly inhibit lipolysis. DXT-MA owns a methyl group and an unsaturation at second position (ω-2) which generates a conjugated system between ester and double bond. Considering the mechanism proposed above where the first step consisted in emulsifier hydrolysis, it seems clear that DXT-MA stabilized emulsions are less reactive for PL than for CALB. Furthermore, demulsification at early stages was faster for olive and sunflower (ω-9 and ω-6 first unsaturation, respectively) than for fish (ω-3 first unsaturation) confirming the hypothesis. Nevertheless, fish oil emulsion finally reaches the 100% FFA_{max} despite of retarding hydrolysis at early stages. *Kleiman et al.* described this retarded hydrolysis especially for *trans*-(ω-3)-unsaturated oils.[42] However, the major component of fish oil (docosahexaeonic acid, DHA) owns a c*is*-conformation in all of its unsaturations. More recently, *Van Kuiken et al.* demonstrated that *cis*-unsaturated fatty acids increased PL activity in the absence of colipase. This said, once sufficient *cis*-unsaturated FFAs are released, PL is activated increasing until 15-fold the demulsification rate observed for those experimental conditions.[43] Hence, selective oil degradation (and eventual release of the cargo) can be achieved by controlling emulsion formulation, enzyme selection and the appropriate hydrolysis conditions.

Previous results have demonstrated that cross-linking at the oil-water interface improves emulsion stability in both highly ionic strength media (see section **4.3.2. Crosslinking assessment by PBS challenge**) and towards CALB lipase. However, these differences were only evaluated qualitatively. With the aim of obtaining quantitative data, we here investigated olive, sunflower and fish oil-based emulsions stabilized with DXT-MA (**D7**). To avoid the effect of droplet size, NEs with hydrodynamic diameter of ca. 300 nm were selected; one of each cross-linked (**E100**, **E101** and **E102** respectively) and one non-crosslinked (**E97**, **E98** and **E99**, respectively). Demulsification was monitored using the pH-stat method.

As can be observed in **Table 8**, for non-cross-linked fish oil emulsion FFA_{max} values of 100 % were achieved at 12 hours in the presence of PL and maintained until the end of the experiment. Contrarily, FFA_{max} of 25% was achieved for fish oil cross-linked emulsion, confirming that interfacial cross-linking significantly improves emulsion stability towards PL (**Figure 46**).

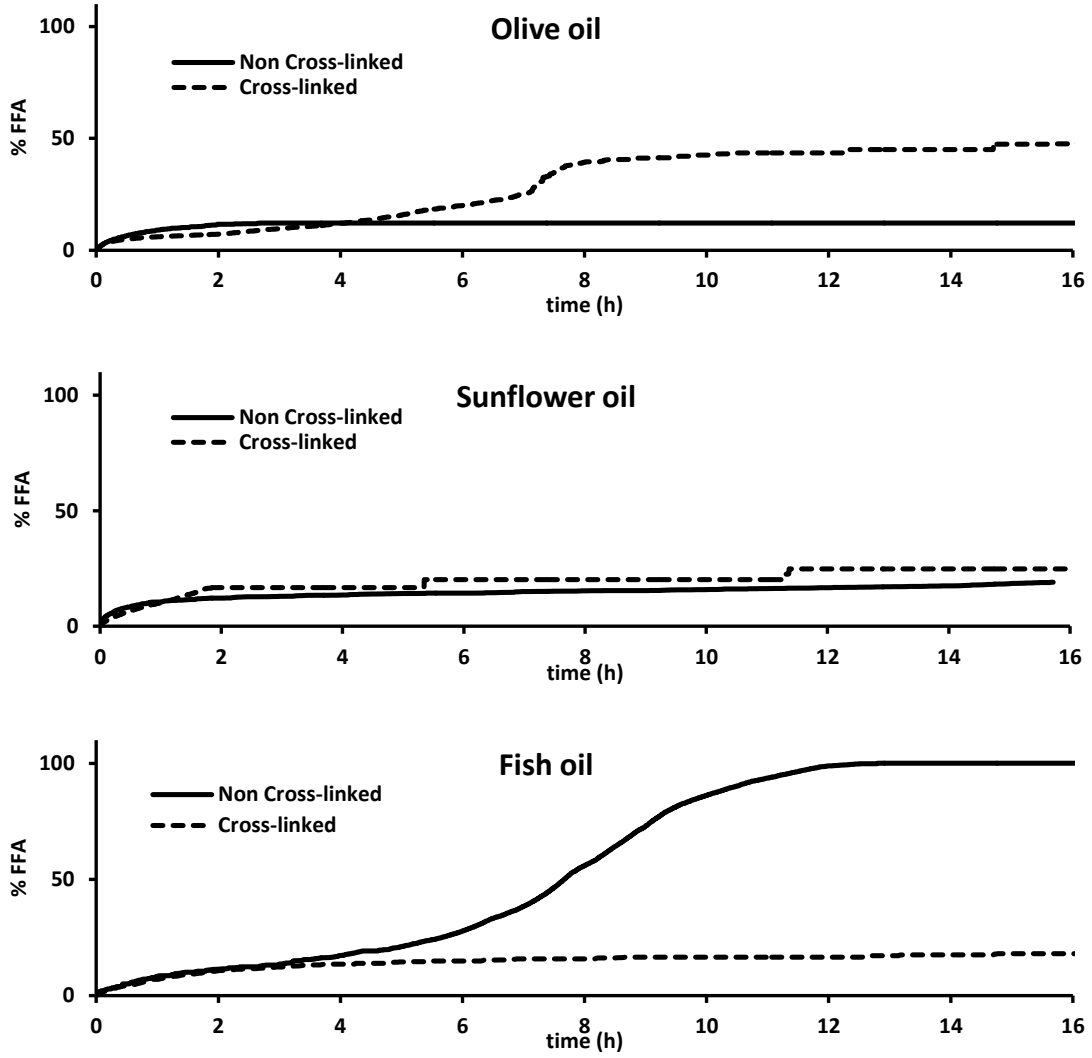

Figure 46. *Cross-linking effect in the quantification of free fatty acids percentage (%FFA) released over time from different oil-in-water emulsions towards PL using pH-stat method. From top to bottom: non-crosslinked and cross-linked emulsions based on olive (**E97**, **E100**), sunflower (**E98**, **E101**), and fish (**E99**, **E102**) oils as dispersed phases using DXT-MA (**D7**) as emulsifier.*

This behavior confirmed previous results obtained for CALB suggesting the possibility of crosslink the emulsion to modulate release. Results are also in accordance with previous discussion as sterically hindered esters (cross-linked) are initially less reactive

than their non-sterically hindered analogous (non-cross-linked). Also in literature, emulsions stabilized by sterically hindered galactose-derivatives slow down the demulsification rate in comparison with their non-hindered analogous.[44] It is worth mentioning that the curves obtained both for cross-linked and non-cross-linked emulsions show similar profiles at t<4h in all cases. However, at longer times the release of the encapsulated phase is dramatically accelerated in the case of non-cross-linked fish oil emulsion, resulting in complete demulsification in a few hours. Contrarily, the cross-linked fish oil emulsion remains stable at t>4h.

Surprisingly, cross-linked emulsions based on olive and sunflower oils have the opposite behavior, being more reactive and reaching higher FFA_{max} values than their non-crosslinked analogous. Possible explanation, based on the demulsification mechanism proposed for CALB, is the fact that cross-linking is preventing coalescence maintaining the initial droplet size and the total surface area available for the enzyme. Thus, cross-linking is contributing to slow down the enzymatic reaction because of the generation of sterically hindered esters which implies the possibility of further degradation before phase separation.

Altogether, our results suggest that DXT-MA, acts as an enzyme-responsive stabilizer, and the enzymatic reaction drives demulsification. The effect of the enzyme can be controlled by cross-linking the stabilizer, suggesting highly tunable properties with high promise in biomedicine.

5.4. Summary and Conclusion

Nanoemulsions based on triglyceride oils as dispersed phase and hydrophobically modified dextran as the emulsifier, are enzyme-responsive materials. We have demonstrated that unspecific lipase enzymes can degrade nanoemulsions stabilized by DXT-MA and DXT-SCPN-MA. These enzymes are able to hydrolyze ester bonds present in both the oil and the emulsifier. Volume-weighted size investigation using LD confirms a decrease in the main droplet size population over time, indicating a lack of stability because of the enzymatic activity. Major differences in demulsification rates

are related to physicochemical properties at the oil/water interface, e.g. the nature of the ester bond and droplet size. Droplet size determines the total surface available for enzyme recognition. Consequently, smaller droplets degrade faster due to the increased surface to volume ratio. Steric hindrance of the ester bond present at the emulsifier also plays a pivotal role in degradation rates. Degradation mechanism proposed consists in two steps. First, the hydrolysis of the ester presented in the emulsifier, followed by the degradation of the encapsulated oil. First step strongly influences the second because emulsifier degradation often results in droplet coalescence reducing the available area for the oil phase hydrolysis. Experiments carried out with a real targetable lipase enzyme, Pancreatic Lipase, suggest that the degradation rate can be tuned by appropriate design of the nanoemulsion.

5.5. Materials and methods

5.5.1. Materials

Dextran from Leuconostoc spp. (DXT-40, Mr ~40 kDa), glycidyl methacrylate (GMA) (97%), 2,2'-(ethylenedioxy)diethanethiol [3,6-dioxa-1,8-octane-dithiol (DODT)] (95%) *Candida Antarctica Lipase B* (CALB), *Rhizomucor miehei Lipase* (RML), *Rhizopus oryzae Lipase* (ROL), *Thermomyces lanuginosa Lipase* (TLL) and *Pancreatic Lipase* (PL) were purchased from Aldrich and used as received. Phosphate-buffered saline (PBS) and dichloromethane were purchased from Scharlau and used as received. 4-(Dimethylamino)pyridine (DMAP) was purchased from Acros-Organics. Water (H_2O) used in the syntheses, unless otherwise stated, was ultrapure water from a MilliQ A10 Gradient equipment (Millipore). DHA rich oil (> 95 wt%) extracted from fish oil was kindly provided by SENDABIO S.L.

5.5.2. Characterization Methods

- *Dynamic Light Scattering* (DLS): DLS analyses were conducted using a Zetasizer Nano ZS, ZEN3600 Model (Malvern Instruments Ltd). All measurements were performed in disposable sizing cuvettes at a laser wavelength of 633 nm and a

scattering angle of 173°, while the zeta-potential measurements were performed in disposable zeta potential cells (pH 7.4, 25°C). Emulsion samples were dispersed in deionized water at a concentration of 2 mg oil/mL. Each measurement was repeated for three runs per sample at 25°C.

- *Laser diffraction (LD)*: LD analyses were conducted using Mastersizer 3000 laser diffraction system (Malvern Instruments Ltd). All measurements were performed at a laser wavelength of 430 nm using 600 mL of deionized water in a glass beaker. Each measurement was repeated for 5 runs per sample and 5 seconds per run at 25°C following Mie dispersion model.
- *Optical Microscopy (OM). OM analyses were conducted using a Leica DM 2000 Model. Sample preparation was performed putting a small droplet of 5 µL of water diluted emulsion (dilution ≥ 1:100, 1 mg oil/mL), in a glass disposable plate. Then, droplet was smashed using a thin plastic plate over there. Sample was leaded for 20 min and then analysed by OM.*
- *PH-stat*: Autotitration was performed in an Excellence Titrator T7 (Mettler Toledo) at pH= 7.2 ± 0.05 using NaOH (0.1M) as titrant agent. Measurements were achieved at regular intervals of 10 seconds (See *5.5.9. Demulsification by pH-Stat method* for further information).

5.5.3. Production of non-crosslinked O/W emulsions (M1-M2)

Emulsifier was dissolved in deionized water in an 8 mL glass vial. To this solution, the oil was added. The relative amounts of emulsifier, water and oil were modified to reach always a final amount of 2 g (M1) or 4 g (M2). Then, emulsion was formed using an UP400S (Hielscher) system at 100% of amplitude and pulse during 4 minutes (400 W) with a H3 sonotrode tip (3 mm diameter, 100 mm length). Sonication step was carried out at 0°C, using an ice bath, and without stirring (M1) or under magnetic stirring (M2).

5.5.4. Production of crosslinked O/W emulsions (M3)

As example, DXT-MA **(D7;** 20 mg, 5% wt. related to oil phase) was dissolved in 3.6 mL of deionized water (aqueous phase, 90% wt.) in a 8 mL glass vial, to this solution 0.4 g

of DHA (oil phase, 10% wt.) were added. Then, 1 µL DODT (0.5 SH eq.) was carefully added over the oil phase and pH was adjusted to 9.5. Emulsion was formed using an UP400S (Hielscher) system at 100% of amplitude and pulse during 4 minutes (400 W) with a H3 sonotrode tip (3 mm diameter, 100 mm length). Sonication step was realized at 0°C, using an ice bath, and under magnetic stirring.

5.5.5. Enzyme-responsiveness analysis by visual inspection

Different fractions of emulsion (**E82**, 100 µL) were mixed with 100 µL of lipase (CALB, RML, ROL or TLL; 20 mg/mL) in an HPLC glass vials. Mixtures were kept in rest for 20 h at room temperature for OM analysis and 40 h for digital pictures acquisition.

5.5.6. Enzyme-responsiveness analysis by LD

Each emulsion (500 µL) was mixed with a solution of *Candida Antarctica Lipase B* (CALB, 500 µL, 0.2 mg/mL) and the mixture was carefully added to 600 mL of water at r.t. and 2000 rpm. Enzymatic degradation was evaluated by volume-weighted size distribution at regular intervals of 30 minutes and determined using a Mastersizer 3000 laser diffraction system (Malvern Instruments Ltd). First measurement (t = 0 h) was acquired before enzyme addition as a control. Further control experiments in the absence of enzyme were also conducted.

5.5.7. Emulsifiers as enzyme substrates

Before emulsion production, 2 mg of emulsifier were solved in 1.8 mL of ultrapure water (aqueous phase, 90% wt.). Then, 10 µL of CALB (20 mg/mL) was added and solution was stirred using a roller mixer for 7 days. The pH is maintained between 4.8 and 6.3. Afterwards, 0.2 g of sunflower oil (oil phase, 10% wt.) were added and emulsion was produced subsequently by sonication with UP400S (Hielscher) system following the methodology described previously. Finally, emulsions prepared were kept in rest 24 h at 4^{o}C and darkness.

5.5.8. Sunflower oil as enzyme substrate

Before emulsion production, a solution of CALB enzyme (10 µL, 20 mg/mL) was poured into 0.4 g of sunflower oil (oil phase, 20% wt.) and stirred using a roller mixer for 7

days. Afterwards, 4 mg of DXT-SCPN-MA (**D12**, 0.1% wt.) and 1.6 mL of ultrapure water (aqueous phase, 80% wt.) were added and the emulsion was produced by sonication with UP400S (Hielscher) system following the methodology described previously. Finally, emulsion was kept in rest 24 h at 4^{o}C and darkness.

5.5.9. Demulsification by pH-Stat method

Emulsion volume corresponding to 100 mg of oil was poured into a solution containing 0.24 mg/mL enzyme (CALB or PL) in 30 mL final volume. Before addition, pH was adjusted to 7.2 (physiological conditions) using HCl (0.1M) and NaOH (0.1M) automatically. Once added, pH was readjusted again reaching pH=7.2 automatically for titration. Increasing amounts of NaOH (0.1M), titrant agent, were automatically added to maintain pH unalterable. Titration was performed at mild conditions (room temperature and stirring) and data was acquired at regular intervals of 10 seconds during 16 hours using an Excellence Titrator T7 (Mettler Toledo). CALB enzyme (solution) was directly added to the dispersion for titration. PL was previously solved in phosphate buffered saline (PBS, 0.7 mM phosphate). Data treatment: transformation of NaOH (mL) volume in free fatty acids percentage (%FFA) in solution has been done according to the following formula:

$$\%FFA = 100 \cdot (V_{NaOH} \cdot M_{NaOH}) / FFA_{\text{total mols}}$$

$FFA_{\text{total mols}}$ were calculated based on the maximum fatty acids (FA) mols present in 100 mg of the corresponding polyunsaturated fatty acid (PUFA; 3 FA per molecule) considering these enzymes are able to break only ester bonds located in positions 1 and 3, keeping position 2 unaltered [5,12]. Initial reaction velocity (V_o) was calculated as the slope of the (%)FFA-time curve at early stages of reaction (t < 5 minutes) and are showed as percentage of free fatty acids released per minute (%FFA min^{-1}). Maximum percentage of free fatty acids FFA_{max} (*plateau*) was calculated at t=15 hours.

5.6. References

1. Ulijn, R. V. Enzyme-responsive materials: A new class of smart biomaterials. *J. Mater. Chem.* **16**, 2217–2225 (2006).

2. de la Rica, R., Aili, D. & Stevens, M. M. Enzyme-responsive nanoparticles for drug release and diagnostics. *Adv. Drug Deliv. Rev.* **64**, 967–978 (2012).

3. McClements, D. J. & Li, Y. Structured emulsion-based delivery systems: Controlling the digestion and release of lipophilic food components. *Adv. Colloid Interface Sci.* **159**, 213–228 (2010).

4. Lee, S. J., Choi, S. J., Li, Y., Decker, E. A. & McClements, D. J. Protein-stabilized nanoemulsions and emulsions: Comparison of physicochemical stability, lipid oxidation, and lipase digestibility. *J. Agric. Food Chem.* **59**, 415–427 (2011).

5. McClements, D. J. & Li, Y. Review of *in vitro* digestion models for rapid screening of emulsion-based systems. *Food Funct.* **1**, 32–59 (2010).

6. Thanki, P. N., Dellacherie, E. & Six, J. L. Prevailing mechanisms of the hydrolytic degradation of oligo(d,l-lactide)- grafted dextrans. *Eur. Polym. J.* **41**, 1546–1553 (2005).

7. Franssen, O., Van Ooijen, R. D., De Boer, D., Maes, R. A. A. & Hennink, W. E. Enzymatic degradation of cross-linked dextrans. *Macromolecules* **32**, 2896–2902 (1999).

8. Brito e Cunha, D. A. *et al.* Structural differences of commercial and recombinant lipase B from Candida antarctica: An important implication on enzymes thermostability. *Int. J. Biol. Macromol.* **140**, 761–770 (2019).

9. Rabbani, G. *et al.* Impact of structural stability of cold adapted Candida antarctica lipase B (CaLB): In relation to pH, chemical and thermal denaturation. *RSC Adv.* **5**, 20115–20131 (2015).

10. Mukherjee, A. K. Hydrophobic-hydrophilic interaction in lipase catalytic triad and possibility of a cofactor mediated catalysis. *Int. J. Agric. Food Sci.* **4**, 84–89 (2014).

11. Zelzer, M. *et al.* Engineering the genetic code of Escherichia coli with methionine analogues and bioorthogonal amino acids for protein immobilization. *Adv. Drug Deliv. Rev.* **1**, 11–39 (2013).

12. Li, Y., Hu, M. & McClements, D. J. Factors affecting lipase digestibility of emulsified lipids using an *in vitro* digestion model: Proposal for a standardised pH-stat method. *Food Chem.* **126**, 498–505 (2011).

13. Reis, P., Holmberg, K., Watzke, H., Leser, M. E. & Miller, R. Lipases at interfaces: A review. *Adv. Colloid Interface Sci.* **147**–**148**, 237–250 (2009).

14. Luna, C. *et al.* Biocatalytic behaviour of immobilized Rhizopus oryzae lipase in the 1,3-selective ethanolysis of sunflower oil to obtain a biofuel similar to biodiesel. *Molecules* **19**, 11419–11439 (2014).

15. Balasubramaniam, B., Sudalaiyadum Perumal, A., Jayaraman, J., Mani, J. & Ramanujam, P. Comparative analysis for the production of fatty acid alkyl esterase using whole cell biocatalyst and purified enzyme from Rhizopus oryzae on waste cooking oil (sunflower oil). *Waste Manag.* **32**, 1539–1547 (2012).

16. Fedosov, S. N. *et al.* Kinetic model of biodiesel production using immobilized lipase Candida antarctica lipase B. *J. Mol. Catal. B Enzym.* **85**–**86**, 156–168 (2013).

17. Bélafi-Bakó, K., Kovács, F., Gubicza, L. & Hancsók, J. Enzymatic biodiesel production from sunflower oil by Candida antarctica lipase in a solvent-free system. *Biocatal. Biotransformation* **20**, 437–439 (2002).

18. Ilmi, M., Hommes, A., Winkelman, J. G. M., Hidayat, C. & Heeres, H. J. Kinetic studies on the transesterification of sunflower oil with 1-butanol catalyzed by Rhizomucor miehei lipase in a biphasic aqueous-organic system. *Biochem. Eng. J.* **114**, 110–118 (2016).

19. Soumanou, M. M. & Bornscheuer, U. T. Improvement in lipase-catalyzed synthesis of fatty acid methyl esters from sunflower oil. *Enzyme Microb. Technol.* **33**, 97–103 (2003).

20. Dizge, N. *et al.* Biodiesel production from sunflower, soybean, and waste cooking oils by transesterification using lipase immobilized onto a novel microporous polymer. *Bioresour. Technol.* **100**, 1983–1991 (2009).

21. Janda, K. The lipolytic activity of Thermomyces lanuginosus strains isolated from different natural sources. *Int. Biodeterior. Biodegrad.* **55**, 149–152 (2005).

22. Eriksson, M. *et al.* One-pot enzymatic polycondensation to telechelic methacrylate-functional oligoesters used for film formation. *Polym. Chem.* **2**, 714–719 (2011).

23. Sen, M. Y., Puskas, J. E., Ummadisetty, S. & Kennedy, J. P. Green polymer chemistry: II. Enzymatic synthesis of methacrylate-terminated polyisobutylenes. *Macromol. Rapid Commun.* **29**, 1598–1602 (2008).

24. Wang, Z. Y., Li, N. & Zong, M. H. A simple procedure for the synthesis of potential 6-azauridine prodrugs by Thermomyces lanuginosus lipase. *J. Mol. Catal. B Enzym.* **59**, 212–219 (2009).

25. De Simone, A. *Engineering the genetic code of Escherichia coli with methionine analogues and bioorthogonal amino acids for protein immobilization*. (2016).

26. Thierry, A. *et al. Lipolysis and Metabolism of Fatty Acids in Cheese*. *Cheese: Chemistry, Physics and Microbiology: Fourth Edition* vol. 1 (Elsevier Ltd, 2017).

27. Perez, C., Daniel, K. B. & Cohen, S. M. Evaluating prodrug strategies for esterase-triggered release of alcohols. *ChemMedChem* **8**, 1662–1667 (2013).

28. Li, Y. & Mcclements, D. J. New mathematical model for interpreting ph-stat digestion profiles: Impact of lipid droplet characteristics on *in vitro* digestibility. *J. Agric. Food Chem.* **58**, 8085–8092 (2010).

29. Naik, S. *et al.* Lipases for use in industrial biocatalysis: Specificity of selected structural groups of lipases. *J. Mol. Catal. B Enzym.* **65**, 18–23 (2010).

30. McCarthy, D. W. *et al.* High purity production and potential applications of copper-60 and copper-61. *Nucl. Med. Biol.* **26**, 351–358 (1999).

31. Takwa, M. *Lipase Specificity and Selectivity*. (2010).

32. Kralovec, J. A., Wang, W. & Barrow, C. J. Production of omega-3 triacylglycerol concentrates using a new food grade immobilized Candida antarctica lipase B. *Aust. J. Chem.* **63**, 922–928 (2010).

33. Dulęba, J., Czirson, K., Siódmiak, T. & Marszałł, M. P. Lipase B from Candida antarctica — the wide applicable biocatalyst in obtaining pharmaceutical compounds. *Med. Res. J.* **4**, 174–177 (2019).

34. Nomura, D. K. & Casida, J. E. Lipases and their inhibitors in health and disease. *Chem. Biol. Interact.* **259**, 211–222 (2016).

35. Kim, J. K. *et al.* Tissue-specific overexpression of lipoprotein lipase causes tissue-specific insulin resistance. *Proc. Natl. Acad. Sci. U. S. A.* **98**, 7522–7527 (2001).

36. Jin, W., Marchadier, D. & Rader, D. J. Lipases and HDL metabolism. *Trends Endocrinol. Metab.* **13**, 174–178 (2002).

37. Ahn, K. *et al.* Mechanistic and pharmacological characterization of PF-04457845: A highly potent and selective fatty acid amide hydrolase inhibitor that reduces inflammatory and noninflammatory pain. *J. Pharmacol. Exp. Ther.* **338**, 114–124 (2011).

38. Karabina, S. & Ninio, E. *Plasma PAFAH/PLA2G7 genetic variability, cardiovascular disease, and clinical trials*. *Enzymes* vol. 38 (Elsevier Inc., 2015).

39. Kim, G. W., Lin, J. E., Blomain, E. S. & Waldman, S. A. Antiobesity pharmacotherapy: New drugs and emerging targets. *Clin. Pharmacol. Ther.* **95**, 53–66 (2014).

40. Bottino, N. R., Vandenburg, G. A. & Reiser, R. Resistance of certain long-chain polyunsaturated fatty acids of marine oils to pancreatic lipase hydrolysis. *Lipids* **2**, 489–493 (1967).

41. Brockerhoff, H. Substrate specificity of pancreatic lipase: Influence of the structure of fatty acids on the reactivity of esters. *BBA - Enzymol.* **212**, 92–101 (1970).

42. Kleiman, R., Earle, F. R., Tallent, W. H. & Wolff, I. A. Retarded hydrolysis by pancreatic lipase of seed oils with Trans-3 unsaturation. *Lipids* **5**, 513–518 (1970).

43. van Kuiken, B. A. & Behnke, W. D. The activation of porcine pancreatic lipase by cis-unsaturated fatty acids. *Biochim. Biophys. Acta (BBA)/Lipids Lipid Metab.* **1214**, 148–160 (1994).

44. Chu, B. S. *et al.* Modulating pancreatic lipase activity with galactolipids: effects of emulsion interfacial composition. *Langmuir* **25**, 9352–9360 (2009).

Chapter 6. COSAN-based omega-3 enriched oil-in-water emulsions as drug nanocarriers for poorly water soluble drugs

6.1. Introduction

Nanoemulsions are described as kinetically stable but thermodynamically unstable systems. Usually, high energy input and the presence of surfactants are required for the formation of the droplets and to ensure colloidal stability, respectively.[1,2] For the latter, surfactants reduce the interfacial tension and form a protective layer to avoid oil droplets coalescence. Classical surfactants consist of molecules with a highly polar head attached to a long hydrophobic tail. These molecules have amphiphilic character and the adequate morphology to act as oil-in-water emulsion stabilizers.[3–5]

The cobalt bis(dicarbollide) anion ($[3,3'\text{-}Co(C_2B_9H_{11})_2]^-$; also known as COSAN) is one of the first metallocarboranes reported [6] and consists of a central cobalt (Co^{3+}) atom sandwiched between two η^5-bonding $[C_2B_9H_{11}]^{2-}$ moieties. The presence of hydridic B–H vertices and charge delocalization over the whole structure confer an amphiphilic character to COSAN, which results in the capacity to self-assemble in monolayer vesicles or micelles.[7–10] Additionally, COSAN can pass directly through synthetic lipid membranes[11] and accumulate in cells without disrupting membrane integrity.[12]

The capacity of COSAN to behave like a classical surfactant opens new possibilities for the rational design of self-organized nano-structures, e.g. nanoemulsions. Based on the unconventional amphiphilic properties of COSAN and its capacity to behave like a classical surfactant,[13] we envisaged the possibility to use COSAN as an efficient stabilizer for oil-in-water (o/w)-NEs.

6.2. Objectives

1. To evaluate the capacity of COSAN to stabilize (o/w)-emulsions.
2. To characterize the resulting nanoemulsions.

3. To evaluate the *in vivo* stability of the resulting nanoemulsions and their capacity to modulate the biodistribution of entrapped drugs, by applying a dual labeling strategy followed by *in vivo* imaging using positron emission tomography.

6.3. COSAN Emulsions

6.3.1. Emulsion production and characterization

Due to its negative net charge delocalized around the whole structure, COSAN is water soluble.[6] This water solubility, together with the previously described amphiphilic character, turn COSAN into a suitable candidate to act as an oil-in-water emulsion stabilizer. In our proof of concept and based on the previously developed experiments, docosahexaenoic acid (DHA) was selected as the oil phase. COSAN (1-8 mg) was added to the water phase (3.6 mL) and the mixture was sonicated in the presence of DHA (400 mg; 425 µL) to produce the emulsions (see **Figure 47**).

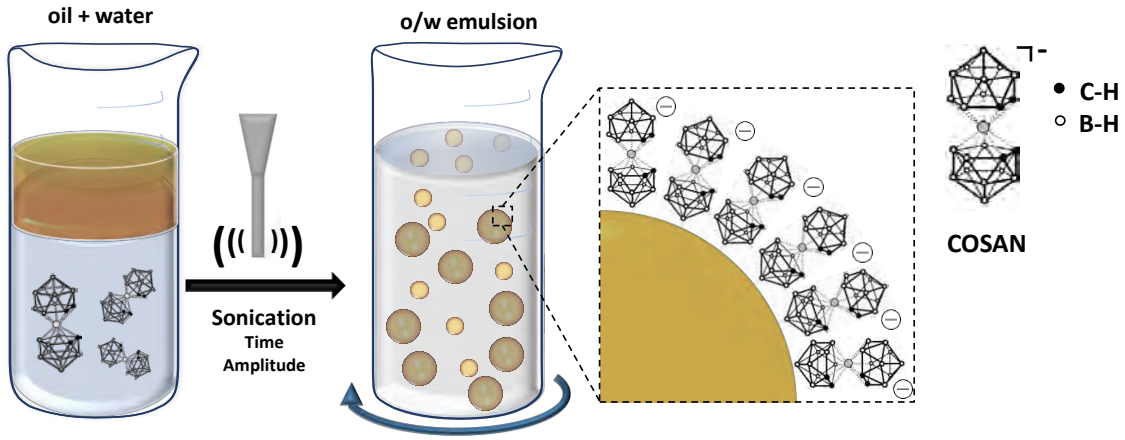

Figure 47. *Schematic representation of COSAN and the production process for the formation of COSAN-stabilised DHA-in-water emulsion.*

Laser diffraction (LD) analyses showed that NEs produced with less than 4 mg of COSAN resulted in large and multimodal size distributions. When the amount of COSAN was higher than 4 mg, smaller and monomodal nanodroplets were obtained.

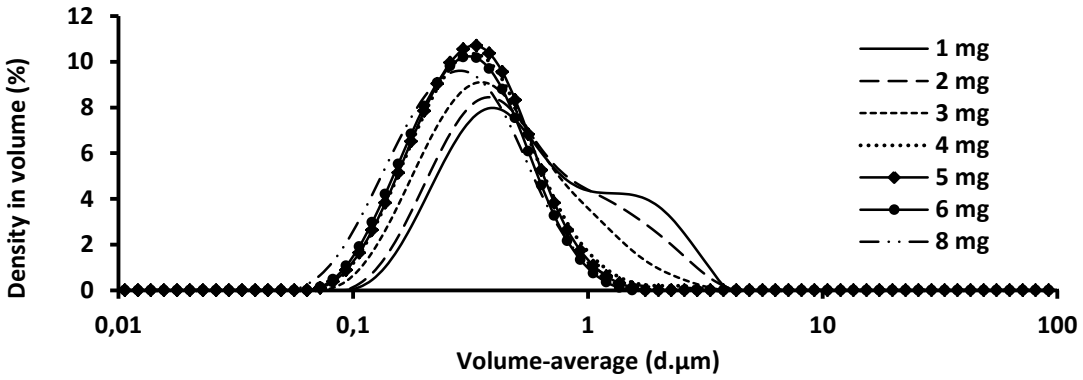

Figure 48. *Size distribution of NEs generated using different amounts of COSAN (1-8 mg) as determined by LD.*

Further characterisation of the NEs prepared with 8 mg of COSAN was carried out using different techniques, i.e. Transmission Electron Cryo-Microscopy (Cryo-TEM), Dynamic Light Scattering (DLS), and Laser diffraction (LD). Cryo-TEM micrographs showed the presence of spherical and highly polydisperse (as expected due the sonication process used) nanodroplets with a number-average diameter (Dn) of 39±27 nm (500 droplets counted) (**Figure 49**). Hydrodynamic diameter (Dh), measured by DLS in ultrapure water revealed a Z-average of 170 nm (PDI=0.18). The significant difference between Dn and Dh can be attributed to the presence of a low number of larger droplets (not seen on Cryo-TEM images), as expected with the high polydispersity of the sample (PDI of 0.18 by DLS) and inherent to the sonication process, which results in an overestimation of Dh, an intensity-average diameter. Z-potential values (-64 mV in 1 mM PBS; pH=7.2), are in good agreement with the delocalized negative charge of the COSAN anion, which confers electrostatic stabilization as a monolayer of tightly packed cylinder at the (o/w) interface (**Figure 47**).

LD measurements conducted at 1500 rpm in ultrapure water showed a volume-average diameter of the NEs droplets at 270 nm. Although LD is not ideal for the determination of the size of submicron particles, the permanent recirculation of the sample makes this technique suitable to evaluate size distributions (multi- vs monomodal) and stability against recirculation flow. Monomodal distributions were

achieved, and overlapping of the curves obtained in consecutive runs indicates good stability of NEs against recirculation (**Figure 49**, LD).

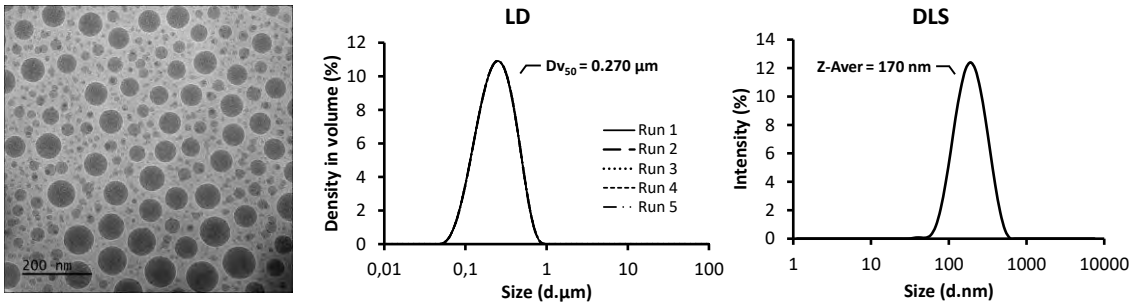

Figure 49. *From left to right: Cryo-TEM micrograph of DHA-in-water emulsion; size distribution as obtained by dynamic light scattering (DLS) and laser diffraction (LD).*

6.4.2. Long-Term Stability: accelerated test

Long term stability of emulsions is a key factor in nanomedicine,[14] as good stability guarantees the possibility to prepare large-scale batches and distribution to end users. To proof the stability over time of COSAN-stabilised NE we performed an accelerated test. To that aim, the hydrodynamic diameter was measured in water over 3 months at 4 different storing conditions: under light at room temperature (r.t.), and in the dark at r.t., 5°C and 40°C. Visual inspection of the NEs showed unaltered aspect over 3 months, while DLS and LD measurements confirmed unaltered droplet size and polydispersity, irrespective of the storing conditions (**Figure 50**). The high stability of our NE is promising especially considering the well-known instability of DHA in the presence of light.

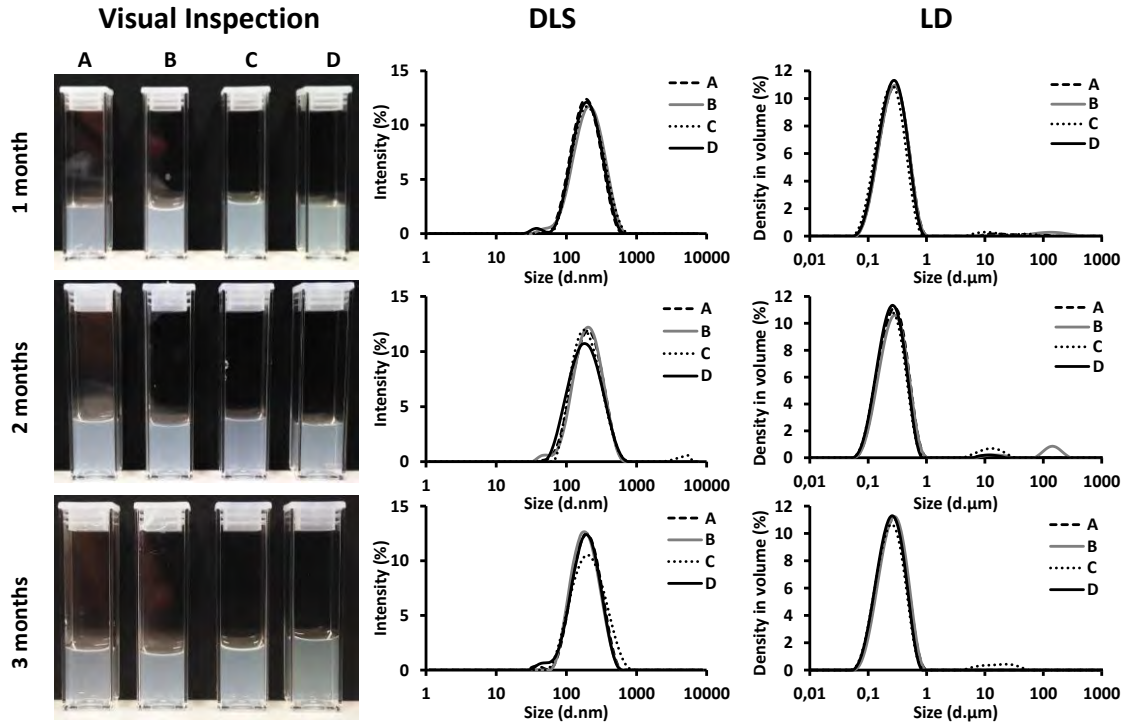

Figure 50. *Accelerated test for COSAN-stabilised DHA-in-water emulsions at 3 different time points (1 month, 2 months and 3 months) after being stored at 4 different conditions (A: light at r.t., B: dark at r.t., C: dark at 5 °C and D: dark at 40 °C). From left to right: Visual aspect of COSAN-stabilised NE; Representative size distribution curves obtained by Dynamic Light Scattering (DLS); representative size distribution curves obtained by Laser Diffraction (LD) at the same time points and storage conditions.*

6.4.3. Media Stability in PBS (1X)

COSAN-based NE was evaluated in extreme dilution conditions (Dil > 1:1000) in water and PBS (1X) under recirculation at 1500 rpm (**Figure 51**). The NE was based on 10 wt. % of fish oil and 0.5 wt. % of COSAN. Water dilution did not show any difference in droplet size over time. However, COSAN-NE diluted in PBS showed a shift in the mean volume from a D_{v50} of 0.25 µm to 0.52 µm in 10 minutes, thus doubling the original size. This trend continues at longer times. Indeed, at t=1 hour a bimodal distribution with maxima at around 0.50 µm (population A) and 10 µm (population B) is observed. Measurements at longer time points showed the formation of a third population at ca. 1000 µm (population C), which can be associated to emulsion destabilization due to phase separation, where the non-encapsulated oil is stacked in the optical detector.

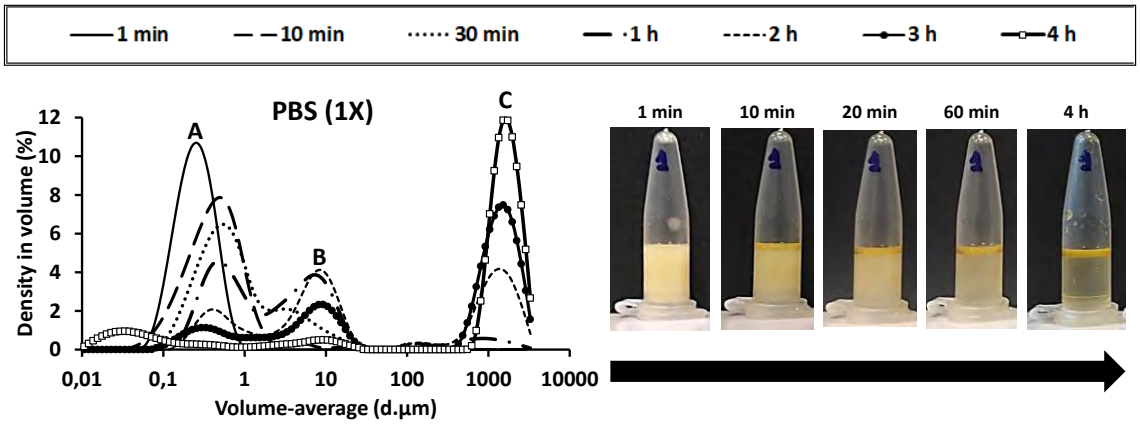

Figure 51. *COSAN-based (o/w)-nanoemulsion stability in PBS (1X). Left) Size distribution measured by LD (1500 rpm, 25 ^{o}C) over 4 hrs in PBS (10 mM phosphate). Right) Visual inspection of the stability of COSAN stabilised DHA-in-water emulsion in PBS (10 mM of phosphate) over time.*

To visually confirm NE instability in highly ionic strength media, the NE was 1:2 diluted in PBS (10 mM phosphate) and digital photographies of the macroscopic behavior of the NE were acquired up to 20 hrs (**Figure 51**). At t=10 minutes, a yellowish oil ring was formed over the emulsion, clearly indicating the initiation of phase separation. Total phase separation could be observed at 4 hrs, confirming previous results obtained with LD.

6.4.3. Emulsion stability towards CALB lipase

As demonstrated in **Chapter 5. Nanoemulsions as lipase-responsive materials**, lipase enzymes are capable to hydrolyse ester bonds present both in the oil and in the surfactant, contributing to emulsion destabilization. However, only certain specific bonds can be degraded by these enzymes. Lipase enzymes can actuate on esters directly attached to a hydrophobic moiety for enzymatic recognition. In this case, COSAN-stabilized DHA-in-water emulsion presented 3 ester bonds per oil molecule (triglyceride) but not in the surfactant. For this reason, we hypothesized that the effect of the lipase on the NE stability should be retarded. To proof our hypothesis, the stability of COSAN-based emulsions towards CALB lipase was evaluated using Laser Diffraction. The stability of the same NE in the absence of the enzyme was also evaluated as a control (**Figure 52**).

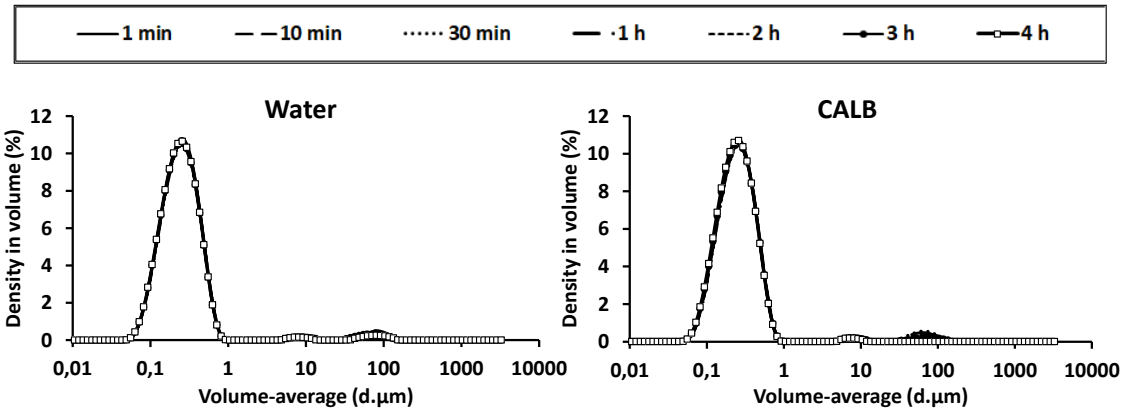

Figure 52. *Size distribution of COSAN-based (o/w)-nanoemulsion as measured by LD (1500 rpm, 25 ^{o}C) over 4 hrs in water (left) and in the presence of CALB enzyme (right)*

The results obtained by LD indicate that the presence of COSAN at the oil/water interface prevents the enzymatic degradation of the nanodroplets. No destabilization was observed during the experiment, despite sample recirculation at 1500 rpm, in both conditions. These results confirm the strong action of COSAN as a stabiliser in the oil-water interface. In spite of the small size of COSAN (which ultimately results in a thin barrier between the two phases) its capacity as stabiliser is sufficient to prevent access of the enzyme to the oil phase, resulting in preserved stability. Although not proven, the negative charge on the surface may play a role in this protective effect. Our results confirm that COSAN-emulsions are not esterase-responsive materials.

6.5. COSAN nanoemulsions as drug carriers

One of the main applications of oil-in-water NE is that they are stable in water but have a hydrophobic core, and hence can be used to carry hydrophobic drugs that either present low water solubility or have low stability after administration into living organisms as demonstrated in **Chapter 4. Stability enhancement: crosslinking at the oil/water interface.** Hence, NEs have been widely used as vehicles for drug delivery. In this case, we evaluated our newly developed nanosystems as hydrophobic drug carriers with the same model drug, 16α-fluoroestradiol (FES), a fluorinated analogue of the estrogen receptor ligand 17β-estradiol (Log Kow=4.01) used previously. Of note, the presence of the fluorine atom enables radiolabelling with the positron emitter fluorine-18 (^{18}F) for subsequent investigation using positron emission tomography (PET).

6.5.1. Emulsion loading capacity using 16α-[^{18}F]Fluoroestradiol (FES) as model drug

NEs were prepared as described above but increased concentrations of FES were solved in the oil phase (2, 3 and 10 % wt.). Trace amounts of [^{18}F]FES, prepared as previously reported by *Mori et al.*[15] (with minor modifications, see experimental section) were subsequently added and the emulsion was produced.

The presence of trace amounts of the radiofluorinated compound enabled a fast and reliable estimation of drug encapsulation capacity. For that purpose, the amount of radioactivity of the reaction mixture was measured after NEs formation. The amount of radioactivity in the emulsion fractions obtained after purification by SEC was also measured, and encapsulation yield was determined as the value of the ratio between these two values. Encapsulation efficiency values of 53, 49 and 59% were obtained for 2, 3 and 10 % wt. concentrations of FES, respectively. These values confirm that encapsulation efficiency is independent of the concentration of the drug in the oil phase, suggesting that encapsulation is mainly driven by the oil/water partition coefficient. Furthermore, FES encapsulation keeps NE physically unaltered in terms of size, polydispersity and stability in different storing conditions, even at the highest loading assayed (**Figure 53**).

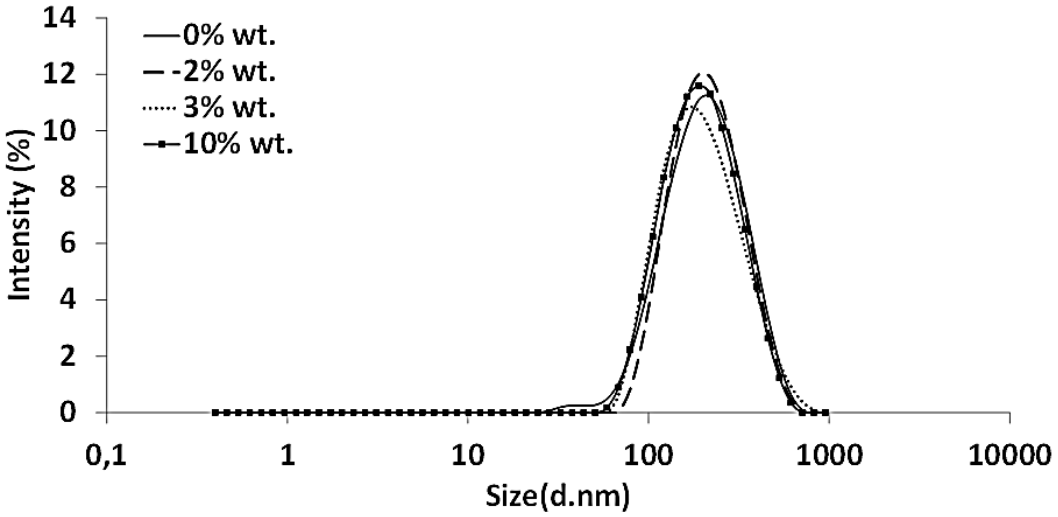

Figure 53. NE size distribution by DLS after encapsulation of different weight percentages (% wt.) of cold FES.

6.5.2. *In vivo* biodistribution of free and encapsulated 16α-[^{18}F]Fluoroestradiol (FES)

Despite the incredibly high stability overtime of COSAN-based NEs at different storage conditions, they showed a very fast destabilization in physiological saline serum. For this reason, we decide to evaluate the capacity of the COSAN-based NEs to modulate the distribution of lipophilic drugs in living organisms via intratracheal instillation using PET imaging. To that purpose, FES was aerosolized and administered intratracheally either as free ([^{18}F]FES) and encapsulated (NE-[^{18}F]FES) drug. As evidenced in the images (**Figure 54**, left) intra-tracheal administration of [^{18}F]FES resulted in a very fast lung clearance, with only 50%, 10% and 5% of the administered labelled compound remaining in the lungs at t=2, t=10 and t=40 minutes after administration, respectively (**Figure 55b**).

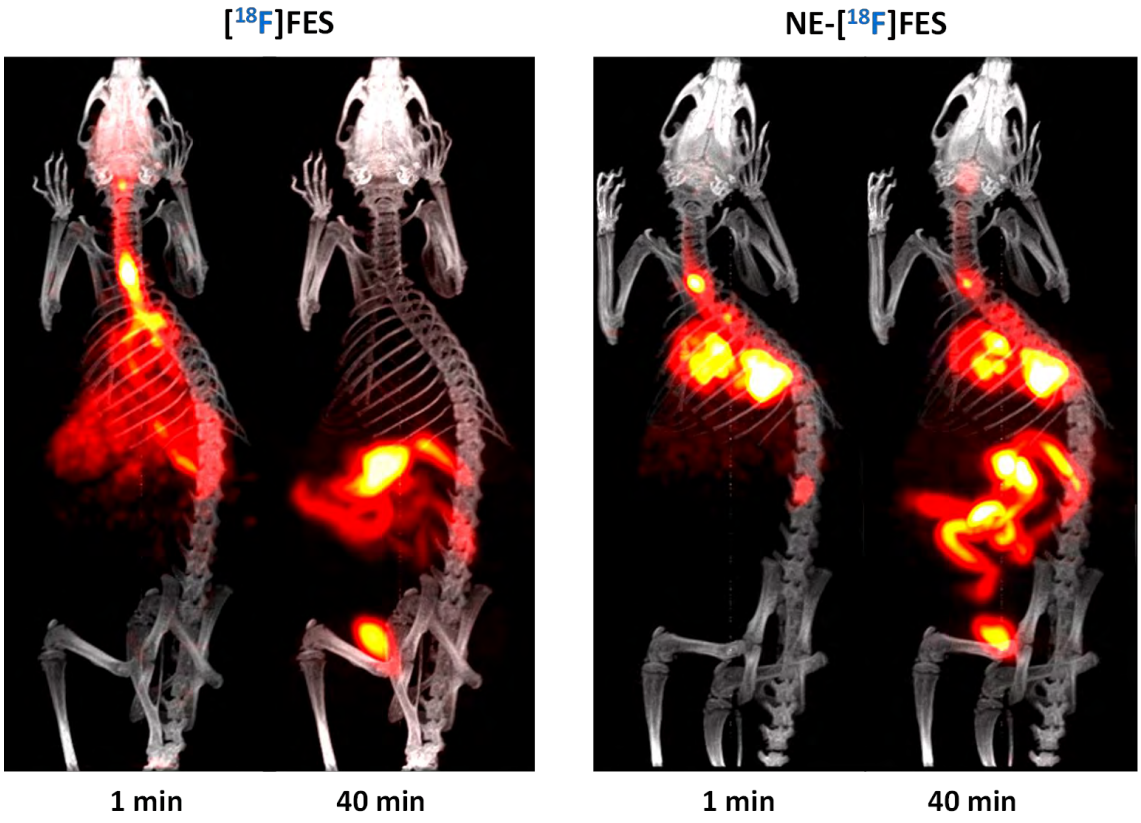

Figure 54. *Representative PET-CT images of the distribution of radioactivity at different time points after intra-tracheal administration of NE-[^{18}F]FES (left) and [^{18}F]FES (right). Maximum intensity projections of PET images have been corregistered with surface-rendered CT-images;*

Contrarily, after administration of NE-[^{18}F]FES most of the activity remained within the lungs at the end of experiment (**Figure 54**, right). Concretely, more than 70% of the radioactivity was still in the lungs at t=10 min, and this value decreased only to 60% at t=40 min **(Figure 55b**). In both cases, lung clearance resulted in the progressive accumulation of radioactivity in the gastrointestinal tract. These results confirm the suitability of the NEs to prolong the residence time of FES in the lungs.

6.5.3. *In vivo* biodistribution of ^{124}I-COSAN

To get further information related to the *in vivo* stability of our NEs, we next explored the biodistribution of the NEs but focusing on the stabiliser, i.e. the COSAN. With that aim, NEs with the same composition and characteristics as those described above were prepared, but a positron emitter (^{124}I, half-life of 4.2 days) was incorporated into the COSAN moiety (**Figure 55**) to yield [^{124}I]NE-FES. The production of the emulsion was performed as described above, but the COSAN solution (containing 7 mg of COSAN) was spiked with ^{124}I-labelled COSAN (1 mg of iodo-COSAN) prepared by isotopic exchange using a previously reported method.[16] Excess of free [^{124}I]COSAN was removed by SEC and the purified fractions containing [^{124}I]NE-FES were pooled and administered to animals. Images obtained at different time points after administration confirmed long residence time in the lungs. Quantification of the images revealed similar activity profiles for both NE-[^{18}F]FES and [^{124}I]NE-FES (**Figure 55c**). These results, together with the fast lung clearance observed after administration of free [^{18}F]FES, suggest a progressive destabilization of the drug-loaded NEs in the lungs followed by fast clearance of both the drug and the stabiliser. The fast elimination of the stabiliser after drug release is positive, as it should enable repeated administration without significant accumulation of the carrier in the lungs.

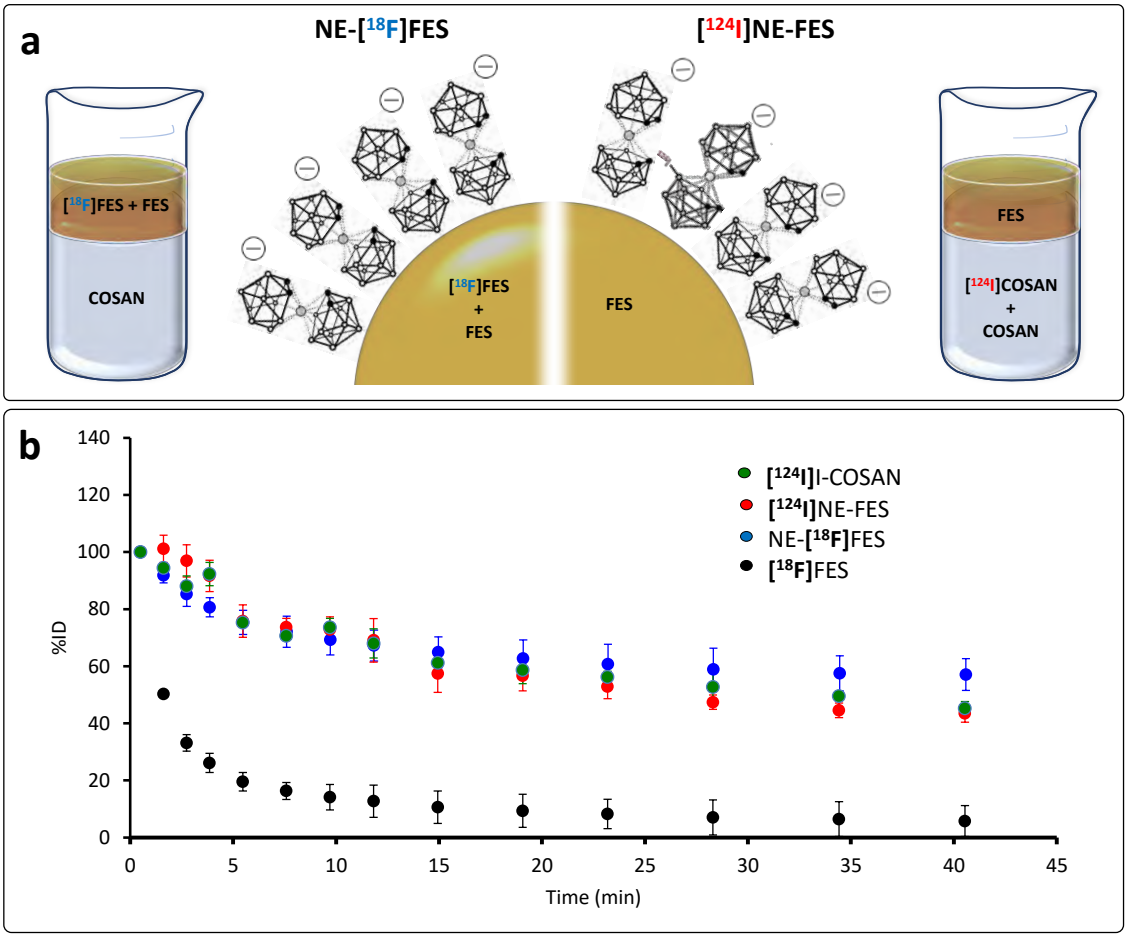

Figure 55. *a) Schematic representation for the preparation of NE-[^{18}F]FES and [^{124}I]NE-FES; b) Time-activity curves in the lungs after intratracheal administration of [^{124}I]I-COSAN, [^{124}I]NE-FES, NE-[^{18}F]FES and [^{18}F]FES. Results are expressed in percentage of injected dose (%ID). Displayed values correspond to mean ± standard deviation, n=2 per compound.*

6.6. Summary and Conclusion

The amphiphilic anion cobalt bis(dicarbollide), commonly known as COSAN, can act as nanoemulsion stabiliser, enabling the formation of drug-loaded, DHA-in-water-based NEs with long term stability in water under different storing conditions. *In vivo* PET imaging studies demonstrated that (i) NEs prolong the residence time in the lungs of the model hydrophobic drug FES after intratracheal aerosolization; and (ii) the stabiliser is rapidly cleared from the lungs after drug release. These results suggest that

the newly developed NEs can be applied for drug delivery of poor water soluble drugs when the lung is the target organ. Therapeutic applications in experimental models of lung inflammation are currently ongoing.

6.7. Materials and methods

6.7.1. Materials

Cesium salt of bis(1,2-dicarbollide)cobaltate (COSAN) and was purchased from Katchem Ltd. (Prague, Czech Republic). Docosahexaeonic acid oil (DHA) (80%) was kindly provided by SendaBio. 3-methoxymethyl-16β,17β-epiestriol-O-cyclic sulfone (MMSE) was purchased from ABX Advanced Biochemical Compounds (Radeberg, Germany). Illustra NAP TM-5 columns were purchased from GE Healthcare Life Sciences. Ultrapure water was obtained from a Milli-Q A10 Gradient equipment (Millipore). Iodine, 17β-estradiol and 4,7,13,16,21,24-Hexaoxa-1,10-diazabicyclo(8.8.8)hexacosane (Kryptofix, K2.2.2) were purchased from Sigma Aldrich Chemical. Phosphate-buffered saline (PBS) and HPLC grade ethanol, dichloromethane and acetonitrile were purchased from Scharlab (Sentmenat, Barcelona, Spain).

6.7.2. Characterization Methods

- *Dynamic Light Scattering* (DLS): DLS analyses were conducted using a Zetasizer Nano ZS, ZEN3600 Model (Malvern Instruments Ltd). All measurements were performed in disposable sizing cuvettes at a laser wavelength of 633 nm and a scattering angle of 173°. Zeta-potential measurements were performed in disposable zeta potential cells (pH 7.2, 25°C). Samples were dispersed at a concentration of 2 mg of oil droplets/mL in ultrapure water for size and in 1 mM phosphate buffer saline for zeta-potential. Measurements were performed in triplicate.
- *Laser diffraction (LD)*: LD analyses were conducted using a Mastersizer 3000 laser diffraction system (Malvern Instruments Ltd). All measurements were performed at a laser wavelength of 430 nm using 600 mL of ultrapure water. Each measurement

was performed 5 times (5 seconds per run) in ultrapure water at 1500 rpm and 25°C following Mie dispersion model.

- *Transmission Electron Cryo-Microscopy (Cryo-TEM):* Cryo-TEM analysis of (o/w)-emulsions were performed on a JEM-2200FS/CR (JEOL Europe, Croissy-sur-Seine, France) transmission electron microscope. This microscope is equipped with a field emission gun (FEG) operated at 200 kV and an in-column Ω energy filter. For sample preparation, freshly glow-discharged 200-mesh grid (R2.2 200 Mesh; QUANTIFOIL) was placed inside the chamber of a Vitrobot Mark III (FEI Company, USA), which is maintained at 8˚C temperature and relative humidity close to saturation (85% rH). Four microliters of non-diluted sample were dropped onto the grid for 15 seconds. After incubation, most of the liquid on the grid was removed by blotting (blot time was 3 seconds, number of blots was set to 1, drain time was zero and blot offset was 1 mm) with absorbent standard Vitrobot filter paper (Ø55/20mm, Grade 595, Thermo Fisher Scientific - FEI). After the blotting step, the grid was abruptly plunged into a liquid ethane bath, previously cooled with liquid nitrogen at approximately -170 ºC. Once the specimen was frozen, the vitrified grid was removed from the plunger and stored under liquid nitrogen inside a cryo-grid storage box. During imaging, no-tilted zero-loss two-dimensional (2D) images were recorded under low-dose conditions, utilizing the 'Minimum Dose System (MDS)' of Jeol software, with a total dose on the order of 10-20 electrons/Å² per exposure, at defocus values ranging from 1.5 to 4.0 µm. The in-column Omega energy filter of the microscope helped us to record images with improved signal-to-noise ratio (SNR) by zero-loss filtering, using an energy selecting slit width of 30 eV centred at the zero-loss peak of the energy spectra. Digital images were recorded on a 4K × 4K (15 µm pixels) Ultrascan4000™ charge-coupled device (CCD) camera (Gatan Inc.) using DigitalMicrograph™ (Gatan Inc.) software, at different nominal magnifications from 4000× to 60000×. Number size distribution was achieved from several micrographs using an automatic image analyser (ImageJ). 500 droplets were selected for the analysis.

6.7.3. Production of COSAN-stabilized (o/w)-emulsions

COSAN (8 mg, 0.2% wt. of the whole emulsion of 4g) was dissolved in ultrapure water (aqueous phase, 3.6 mL, 90% wt.) in an 8 mL glass vial. To this solution, 0.4 g of DHA (oil phase, 10% wt.) was added. The emulsion was then formed by sonication (0°C, under stirring) using an UP400S (Hielscher) system at 100% of amplitude and pulse during 4 minutes (400 W) with a H3 sonotrode tip (3 mm diameter, 100 mm length). For *in vivo* studies of NE-[^{18}F]FES, 50 µL of a trace solution of [^{18}F]FES in dichloromethane (containing ca. 806.6 MBq, see *6.3.12. Aerosol administration* for *in vivo* details) were poured into the DHA phase and mixed before sonication. For *in vivo* studies of COSAN labelled emulsion ([^{124}I]NE-FES), a COSAN solution (containing 7 mg of COSAN) was spiked with ^{124}I-labelled COSAN (1 mg of iodo-COSAN containing ca. 14.06 MBq see *6.3.12. Aerosol administration* for *in vivo* details) in 3.6 mL of ultrapure water. In both cases the emulsion was purified before injection by Size Exclusion Chromatography (SEC) using an Illustra NAP TM-5 column.

6.7.4. Medium stability over time in PBS (1X)

Medium stability studies were performed over time and under recirculation in phosphate buffered saline (PBS, 10 mM phosphate) followed by volume-weighted size distribution at regular intervals of 1 minute, determined using a Mastersizer 3000 laser diffraction system (Malvern Instruments Ltd). COSAN-based emulsion was added dropwise over 100 mL of PBS (1X) in the Hydro SM (Small volume entry level wet dispersion unit) at 1500 rpm. For digital picture acquisition, 500 µL of emulsion were diluted with 500 µL of PBS (10 mM phosphate) in a regular 1.5 mL eppendorf and the mixture was kept at room temperature, under light and without stirring.

6.7.5. Emulsion stability towards CALB lipase by LD

COSAN-stabilized (o/w)-nanoemulsion (500 µL) was mixed with a solution of *Candida Antarctica Lipase B* (CALB, 500 µL, 0.2 mg/mL) and the mixture was carefully added to 600 mL of water at r.t. and 1500 rpm. Enzymatic degradation was evaluated by volume-weighted size distribution at regular intervals of 10 minutes during 4 hours and determined using a Mastersizer 3000 laser diffraction system (Malvern Instruments

Ltd). First measurement was acquired before enzyme addition as a control. Further control experiments in the absence of enzyme were also conducted.

6.7.6. Long-term stability at different storing conditions (accelerated test conditions)

COSAN-stabilized DHA-in-water emulsion was freshly prepared as described above and fractions of 1 mL were stored at 4 different conditions (A: light at r.t., B: dark at r.t., C: dark at 5 °C and D: dark at 40 °C) over 3 months. Emulsion stability was subsequently evaluated by visual inspection, and determination of hydrodynamic diameter (using DLS) and volume average diameter (using LD) at 3 different time points (1 month, 2 months and 3 months).

6.7.7. Emulsion loading capacity

Increasing amounts of cold 17β-estradiol (20 mg, 30 mg and 100 mg) were solved in 1 g of DHA oil. After dissolution, 400 mg of each mixture (2, 3 and 10 % wt.) and 50 µL of a solution containing [^{18}F]FES in dichloromethane (ca. 100 ng, 1.11-2.59 MBq) were poured into 3.6 mL of ultrapure water containing 8 mg of COSAN. Emulsions were produced as described above. Once produced, 500 µL of each emulsion were purified by SEC using an Illustra NAP TM-5 column. The purified fractions were pooled, diluted with ultrapure water to reach a final volume of 2 mL, and transferred to Gamma Counter-compatible tubes. The same dilution was applied for 500 µL of non-purified emulsions. The amount of radioactivity in each sample was determined in counts per second (cps) using an automated Gamma Counter. The incorporation of [^{18}F]FES was subsequently calculated as the ratio between the amount of radioactivity in the purified fraction and the amount of radioactivity in the non-purified fraction, and expressed in percentage.

6.7.8. Synthesis of Cs[8-I-3,3'-Co(1,2-$C_2B_9H_{10}$)(1',2'-$C_2B_9H_{11}$)] (I-COSAN)

Iodine (0.83 g, 3.28 mmol) was added to a solution of cobalt bis (dicarbollide) (0.75 g, 1.64 mmol) in EtOH (10 mL). The reaction mixture was left to stand overnight at room temperature and was then heated under reflux for 2.5 h. The excess iodine was decomposed by the addition of a solution of $Na_2S_2O_3$ (0.42 g, 2.63 mmol) in water (8

mL) and the resulting mixture was boiled for 5 min. The mixture was concentrated until the formation of an orange precipitate. This was filtered off, washed with water and hexane, and dried under vacuum (0.58 g, 36 %). ^{1}H NMR (500 MHz, acetone-d6): δ 4.54 [C–H, 2H, s], 4.29 [C–H, 2H, s], 2.83 [B-H, 17 H, m]; ^{11}B{^{1}H} NMR (500 MHz, acetone-d6): δ 6.15 [1B, s], 3.19 [1B, s], 0.97 [1B, s], -2.01 [2B, d], -5.01 [5B, s], -5.74 [2B, s], -16.32 [2B, s], -17.77 [2B, s], -21.20 [1B, s], -23.40 [1B, s].

6.7.9. Radiochemistry (I): Radiolabeling of Iodo-COSAN with ^{124}I

Acetonitrile (200µL) was added to a NaOH (0.1M) solution containing Na[^{124}I]I (50 µL, 44.8 MBq) and the resulting mixture was introduced in a 2.5 mL conic vial. The solvent was evaporated to dryness (110°C, 30 min) and 1 mg of iodo-COSAN dissolved in acetonitrile (100 µL) was added together with *trans-bis*(acetate)*bis*[o-(di-o-tolylphosphino)benzyl] dipalladium (II) (Herrmann's catalyst, HC, 0.1 mg, 0.101 µmol) dissolved in toluene (100 µL). The reaction mixture was heated at 100°C for 5 min, the solvent was removed under a constant helium flow and the resulting solid was dissolved in 0.5 mL of 0.1M ammonium formate (AMF)/acetonitrile (1/2) and purified by and passing through a Sep-Pak C18 plus cartridge (Sep-Pak® Light, Waters) after 1:100 water dilution. Compound retained was eluted with ethanol (3x500 µL). The solvent was finally evaporated to dryness. Quality control was performed by radio-HPLC after diluting the solid residue with mobile phase. Analytical conditions were: Stationary phase: Mediterranea Sea18 column (4.6x150 mm, 5 µm particle size, Teknokroma, Spain); mobile phase A: 0.1M ammonium formate (AMF) buffer pH= 3.9; B: acetonitrile; flow rate = 1mL/min; gradient: 0 min: 60% A- 40% B; 2min: 60% A- 40% B; 6min: 20% A- 80% B; 14min: 0% A- 100% B; 16min: 0% A- 100% B; 18min: 60% A- 40% B; 20min: 60% A- 40% B (retention time: 13.5min, **Figure 56**).

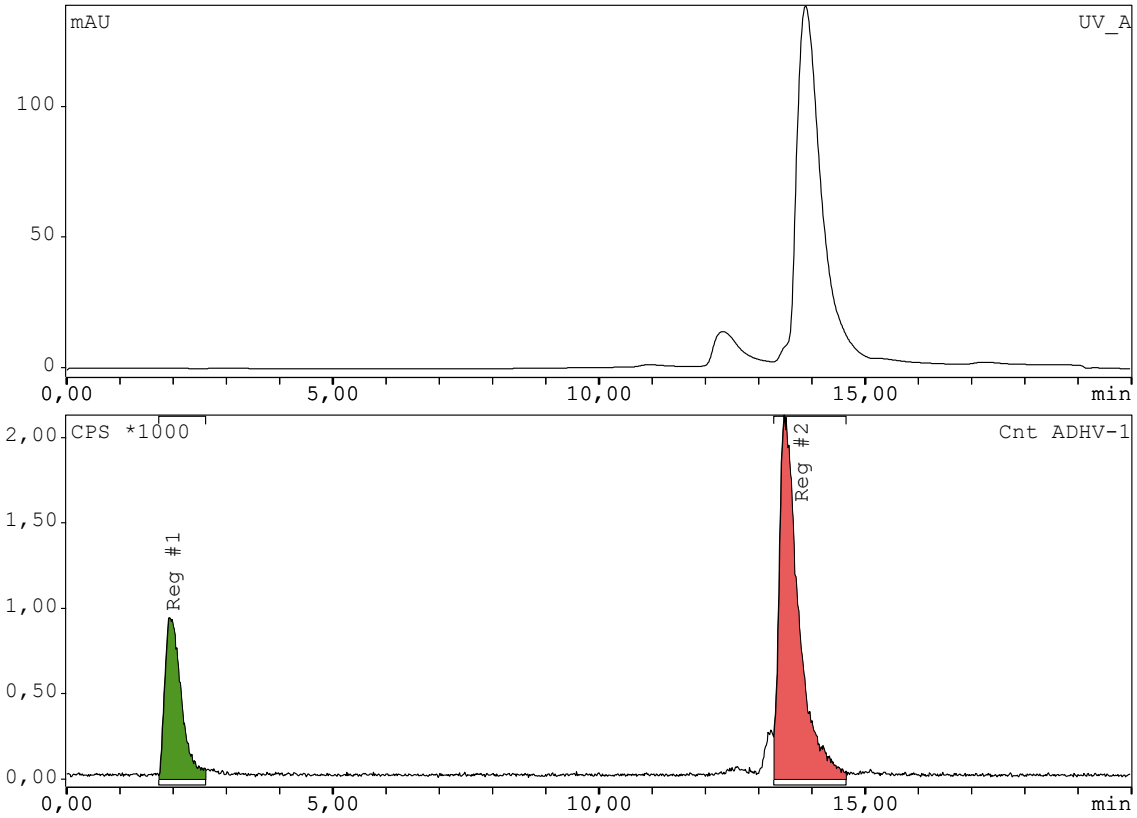

Figure 56. *Chromatogram obtained before purification of the reaction mixture containing [^{124}I]-I-COSAN and free iodide. UV detector (top) and radioactivity detector (bottom) signals are shown. The peak corresponding to [^{124}I]-I-COSAN elutes at 13.5 min.*

6.7.10. Radiochemistry (II): Synthesis of 16α-[^{18}F]Fluoroestradiol (FES)

[^{18}F]fluorine was produced by irradiation of [^{18}O]H_2O with 18MeV protons using an IBA Cyclone 18/9 cyclotron. The production of 16α-[^{18}F]Fluoroestradiol was carried out following a previously described method [17] with minor modifications. In brief, [^{18}F]F^- was trapped in an Accell™ Plus QMA anion exchange resin (Waters) and eluted into a V-shaped vial using sequentially a solution of Kryptofix $K_{2.2.2}$ in MeCN (15 mg/mL; 1 mL) and an aqueous K_2CO_3 solution (6 mg/mL; 0.5 mL). The solvent was evaporated to dryness via azeotropic distillation in two steps (80°C, 10 min; 100°C, 5 min) under helium flow. Subsequently, a solution containing 1 mg of 3-methoxymethyl-16β,17β-epiestriol-O-cyclic sulfone (MMSE) in anhydrous MeCN (1 mL) was added and the mixture was heated at 100°C for 10 min. After fluorination, a 0.1M HCl solution in CH_3CN (prepared by mixing 9 parts of MeCN and 1 part of 1 M HCl) was added and the solvent was evaporated to dryness at 100°C under helium flow. After repeating this

operation and cooling to 40°C, the reaction crude was diluted with Water/MeCN (40/60, 2.5 mL) and the resulting mixture was eluted through a Sep-Pak C18 plus cartridge (Waters) and purified by high performance liquid chromatography (HPLC) using radioactive detection. A Nucleosil™ 100-7 C18 column (10 x 250 mm, 5 µm) was used as stationary phase and Water/MeCN (40/60) as the mobile phase at a flow rate of 5 mL/min. The desired fraction (retention time: 11.6 min, see **Figure 57**) was collected, diluted with water (40 mL) and reformulated by trapping in a Sep-Pak C18 Plus Short Cartridge (waters) and further eluting with dichloromethane (2 mL). Quality control analysis was performed using a Mediterranea Teknokroma C18 column (150 mm) as stationary phase. The column was eluted with A (water) and B (Acetonitrile) using a gradient: t=0 min, 80% A, 20% B; t=2min, 80% A, 20% B; t=10 min, 10% A, 90% B; t=12 min, 10% A, 90% B; t=14 min, 80% A, 20% B at 1 mL/min flow rate. The retention time was 9 min.

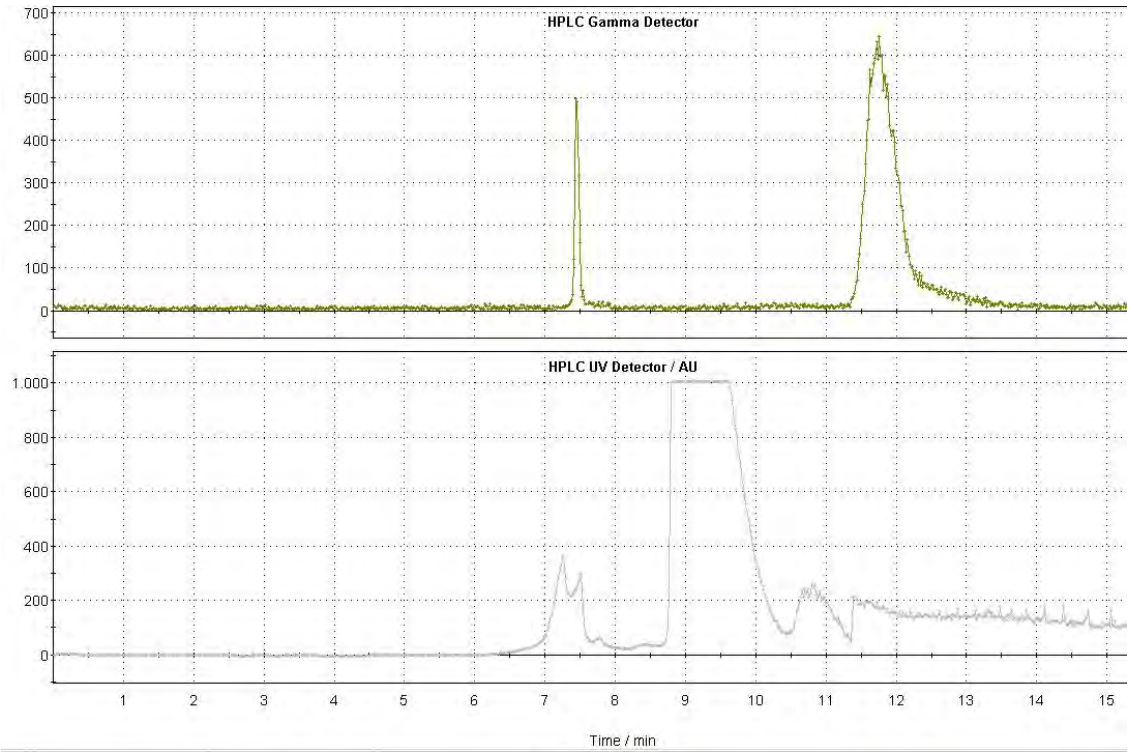

Figure 57. *Chromatogram obtained during purification of 16α-[^{18}F]Fluoroestradiol. UV detector (bottom) and radioactivity detector (top) signals are shown. The peak corresponding to 16α-[^{18}F]Fluoroestradiol elutes at 11.6 min.*

6.7.11. Animal experiments

The animals were maintained and handled in accordance with the Guidelines for Accommodation and Care of Animals (European Convention for Protection of Vertebrate Animals Used for Experimental and Other Scientific Purposes) and internal guidelines. Experimental procedures were approved by the ethical committee and local authorities. All animals were housed in ventilated cages and fed on standard diet *ad libitum*.

6.7.12. Aerosol administration

Endotracheal insufflations were carried out using the Penn-Century MicroSprayer® Aerosolizer (FMJ-250 High Pressure Syringe Model, Penn-Century. Inc. Wyndmoor, USA; henceforth "Penn-Century Aerosolizer") following a previously reported method by Cossío *et al.* (2018).[18] In brief, deep sedation was induced to the animals by inhalation of 5% isoflurane in pure O_2. The tip of the delivery needle was carefully positioned just above the carina and 50 µL of injectable emulsion diluted with ultrapure water (1:10), containing 1.85-9.32 MBq for [^{18}F]FES or 0.84-1.15 MBq for [^{124}I]-I-COSAN, was administered. A small animal Laryngoscope (Penn-Century, Model LS-2) was used for correct visualization of the epiglottis. Immediately after administration, rats were submitted to *in vivo* imaging studies.

6.7.13. *In vivo* Imaging experiments

After aerosol administration and without recovering from sedation, animals were positioned in an eXploreVista-CT small animal PET-CT system (GE Healthcare, USA) to perform *in vivo* studies. During imaging, rats were kept normothermic using a heating blanket (Homeothermic Blanket Control Unit; Bruker). Anesthesia was maintained by inhalation of 1.5-2% isoflurane in pure O_2. Dynamic PET images (energy window: 400-700 KeV) were acquired with the following frames: 4 x 15 s, 4 x 30 s, 3 x 60 s and 3 x 90 seconds. In all cases, four beds were defined to acquire whole body images (total acquisition time = 42 min). After each PET acquisition, a CT scan (X-Ray energy: 40 kV, intensity: 140 µA) was performed for a later attenuation correction in the image reconstruction and for unequivocal localization of the radioactivity. PET Images were

reconstructed using random and scatter corrections using filtered back projection. PET-CT images of the same animal were co-registered and analyzed using PMOD image analysis software (PMOD Technologies Ltd, Zürich, Switzerland). Volumes of interest (VOIs) were manually delineated on the organs of interest on CT images. VOIs were transferred to PET images and time–activity curves (decay corrected) were obtained as cps/cm^3 in each VOI and values were then normalised to the starting amount of radioactivity.

6.8. References

1. Tadros, T., Izquierdo, P., Esquena, J. & Solans, C. Formation and stability of nano-emulsions. *Adv. Colloid Interface Sci.* **108–109**, 303–318 (2004).

2. Tayeb, H. H. & Sainsbury, F. Nanoemulsions in drug delivery: Formulation to medical application. *Nanomedicine* **13**, 2507–2525 (2018).

3. Gupta, A., Eral, H. B., Hatton, T. A. & Doyle, P. S. Nanoemulsions: formation, properties and applications. *R. Soc. Chem.* **12**, 2826–2841 (2016).

4. Ghorabi, S., Rajabi, L., Madaeni, S. S., Zinadini, S. & Derakhshan, A. A. Effects of three surfactant types of anionic, cationic and non-ionic on tensile properties and fracture surface morphology of epoxy/MWCNT nanocomposites. *Iran. Polym. J. (English Ed.* **21**, 121–130 (2012).

5. Holland, P. M. & Rubingh, D. N. Mixed Surfactant Systems. *Fuel Sci. Technol. Int.* **11**, 241–242 (1993).

6. Hawthorne, M. F. *et al.* π-Dicarbollyl Derivatives of the Transition Metals. Metallocene Analogs. *J. Am. Chem. Soc.* **90**, 879–896 (1968).

7. Bauduin, P. *et al.* A theta-shaped amphiphilic cobaltabisdicarbollide anion: Transition from monolayer vesicles to micelles. *Angew. Chemie - Int. Ed.* **50**, 5298–5300 (2011).

8. Brusselle, D. *et al.* Lyotropic lamellar phase formed from monolayered θ-shaped carborane-cage amphiphiles. *Angew. Chemie - Int. Ed.* **52**, 12114–12118 (2013).

9. Ďorďovič, V. *et al.* Stealth Amphiphiles: Self-Assembly of Polyhedral Boron Clusters. *Langmuir* **32**, 6713–6722 (2016).

10. Fernandez-Alvarez, R., Ďorďovič, V., Uchman, M. & Matějíček, P. Amphiphiles without Head-and-Tail Design: Nanostructures Based on the Self-Assembly of Anionic Boron Cluster Compounds. *Langmuir* **34**, 3541–3554 (2018).

11. Verdiá-Báguena, C. *et al.* Amphiphilic COSAN and I2-COSAN crossing synthetic lipid membranes: Planar bilayers and liposomes. *Chem. Commun.* **50**, 6700–6703 (2014).

12. Tarrés, M., Canetta, E., Viñas, C., Teixidor, F. & Harwood, A. J. Imaging in living cells using νb-H Raman spectroscopy: Monitoring COSAN uptake. *Chem. Commun.* **50**, 3370–3372 (2014).

13. Uchman, M., ɯormǰovič, V., Tošner, Z. & Matějíček, P. Classical Amphiphilic Behavior of Nonclassical Amphiphiles: A Comparison of Metallacarborane Self-Assembly with SDS Micellization. *Angew. Chemie - Int. Ed.* **54**, 14113–14117 (2015).

14. Lerche, D. & Sobisch, T. Direct and accelerated characterization of formulation stability. *J. Dispers. Sci. Technol.* **32**, 1799–1811 (2011).

15. Mori, T. *et al.* Automatic synthesis of 16α-[18F]fluoro-17β-estradiol using a cassette-type [18F]fluorodeoxyglucose synthesizer. *Nucl. Med. Biol.* **33**, 281–286 (2006).

16. Gona, K. B., Gómez-Vallejo, V., Padro, D. & Llop, J. [18F]Fluorination of o-carborane via nucleophilic substitution: Towards a versatile platform for the preparation of 18F-labelled BNCT drug candidates. *Chem. Commun.* **49**, 11491–11493 (2013).

17. Römer, J., Füchtner, F., Steinbach, J. & Johannsen, B. Automated production of 16α- [18F]fluoroestradiol for breast cancer imaging. *Nucl. Med. Biol.* **26**, 473–479 (1999).

18. Cossío, U. *et al.* Preclinical evaluation of aerosol administration systems using Positron Emission Tomography. *Eur. J. Pharm. Biopharm.* **130**, 59–65 (2018).

Chapter 7. General Conclusions

1. Dextran derivatives with different functionalities can stabilize oil in water (o/w)-emulsions. Among all experimental scenarios tested, small-sized nanoemulsions (Z-Average = 270 nm) with low polydispersion values (PDI<0.22) could be achieved when methacrylate-functionalized dextran (DXT-MA) with a substitution range (DS) of 15-36% was used as the stabiliser.
2. The stability of the nanoemulsion can be enhanced via cross-linking reaction at the oil-water interface by dissolving the linker in the oil phase. Crosslinking nanoemulsions with >1eq. of 2,2'-(ethylenedioxy)diethanethiol (DODT; 0.5 eq. thiol) linker proved to be more stable than their non-crosslinked analogous over time, under different storing conditions and in physiologically relevant media.
3. Cross-linked nanoemulsions can prolong the residence time of encapsulated hydrophobic drugs in the lungs after direct pulmonary administration, as demonstrated using multi-isotopic radiolabelling followed by positron emission tomography (PET) imaging and 16α-fluoro-17β-estradiol (fluoroestradiol) as a model drug. The stabilizer is rapidly cleared from the lungs after drug release.
4. Nanoemulsions based on triglyceride oils (oil phase) and DXT-MA (emulsifier) are lipase-responsive materials. The enzymes, Candida Antarctica Lipase B (CALB) and Pancreatic Lipase (PL), are able to hydrolyse ester bonds present both in the oil and the emulsifier, triggering an eventual release of the cargo.
5. The amphiphilic anion cobalt bis(dicarbollide) (COSAN) can act as (o/w)-nanoemulsion stabiliser, enabling the formation of oil-in-water NEs with long term stability in water under different storing conditions. The resulting nanoemulsions can act as drug carriers, and prolong the residence time of encapsulated hydrophobic drugs in the lungs after direct pulmonary administration, as demonstrated using multi-isotopic radiolabelling followed by PET imaging and fluroestradiol as a model drug. The stabiliser is rapidly cleared from the lungs after drug release.

Appendix I. Production and Characterization of dextran-based emulsions

Table 9. *Experimental conditions for emulsion formation and their characterization. Weight percentages (% wt) are based on the whole emulsion except in the case of the stabilizer, (*): % wt. based on the oil phase. Size distribution values in Intensity (DLS: Dynamic Light Scattering) and Volume (LD: Laser Diffraction). "N/A": data not available.*

	Oil phase			Water phase		Stabilizer			DLS characterization		LD characterization		Production Method
Name	**Class**	**% wt.**	**mass (g)**	**% wt.**	**mass (g)**	**Type**	**% wt.***	**mass (mg)**	**Z-Average (d.nm)**	**PDI**	**Volume-average (d.µm)**	**Uniformity**	
E0	Dodecane	50	1	50	1	DXT	1	10	N/A	N/A	N/A	N/A	M1
E1	Dodecane	50	1	50	1	D12	1	10	3100	0.31	7.3	2.56	M1
E2	Dodecane	50	1	50	1	D17	1	10	2070	0.14	14.2	1.8	M1
E3	Dodecane	50	1	50	1	D15	1	10	1740	0.33	6.4	0.75	M1
E4	Dodecane	50	1	50	1	D16	1	10	1640	0.53	19.2	1.4	M1
E5	Olive	50	1	50	1	D17	1	10	1470	0.78	50.8	6.8	M1
E6	Olive	40	0.8	60	1.2	D17	1	8	390	0.45	17.7	2.7	M1
E7	Olive	30	0.6	70	1.4	D17	1	6	340	0.65	75.2	4.6	M1
E8	Olive	20	0.4	80	1.6	D17	1	4	430	0.73	17.0	5.8	M1
E9	Olive	10	0.2	90	1.8	D17	1	2	300	0.45	11.9	1.3	M1
E10	Sunflower	50	1	50	1	D17	1	10	960	0.63	45.5	7.2	M1
E11	Sunflower	40	0.8	60	1.2	D17	1	8	540	0.69	65.2	16.7	M1
E12	Sunflower	30	0.6	70	1.4	D17	1	6	330	0.50	6.1	1.0	M1
E13	Sunflower	20	0.4	80	1.6	D17	1	4	350	0.87	3.4	5.4	M1
E14	Sunflower	10	0.2	90	1.8	D17	1	2	410	0.48	7.6	3.5	M1
E15	Olive	30	0.6	70	1.4	D16	1	2	300	0.66	19.4	0.6	M1
E16	Olive	20	0.4	80	1.6	D16	1	2	410	0.74	55.4	1.2	M1
E17	Olive	10	0.2	90	1.8	D16	1	2	430	0.64	8.1	2.1	M1
E18	Sunflower	30	0.6	70	1.4	D16	1	2	340	0,48	9.0	7.4	M1
E19	Sunflower	20	0.4	80	1.6	D16	1	2	370	0.78	1.4	1.2	M1

	Oil phase			Water phase		Stabilizer			DLS characterization		LD characterization		Production Method
Name	Class	% wt.	mass (g)	% wt.	mass (g)	Type	% wt.*	mass (mg)	Z-Average (d.nm)	PDI	Volume-average (d.µm)	Uniformity	
E20	Sunflower	10	0,2	90	1,8	D16	1	2	480	0,65	2,5	1,2	M1
E21	Eucalyptus	30	0,6	70	1,4	D16	1	2	193	0,69	N/A	N/A	M1
E22	Eucalyptus	20	0,4	80	1,6	D16	1	2	1220	0,77	N/A	N/A	M1
E23	Eucalyptus	10	0,2	90	1,8	D16	1	2	470	0,14	N/A	N/A	M1
E24	Olive	30	0,6	70	1,4	D15	1	2	1430	0,88	17,8	4,7	M1
E25	Olive	20	0,4	80	1,6	D15	1	2	1050	0,82	6,2	1,7	M1
E26	Olive	10	0,2	90	1,8	D15	1	2	390	0,76	2	3,4	M1
E27	Sunflower	30	0,6	70	1,4	D15	1	2	830	0,65	4	1,2	M1
E28	Sunflower	20	0,4	80	1,6	D15	1	2	680	0,65	17,4	0,7	M1
E29	Sunflower	10	0,2	90	1,8	D15	1	2	380	0,69	1,6	2,3	M1
E30	Peppermint	30	0,6	70	1,4	D15	1	2	3180	0,33	N/A	N/A	M1
E31	Peppermint	20	0,4	80	1,6	D15	1	2	1160	0,49	N/A	N/A	M1
E32	Peppermint	10	0,2	90	1,8	D15	1	2	400	0,34	N/A	N/A	M1
E33	Eucalyptus	30	0,6	70	1,4	D15	1	2	1420	0,34	N/A	N/A	M1
E34	Eucalyptus	20	0,4	80	1,6	D15	1	2	990	0,32	N/A	N/A	M1
E35	Eucalyptus	10	0,2	90	1,8	D15	1	2	600	0,21	N/A	N/A	M1
E36	Olive	10	0,2	90	1,8	D12	1	2	860	0,69	3,2	0,8	M1
E37	Olive	10	0,2	90	1,8	D15	1	2	290	0,62	2,3	3,6	M1
E38	Olive	10	0,2	90	1,8	D17	2	4	270	0,57	2,5	3,3	M1
E39	Olive	10	0,2	90	1,8	D12	2	4	1400	0,44	1,5	0,5	M1
E40	Olive	10	0,2	90	1,8	D16	2	4	1050	0,79	3,4	0,8	M1
E41	Olive	10	0,2	90	1,8	D15	2	4	770	0,68	3,8	0,9	M1
E42	Olive	10	0,2	90	1,8	D17	5	10	300	0,42	2,3	2,1	M1

	Oil phase			Water phase		Stabilizer			DLS characterization		LD characterization		Production Method
Name	**Class**	**% wt.**	**mass (g)**	**% wt.**	**mass (g)**	**Type**	**% wt.***	**mass (mg)**	**Z-Average (d.nm)**	**PDI**	**Volume-average (d.µm)**	**Uniformity**	
E43	Olive	10	0,2	90	1,8	D12	5	10	460	0,5	1	0,7	M1
E44	Olive	10	0,2	90	1,8	D16	5	10	530	0,5	0,9	1,3	M1
E45	Olive	10	0,2	90	1,8	D15	5	10	1180	0,72	4,3	0,8	M1
E46	Sunflower	10	0,2	90	1,8	D12	1	2	840	0,77	2,8	0,7	M1
E47	Sunflower	10	0,2	90	1,8	D15	1	2	380	0,63	1,6	2,3	M1
E48	Sunflower	10	0,2	90	1,8	D17	2	4	310	0,46	14,2	6,8	M1
E49	Sunflower	10	0,2	90	1,8	D12	2	4	510	0,54	1,3	0,6	M1
E50	Sunflower	10	0,2	90	1,8	D16	2	4	370	0,61	1,9	1	M1
E51	Sunflower	10	0,2	90	1,8	D15	2	4	530	0,56	9,8	2,7	M1
E52	Sunflower	10	0,2	90	1,8	D17	5	10	220	0,34	5,6	4,6	M1
E53	Sunflower	10	0,2	90	1,8	D12	5	10	380	0,42	1	0,6	M1
E54	Sunflower	10	0,2	90	1,8	D16	5	10	310	0,46	1,5	0,9	M1
E55	Sunflower	10	0,2	90	1,8	D15	5	10	1620	0,52	1,9	1,3	M1
E56	Fish	10	0,2	90	1,8	D12	1	2	530	0,58	1,4	0,8	M1
E57	Fish	10	0,2	90	1,8	D12	2	4	420	0,44	1,1	0,7	M1
E58	Fish	10	0,2	90	1,8	D12	5	10	460	0,46	0,8	0,7	M1
E59	Fish	10	0,4	90	3,6	D1	5	20	700	0,54	1,9	0,6	M2
E60	Fish	10	0,4	90	3,6	D2	5	20	250	0,25	0,8	1,6	M2
E61	Fish	10	0,4	90	3,6	D5	5	20	280	0,22	0,6	0,7	M2
E62	Fish	10	0,4	90	3,6	D6	5	20	340	0,36	1,1	2,7	M2
E63	Fish	10	0,4	90	3,6	D8	5	20	460	0,42	0,5	0,7	M2
E64	Fish	10	0,4	90	3,6	D9	5	20	550	0,38	0,6	0,6	M2
E65	Fish	10	0,4	90	3,6	D11	5	20	420	0,44	0,8	0,7	M2

	Oil phase			Water phase		Stabilizer			DLS characterization		LD characterization		Production Method
Name	**Class**	**% wt.**	**mass (g)**	**% wt.**	**mass (g)**	**Type**	**% wt.***	**mass (mg)**	**Z-Average (d.nm)**	**PDI**	**Volume-average (d.µm)**	**Uniformity**	
E66	Sunflower	10	0,4	90	3,6	D4	5	20	N/A	N/A	0,99	2	M2
E67	Sunflower	10	0,4	90	3,6	D9	5	20	N/A	N/A	0,82	0,5	M2
E68	Sunflower	10	0,4	90	3,6	D11	5	20	N/A	N/A	0,97	0,6	M2
E69	Sunflower	10	0,4	90	3,6	D14	5	20	N/A	N/A	1,21	0,6	M2
E70	Fish	10	0,4	90	3,6	D7	5	20	305	0,27	0,38	0,5	M2

Appendix II. Production and Characterization of Cross-linked emulsions

Table 10. *Experimental conditions for emulsion formation, and size distribution values as obtained by Dynamic Light Scattering (DLS, intensity) and Laser diffraction (LD, volume). In all cases, the relative amounts used were: 10 wt.% fish oil; 90 wt.% water; 5 wt.%* ***D7*** *(relative to oil phase). "N/A": data not available.*

	DLS characterization		LD characterization		Method	DODT / µL (thiol equivalents)
Name	**Z-Average (d.nm)**	**PDI**	**Volume-average (d.µm)**	**Uniformity**		
E71	305	0.27	0.38	0.5	M2	0.0 (0.0)
E72	N/A	N/A	0.43	0.6	M2	0.0 (0.0)
E73	N/A	N/A	0.44	0.6	M3	0.5 (0.25)
E74	N/A	N/A	0.38	0.6	M3	1.0 (0.5)
E75	N/A	N/A	0.38	0.7	M3	1.5 (0.75)
E76	N/A	N/A	0.39	0.8	M3	2.0 (1.0)
E77	N/A	N/A	0.47	1.1	M3	3.0 (1.5)
E78	300	0.24	0.55	0.5	M2	0.0 (0.0)
E79	300	0.24	0.51	0.5	M3	1.0 (0.5)
E80	260	0.19	0.38	0.5	M3	1.0 (0.5)
E81	330	0.26	0.38	0.7	M3	1.0 (0.5)

Appendix III. Production and Characterization of Lipase-Responsive Emulsions

Table 11. *Experimental conditions for emulsion formation and their characterization. Weight percentages (% wt.) are based on the whole emulsion except in the case of the stabilizer, (*): % wt. based on the oil phase. Size distribution values in Intensity (DLS: Dynamic Light Scattering) and Volume (LD: Laser Diffraction). "N/A": data not available.*

	Oil phase			Water		Stabilizer			DLS characterization		LD characterization		Production Method
Name	**Class**	**% wt.**	**mass (g)**	**% wt.**	**mass (g)**	**Type**	**% wt.***	**mass (mg)**	**Z-Average (d.nm)**	**PDI**	**Volume-average (d.µm)**	**Uniformity**	
E82	Sunflower	40	0.8	60	1.2	D15	1	8	1090	0.62	1.72	1.32	M1
E83	Sunflower	10	0.2	90	1.8	D15	1	2	N/A	N/A	N/A	N/A	M1
E84	Sunflower	10	0.2	90	1.8	D12	1	2	N/A	N/A	N/A	N/A	M1
E85	Sunflower	10	0.2	90	1.8	D17	1	2	N/A	N/A	N/A	N/A	M1
E86	Sunflower	10	0.2	90	1.8	T20	1	2	N/A	N/A	N/A	N/A	M1
E87	Sunflower	10	0.2	90	1.8	TX100	1	2	N/A	N/A	N/A	N/A	M1
E88	Sunflower	20	0.4	80	1.6	D15	1	4	N/A	N/A	N/A	N/A	M1
E89	Olive	10	0.4	90	3.6	D7	1	20	N/A	N/A	0.93	0.71	M2
E90	Sunflower	10	0.4	90	3.6	D7	1	20	N/A	N/A	0.69	0.48	M2
E91	Fish	10	0.4	90	3.6	D7	5	20	N/A	N/A	0.51	0.51	M2
E92	Fish	10	0.4	90	3.6	D7	5	20	N/A	N/A	0.53	0.61	M3
E93	Sunflower	10	0.4	90	3.6	D7	5	20	310	0.25	N/A	N/A	M2
E94	Sunflower	10	0.4	90	3.6	T20	5	20	240	0.32	N/A	N/A	M2
E95	Sunflower	10	0.4	90	3.6	TX100	5	20	240	0.28	N/A	N/A	M2
E96	Sunflower	20	0.8	80	3.2	D9	5	40	3940	0.44	N/A	N/A	M2
E97	Olive	10	0.4	90	3.6	D7	5	20	280	0.26	N/A	N/A	M2
E98	Sunflower	10	0.4	90	3.6	D7	5	20	290	0.28	N/A	N/A	M2
E99	Fish	10	0.4	90	3.6	D7	5	20	280	0.23	N/A	N/A	M2
E100	Olive	10	0.4	90	3.6	D7	5	20	290	0.27	N/A	N/A	M3
E101	Sunflower	10	0.4	90	3.6	D7	5	20	280	0.25	N/A	N/A	M3
E102	Fish	10	0.4	90	3.6	D7	5	20	290	0.21	N/A	N/A	M3